Fusing Bio-Inspired Surface Modification with Cycloaddition-Driven Polymer Conjugation

Zur Erlangung des akademischen Grades eines

DOKTORS DER NATURWISSENSCHAFTEN

(Dr. rer. nat.)

Fakultät für Chemie und Biowissenschaften

Karlsruher Institut für Technologie (KIT) - Universitätsbereich

genehmigte

DISSERTATION

von

Dipl.-Chem. Corinna Marina Preuß

aus

Nürtingen, Deutschland

Dekan: Prof. Dr. Peter W. Roesky
Referent: Prof. Dr. Christopher Barner-Kowollik
Korreferent: Prof. Dr. Michael A. R. Meier
Mündliche Prüfung: 17.04.2015

Die vorliegende Arbeit wurde von Oktober 2011 bis März 2015 unter Anleitung von Prof. Dr. Christopher Barner-Kowollik am Karlsruher Institut für Technologie (KIT) - Universitätsbereich angefertigt.

Erklärung

Ich erkläre hiermit, dass ich die vorliegende Arbeit im Rahmen der Betreuung durch Prof. Dr. Christopher Barner-Kowollik selbstständig verfasst und keine anderen als die angegebenen Quellen und Hilfsmittel verwendet habe. Wörtlich oder inhaltlich übernommenen Stellen sind als solche kenntlich gemacht und die Satzung des Karlsruher Instituts für Technologie (KIT) zur Sicherung guter wissenschaftlicher Praxis wurde beachtet.
Des Weiteren erkläre ich, dass ich mich derzeit in keinem weitern laufenden Promotionsverfahren befinde und auch keine vorausgegangenen Promotionsversuche unternommen habe.

Karlsruhe, den 02.03.2015

_____

Corinna Preuß

Life has three rules: ***Paradox, Humor****, and* ***Change.***

Paradox: *Life is a mystery; don't waste your time trying to figure it out.*

Humor: *Keep a sense of humor, especially about yourself. It is a strength beyond all measure.*

Change: *Know that nothing ever stays the same.*

- Dan Millman, Way of the Peaceful Warrior -

Publications Arising from this Thesis

[1] ***Biomimetic Dopamine-Diels-Alder Switches***

Preuss, C. M.; Goldmann, A. S.; Trouillet, V.; Walther, A.; Barner-Kowollik, C. ***Macromol. Rapid Commun.*** **2013**, *34*, 640.

[2] ***Controlled Cell Adhesion on Poly(dopamine) Interfaces Photo-Patterned with Non-Fouling Brushes***

Rodriguez-Emmenegger, C.;* Preuss, C. M.;* Yameen, B.; Pop-Georgievski, O.; Bachmann, M.; Mueller, J. O.; Bruns, M.; Goldmann, A. S.; Bastmeyer, M.; Barner-Kowollik, C. ***Adv. Mater.*** **2013**, *25*, 6123.

[3] ***A Bioinspired Light Induced Avenue for the Design of Patterned Functional Interfaces***

Preuss, C. M.; Tischer, T.; Rodriguez-Emmenegger, C.; Zieger, M. M.; Bruns, M.; Goldmann, A. S.; Barner-Kowollik, C***. J. Mater. Chem. B*** **2014**, *2*, 36.

[4] ***Fusing Catechol-Driven Surface Anchoring with Rapid Hetero Diels-Alder Ligation***

Preuss, C. M.; Zieger, M. M.; Rodriguez-Emmenegger, C.; Zydziak, N.; Trouillet, V.; Goldmann, A. S.; Barner-Kowollik**,** C. ***ACS Macro Lett.*** **2014**, *3*, 1169.

* both authors contributed equally.

Additional Publications

[1] ***Synthesis of Enantiomeric Pure Lithium and Potassium Benzamidinate Complexes‡***

Benndorf, P.; Preuß, C., Roesky; P. W. ***J. Organom. Chem.*** **2011,** *696*, 1150.

[2] ***The Influence of a Potential Diffusion Control on the Outcome of Modular Polymer-Polymer Click Conjugations†***

Preuss, C. M.; Barner-Kowollik, C. ***Macromol. Theory Simul.*** **2011**, *20*, 700.

[3] ***Chiral Benzamidinate Ligands in Rare-Earth-Metal Coordination Chemistry‡***

Benndorf, P.; Kratsch, J.; Hartenstein, L.; Preuss, C. M.; Roesky, P. W. ***Chem. Eur. J.*** **2012**, *18*, 14454.

[4] ***Hetero Diels-Alder Chemistry for the Functionalization of Single-Walled Carbon Nanotubes with Cyclopentadienyl End-Capped Polymer Strands***

Zydziak, N.; Preuss, C. M.; Winkler, V.; Hübner, C.; Bruns, M.; Barner-Kowollik, C. ***Macromol. Rapid Commun.*** **2013**, *34*, 672.

[5] ***A Facile One-Pot Route to Poly(carboxybetaine acrylamide) Functionalized SWCNTs***

Yameen, B.; Rodriguez-Emmenegger, C.; Ahmed, I.; Preuss, C. M.; Dürr, C. J.; Zydziak, N.; Trouillet, V.; Fruk, L.; Barner-Kowollik, C. ***Chem. Commun.*** **2013**, *49*, 6734.

†Publication resulting from the Diploma thesis.
‡Results from the 'Vertieferarbeit' in collaboration with Professor P. W. Roesky.

[6] ***A Facile Avenue to Conductive Polymer Brushes via Cyclopentadiene-Maleimide Diels–Alder Ligation***

Yameen, B.; Rodriguez-Emmenegger, C.; Preuss, C. M.; Pop-Georgievski, O.; Verveniotis, E.; Trouillet, V.; Rezek, B.; Barner-Kowollik, C. ***Chem. Commun***. **2013**, *49*, 8623.

[7] ***Suppressing Pseudomonas aeruginosa Adhesion via Anti-Fouling Polymer Brushes***

Rodriguez-Emmenegger, C.; Decker, A.; Surman, F.; Preuss, C. M.; Sedlákova, Z.; Zydziak, N.; Barner-Kowollik, C.; Schwartz, T.; Barner, L. ***RSC Adv.*** **2014,** *4*, 64781.

Abstract

In order to cope with future challenges in areas concerning the environment, medicine, transportation, construction industry and nutrition, an enormous amount of specific solutions is required. Especially, new developments in (bio)material fabrication are essential for progress in fields such as material science, nanotechnology, biosensing, life science, information technology or electronics, among others. Thus, advanced protocols for designing new materials that tailor certain properties are required. This is particularly important for surface-based applications in which the uppermost layer controls the material's performance to a significant extent. Different surface modification techniques, such as self-assembling monolayer (SAM) formation, lithography or chemical vapor deposition have already been widely employed, yet only being applicable on certain surfaces. In order to target various types of substrates, such as metals, minerals or even polymers or polymer coatings, a more versatile and substrate-independent modification route is inevitable. In this context, maritime organisms, such as marine mussels, have proven as excellent natural examples as these organisms possess the extraordinary ability to adhere to virtually all types of surfaces,

even rocks, wood or ship coatings and withstand rough tidal zones. The strong adhesion properties origin from catechol units provided in the mussel foot proteins (mfps) in the mussel's plaque at the distal end of the mussel byssus. Several research groups precisely investigated the described phenomenon and performed approaches to mimic this behavior in a synthetic fashion. Two different paths of exploiting these strong adhesion abilities were discovered: On the one hand, the attachment of catechol-anchor molecules based on catecholamines, such as dopamine or 3,4-dihydroxyphenyl-alanine (DOPA), on the other hand, the preparation of polydopamine films in slightly alkaline media and their post-modification.

In the present thesis, various routes to tailor the properties of surfaces were developed by fusing the modularity of advanced polymer chemistry with the imitation of the strong adhesion abilities of marine organisms by employing thermal or light-induced orthogonal ligation techniques in order to achieve precise functionalization of well-defined polymers and biomacromolecules, as well as regional and temporal control of the same, on variable surfaces. The former methods led to fast conjugation at ambient temperature while the latter enabled to gain access to spatial control. By shining light on defined areas, a precise encoding of the desired functionalities was achieved.

Firstly, an *α*-catechol polymer was prepared in a Diels–Alder (DA) reaction of a cyclopentadiene (Cp) terminated poly(ethylene glycol) (PEG) chain and a maleimide containing catechol. The polymer was readily grafted to surfaces *via* the interactions with the catechol. By simply increasing the temperature over the retro-DA (rDA) temperature the polymer was degrafted (cleavage of the maleimide-Cp moiety). The switch was reversed by conducting a subsequent DA reaction with the Cp-baring polymer. Thus, a surface modification tool was designed that allows to switch between these two states repeatedly. In a second thermally driven *grafting-to* approach, a new dithioester-based DOPA molecule was synthesized and attached to silicon wafers *via* its catechol moiety. The rapid ligation abilities of such a dithioester group with Cp-bearing polymers was exploited in a one-pot retro-hetero-DA (rHDA)/HDA sequence for the attachment of specific polymers (PEG, poly(2,2,2-trifluoroethyl meth acrylate (PTFEMA)). In a third catechol-anchor-based approach, surface grafting with previously prepared maleimide-carrying (bio)macromolecules, more precisely PEG, PTFEMA and a peptide, was conducted by applying a photo-induced DA protocol,

namely photoenol ligation. Furthermore, spatially controlled grafting of PTFEMA chains was also achieved by employing this method. Finally, the availability of nucleophilic groups on polydopamine (PDA) films was exploited to attach tetrazole moieties, which are capable of performing nitrile-mediated tetrazole-ene cycloadditions (NITECs) with a suitable dipolarophile during UV-irradiation. Hence, a maleimide-based compound, capable to initiate polymerization from surfaces, was ligated *via* a spatially controlled NITEC reaction. In a consecutive surface-initiated (SI) atom-transfer radical-addition polymerization (ATRP) (*grafting-from*) non-fouling polymer brushes were generated in order to control cell adhesion on the substrate.
In summary, four different projects were realized employing the catechol-anchor (Project 1-3) and the PDA film (Project 4) approach. The grafting of catechol anchored compounds led to thin, SAM-like coatings on gold, silicon wafers, graphite and polymers (PE, PET). The subsequent thermal or light-triggered ligation or switching of specific (bio)macromolecules (polymers, peptide) (*grafting-to*) allowed the generation of different on-demand surface modification protocols, especially with the focus on their versatile applicability, no matter what type of surface was employed. Furthermore, even spatial control of the attachment of polymers and a biomacromolecule on the microscale was achieved utilizing the described light-triggered photoenolization protocol. By exploiting the availability of functional groups on previously prepared PDA films, these films were functionalized with non-fouling polymer brushes in several steps in a spatially controlled fashion (Project 4) (*grafting-from*). The non-fouling polymer brushes exhibited extraordinary resistance towards cell adhesion in the micropatterned areas. Owing to the strong adhesion properties of these PDA films and catechol anchors, the described concepts are envisioned to be transferable to virtually any substrate.

By merging advanced polymer chemistry and modular orthogonal ligation techniques with the mimicry of the extraordinary adhesion abilities of marine mussels, this thesis opens new perspectives with regard to the development of novel tailored and well-defined surface modifications. The objective was to generate (i) versatile, (ii) substrate independent, (iii) modular, (iv) efficient and (v) mild polymer surface conjugation protocols in order to create a base for the future preparation of highly defined – in

terms of spatial resolution but also properties – (bio)materials. The targeted applications range from medical areas, such as point-of-care diagnostics or fabrication of non-fouling interfaces for cardiovascular devices, over (bio)chemical or (bio)medical fields, for instance, the preparation of biosensors or cell behavior tests, to the precise fabrication of conductive surfaces for electronic devices. Owing to the versatility of the concepts, even more fields of application are envisioned to become accessible.

Zusammenfassung

Um den aktuellen und zukünftigen Anforderungen in Bereichen wie Umwelt, Medizin, Transport, Bauwesen und Ernährung gerecht zu werden, wird eine große Bandbreite an spezifischen Lösungsansätzen benötigt. Insbesondere die Entwicklung neuer Materialien oder Biomaterialien ist entscheidend für die Herstellung funktionaler Anwendungen in Disziplinen wie unter anderem Materialwissenschaften, Nanotechnologie, Biosensorik, Biowissenschaften, Informationstechnologie und Elektronik. In diesem Zusammenhang ist es erforderlich, neue Materialien zu entwickeln, die gewisse anwendungsspezifische Eigenschaften aufweisen. Gerade bei oberflächenbasierten Anwendungen ist die sorgfältige Gestaltung der obersten Oberflächenschicht von enormer Bedeutung, um die erwünschten Eigenschaften zu generieren. Unterschiedlichste Oberflächenmodifikationstechniken wie beispielsweise die Bildung selbstorganisierender Monolagen (SAM), Lithografie oder die chemische Gasphasenabscheidung werden häufig eingesetzt, sind aber auf gewisse Oberflächentypen begrenzt. Um verschiedenste Substratarten, wie unter anderem Metalle, Mineralien oder sogar Polymere und polymerbasierte Beschichtungen

anzusprechen, ist eine vielseitige und substratunabhängige Oberflächenmodifikations-methode nötig. In diesem Zusammenhang haben sich maritime Organsimen wie Muscheln als exzellente natürliche Vorbilder erwiesen, da sie die außergewöhnliche Fähigkeit besitzen, auf praktisch allen Arten von Oberflächen, sogar Felsen, Holz oder Schiffslacken, anzuhaften und dabei den stürmischen und rauen Bedingungen in Brandungszonen standzuhalten. Diese starken Haftungseigenschaften werden von Catecholeinheiten erzeugt, die in speziellen Proteinsequenzen – den „Mussel Foot Proteins“ (mfps) – in den Byssusfäden der Muscheln vorkommen. Zahlreiche Forschergruppen haben dieses Phänomen schon genauer untersucht und Versuche zu dessen synthetischer Imitation unternommen. Dabei wurden zwei unterschiedliche Wege gefunden diese starke Anhaftungsfähigkeit zu nutzen. Einerseits können die Catechole in Catecholaminen wie Dopamin oder 3,4-Dihydroxyphenylalanin (DOPA) als Catecholanker verwendet werden. Auf der anderen Seite dient die Bildung von Polydopaminfilmen (PDA) unter leicht alkalischen Bedingungen und die nachfolgende Modifikation der PDA-Filme als Basis.

Durch die Verbindung von moderner Polymerchemie, der Nachahmung der außerordentlich starken Haftungsfähigkeit von Meeresorganismen und thermischen und lichtinduizerten orthogonalen Konjugationsmethoden, wurden in der vorliegenden Doktorarbeit unterschiedlichste Verfahren zur Herstellung solcher funktionaler Oberflächen entwickelt. Diese Konjugationsmethoden wurden verwendet, um eine präzise und/oder räumlich und zeitlich gesteuerte Funktionalisierung von unterschiedlichsten Oberflächen durch gezieltes Anbringen von Polymeren und Biomakromolekülen zu erreichen. Zu diesem Zweck wurden sowohl sehr schnelle thermische Konjugationsmethoden als auch lichtinduzierte Techniken – zur Gewinnung räumlicher Kontrolle – verwendet. Durch die Bestrahlung mit Licht einer bestimmten Wellenlänge konnte eine präzise Funktionalisierung erreicht werden.

Zunächst wurde ein α-Makrocatechol durch eine Diels–Alder (DA) Reaktion zwischen einem Maleimid-Dopaminderivat und einer cyclopentadientragenden (Cp) Poly(ethylenglycol) (PEG) erzeugt. Diese wurde dann über seine Catecholeinheit auf Oberflächen angebracht. Durch eine Temperaturerhöhung über die retro-DA (rDA) Temperatur konnte das Polymer wieder von der Oberfläche abgespalten werden

(Spaltung der Maleimide-Cyclopentadien-Einheit). Die Schaltereigenschaft konnte durch eine weitere DA Reaktion mit einem Cp-tragenden Polymer wieder umgekehrt werden. Hierdurch wurde eine Oberflächenmodifiktionsmethode entwickelt, die es erlaubt, zwischen diesen beiden Zuständen gezielt umzuschalten. In einem zweiten thermischen Ansatz wurde zuerst ein neues dithioesterbasierendes DOPA-Derivat synthetisiert und über seine Catecholeinheit auf Siliziumscheiben aufgebracht. Die enorm schnelle Cycloadditionsfähigkeit einer solchen Dithioestergruppe mit Cp-terminierten Polymerketten (PEG, Poly(2,2,2-Trifluoroethylmethacrylat (PTFEMA)) konnte ausgenutzt werden, um in einer Eintopf-retro-Hetero-DA (rHDA)/HDA-Sequenz die Anbindung von Polymeren auf Oberflächen zu ermöglichen. In einem dritten Catechol-Anker basierten Ansatz konnten bestimmten Makromoleküle (PEG, PTFEMA und ein Peptid) auf vorher modifizierte Substrate durch eine lichtinduzierte DA-Reaktionsmethode, genauer gesagt die Photoenolreaktion, aufgepfropft werden. Außerdem wurde für einem Modellsystem mit PTFEMA räumliche Kontrolle dieses Vorgangs erreicht. Im letzten Projekt wurde das Vorliegen von nukleophilen Gruppen auf zuvor generierten Polydopamin (PDA) Filmen genutzt, um Tetrazoleinheiten anzubringen. Diese können in einer Nitril-Imin vermittelten Tetrazole-en Cycloaddition (NITEC) durch Lichteinstrahlung mit geeigneten Dipolarophilen reagieren. Auf diesem Weg wurde ein Initiator eingeführt, welcher fähig ist, Polymerisationen von Oberflächen zu initiieren. Dadurch konnten Polymerbürsten mit „non-fouling“ Eigenschaften erzeugt werden (*„grafting-from“*), die wiederum die Fähigkeit besitzen, die räumliche Adhäsion bestimmter Zellen auf den Oberflächen zu kontrollieren.

Zusammenfassend wurden vier Projekte verwirklicht, von denen drei auf die Anhaftung von Catecholankern (Projekt 1-3) (*„grafting-to“*) und eins auf die nachträgliche Modifikation von PDA-Filmen (Projekt 4) (*„grafting-from“*) basieren. Das Aufpfropfen von catecholtragenden Molekülen auf Oberflächen wie Gold, Siliziumscheiben, Grafit und polymeren Werkstoffen (PE, PET) führte zu dünnen, SAM-artigen Beschichtungen. Die nachfolgende thermische oder lichtinduzierte Konjugation oder die Schaltung von spezifischen (Bio-)Makromolekülen (Polymere, Peptide), ließ die Entwicklung von verschiedenartigen, gezielten Oberflächenmodifikationsprotokollen zu. Dies ist insbesondere im Hinblick auf ihre

vielseitigen und substrattypunabhängigen Anwendungsbereiche von Bedeutung. Des Weiteren konnte durch den Einsatz des beschriebenen Photoenolkonzepts die Anbringung von Polymeren in räumlich aufgelöster Weise im Mikromaßstab realisiert werden. Im vierten Projekt wurden die auf den zuvor erzeugten PDA-Filmen vorhandenen funktionellen Gruppen ausgenutzt, um diese Oberflächen in mehreren Schritten mit „non-fouling“ Polymerbürsten in räumlich gezielter Weise zu bestücken. Diese „non-fouling“ Polymerbürsten wiesen eine außerordentliche Resistenz gegenüber Zellanhaftung auf. Auf Grund der starken Anhaftungsfähigkeit dieser PDA Filme und der Catecholanker, können die beschriebenen Konzepte voraussichtlich auf jede Art von Substraten übertragen werden.

Durch die Zusammenführung von fortschrittlicher Polymerchemie und modularen orthogonalen Konjugationsmethoden mit der Nachahmung der außergewöhnlichen Anhaftungsfähigkeiten von Muscheln, eröffnet diese Doktorarbeit Perspektiven bezüglich der Entwicklung neuer, maßgeschneiderter und wohldefinierter Oberflächenmodifikationen. Die Zielsetzung lag darin, (i) vielseitige, (ii) substratunabhängige, (iii) modulare, (iv) leistungsfähige und (v) milde Polymeroberflächenkonjugationsmethoden zu entwickeln, welche als Grundlage für die zukünftige Herstellung von wohldefinierten – bezüglich räumlicher Auflösung aber auch bezüglich der Eigenschaften – (Bio-)Materialien dienen sollen. Die angestrebten Anwendungen reichen von medizinischen Bereichen, wie „Point-of-Care Testing“ oder der Herstellung von Oberflächen mit „non-fouling“ Eigenschaften für kardiovaskuläre Anwendungen, über (bio-)chemische oder (bio-)medizinische Gebiete, wie beispielsweise die Entwicklung von Biosensoren oder das Testen von Zellverhalten, hin zu der präzisen Fertigung von leitenden Oberflächen für elektronische Geräte. Auf Grund der Vielseitigkeit der Konzepte wird erwartet, dass sogar noch mehr Anwendungsgebiete erschlossen werden können.

Contents

List of Abbreviations

Ag	silver
AGET ATRP	activator generated by electron transfer ATRP
AIBN	azobisisobutyronitrile
AM	acrylamide
AN	acrylonitrile
ARGET ATRP	activator regenerated by electron transfer ATRP
ATRA	atom-transfer radical-addition
ATRP	atom transfer radical polymerization
Au	gold
BiPy	2,2'-bipyridyl
CBAA	carboxybetaine acrylamide
CCl_4	carbon tetrachloride
$CDCl_3$	deuterated chloroform
CNT	carbon nanotubes
Cp	cyclopentadiene
Đ	dispersity
DA	Diels–Alder
DAPI	4´,6-diamidino-2-phenylindole
DBU	1,8-diazabicyclo[5.4.0]undec-7-ene
DCM	dichloromethane
DLW	direct laser writing
DMAP	4-(dimethyl amino)-pyridine
DMSO-D6	deuterated dimethyl sulfoxide
DOPA	3,4-dihydroxyphenylalanine
EDC·HCl	1-ethyl-3-(3-dimethylaminopropyl)carbodiimide hydrochloride
EDG	electron donating group
eq.	equivalent
ESI-MS	electrospray ionization mass spectrometry

EtOH	ethanol
EWG	electron withdrawing group
FMP	2-formyl-3-methylphenoxy
FRP	free radical polymerization
GPC	gel permeation chromatography
H_2SO_4	sulfuric acid
HCl	hydrochloric acid
HDA	hetero-Diels-Alder
HEMA	2-hydroxyethyl methacrylate
HOEGMA	hydroxy-capped oligoethylene glycol methacrylate
HOMO	highest occupied molecular orbital
HPMAM	*N*-(2-hydroxypropyl)meth acrylamide
*i*BA	*iso*-bornyl acrylate
LUMO	lowest unoccupied molecular orbital
MA	methyl acrylate
MADIX	macromolecular design *via* the interchange of xanthates
Mal	maleimide
Me_4Cyclam	*N,N',N'',N'''*-tetramethyl-1,4,8,11-tetraazacyclotetradecane
MeCN	acetonitrile
MeOD-D4	deuterated methanol
MeOEGMA	oligo(ethylene glycol) methyl ether methacrylate
mfp	mussel food protein
$MgSO_4$	magnesium sulfate
MMA	methyl methacrylate
$NaNO_2$	sodium nitrite
NITEC	nitrile-imine mediated tetrazole-ene cycloaddition
NMR	nuclear magnetic resonance
NP	nanoparticle
NVC	*N*-vinylcarbazole
OEG	oligo(ethylene glycol)
P3HT	poly(thiophene)
PCBAA	poly(carboxybetaine acrylamide)
PDA	polydopamine
PE	polyethylene

PEG	poly(ethylene glycol)
PEP	peptide (Gly-Arg-Gly-Asp-Ser)
PET	poly(ethylene terephthalate)
P*i*BA	poly(*iso*-bornyl acrylate)
PMDETA	*N,N,N′,N′,N″*-pentamethyldiethylenetriamine
PMeOEGMA	poly(oligo(ethylene glycol) methyl ether methacrylate)
PMMA	poly(methyl methacrylate)
preCOLs	prepolymerized collagenes
PS	poly(styrene)
pSAM	pseudo-self-assembling monolayer
PTFEMA	poly(2,2,2-trifluoroethyl methacrylate
RAFT	reversible addition-fragmentation chain transfer
RATRP	reverse ATRP
rDA	retro-Diels-Alder
RDRP	reversible-deactivation radical polymerization
REFs	rat embryonic fibroblasts
rHDA	retro-hetero-Diels-Alder
ROP	ring-opening polymerization
S	styrene
SAM	self-assembling monolayer
SCNPs	single chain polymeric nanoparticles
SEC	size exclusion chromatography
SEC-ESI-MS	SEC coupled with ESI-MS
SET	single-electron-transfer
SET-LRP	single-electron-transfer living radical polymerization
SI	surface initiated
Si	silicon
SI-ATRP	surface initiated ATRP
$Sn(EH)_2$	Tin(II) 2-ethylhexanoate
$SOCl_2$	thionyl chloride
SR&NI ATRP	simultaneous reverse and normal initiation ATRP
TBAF	tetra-*n*-butyl ammonium fluoride
TBDMS-Cl	*tert*-butyldimethylsilyl chloride
TEA	triethyl amine

TFA	trifluoroacetic acid
TFEMA	2,2,2-trifluoroethyl methacrylate
THF	tetrahydrofuran
tmps	thread matrix proteins
ToF-SIMS	time-of-flight secondary ion mass spectrometry
Tris	tris(hydroxymethyl)methylamine
Vac	vinyl acetate
VASP	vasodilator-stimulated phosphoprotein
XPS	X-ray photoelectron spectroscopy

1

Introduction and Motivation

The increasing need of new functional materials that exhibit certain properties, depending on the tasks they are targeted to fulfill, challenges scientists in a plethora of fields all over the globe. Whether these demands concern substances on the macroscale, such as lightweight or tough material for construction or vehicles, or on the microscale, especially for the establishment of novel (bio)medical or electrical devices, polymer chemistry is always present as a versatile and modular tool in terms of preparing novel and innovative tailored material. A vast amount of different synthetic methods has already been developed.[1-5] The design of a (bio)material's surface is crucial for its properties and interactions.[3] Therefore, the generated (bio)material has to be precisely engineered on the nanoscale to serve particular requirements.[3] Typically employed strategies such as surface-initiated (SI) growth of polymer brushes,[6] self-assembling monolayers (SAMs) using anchoring groups as silanes for silane-oxide interaction or alkane-thiol attachment on gold surfaces,[6-8] lithographic techniques or chemical vapor deposition are topics of the contemporary research.[9-12] However, from the vast number of reactions none can cope with the

variability of surface chemistries and energies. Thus an universal approach for grafting polymer to substrates to tailor the surfaces' properties remains elusive.

Nature has developed enormous amounts of mechanisms, metabolism and (bio)materials over the last 3.8 billion years[13] and thus, has proven to be an excellent teacher. The naturally strong adhesion properties of maritime organisms, more precisely marine mussels or other bivalves, which originates from catechol units presented in several protein sequences in the mussel's plaque, has caught the strong attention of researchers in different scientific areas. Further investigations led to the discovery that dopamine (3,4-dihydroxyphenethylamine), a small molecule that also contains a catechol, serves as a suitable precursor for the formation of mussel-glue-like films under slightly alkaline conditions.[14] Perhaps the most remarkable property of these polydopamine (PDA) films is that – similarly to mussels – they can bind to any surface even in the most hostile environments.[15] Furthermore, catechol units were identified to be capable for serving as anchors to inorganic, organic or polymeric surfaces.[15-17] Inspired by these findings, researchers have been investigating and mimicking these behaviors in order to create functional materials in differing fields.[14,15,18] Especially in the area of biological or medical applications,[19-21] the advantage of highly adherent films that are generated in aqueous media and that can be modified to certain extend, possess strong potential for the generation of functional and non-toxic surfaces. Thus, by exploiting the described capabilities of such PDA films or catechol anchors, universal surface modification protocols are envisioned to become accessible.

In the present thesis, the second-layer modification of PDA films, as well as the extraordinary capability of catechol groups, provided in dopamine or 3,4-dihydroxyphenylalanine (DOPA), to adhere to virtually any kind of surface are merged with reversible-deactivation radical polymerization (RDRP) methods and advanced polymer ligation protocols. For this purpose, well-established cycloadditions are utilized as conjugation tools. In general, two main types of conjugation triggers – thermal and light – were exploited in order to generate novel tailored materials by selective surface design employing *grafting-from* and *grafting-to* approaches. The thermal ligation techniques include well-developed Diels–Alder (DA) and hetero-Diels–Alder (HDA) reactions, whereas highly specific photo-induced surface

conjugation was implemented *via* photoenol (light-induced DA reaction) ligation and nitrile-imine mediated tetrazole-ene cycloaddition (NITEC) (light-induced 1,3-dipolar cycloaddition).[22-25] The advantage of the thermal approaches rests upon the exceptionally mild temperatures (ambient temperature) under which the (H)DA reactions operate and, in the case of HDA ligation, also its fast rate.[24,26,27] Thus, these systems can be envisioned to be employed in applications requiring mild conditions, such as in biological environments, as well as for medical devices. Some examples include coating of sensors, design of surfaces or controlled cell seeding, coating of stents, as well as suturing during surgical procedures. By introducing photo-triggered conjugation methods, a higher level of selectivity can be achieved.[28,29] The spatial and time control of the surface modification opens up a plethora of applications, such as for the improvement of the fields mentioned above, as well as for optical and electrical systems.

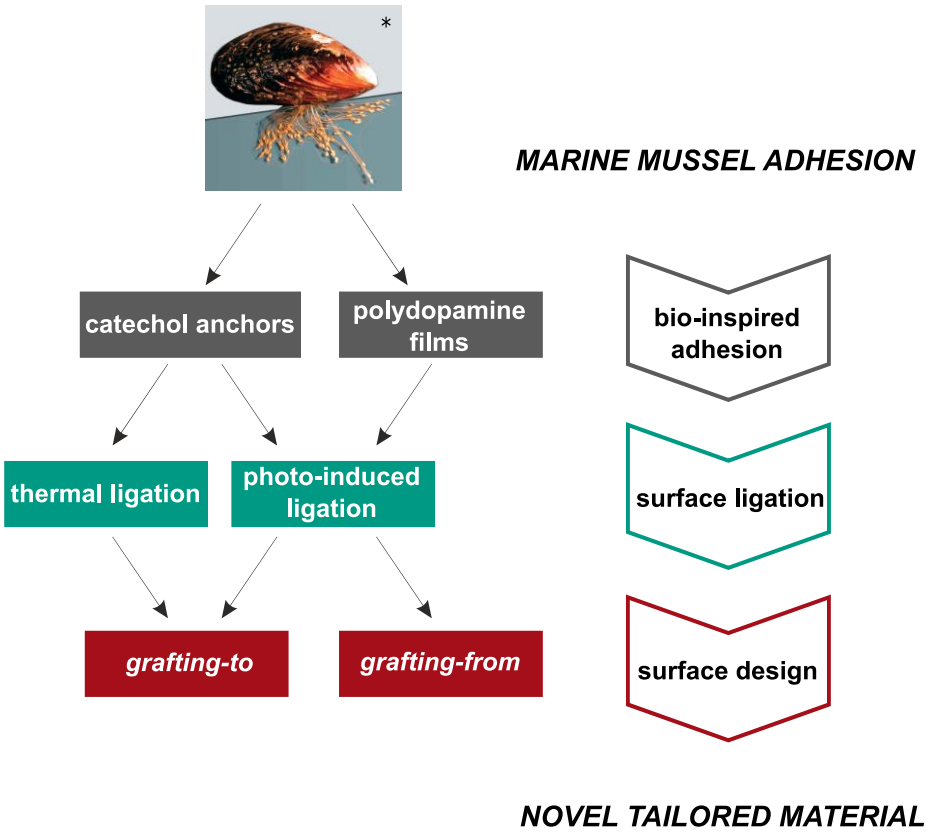

* Picture reprinted with permission from Ref. 15. Copyright 2011 Annual Reviews.

Gazing into the fields of applications for such systems in more detail, a certain number of areas could benefit from the novel methodologies developed herein. Yet, further

improvement is essential. In medical areas, such as the creation of point-of-care devices, the fabrication of more compact, portable and user-friendly diagnostics, without the need of external analytic methods, provides a challenging interdisciplinary field.[30,31] Thinking of simple dip-stick technology employed in pregnancy tests or tests strips for diabetes diagnostics, which have already proven as appropriate and reliable tools, the development and availability of facile point-of-care self-tests that can be performed at home without assistance of a medical practitioner or in regions where medical support is not area-wide provided, is likely to be fundamental for future health care systems.[30,32] Such point-of-care devices operate, for instance, on the base of immunoassays, which can detect different target analytes, such as hormones or proteins, as on-site and immediate diagnostic systems. These systems are important for in-field examinations for the military, as well as in the environmental and nutrition sector.[32] The detection of pesticides, bacteria or insecticides in drinking water, as well as any undesired contamination in food or drinks can be achieved by such instruments.[32] In order to create more versatile and low cost point-of-care devices, the design of novel surface technologies is essential, as the major detection progress in such assay applications operates on interface-based interactions with the target analytes. For the fabrication of these surfaces, advanced polymer chemistry provides a plethora of tools, such as orthogonal polymer grafting to or precisely controlled growth of polymer brushes from surfaces, and has therefore, already widely been used in this context.[33] For the preparation of biosensors the surface needs to meet the following requirements. The interface must be able to prevent any non-specific adsorption or fouling of any biological entities (proteins, lipids, bacteria or cells), whilst – at the same time – containing biorecognition elements able to capture the desired analyte from a complex biological milieu. So far the only chemical modification able to meet these challenges are those based on polymer brushes from few hydrophobic monomers.[34,35] These brushes can be further functionalized with bioreceptors and utilized to detect pathogens, biomarkers or antibodies, among other biomolecules.[33] For this purpose, precise design and selective choice of the polymer brushes grown from or attached to the surface, as well as further functionalization in some cases, is required in order to avoid any non-specific adsorption or side reactions in more complexly composed samples.[33] Another application for precisely designed polymer brushes on substrates

that involves spatially control of the same, is the preparation of micropatterns in order to keep cells located in restricted and specifically shaped areas.[36] Thus, key parameters of the cell environment can be controlled (e.g. the shape, chemical composition, topography, elastical and mechanical properties) or manipulated to investigate how cells sense and react on changes in their microenvironments, which is crucial for a deeper understanding of cell behavior.[33,36] In addition, the preparation of protein and cell anti-fouling surfaces is fundamental for medical applications.[33] A typical application in which these surfaces are of interest is the fabrication of stents.[33] An ideal stent surface must prevent bacterial colonization (and biofilm formation), which can prove lethal, minimize restenosis, a process by which muscular cells close the lumen of the stent and, finally, be hemocompatible. Precisely designed polymer brushes are now investigated as they can meet the challenges of prevention of bacterial attachment and reduce restenosis.[33] Apart from biological, biochemical or medical applications, precisely designed interfaces are also in the scope of molecular electronics, for instance, for the preparation or organic or polymeric conductive surfaces.[37,38]

The combination of advance polymer chemistry with modular thermal and light-induced ligation tools and the extraordinary ability of marine organisms to adhere to a plethora of different surfaces is envisioned to contribute to the development of novel and versatile surface modification routes in order to generate material with tailored properties for even more fields of applications as described.

Within the next chapter (Chapter 2), the theoretical background of the current thesis is given before the results and discussions (Chapter 3-6) provide a detailed presentation of the findings obtained in the context of this PhD thesis. In Chapter 7, the different projects presented in this thesis are compared and discussed with regard to the combined approaches (see flow chart above), i.e. the attachment process, the ligation tool and the type of polymer grafting. The conclusion and outlook are summarized in Chapter 8 and give an overview of the projects. Detailed experimental data, as well as information on the employed chemicals and equipment is provided in Chapter 9.

2

Theoretical Background

The current chapter presents an overview of the topics treated in the context of the present thesis, as well as the chemical methods and mechanisms that were employed and the latest state of the art published in the examined fields.

First, the motivation for preparing bio-inspired surfaces by mimicking the adhesive behavior of marine mussels is specified in more detail (2.1), before different reversible-deactivation radical polymerization (RDRP) techniques, which are applied in solution and on surfaces, are outlined (2.2). Finally, miscellaneous thermal or light-induced cycloadditions for conjugations of polymers and/or small molecules in solution, as well as on surfaces, are described (2.3).

2.1. Surface Modification by Bio-Inspired Ad-Layer Attachment or Catechol Anchoring

The present chapter provides an overview of the idea behind and the state of the art of PDA film formation and catechol attachment onto various surfaces and their corresponding modification. First, the extraordinary adhesion properties of marine mussels are highlighted (2.1.1), then dopamine as a precursor for the formation of highly adherent polydopamine (PDA) films is introduced (2.1.2) and, finally, the development of useful surface modification protocols based on second-layer modification of PDA films (2.1.3) catechol anchoring (2.1.4) is outlined.

2.1.1. Marine Mussels and their Adhesion Properties

Marine mussels, as well as other bivalves, possess extraordinary adhesion properties to a wide selection of materials such as rocks, wood, metal and coated ships, even under harsh conditions in their naturally rough environment.[15,18] Although the resistance in the wavy, rocky seaside zones cost between 8% to 12% of the mussels' metabolic energy, the marine mussel benefits from its habitat due to the availability of aerated seawater, provision of nutrition and fast waste disposal.[15] The strong adhesion properties of marine mussels stem from an extraordinary adhesion system, the mussel byssus. The mussel byssus originates from the mussel's stem and consist of bundles of radially distributed threads (50-100 threads depending on the species) with plaque at their distal ends (**Figure 1**).[15] The plaque exhibits approximately 7-8 different proteins, however, only five are exclusively provided in the plaque.[15] Mussel food protein (mfp)-1 (key protein of byssal cuticle), as well as thread matrix proteins (tmps) and pre-polymerized collagens (preCOLs) (that form the core of the byssal threads) are not confined to the plaque. All the sequences of the five proteins existing exclusively in the plaque, namely mfp-2, -3, -4, -5 and -6, contain the amino acid 3,4-dihydroxyphenyl-L-alanine (DOPA) (due to posttranslational modification of tyrosine),[39] whose catechol moieties are assumed to be responsible for the strong attachment of the mussel to different surfaces, whereas the remaining parts of the sequences differ strongly for every protein.[15] Besides mfp-2 (most abundant mfp),

mfp-4 (largest mfp with 90 kDa, interaction with preCOL) and mfp-6 (high level of lysine, tyrosine, glycine), which all only exhibit low amounts of DOPA (< 5 %), the DOPA rich mfps, mfp-3 (some sequences possess ≥ 20 mol % DOPA) and mfp-5 (≈ 30 mol % DOPA), are present in the plaque.[15] Mfp-3 and mfp-5, which were identified to operate as the best adhesives of these five proteins (mfp-5 even nearly 3 times stronger as mfp-3), are located in the plaque near the plaque-substrate interface (**Figure 1**).[15,39,40] Furthermore, the side chain of these two protein types is exploited for tough bidentate interactions with surfaces, owing to the two phenolic hydroxyl groups provided in DOPA.[15] Moreover, mfp-6 might also serve as potent antioxidants in order to preserve a certain amount of the interfacial DOPA in a reduced state to achieve good adsorption, besides its abilities as cross-linker to form S-cysteine-DOPA adducts once its reducing capacity is depleted.[15]

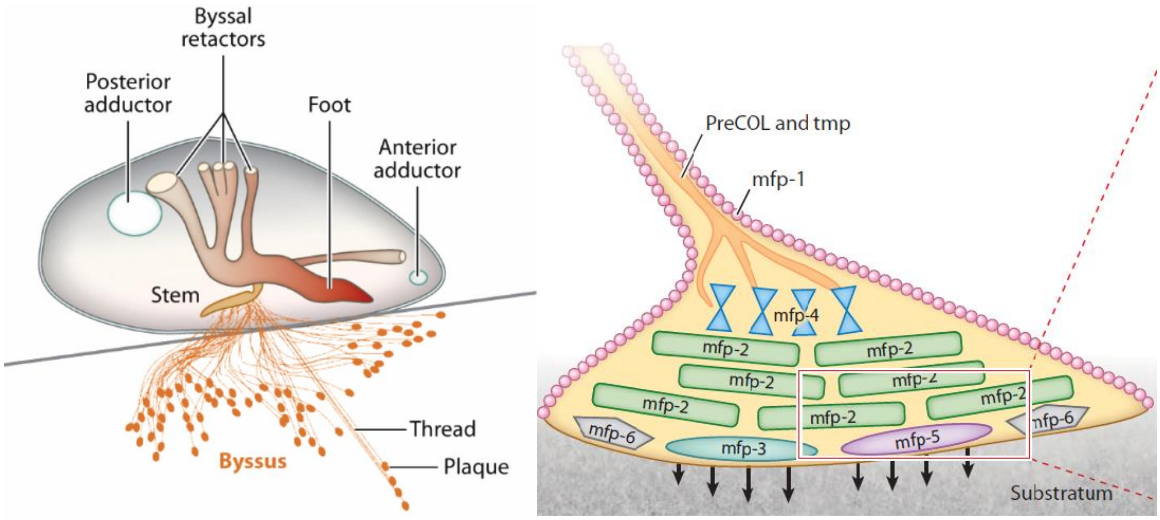

Figure 1: Schematic depiction of a marine mussel on a half-shell (left). The mussel attaches to surfaces *via* its plaque that is located at the distal thread ends. The threads are bundled (byssus) and distributed in a radial fashion from the stem. An excerpt of the byssal plaque and an illustration of the availability of the major mussel foot proteins (mfps), as well as their interaction with the preCOLs that form the core of the byssal threads is presented on the right. Figures reprinted with permission from Ref. 15. Copyright 2011 Annual Reviews.

Inspired by these findings, several researchers turned their attention to the synthetic imitation of these abilities in order to generate artificial adhesives for wet polar surfaces, by employing dopamine (3,4-dihydroxyphenethylamine) and DOPA as precursors for strongly adherent films – a topic that is further introduced in the following section.

2.1.2. Strongly Adherent Films

In 2007, the group of Messersmith firstly published the formation of strongly adherent films on various substrates, even Teflon®, by employing dopamine as starting material in a dopamine self-polymerization procedure in slightly alkaline media.[14] Based on the findings of Waite *et al.* concerning the role of the amino acids DOPA and lysine in the mfp-5,[18,41] Messersmith and co-workers identified dopamine as a promising precursor for the preparation of mussel-inspired glues as dopamine exhibits both, the catechol units of DOPA, as well as the primary amino functionality found in lysine (**Figure 2**).[14] By immersing different types of substrates (e.g. metal, polymers, glass, among others) in an aqueous slightly alkaline Tris-buffer solution (pH=8.5 ≙ pH typical for marine environments) of dopamine, deposition of a polymer film that adheres to the substrates and whose thickness increases with time (≈ 50 nm after 24 h), occurs.[14]

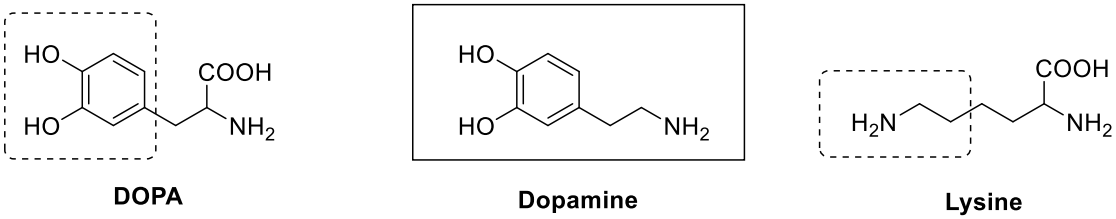

Figure 2: Depiction of the composition of dopamine (center), which contains the catechol moiety of DOPA (left), as well as the amino-functionality of lysine (right). Dopamine was, therefore, identified to operate as a suitable base substance for the formation of strongly adherent films.[14]

The mechanism of the film formation is assumed to be induced by the spontaneous oxidation of dopamine in alkaline media, where readily reactive intermediates such as 5,6-indole quinone, 5,6-indole semiquinone and 5,6-dihydroxyindole are generated and further react in several oxidative coupling step between the indole units to form water-insoluble oligomeric/polymeric PDA (**Figure 3**).[42,43] Through the self-assembly of these oligomers, colloidal particles are generated, which further aggregate to form a thin adherent film on the surface that is in touch with the solution, as well as a black precipitated floating in the mixture.[42,43] The PDA formation most likely proceeds by adsorption of the colloidal particles, as well as polymerization from the substrate's surface.[42,43] Still, the precise structure of the PDA films is elusive.[42]

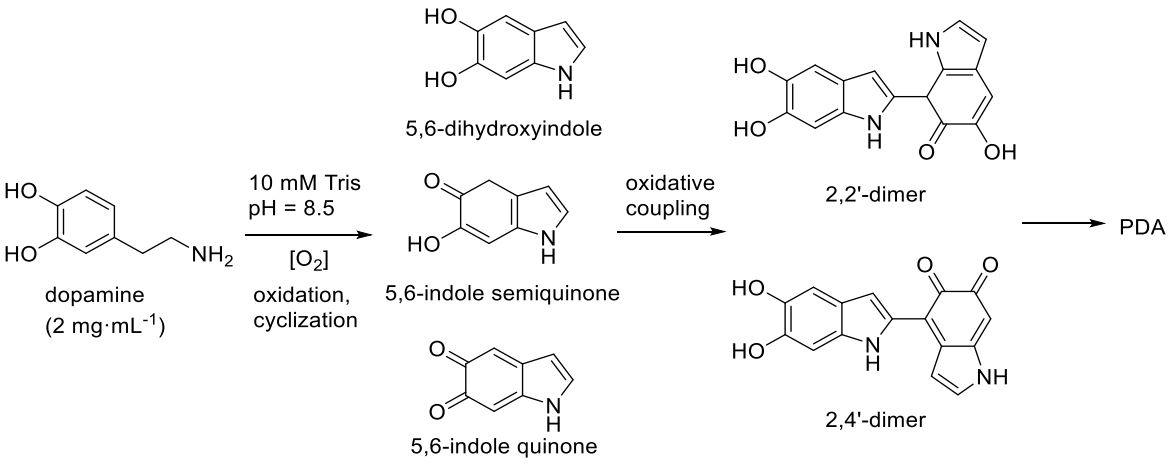

Figure 3: Schematic overview of the suggested formation of PDA films. In a first step, dopamine is oxidized to different indole-derivatives (5,6-dihydroxyindole, 5,6-indole semiquinone, 5,6-indole quinone). Subsequently, dimers and then oligomers are generated by oxidative coupling reactions, which finally results in the formation of PDA films on the surface in contact with the solution. Adapted and redrawn with permission from Ref. 43. Copyright (2012) American Chemical Society.

By employing dopamine as a building block for the formation of adherent films as surface coatings, the modification of substrates that are non-amenable to functionalization or that possess low surface energy, becomes accessible.[14,42] The strong adhesion properties of PDA originates from the interaction of the *o*-quinone/catechol species in the layer by either creating coordinative bonds with metal oxides on the surface of the substrate or covalent bonds formed by nucleophiles from the surface, as well as weaker interactions, such as π-π-stacking, van-der-Waals and hydrophobic interaction and hydrogen bonds.[42] Other catecholamines are also capable to generate these films.[15] The availability of a significant selection of functional groups on the PDA surface emerges as an important tool for second-layer modification on top of the PDA films, which leads to bio-inspired coatings that bear the ability to attach to a wide variety of surfaces and to adjust the surfaces' properties on demand.

In the following section, recent developments based on PDA-film modification and applications are introduced.

2.1.3. Ad-Layer PDA Film Modification

The remaining moieties on PDA after the film formation are applicable for further reactions with organic substances (e.g. polymers or small molecules) to create an interesting functional organic second-layers on top.[43,44] For instance, the catechol moieties, as well as the unsaturated indole-groups in the PDA film are capable of undergoing Michael additions or Schiff base reactions with nucleophilic groups such as amino- or thiol-moieties.[14,43]

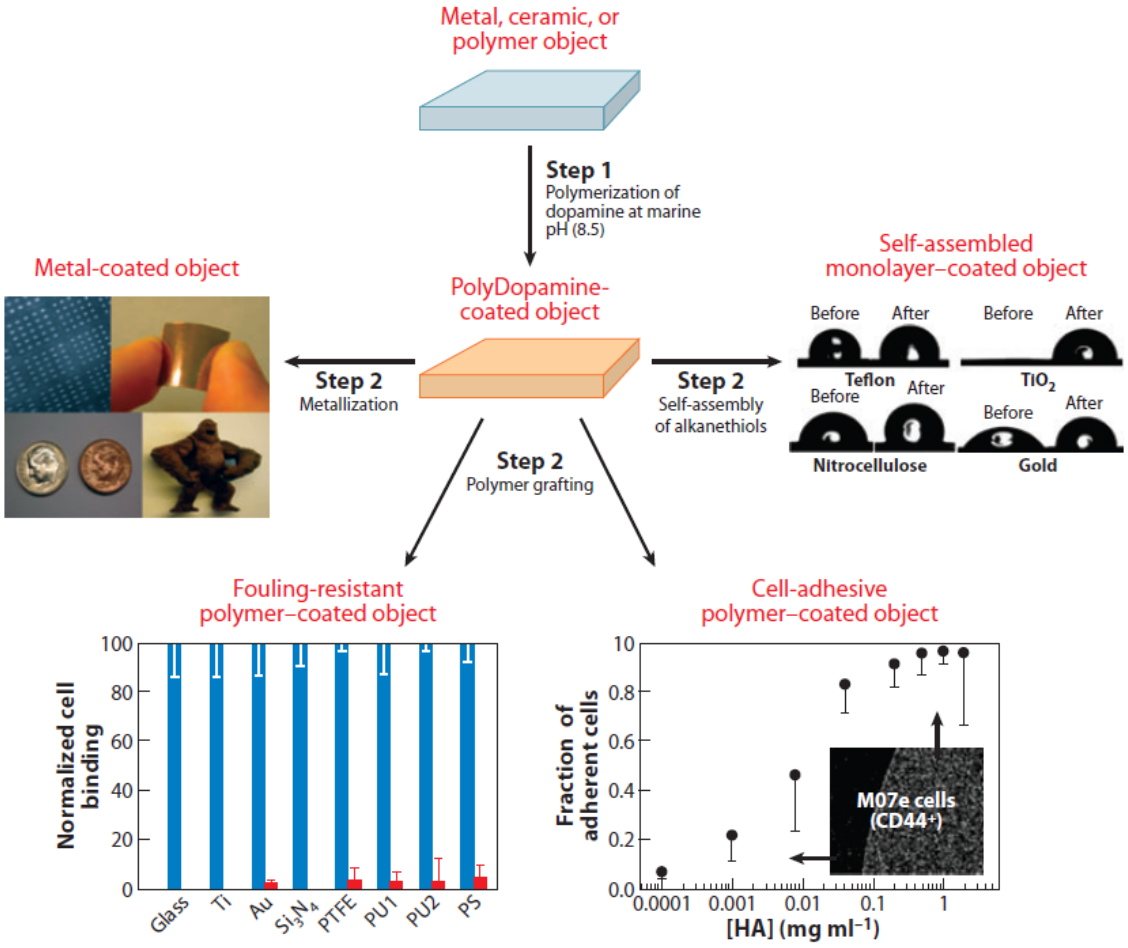

Figure 4: Potential methods for second layer deposition on PDA films. In a first step, the PDA substrate is generated by dip-coating in a dopamine containing Tris buffer solution (pH = 8.5) in order to mimic the maritime environment. In a second step, pSAM formation of alkanethiols, polymer grafting or metallization on the prepared PDA surface is performed.[15] Figure reprinted with permission from Ref. 15. Copyright 2011 Annual Reviews.

Pop-Georgievski *et al.* recently employed the described approach by tethering anti-fouling poly(ethylene oxide) brushes that possess thiol- or amino-head groups on PDA films to form a substrate-independent surface modification route for the preparation

of anti-fouling surfaces, which resist the fouling from complex protein solutions (blood plasma and blood serum),[43,45] and the non-specific attachment of cell lines, such as mouse embryonic fibroblast cells and human embryonal carcinoma cells.[46] The formation of pseudo-self-assembling monolayers (pSAMs) of alkanethiols (interaction of thiols with catechol/quinone moieties on PDA) or oligo(ethylene glycol) (OEG) was presented by Lee *et al.* (**Figure 4**).[14] The latter approach depicts strong resistance towards fibroblast cell attachment,[14] comparable with non-fouling SAMs formed on gold substrates.[14,47] In addition, the metal-binding properties of catechols was exploited to generate adherent metal coatings on PDA films by simple dip-coating of PDA on substrates in metal-ion solutions such as copper (II) chloride or silver nitrate (**Figure 4**).[14,15] Thus, the latter method was also employed for generating PDA-based films that show antibacterial resistance and even kill bacteria by silver release.[48]

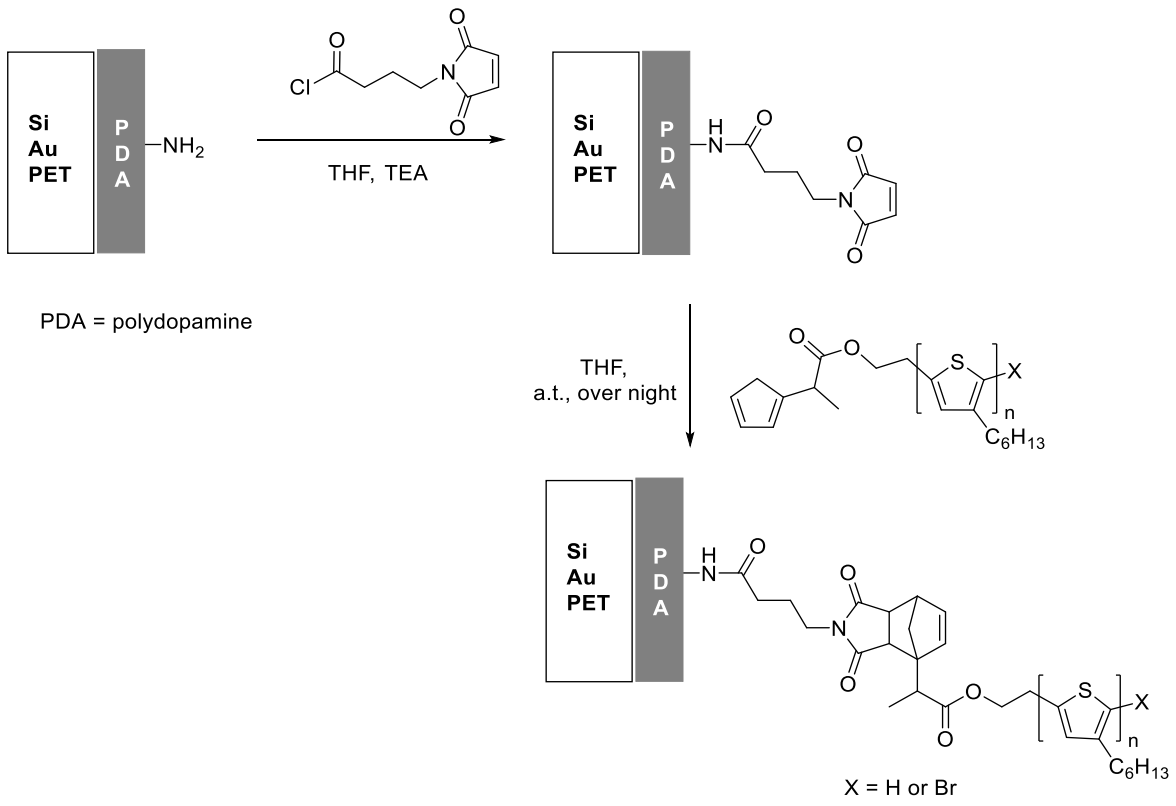

Figure 5: Short reaction sequence for the functionalization of a PDA substrate with conductive P3HT. The amino groups on the PDA surface, first, undergo a amidation reaction with a maleimide carrying small molecule before a catalyst-free Diels–Alder ligation with P3HT-Cp is performed.[38] Adapted and redrawn from Ref. 38 with permission from The Royal Society of Chemistry (Copyright 2013).

Besides the grafting of metal ions, small organic molecules or polymers to the sole PDA surface, grafting of functional small molecules for either conjugation of polymer chains

or as initiators for controlled surface polymerizations was performed.[38,42,49] Yameen *et al.* recently presented a catalyst free and efficient method for conjugating cyclopentadiene (Cp)-carrying conductive polymers brushes (polythiophene (P3HT)) with maleimides provided on a previously modified PDA surfaces in a Diels–Alder reaction (**Figure 5**).[38] The amino-rich PDA surfaces[44] were reacted with 4-maleimidobutyroyl chloride in a base-catalyzed amidation reaction in THF to generate the maleimide functionalized PDA substrate (**Figure 5**). The precisely designed conductive P3HT-Cp brushes merged with the ability of PDA films to adhere to virtually any surface, provide a promising tool for future applications in the field of electronic devices.

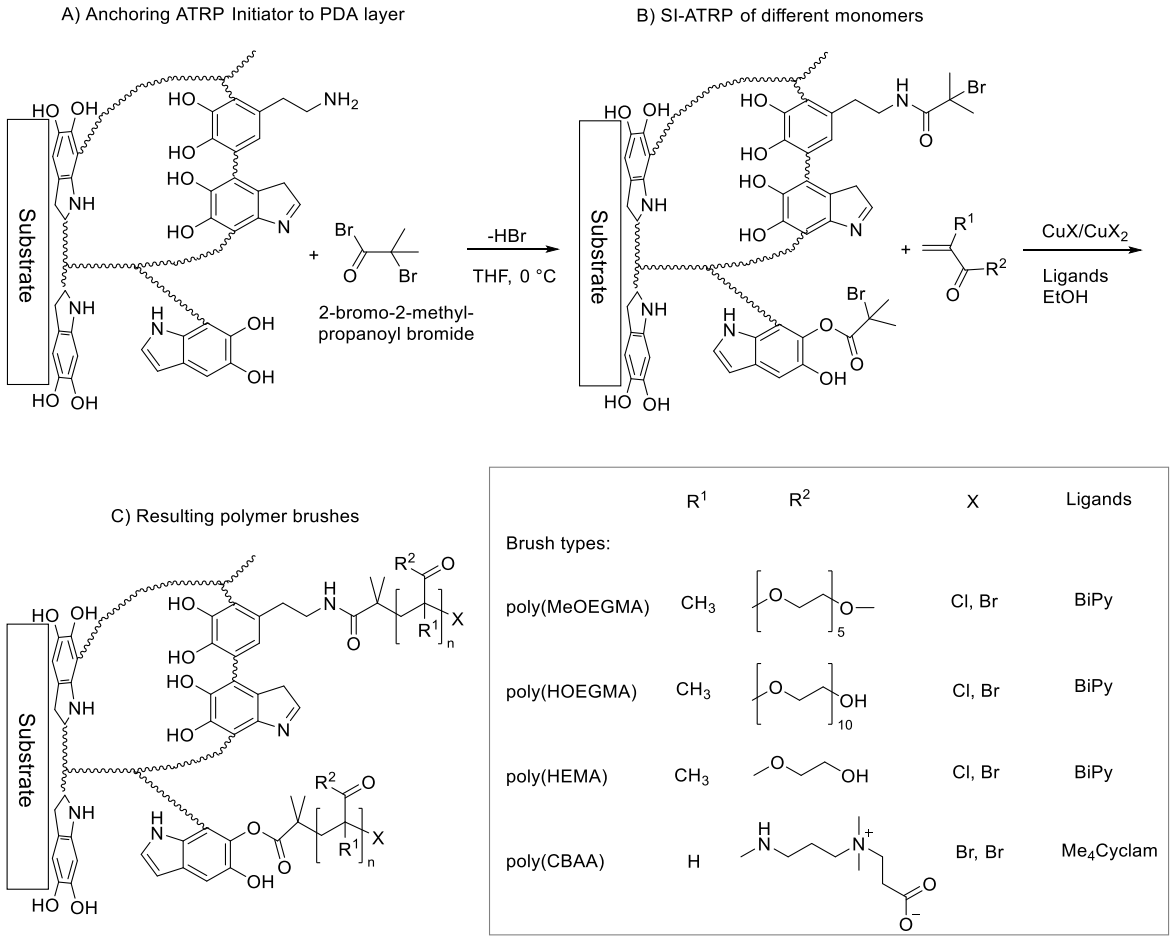

Figure 6: Overview of the preparation of anti-fouling surfaces. The remaining amino- and hydroxyl-moieties on a PDA substrate are reacted in an amidation with an ATRP initiator (2-bromo-2-methylpropanoyl bromide), which was further employed in different surface-initiated ATRPs (SI-ATRPs) utilizing MeOEGMA, HOEGMA, HEMA and CBAA as monomers to generate surfaces with anti-fouling properties. Adapted and redrawn from Ref. 42 with permission from The Royal Society of Chemistry (Copyright 2013).

Gazing into a different area – medical and biochemical applications – Pop-Georgievski and co-workers utilized PDA films for the preparation of substrate-independent anti-fouling interfaces by growing anti-fouling polymer brushes *via* controlled atom-transfer radical-polymerization (ATRP) (further described in Section 2.2.2 and 2.2.4) from PDA surfaces (**Figure 6**).[42] The ATRP initiator (2-bromo-2-methylpropanyl bromide) was attached to the amino- and catechol-moieties provided by the PDA substrate, before the surface-initiated ATRP (SI-ATRP) (for further information concerning SI-ATRP refer to Section 2.2.4) was conducted, employing OEG methacrylates (MeOEGMA, HOEGMA), carboxybetaine acrylamide (CBAA) and 2-hydroxyethyl methacrylate (HEMA) (**Figure 6**).[42] The anti-fouling behavior of the generated substrates was confirmed as the polymer brushes thoroughly prevented the fouling from main blood plasma protein solutions and by 97 % reduced fouling from undiluted human blood plasma.[42] Hence, the proposed method raises the opportunity to design substrates that are resistant to fouling by not requiring additional chemical pre-activation in a simple fashion.[42]

Within the current chapter, general PDA modification methods were described. All transformation techniques are predicated on the functionalization of previously fabricated PDA films. In contrast, the following section covers surface modifications based on catechol anchoring of dopamine- and other catecholamine-precursor molecules or polymers.

2.1.4. Surface Modification by Catechol Anchoring of Catecholamines

Thiol-based compounds that bind to metals, such as silver (Ag) or gold (Au) and functional silanes, employed for the attachment to silicon or miscellaneous oxide surfaces, have proven to act as well-established anchoring groups for surface modifications.[6,7,50-53] Although both strategies have been widely applied, some disadvantages need to be taken into account. Recently, Klok and coworkers called the stability of poorly formed silane SAMs into question by discovering that long polymer chains that are attached to a surface, which is exposed to a good thermodynamic solvent, are cleaved off owing to the imposed osmotic pressure.[54,55] In addition, the inherent problems of multilayer formation of various silanes has been shown to lead to stability problems for further surface modifications.[56-58] Regarding thiol-based linkage that is only applicable on specific material (Au and Ag), surfaces are generated that are neither stable to heating over 60 °C, nor to ligand exchange if other functional thiols are present.[59]

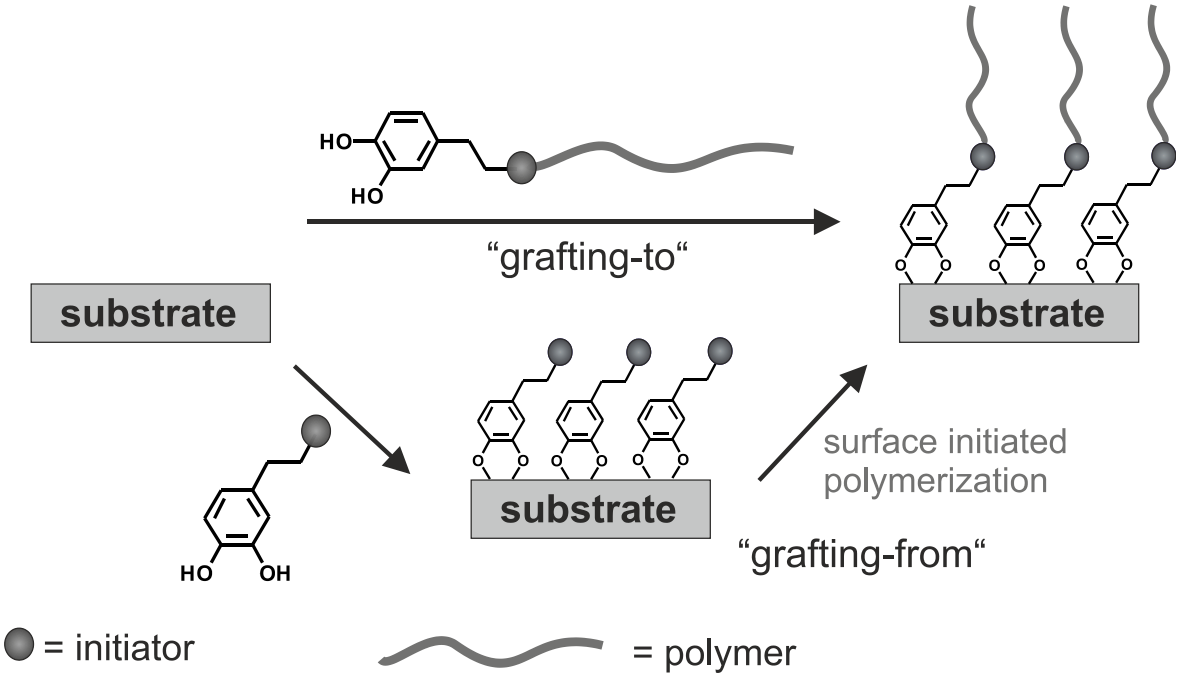

Figure 7: Schematic overview of the types of surface modification by catechol anchoring on a substrate. At the top, grafting of a previously prepared polymer brush to a surface (*grafting-to*) is depicted. At the bottom, a suitable catechol-anchor carrying initiator is attached to the substrate, before a surface-initiated polymerization is conducted (*grafting-from*).

These results have turned the attention of researchers towards more versatile linkers, such as catechols that are available in dopamine and other catecholamines, and that are capable of operating as strong anchors to a considerable number of materials.[15,16] In the context of surface functionalization with precise polymer chains by exploiting catechol anchoring, two widely utilized approaches – *grafting-from* and *grafting-to* – exist (**Figure 7**).[15,16,40,60-63] In this regard, *grafting-to* denotes the tethering of catechol-capped polymer brushes that were previously prepared in solution.[40,61,63] An additional route for grafting polymers to a suitable substrate concerns the attachment of catechol units that are provided in the backbone of the polymer, instead of in the chain end.[15,64,65] Furthermore, *grafting-from* can, for instance, be conducted by the attachment of a catechol-bearing ATRP initiator, followed by surface-initiated controlled ATRP (SI-ARTP) of the desired monomer to generate polymers that exhibit anti-fouling properties or/and better biocompatibility.[16,62,66,67] For further information concerning SI-ATRP, refer to Section 2.2.4. Besides for the functionalization of surfaces, catechol-capped molecules and polymers are also capable of anchoring to nanoparticles (NP), such as Fe_3O_4 or TiO_2 NPs.[68-71]

Within the current chapter (2.1), the background behind the concept of mimicking the abilities of adhesives produced by marine mussels, as well as the current state of research and the already developed applications were introduced. In the present thesis, these concepts were further merged with different cycloaddition reactions and RDRP techniques to generate widely applicable surface modification routes beneficial for a considerable number of materials. The next chapter focuses on RDRP techniques, in particular, ATRP and RAFT polymerization.

2.2. Reversible-Deactivation Radical-Polmerization (RDRP) in Solution and on Surfaces

The following chapter provides an overview of the main RDRP techniques utilized within the current thesis, starting with the classification of atom-transfer radical-polymerization (ATRP) and reversible addition-fragmentation chain transfer (RAFT) polymerization in the context of general RDRPs (2.2.1), over the detailed description of ATRP (2.2.2) and RAFT (2.2.3), to surface initiated ATRP (2.2.4), which is also within the scope of the thesis.

2.2.1. Reversible-Deactivation Radical-Polymerization (RDRP) – a Summary

Within recent decades, the development of application-oriented functional materials has been in the focus of global research teams and several industries. Concerning large scale applications, such as in construction or transportation industry, as well as in micro- or nanoscale fields in medical or (bio)chemical scopes, a large amount of different methods and substances have been investigated and developed. Polymer chemistry has provided extraordinary capacities for creating materials with certain properties on demand. Besides well-established step growth and free radical polymerization (FRP), polymerization techniques such as anionic polymerization, ring opening polymerization (ROP) and RDRPs[72] are gaining more and more importance due to their potential for fabricating precisely controlled macromolecules. Among these three methods, ROP and RDRP exhibit more user friendly conditions than anionic polymerization, which is highly susceptible to water, as well as oxygen and impurities.[73] Herein, the focus rests on RDRPs as these techniques are mainly utilized in the current thesis. RDRP stands for the controlled/living radical polymerization of vinyl-based monomers.[74] Starting from the pioneering work of Otsu in 1982,[75,76] a large number of proposed methodologies for controlled radical polymerization have been investigated and have become available.[74] In 2001, Kamigaito *et al.* presented a selection of different RDRP techniques (**Figure 8**), and categorized them by their

covalent bonds in the dormant species, for instance C–C (1), C–S (2 and 9), C–O (4 and 5), C–Se (3), C–halogen (6 and 8) and C–metal (7).[74] All these types of covalent bonds can be reversibly transferred to a reactivated growing radical species by different chemical (metal catalyst or other radicals) or physical (light or heat) stimuli.[74] The reversibility of the transfer reactions is a general requirement to retain control over the polymerization processes. In the current thesis, the – in the meantime – widely extended concepts of metal catalyzed living radical polymerization (6) and RAFT polymerization (9) were employed.

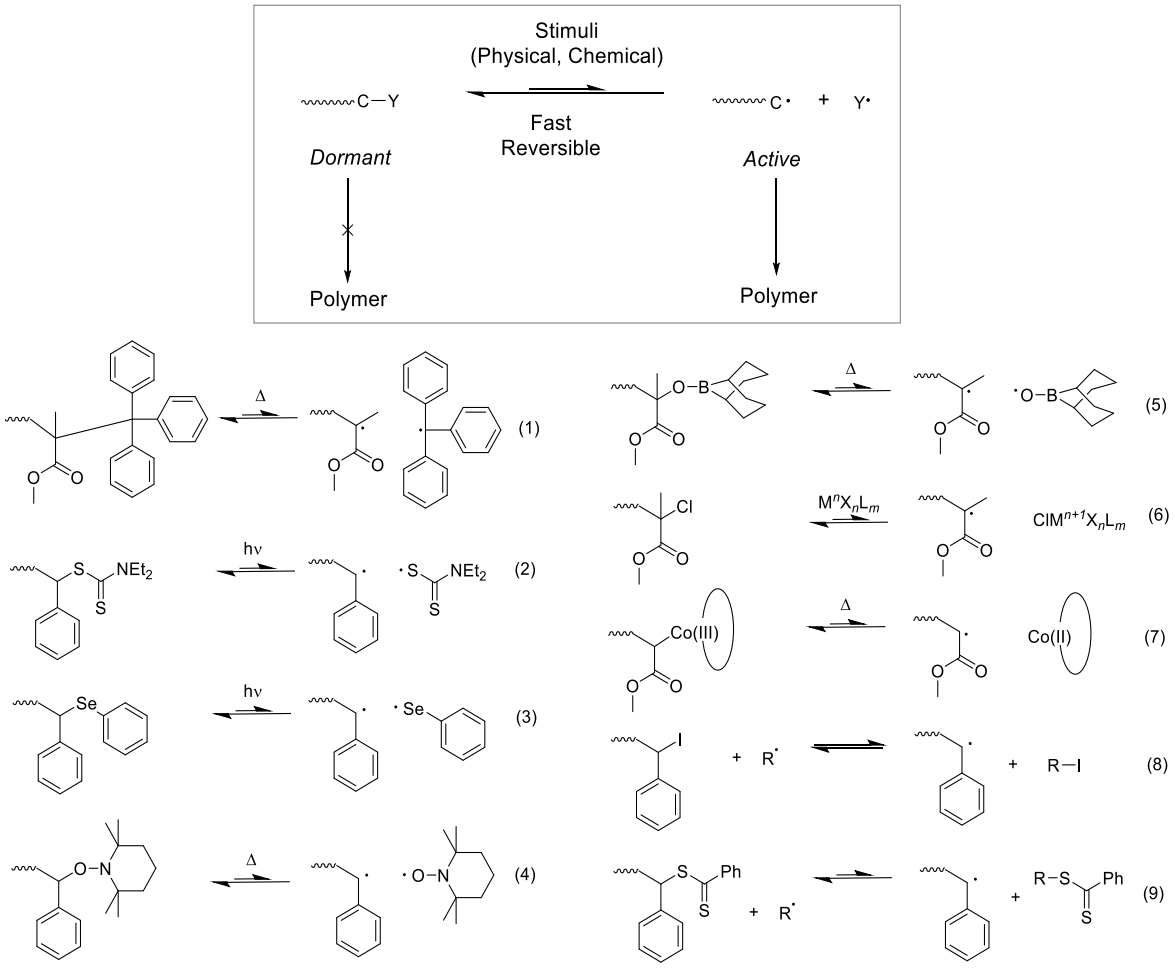

Figure 8: An overview of diverse RDRP techniques is depicted. A dormant species is activated by chemical or physical stimuli by generating a radical, which is capable to perform controlled polymerization. Enhanced versions of (6), as well as (9) were utilized in the current thesis. Adapted and redrawn with permission from Ref. 74. Copyright (2001) American Chemical Society.

Given that RDRP methods combine the benefits of FRP (simple synthetic procedures, availability of a wide variety of initiators and extraordinary tolerance towards functional groups) and anionic polymerization (linear growth of polymer chains,

narrow molecular weight distributions and – of major importance for block copolymer formation – reactivation of polymer chains), they provide enormous advantages in comparison to other polymerization techniques.[77,78] In addition, the selection of monomers that undergo radical polymerization is much higher than the one that can be employed in, for instance, ionic polymerizations.[79] The general idea behind all RDRP techniques is the decrease of the terminating radicals chains in solution or in bulk by adding a suitable compound (controlling agent) capable of generating an equilibrium-dependent dormant (or transferring) species, which can be reactivated and propagate before it is deactivated (or retransferred) to generate the dormant (or transferring) species again.[74,80] Both species – growing and dormant (or transferring) – stand in constant rapid and dynamic equilibrium minimizing the chance of termination of a growing radical with a second radical and thus, providing the opportunity for all growing radicals to propagate in an equal fashion.[74] Thus, narrow dispersities $Đ$ are achieved. In the current thesis, RDRP techniques, namely ATRP and RAFT, were employed and are described in detail in the following sections (2.2.2, 2.2.3).

2.2.2. Atom-Transfer Radical-Polymerization (ATRP)

ATRP was first introduced by Matyjaszewski and co-workers in 1995 by enhancing the well-known atom-transfer radical-addition (ATRA) method, which was – until then – solely applied in organic synthesis for carbon-carbon bond formation.[81] At the very same time, Sawamoto and colleagues presented a new type of living polymerization by employing a ruthenium based organometallic compound ($RuCl_2PPh_3$) with carbon tetrachloride (CCl_4) and methyl methacrylate (MMA) to form PMMA with narrow dispersities $Đ$ in solution.[82] Although Matyjaszewski and Sawamoto developed the process of metal-catalyzed living radical polymerization independently, the principle is the same. In comparison to some other RDRP methods, such as RAFT polymerization, ATRP is an example for reversible-termination RDRP techniques. Dormant and activated species of radicals are present in a reaction mixture. The activated radicals (growing radicals) are deactivated by a controlling agent after some propagation steps and the dormant species are reactivated due to the equilibrium-dependent release of the controlling agent (metal complex M_t^n-Y/Ligand; M = transition metal, n = oxidation

state, Y = counter ion or another ligand).[80,81] **Figure 9** depicts the general mechanism of such a transition metal catalyzed ATRP. Dormant radicals (R-X) are reactivated in a reversible redox process, which is catalyzed by a metal complex (M_t^n-Y/Ligand) in its oxidation state *n*. The metal complex undergoes an one-electron oxidation, accompanied by the abstraction of the halogen or pseudo halogen atom (X), which is bound to the radical in the dormant species R-X.[80] The radical R· is released and performs further propagation steps, before it is deactivated again by re-transfer to the organic halide (R-X) caused by the oxidized species of the transition metal complex (X-M_t^{n+1}-Y/Ligand).[80] The redox process operates with a rate coefficient of deactivation (k_{deact}) and activation (k_{act}). Owing to the low concentration of radicals in comparison to conventional FRP, termination of two radicals is minimized.[80]

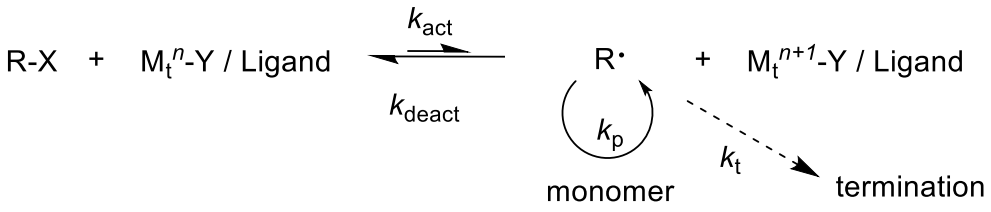

Figure 9: The general activation/deactivation steps of transition metal catalyzed ATRP are depicted. The reactivation of a dormant radical species R-X occurs *via* a reversible redox reaction with a transition metal complex (M_t^n-Y/Ligand). The released radical R· propagates for some steps, before it is deactivated again by the oxidized metal complex (X-M_t^{n+1}-Y/Ligand). M_t: transition metal, *n*: oxidation state, Y: counter ion or additional ligand, X: (pseudo)halogen, k_{act} or k_{deact}: rate coefficient of the activation or the deactivation, k_p: rate coefficient of the propagation, k_t: rate coefficient of the termination. Reprinted with permission from Ref. 80. Copyright (2001) American Chemical Society.

In addition to normal ATRP, further methods have been extensively studied and described. **Figure 10** demonstrates an overview of different types of ATRP reactions in comparison to normal ATRP (**a**). The advantage of alternative or reverse ATRP (RATRP) (**b**) is the non-sensitivity to air of the technique.[83,84] In comparison to conventional ATRP, the catalyst is employed in its oxidized state (X-M_t^{n+1}-Y/Ligand), initiation is performed *via* common FRP initiators, such as AIBN and the generated initiating radical can either react with the monomer or the oxidized catalyst species to form the catalyst's reduced version M_t^n-Y/Ligand.[83,84] The next steps follow the classic ATRP mechanism.[83] However, the concentration of the catalyst needs to be comparable to the amount of initiator.[84] In simultaneous reverse and normal initiation (SR&NI) ATRP (**c**), the methods mentioned above are combined, leading to a versatile dual initiation system where all types of polymers and block copolymers generated by

classical ATRP can be prepared.[84] However, this system suffers from partial loss of control owing to the chains initiated by the standard FRP initiator.[84] The basic idea of activator generated by electron transfer (AGET) ATRP is the utilization of an electron transfer (for instance by employing $Sn(EH)_2$) instead of organic radicals for the reduction of the oxidized catalyst.[84] Matyjaszewski and co-workers improved the AGET concept and introduced activator regenerated by electron transfer (ARGET) ATRP, which employs a non-radical generating reducing agent, such as ascorbic acid, to form the reduced species of the catalyst *in situ* in order to achieve better control over the system.[85]

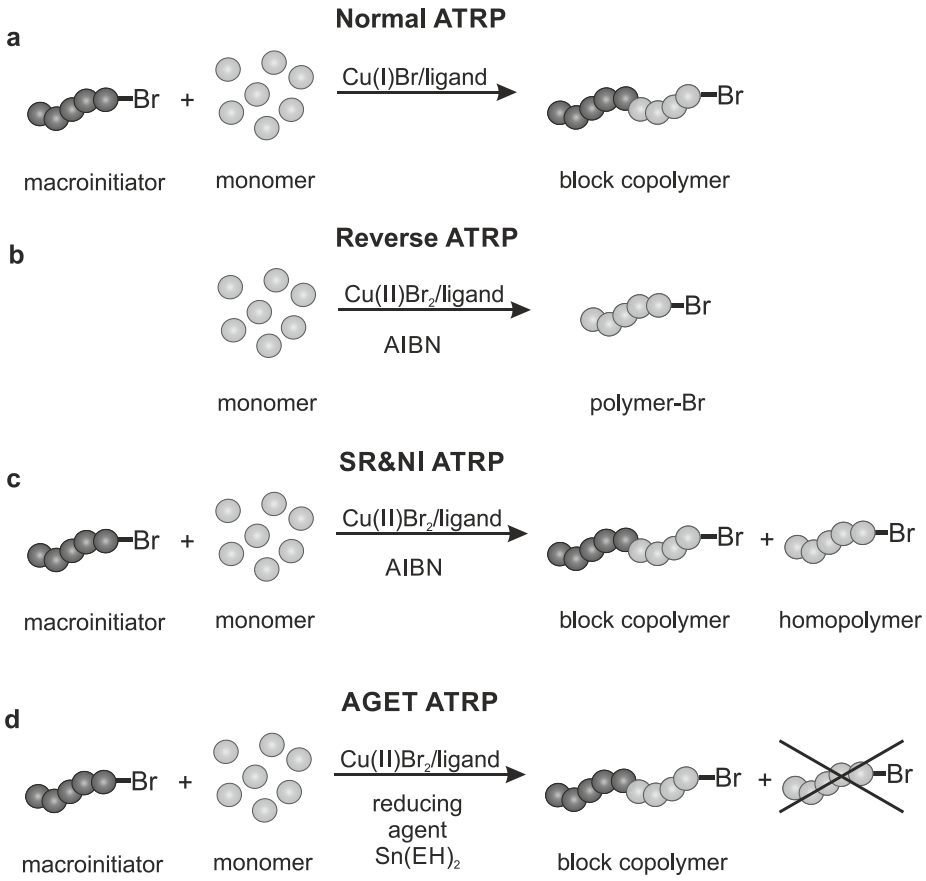

Figure 10: Different types of ATRP-based polymerizations are depicted. Normal ATRP (**a**) only functions under air exclusion, whereas in reverse ATRP (RATRP) (**b**) the air-stable oxidized version of the catalyst is employed.[84] A combination of **a** and **b**, the so called simultaneous reverse and normal initiation (SR&NI) ATRP is illustrated in **c**. Activator generated by electron transfer (AGET) ATRP describes a low copper concentration type reaction (**d**).[84] Adapted and redrawn with permission from Ref. 84. Copyright (2005) American Chemical Society.

Besides copper, which is widely employed in ATRP, other transition metals such as iron, ruthenium, nickel or palladium, to name but a few, have caught the attention of researchers to create novel transition metal complexes for metal catalyzed living

radical polymerization.[74] A wide variety of vinyl-based monomers have already been successfully polymerized, however, ATRP of non-activated monomers such as ethylene, vinyl acetate or vinyl chloride still causes difficulties.[74,86,87] In this context, especially in case of vinyl chloride, single-electron-transfer living radical polymerization (SET-LRP) was presented as a promising tool to achieve control of the polymerization.[87,88] The reactive Cu(0) species, which operates as electron donor, is oxidized to Cu(I) *in situ* and initiates the polymerization *via* heterogeneous SET on the alkyl halide.[87,89] Cu(I) immediately disproportionates in Cu(0) and Cu(II).[87,89] In turn, Cu(II) serves as the electron acceptor, which is necessary as deactivator for the reversible termination step, as established from typical ATRPs.[87,89] The advantages of the described technique are its ability to operate under mild conditions (at ambient temperature or below), the application of only catalytic amounts of catalyst, its high reaction rate, and – of major importance – the amount of bimolecular terminations is decreased and can, under suitable reaction conditions, not even be detected.[87,89]

2.2.3. Reversible Addition-Fragmentation Chain Transfer (RAFT) Polymerization

Unlike ATRP, which operates according to a reversible termination principle, RAFT polymerization is a degenerative chain transfer RDRP technique.[90] The essential difference between the two RDRP types originates from the amount of activated radicals available in the reaction mixture.[91] In case of ATRP, the low radical concentration is necessary to preserve the living character, whilst in the RAFT process, the number of activated radicals is comparable to the one in free radical polymerization (FRP), since once a growing radical chain is transferred to an deactivated state (dormant state) a former dormant species is immediately reactivated.[92] Thus, the overall number of radicals remains constant.[91] In 1998, the principle of RAFT polymerization was introduced by Rizzardo, Moad and the CSIRO team whilst Zard and Destarac contemporaneously and individually developed the equivalent technique of macromolecular design *via* the interchange of xanthates (MADIX).[77,93,94]

For simplification, RAFT is employed for both expressions in the current thesis since both methods originate from the same mechanism. The key step in the RAFT process

is the transfer of growing radical chains in an equilibrium reaction, utilizing, for instance, trithiocarbonates, dithioesters, dithiocarbamates or xanthates as controlling agents – namely RAFT agents (**Figure 11**).[95]

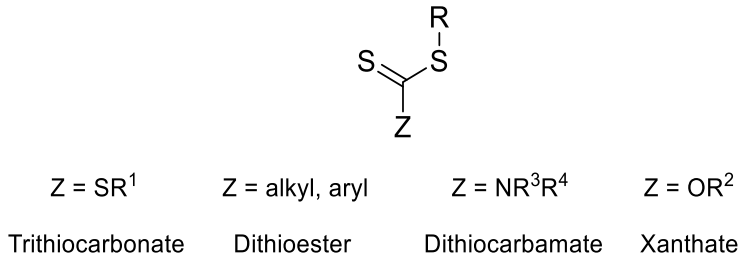

Figure 11: Different types of RAFT controlling agents are depicted. The choice of the employed RAFT agent, for instance, trithiocarbonates, dithioesters, dithiocarbamates or xanthates (from left to right), is monomer dependent.

The initiation step of a RAFT polymerization proceeds in the same fashion as in conventional FRP by the generation of primary radicals from a suitable initiator (thermal, redox, photo induced).[96] The most common initiator for radical-mediated processes is 2,2'-azobisisobutyronitrile (AIBN), which generates radicals due to the release of nitrogen.[79] A simplified overview of the RAFT mechanism is depicted in **Figure 12**. A initiator radical I· is generated, which propagates by adding monomer units (M) to form the propagation radical P_n·.[96] Owing to the high chain-transfer constant of such RAFT agents, it is most likely that only a couple of monomers are added before P_n· enters the pre-equilibrium with a RAFT agent (thiocarbonylthio compound).[96,97] Ideally, the forward fragmentation is favored, meaning that the previously generated P_n remains attached to the RAFT agent (macro RAFT agent) and the freshly released radical R· reinitiates polymerization and starts new propagation steps with the monomer.[97] The described characteristic is achieved when R is a better leaving group than P_n and when R· presents good reinitiating properties.[96] The freshly grown polymer chain P_m· enters the main equilibrium by addition to a macro RAFT agent.[78] A polymer chain (P_n or P_m) is released, propagates and re-enters the degenerative chain transfer again.[96] Due to the rapid equilibrium between the growing radical species (P_n· and P_m·) and the macro RAFT agent (thiocarbonylthio compound), all activated radical chains possess equal probabilities to propagate and, therefore, narrow dispersities (*Đ*s) are achieved.[97] Although most of the side reactions, such as termination or conventional chain transfer, are suppressed, a certain amount of these undesired processes still occurs, leading to dead polymer chains that remain in the final

material.[96] It has to be noted that the RAFT mechanism described herein illustrates a simplified and generally accepted theory for the process, however, some aspects are still not fully understood.[96]

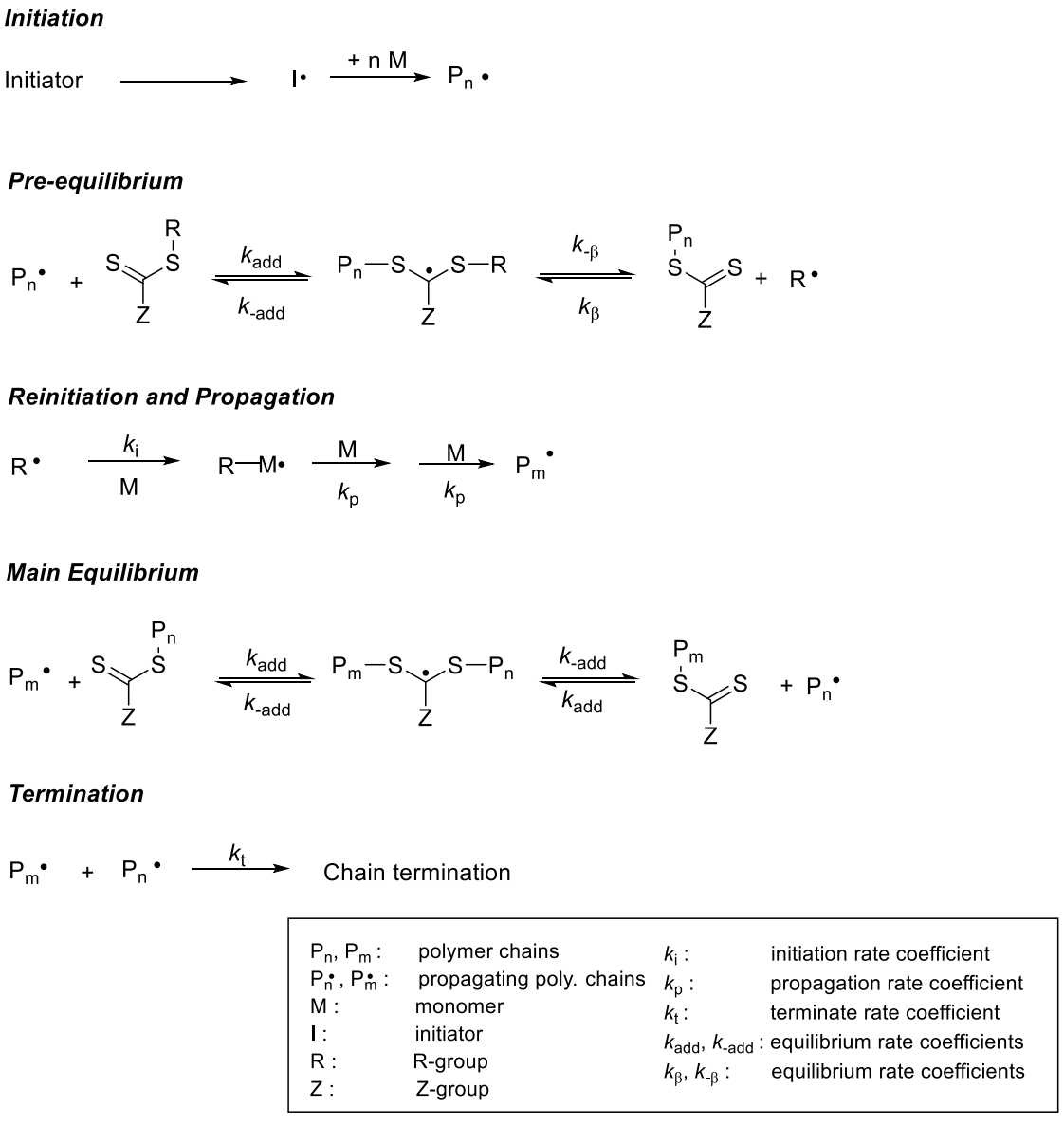

Figure 12: Schematic illustration of the RAFT process. The general steps of the RAFT mechanism are depicted: initiation, pre-equilibrium, reinitiation and propagation, main equilibrium and termination steps. Adapted with permission from Ref. 78 (John Wiley & Sons) and Ref. 98 (CSIRO PUBLISHING, 2005) (http://www.publish.csiro.au/nid/51/paper/CH05072.htm).

The choice of the R- and Z-group is predominantly dictated by the type of monomer which is to be polymerized *via* RAFT. The selection of the Z-group affects the addition and fragmentation rates by modification of the stability of the intermediate radical. Dithioesters, for instance, are suitable for the polymerization of acrylates,

methacrylates or styrene, whereas control of RAFT polymerization of vinyl acetate is only achieved by employing dithiocarbamates or xanthates.[99,100] The R-group, on the other hand, needs to be a good leaving group, implying that the radical generated by the R-group is more stable than the attaching one, yet must also be capable of reinitiating polymerization.[100] In summary, the reactivity of the C=S double bond in the thiocarbonylthio compound must be high, the intermediate radicals should fragment rapidly and should not undergo side reactions, the intermediate should favor the forward fragmentation and the freshly generated radicals should reinitiate well.[100] **Figure 13** provides general guidelines for the choice of an appropriate RAFT agent, depending on the type of monomer to be polymerized.

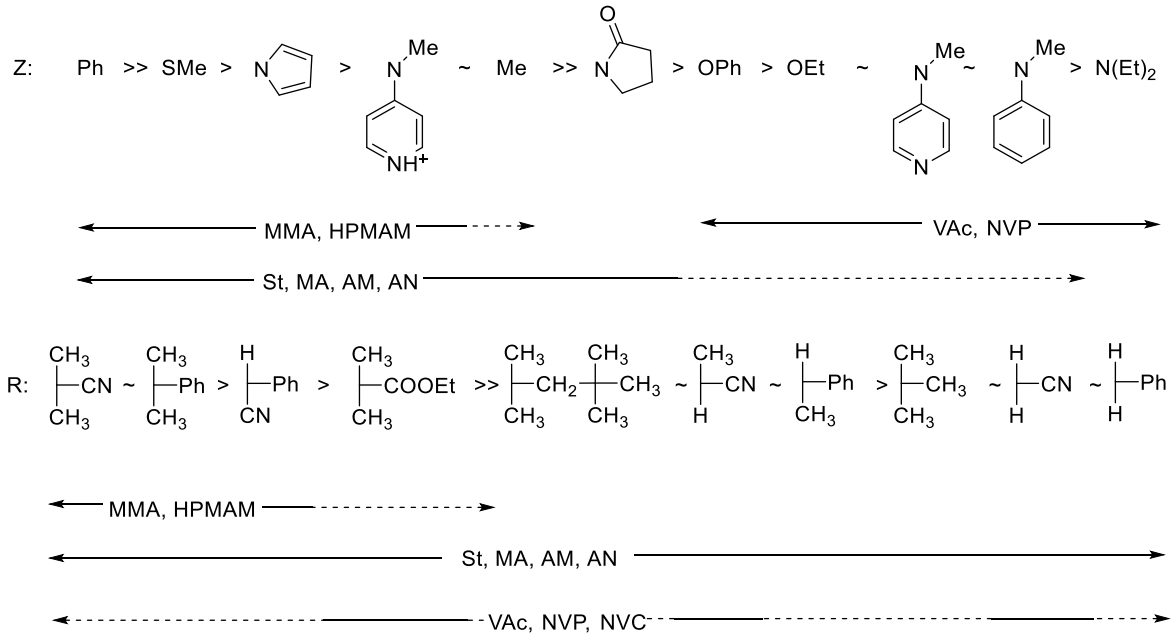

Figure 13: General guideline for the selection of a suitable RAFT agent (Z-C(=S)-S-R) for the polymerization of certain monomers. Continuous lines indicate full control, whereas dashed lines imply partial control of the polymerization process. MMA: methyl methacrylate, HPMAM: *N*-(2-hydroxypropyl)meth acrylamide, VAc: vinyl acetate, NVP: *N*-vinylpyrrolidone, St: styrene, MA: methyl acrylate, AM: acrylamide, AN: acrylonitrile, NVC: *N*-vinylcarbazole. Adapted and redrawn with permission from Ref. 101. Copyright (2012) American Chemical Society.

2.2.4. Polymer Brushes on Surfaces – Surface Initiated ATRP (SI-ATRP)

Coating a surface with a certain polymer type alters the surface's properties critically.[102] In general, two strategies for preparing surfaces that feature polymer brushes – *grafting-from* and *grafting-to* – have already been widely employed to modify interfaces and generate novel material for defined applications.[103,104]

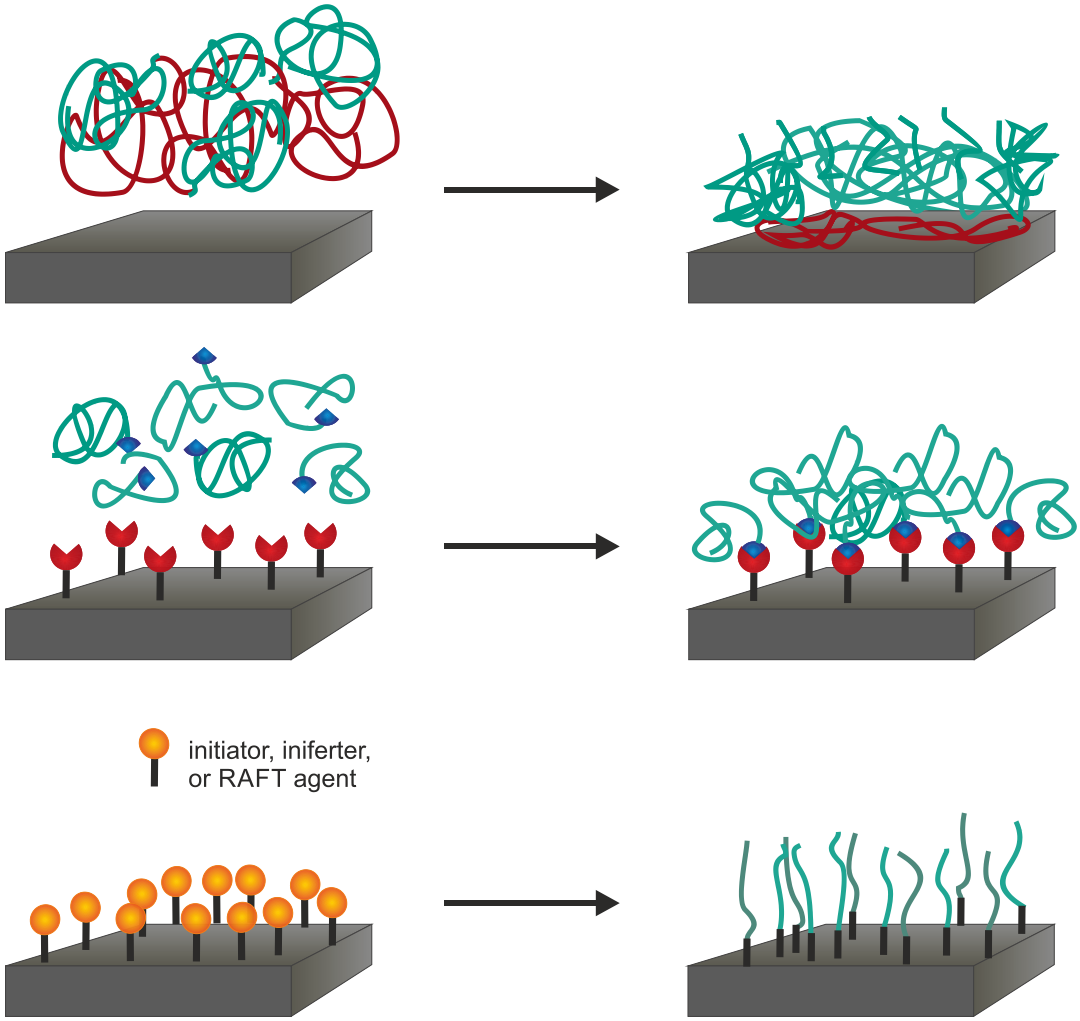

Figure 14: Different routes for the preparation of surfaces that contain polymer brushes are depicted. By employing *grafting-to* approaches, the polymer attachment is conducted by either physisorption (**A**) or chemisorption (**B**), whereas *grafting-from* implies the growth of polymer brushes from a previously attached initiator, iniferter or RAFT-agent on the surface (**C**).[103] Adapted and redrawn with permission from Ref. 103 . Copyright (2009) American Chemical Society.

In a *grafting-from* approach, the polymerization is initiated straight from the initiator-carrying surface, whereas *grafting-to* implies the tethering of readily prepared polymer brushes to a surface.[103,105] Both methods exhibit different advantages and the

most suitable technique must be selected individually, depending on the type of application. In a *grafting-from* approach, the polymer chains are grown in a controlled fashion in terms of chain length and composition, from the entire surface, achieving high grafting densities.[103] *Grafting-to* approaches, on the other hand, allow the full characterization of the polymer chains prepared in solution previously to the attachment *via* variable techniques, however, lower grafting densities are obtained owing to steric hindrance.[103] **Figure 14** depicts an overview of the general synthetic strategies for the preparation of polymer brushes on surfaces. Typical *grafting-to* approaches are conducted by the attachment of previously prepared polymer brushes by either physisorption (**Figure 14 A**) or chemisorption (covalent bond formation) (**Figure 14 B**).[103] Within the current thesis, *grafting-to* approaches based on covalent bond formation *via* thermal or light-induced cycloaddition reactions play a key role and will be further described and discussed in Chapter 3 to 5. Furthermore, as an example for SI controlled polymerization from PDA substrates, a corresponding *grafting-from* approach is presented in Chapter 6. A schematic overview of SI-polymerizations is presented in **Figure 14 C**. The initiator (for instance an ATRP initiator), the iniferter or the RAFT agent – depending on the type of SI polymerization – is attached to the surface and the desired polymer brush is grown from there.[103]

A considerable number of surface-initiated (*grafting-from*) strategies in the field of RDRPs has already been studied extensively.[103] Within the current chapter, the focus lies on the *grafting-from* approach in combination with a RDRP technique, more precisely surface initiated ATRP (SI-ATRP). In general, different methods for the attachment of the surface-initiating molecule are available, apart from the already discussed systems based on PDA films or catechol anchoring (2.1.3, 2.1.4). These tethering techniques include, for instance, SAM formation of thiols or dithiols on gold or other noble metal surfaces, as well as silanes on oxidized substrates.[6-8,103,105-107] In order to clarify the reaction steps on the surface within a SI-ATRP, a reaction scheme published by Rodriguez-Emmenegger *et al*. concerning the preparation of anti-fouling polymer brushes from gold is presented in **Figure 15**.[6] The initiator-carrying SAM on the gold surface (ω-mercaptoundecyl bromoisobutyrate) (**Figure 15 A**), undergoes two consecutive SI-ATRP polymerizations were oligo ethylene glycol methyl ether methacrylate (MeOEGMA) is employed as a first monomer (**Figure 15 B**), followed by

either MeOEGMA again (**Figure 15 C**) or carboxybetain acryl amide (CBAA) (**Figure 15 D**) to confirm the living nature of the system and its ability for block copolymer formation.[6] In addition, it is worth noticing that a mixed halide catalyst system (Cu(I)Cl/Cu(II)Br_2/Ligand) was employed owing to the higher bond energy of C–Cl in comparison to C–Br, which shifts the equilibrium to the dormant species. As a result, the rate of polymerization is decreased and, therefore, the control of the system increases.[6,103,108]

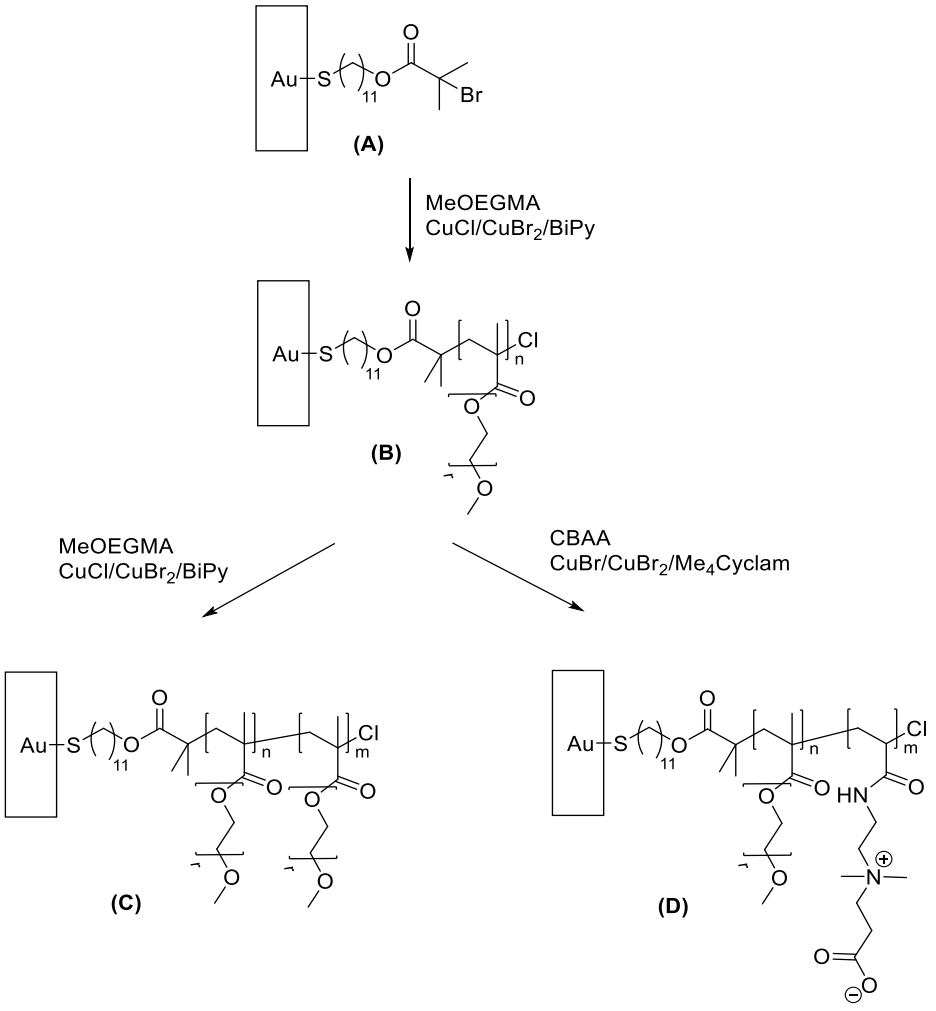

Figure 15: The surface initiated (SI) ATRP from an initiator-carrying SAM on gold (**A**) is depicted. First, oligo ethylene glycol methyl ether methacrylate (MeOEGMA) is polymerized (**B**), before either an additional poly(MeOEGMA) (**C**) or a poly(CBAA) (**D**) layer is grown to confirm the living behavior of the system and its ability to form block copolymers.[6] Adapted with permission from Ref. 6. Copyright (2012) John Wiley and Sons.

The current example clearly indicates that SI-ATRP provides high potential with regard to substrate modification for applications in biological systems, as well as related areas. Hence, SI-ATRP was conducted in the current thesis in combination with NITEC

chemistry (2.3.3) to generate a substrate independent surface modification tool allowing spatially resolved controlled cell adhesion (Chapter 6).

Within the present section, general RDRP techniques were described as well as SI types. The following and last chapter summarizes different thermal- and photo-induced cycloaddition reactions, which combine the topics already described in the current and the preceding section (2.2 and 2.1).

2.3. Cycloadditions in a Polymer Context

The current chapter presents an overview of different types of cycloadditions with regard to polymer conjugation, commencing with the general classification of cycloadditions (2.3.1), followed by thermal and photo-induced DA type reactions (2.3.2) in solution and on surfaces, and finally, introducing a specific 1,3-dipolar cycloaddition, namely NITEC for surface modification (2.3.3).

2.3.1. Cycloadditions – Classification

Most reactions in organic chemistry are ionic.[109] In contrast, pericyclic reactions, such as sigmatropic rearrangements, electrocyclic reactions, as well as cycloadditions, are based on the cyclic movement of electrons without any intermediates.[109] **Figure 16** presents an overview of the different pericyclic reactions and the corresponding number of generated or broken σ-bonds.[109]

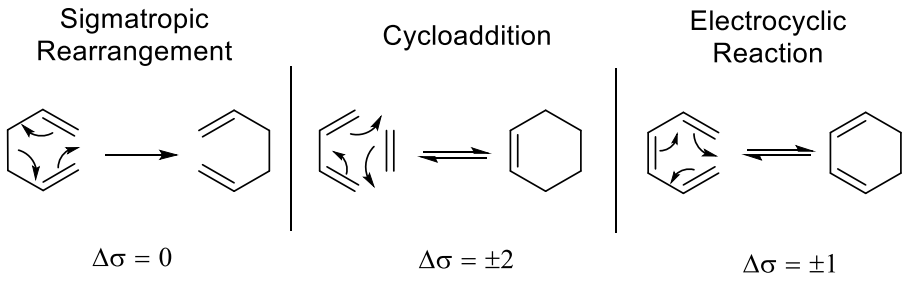

Figure 16: Overview of different pericyclic reactions and the number of σ-bonds that are generated or broken, respectively. From left to right: Sigmatropic rearrangement, cycloaddition, electrocyclic reaction.[109]

Within the current thesis, diverse types of cycloadditions were employed, namely thermal or photo-induced DA, thermal HDA reactions and light-induced 1,3-dipolar cycloadditions – NITEC – in order to tether previously prepared polymer brushes or SI-ATRP initiators to surfaces. These methods are described in the following sections.

2.3.2. Thermal and Photo-Induced Diels–Alder Type Cycloadditions as Tools for Polymer Ligation in Solution and on Surfaces

DA and HDA reactions belong to the group of [4 + 2] – cycloadditions and proceed between a molecule bearing two conjugated double bonds (diene) and another compound carrying a double bond (dienophile) (**Figure 16**, center). These reactions are, in general, thermodynamically favored due to the generation of two additional σ-bonds, whilst two π-bonds and the conjugation of the diene disappear.[109] Especially in polymer chemistry, the post-modification of synthetically prepared polymers by, for instance, transformation of the polymer-end group and subsequent generation of well-defined architectures or modular structures, such ligation reactions have gained high importance.[110] In normal DA reactions,[111] the energies of the highest occupied molecular orbital (HOMO) of the diene and the lowest unoccupied molecular orbital (LUMO) of the dienophile are closer to each other than the inverse pair (HOMO of dienophile and LUMO of diene), and these orbitals are, therefore, interacting.[111] Typical dienophiles that undergo such a normal DA reaction exhibit an electron-poor double bond (due to electron withdrawing groups), which decreases the dienophile's LUMO energy.[111] Hence, maleimides that are attached to a polymer strand serve as highly reactive dienophiles able to conjugate with polymers that carry dienes, such as linear pentadiene (elevated temperature required) or cyclopendtadiene (Cp) (ambient temperature) in solution.[38,112,113] An advantage of conjugation reactions with Cp-polymers is the relatively low temperature of the reverse retro-DA (rDA) process.[114] Furthermore, Cp-polymers can also be employed in HDA conjugations and their corresponding retro-HDA (rHDA) reactions with dithioesters (dienophile).[115] These dithioesters have already been introduced in the context of RAFT polymerizations.[23,116-118] Adopting the nomenclature of RAFT agents, in HDA reactions the Z-group is required to contain electron withdrawing moieties, such as phosphoryl or pyridinyl groups that can be further activated by Lewis or Brønsted acids, such as $ZnCl_2$ or trifluoro acetic acid (TFA), respectively.[23,119] However, Glassner *et al.* showed the applicability of such dithioester-based HDA conjugations with Cp- and open chain dienes-bearing water-soluble polymers in aqueous media under mild and catalyst-free conditions.[120] Moreover, Oehlenschlaeger *et al*. recently presented a novel catalyst-free

HDA system, exploiting the electron withdrawing properties of a cyano-moiety that serves as the Z-group of a dithioester, which was applied to generate a HDA-based reversible step growth polymerization technique, as well as a novel self-healing material.[121,122] Blinco *et al.* introduced Cp-moieties on silicon wafers, before several (H)DA reactions with different polymers that contained a dienophile-moiety (dithioesters, maleimide) were conducted on the surface.[114] **Figure 17** depicts the step-by-step surface functionalization, starting with the attachment of the bromine terminated silane to the silicon wafer. Consequently, a Cp-transformation of the bromine is performed, followed by the accomplishment of the (H)DA reactions with the polymers bearing a suitable dienophile, at ambient temperature.[114] In this regard, dithioesters attached to poly(*iso*-bornyl acrylate) (P*i*BA) (**Figure 17**, top) or poly(styrene) (PS) (**Figure 17**, center) were attached to the Cp-functionalized surfaces *via* HDA conjugation.[114] As an example for DA surface ligation, poly(ethylene glycol)-maleimide (**Figure 17**, bottom) was reacted with the Cp-carrying silicon wafer at ambient temperature.[114] In addition, the appropriate rDA and rHDA reactions were also conducted on the surface and confirmed *via* XPS.[114]

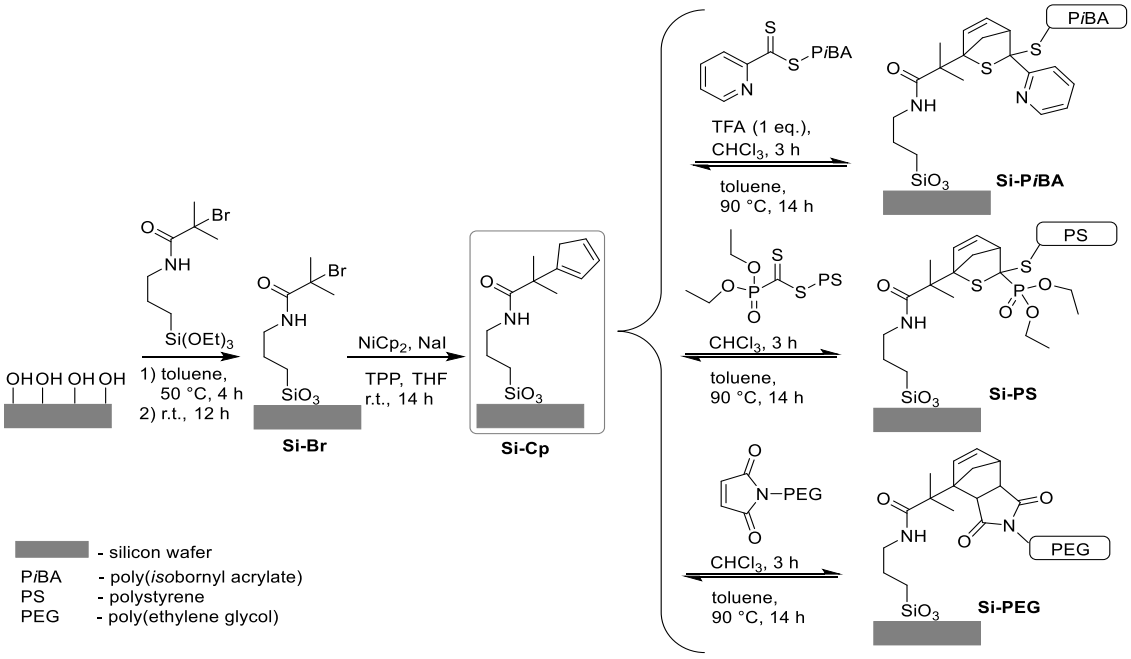

Figure 17: The stepwise modification of a silicon wafer is depicted. First, a bromine-carrying silane is attached, before the terminal bromine is transformed to a Cp-moiety, which is capable of (H)DA conjugation with suitable dienophiles at ambient temperature. The top and center approaches describe HDA-ligation with dithioesters (phosphoryl, pyridinyl)-carrying polymers, whereas the bottom part shows a DA reaction with polymers that possess maleimide functionalities. The corresponding retro-(H)DA reactions are performed at 90 °C. Adapted and redrawn with permission from Ref. 114. Copyright (2011) John Wiley and Sons.

Besides DA and HDA conjugation on silicon substrates,[38,114] several approaches employing fullerenes[123,124] or carbonanotubes (CNTs)[125-128] as dienophiles with Cp-polymers, as well as HDA reactions between Cp-functionalized cellulose[129,130] or microspheres[131] with dithioester-carrying RAFT (bio)polymers or thioamide-bearing peptides, among others, have already been reported.

Recently, a concept combining special photo-induced DA reactions – namely photoenol conjugation or photoenolization[132-134] – with polymer chemistry was introduced by Gruendling *et al*.[22] The general mechanism of such a photoenol reaction is depicted in **Figure 18**.[22] A *o*-methylphenyl ketone (or aldehyde if R=H) is excited with UV light and a intramolecular H-abstraction occurs, followed by a rearrangement process to form a highly reactive diene, which undergoes rapid DA ligation with dienophiles that bear electron withdrawing groups (EWGs), such as maleimides.[22] R^1 and R^2 represent either organic residues or polymers.

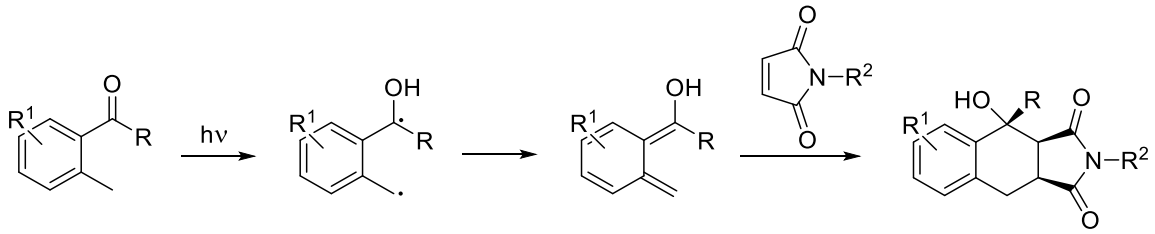

Figure 18: General procedure for photoenol-maleimide ligation. A *o*-methylphenyl ketone (or aldehyde if R=H) is excited leading to an intramolecular hydrogen abstraction and a rearrangement step to form an *o*-xylylene intermediate, which operates as a highly reactive diene in DA reaction with dienophiles, such as maleimides.[22] R^1 and R^2 represent either organic residues or polymers. Reprinted with permission from Ref. 22. Copyright (2011) John Wiley and Sons.

The described approach has already been applied for catalyst free advanced polymer design, for instance, to generate single-chain polymeric nanoparticles (SCNPs),[135] as well as for conjugation of hetero-dienophiles, namely dithioester-RAFT polymers, with a photoenol-capable terminated polymer strands or microspheres.[136,137] Moreover, the sequential preparation of ABC triblock copolymers employing two generations of photoenols in light-triggered conjugations with carefully selected dienes,[138] as well as the generation of more complex ABA- and ABC- block copolymers using photoenolization-capable moieties in combination with other ligation techniques, were also presented.[139] In this context, the light-triggered photoenol ligation reaction was presented to proceed orthogonally to thermally induced DA reactions.[110,139] Furthermore, the applicability of the photoenol reactions in biochemical systems was

presented by Bauer *et al.*, who conjugated a DNA strand bearing a photoenol-capable moiety with maleimide-capped protein under relatively mild conditions.[140] In addition, silver core NPs were functionalized with photoenol capable moieties and covalently conjugated with polymers under irradiation.[141]

Besides photoenol reactions in solution, several spatially controlled light-triggered photoenol surface reactions on (bio)substrates based on the modification of silanes, hyaluronic acid or cellulose (**Figure 19**) have been introduced.[28,29] Moreover, the fabrication and photo-functionalization of 3D scaffolds prepared by direct laser writing (DLW),[142] as well as the precise functionalization of previously generated free-standing DLW 3D microscaffolds have already been presented.[143]

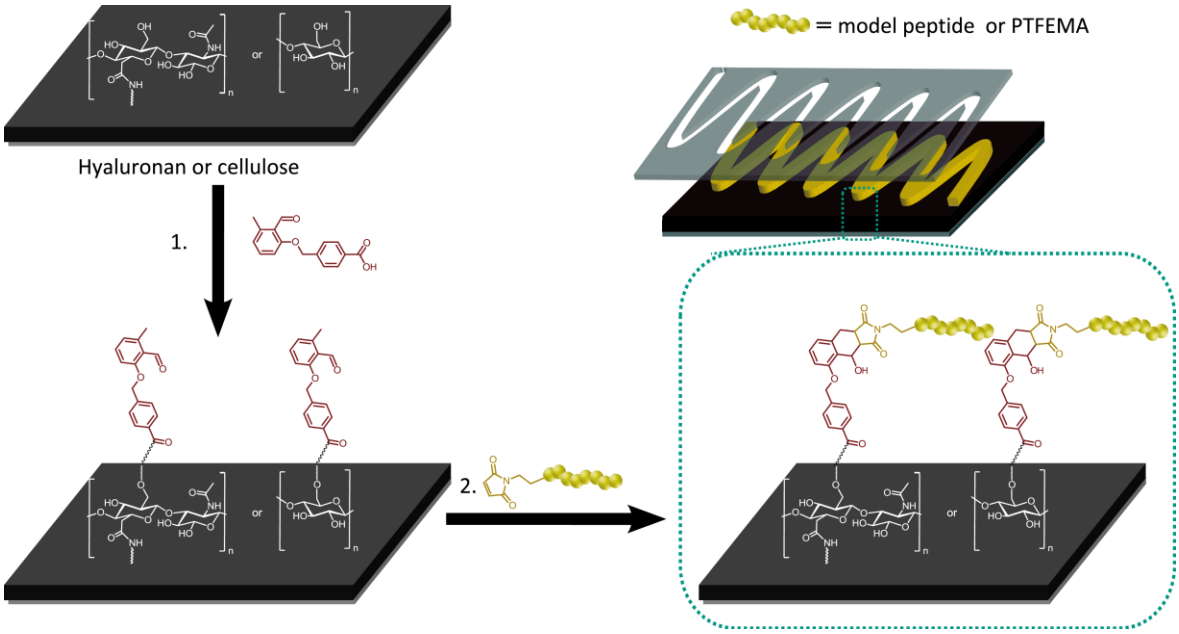

Figure 19: Spatially controlled light-induced photoenol reaction on cellulose or hyaluronic acid is illustrated. Photoenol-moieties are attached to the substrates by Steglich-type esterifications, followed by irradiation (λ_{max} = 320 nm) in the presence of a maleimide-terminated peptide sequence or polymer (poly(2,2,2-trifluoroethyl methacrylate) (PTFEMA)). Spatial control is achieved by covering selective regions on the surface with a meander-shaped shadow mask prior irradiation.[29] Reprinted with permission from Ref. 29. Copyright (2013) American Chemical Society.

The functionalization of biosubstrates, such as cellulose and hyaluronic acid, with a photoenol moiety and the subsequent photo-induced DA reaction with either maleimide-carrying polymer strands (poly(2,2,2-trifluoroethyl methacrylate) (PTFEMA)) or a model peptide sequences was presented by Tischer *et al.* (**Figure 19**).[29] Regional control of the tethering was accomplished by application of a

sophisticated meander-shaped shadow masked on the substrate prior to irradiation (λ_{max} = 320 nm).[29] Thus, highly resolved polymer patterning was generated with variable types of polymers or peptides which establishes novel pathways for the preparation of substrates in the context of medical or (bio)chemical applications. Recently, the fabrication of 2D micropatterns from gold NPs by combining DLW with multiphoton-induced Diels–Alder protocols, as well as their functionalization with polymers in a second photo-ligation step exploiting the remaining photoenol-capable moieties not consumed before, was presented by Stolzer *et al*.[144]

2.3.3. Nitrile Imine-Mediated Tetrazole-Ene Cycloaddition (NITEC) for Surface Modification

The concept of nitrile imine-mediated tetrazole-ene cycloaddition (NITEC) was first introduced by Sustmann and Huisgen in 1967,[145] and further enhanced for use in a (bio)chemical or medical context by Lin and co-workers.[25,146,147] The general mechanism of such NITEC reactions is depicted in **Figure 20**. NITEC represents a [3+2]-cycloaddition, also known as 1,3-dipolar-cycloaddition.

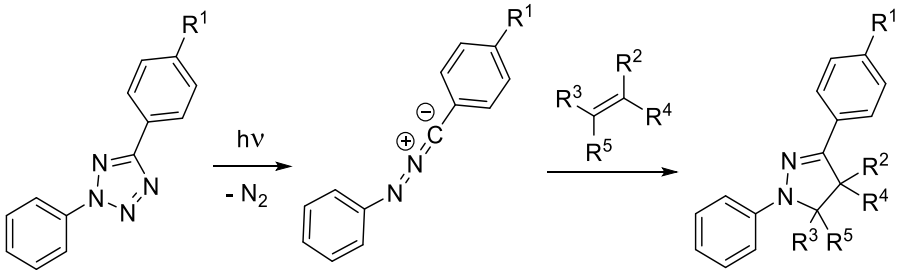

Figure 20: General mechanism of a NITEC reaction. A highly reactive propargyl-allenyl type nitrile imine (1,3-dipole) is generated by nitrogen release during UV-irradiation. Subsequently, the nitrile imine undergoes a 1,3-diploar cycloaddition with a suitable dipolarophile. Adapted (and extended) with permission from Ref. 148. Copyright (2012) John Wiley and Sons.

A tetrazole moiety, which can be attached to organic or polymeric residues, is irradiated with UV light, whereby nitrogen is released and a highly reactive propargyl-allenyl type 1,3-dipole is formed, namely a nitrile imine. The dipole further reacts with a convenient dipolarophile (organic or polymeric residues) to form a pyrazoline-type linker.[25,145,148] In this respect, maleimides serve as suitable dipolarophiles due to their electron-deficient double bond.[25,148] Recently, the principle of NITEC reactions was

applied in several new systems, for instance for protein modification,[146,147] polymer-enzyme ligation,[149] polymer-polymer conjugation,[150] polymer crosslinking,[151] or step-growth polymerization,[152] to name but a few. Remarkably, Hiltebrandt *et al.* merged the NITEC and the photoenol protocol and created a λ-orthogonal wavelength-dependent polymer conjugation system.[153]

Furthermore, NITEC was already employed on surfaces or biosubstrates for either grafting streptavidin, polymers or photo-responsive azobenzene moieties to the surfaces or substrates,[35,51,148,154] or for grafting polymers *via* SET-LRP from a substrate where the initiator was previously attached *via* NITEC.[35]

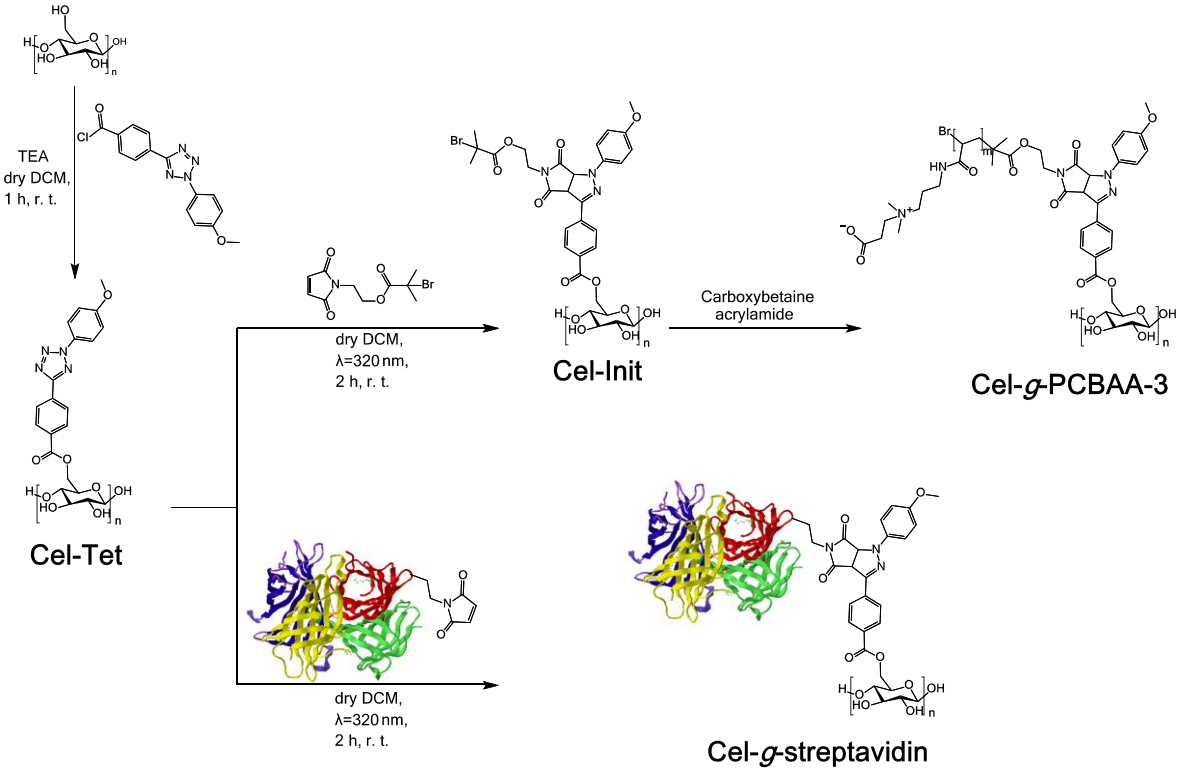

Figure 21: NITEC-based *grafting-to* and *grafting-fro*m approaches on cellulose. First, cellulose is modified with a tetrazole moiety (**Cel-Tet**), before either streptavidin (**Cel-*g*-streptavidin**) (lower part) or a suitable SET-LRP initiator (**Cel-Ini**) is grafted to the bio-substrate (upper part). In a SET-LRP, non-fouling poly(CBAA) (**Cel-*g*-PCBAA-3**) is generated. The described principle can also be adapted for spatially resolved surface patterning. Reprinted with permission from Ref. 35. Copyright (2012) John Wiley and Sons.

In **Figure 21**, *grafting-to* and *grafting-from* approaches, applying NITEC as conjugation method, on the biosubstrate cellulose are depicted.[35] Cellulose, which is the most widely employed organic polymer,[155] was first modified with a suitable tetrazole moiety (**Cel-Tet**), before the NITEC reaction with a streptavidin-maleimide (**Cel-*g*-streptavidin**) (lower part) or a maleimide-carrying SET-LRP initiator (**Cel-Ini**) (upper

part) was conducted under UV irradiation.[35] In the *grafting-from* approach, non-fouling poly(carboxybetaine acrylamide) (PCBAA) was polymerized from the initiator on the substrate *via* SET-LRP (**Cel-*g*-PCBAA-3**). The immobilization of such biomolecules or non-fouling polymers on a simple and highly available substrate as cellulose can be envisioned for future medical or (bio)chemical applications, such as point-of-care devices.

The current and last chapter (2.3) of the theoretical background section treated different types of cycloaddition reactions, namely thermal and photo-induced (H)DA reactions, as well as a special photo-induced 1,3-diploar cycloaddition, NITEC. These conjugation reactions form the core of the concept of bio-inspired surface ligation with small molecules, polymers or peptides. In the following chapters, different approaches for novel surface modification methods based on PDA films or catechol anchors employing thermal cycloadditions (Chapter 3 and 4), on the one hand, and photo-induced conjugations (Chapter 5 and 6), on the other hand, are presented and discussed in detail.

3

Thermal Polymer Diels–Alder Ligation on Catechol-Anchor based Substrates

Thermally driven [4+2] cycloadditions, more precisely Diels–Alder (DA) reactions, and their reversible counterparts have proven to be beneficial tools for orthogonal ligation of small molecules or polymers (2.3.2). Well-established diene-dienophile pairs in such thermal Diels–Alder ligations are furan-*N*-maleimide and anthracene-maleimide. However, these ligation-pairs suffer from the necessity of elevated temperature for successful Diels–Alder conjugation.[24,156,157] By careful selection of the conjugating moieties – dienes and dienophiles – the HOMO-LUMO interaction of the reacting species can be manipulated to the extent that the DA ligation operates even under ambient conditions.

Parts of the chapter were reproduced from Preuss, C. M.; Goldmann, A. S.; Trouillet, V.; Walther, A.; Barner-Kowollik, C. *Macromolecular Rapid Communications* **2013**, *34*, 640 by permission from John Wiley and Sons (Copyright 2013).

Therefore, the combination of maleimide (Mal) and Cp groups serves as such an ambient temperature conjugation method.[24] In addition, its corresponding rDA reaction was identified to fully perform at 90 °C.[114] Moreover, the described system has already been adopted for the preparation of linear multiblock copolymers,[139] as well as dynamic covalent ligations on silicon wafers.[114]

In order to broaden the scope of applications, the principle of dynamic covalent reactions of polymer strands on silicon surfaces was fused herein with strongly adherent catechol chemistry. Inspired by the strong adhesion abilities of maritime organisms, such as marine mussels, which adhere to a wide variety of materials, such as wood, rocks, metal or ship coatings, to mention but a few,[15,18] many research groups have investigated these adhesive properties and applied them in different surface projects (2.1.4). Herein, a maleimide-carrying dopamine derivative was employed in DA ligations with a PEG-strand that exhibits a Cp-end group in solution at ambient temperature. PEG was chosen owing to its non-toxicity and water solubility.[158] Due to these abilities PEG already serves as a well-established macromolecular material in medical or pharmaceutical areas.[158,159] The generated PEG-based macro-catechol was attached to different surface (Au, Si, polyethylene (PE)) and several DA/rDA cycles were performed for the model system on gold substrates. Thus, a thermally driven switching system capable to modify surfaces' properties on demand by simply detaching and attaching Cp-functionalized polymers was designed. A schematic overview of the reaction sequence is depicted in **Figure 22**.

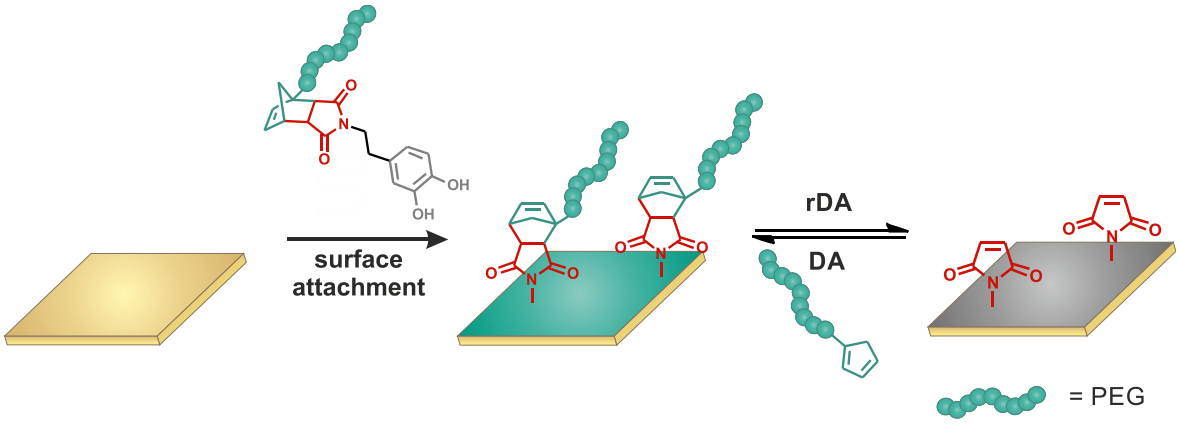

Figure 22: Schematic overview of the attachment of the previously generated macro-catechol (PEG-based) to different substrates (Au, Si, poly(ethylene)) and the thermally driven switching system (DA/rDA) on the model system (Au surface).

Characterization of the small molecules and polymers was conducted by electrospray ionization mass spectrometry (ESI-MS), size-exclusion chromatography (SEC) ESI-MS and nuclear magnetic resonance (NMR) spectroscopy, whilst surface characterization was performed by X-ray photoelectron spectroscopy (XPS).

The detailed experiments and results in solution as well as on the surface are described in the following chapters.

3.1. Diels–Alder conjugation of PEG-Cp and dopamine-maleimide (dM) in solution

In order to verify the DA ability of the presented system, the conjugation reaction was first tested in solution. A catechol based maleimide, namely dopamine maleimide (dM) **(1)**,[69] was ligated with Cp-capped PEG (PEG-Cp) **(2)** (M_n = 2200 g·mol^{-1}) in a DA reaction in DCM at ambient temperature (**Figure 23**).

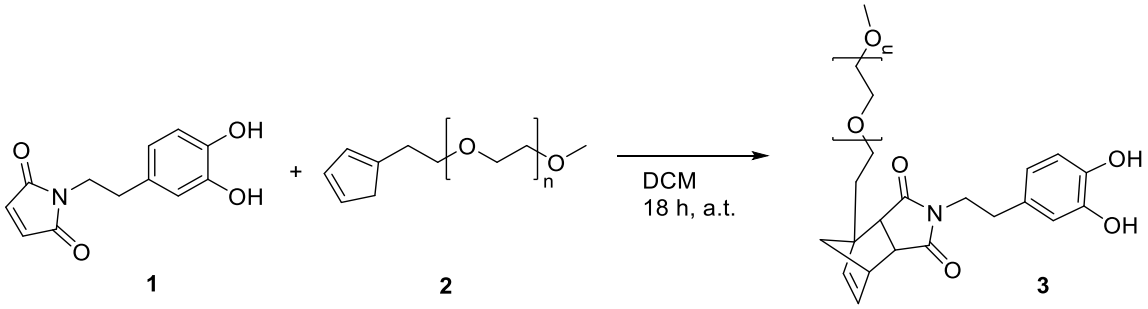

Figure 23: DA conjugation of dopamine maleimide (dM) with PEG-Cp (M_n = 2200 g·mol^{-1}) in DCM at ambient temperature. The macro-catechol dM-PEG **(3)** is generated.

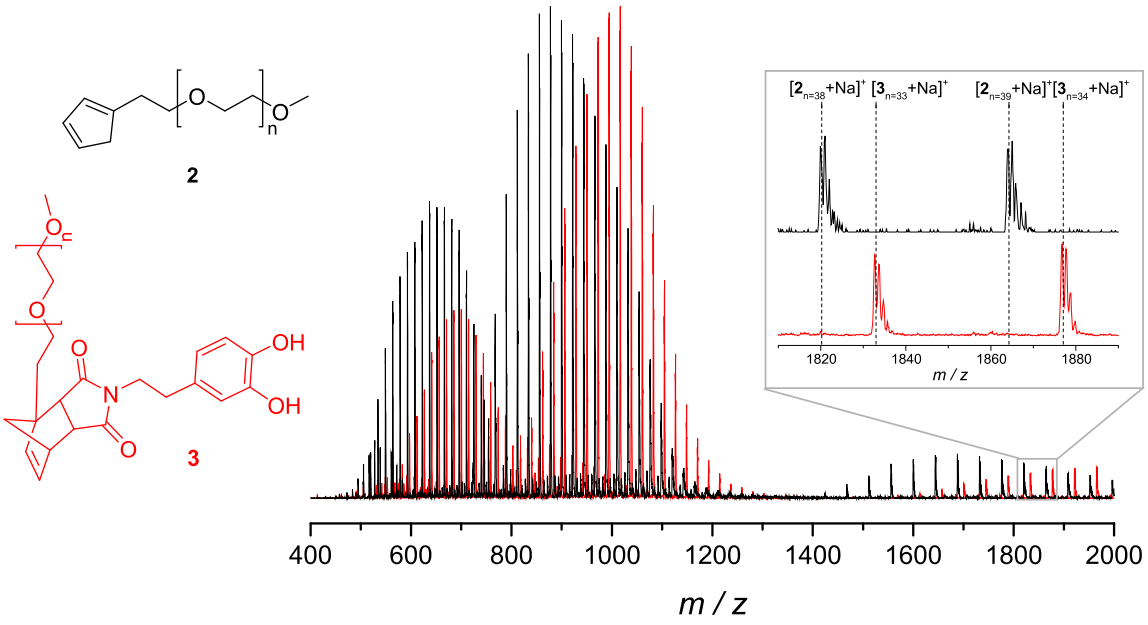

Figure 24: Full ESI-MS spectrum of PEG-Cp **(2)** (black) and the DA product PEG-dM **(3)** (red) including single, double and triple charges. The inset depicts an enlarged area of the spectrum and verifies full conversion of the presented conjugation owing to the disappearance of the signals assigned to pure PEG-Cp **(2)** (black) (e.g. at *m/z* $[\mathbf{2}_{n=38}+Na]^+_{exp}$ = 1820.07) and the appearance of the corresponding signals of PEG-dM **(3)** (red) (e.g. at *m/z* $[\mathbf{3}_{n=34}+Na]^+_{exp}$ = 1877.03). The experimentally detected ESI-MS masses matched the theoretically ones within experimental error.

Complete conversion was evidenced by ESI-MS. **Figure 24** exhibits the full ESI-MS spectra of PEG-Cp **(2)** (black) and the DA cycloadduct PEG-dM **(3)** (red). The molecular weight of the repeating unit (n) for PEG in the molecular weight distribution equals 44.03 g·mol^{-1}. As depicted in the inset, the DA reaction proceeded to full extend as **(2)** (*m/z* [**2**$_{n=38}$+Na]$^{+}_{exp}$ = 1820.07) was completely consumed. In addition, the experimentally detected *m/z* value for n = 34 of **(3)** at 1877.03 is almost identical to the theoretically calculated value (*m/z* [**3**$_{n=34}$+Na]$^{+}_{theo}$ = 1877.04).

As the conducted DA ligation was evidenced to reach full conversion in solution, its applicability to surfaces was assumed. The following steps concerning the desired surface modification and the corresponding results are presented in detail in the next section.

3.2. Diels–Alder/retro-Diels–Alder Ligation of PEG-Cp on dM-Modified Surfaces

The initial path for designing a DA-based switching system was intended to be performed by the simple attachment of pure dM **(1)** straight on a surface by dissolving the starting material in mixture of a 0.3 M tris(hydroxymethyl)methylamine (Tris) buffer solution (pH = 8.5) and MeOH (1 : 1) and immersing a previously cleaned gold substrate over night at ambient temperature. In **Figure 25**, the conducted surface reaction is depicted on the right and was confirmed by XPS characterization (left).

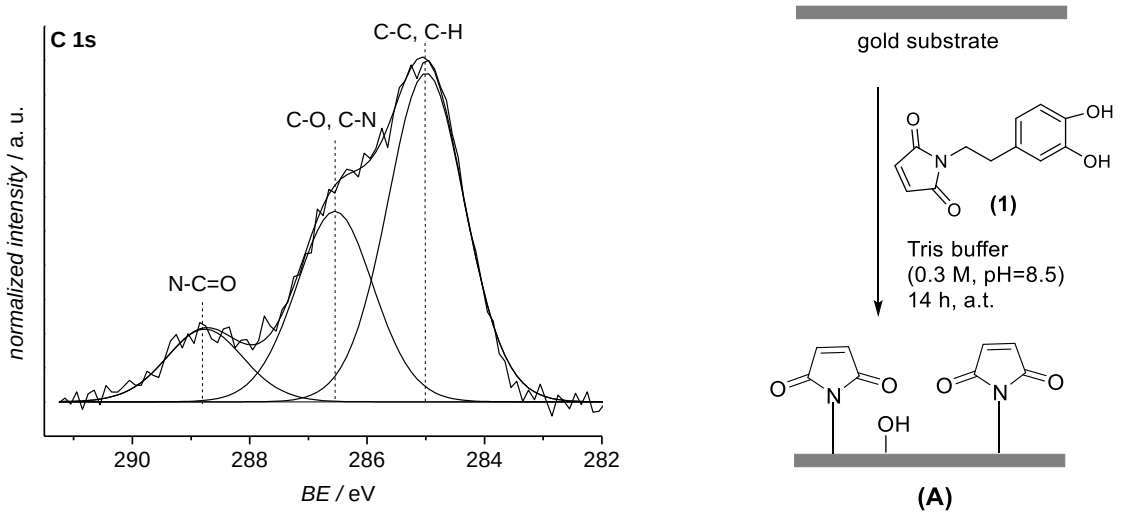

Figure 25: The C 1s XPS spectrum of pure dM **(1)** on a gold substrate **(A)** is depicted on the left. All expected signals were detected. The corresponding attachment reaction is presented on the right.

The C 1s XPS spectrum of pure dM **(1)** on the gold surface **(A)** can be deconvoluted into three components: C-C, C-H at 285.0 eV, C-O, C-N at 286.5 eV and N-C=O at 288.5 eV,[160] which matches the predicted types of functional groups. Interestingly, the peak assigned to the N-C=O bond shows less intensity as expected, which was assumed to result from nucleophilic attacks at the maleimide moiety within the attachment process, due to the slightly basic conditions the system was exposed to. Thus, maleimide functionalities on the surface seemed to be deactivated. These findings were further supported by an additional experiment that was performed to investigate the

desired DA-conjugation ability of the surface-maleimides with PEG-Cp **(2)**, which did not proceed.

Therefore, a second approach, employing the previously prepared PEG-dM **(3)** (Section 3.1) straight on the gold surface, was explored. The complete reaction sequence of the attachment of **(3)** is depicted in **Figure 26**. The starting material **(3)**, in this case, was dissolved in either pure 0.3 M Tris buffer solution (pH = 8.5) or the previously described Tris-MeOH mixture (0.3 M Tris buffer solution (pH = 8.5) : MeOH = 1 : 1) and a gold substrate was immersed for 14 h at ambient temperature to generate the macro-catechol carrying substrate **(B)**. Furthermore, silicon wafers and poly(ethylene) substrates were also treated in the same fashion and showed similar results. Nevertheless, gold was chosen as the model system for the consecutive reactions.

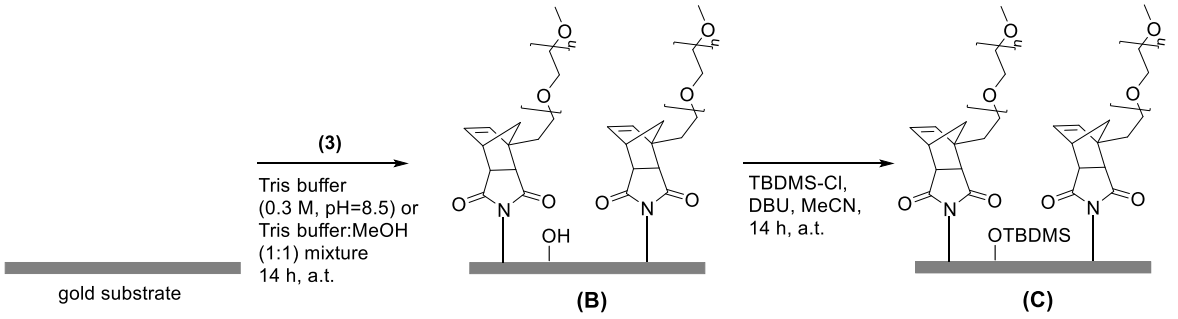

Figure 26: The stepwise surface attachment of PEG-dM and protection of the remaining –OH moieties is illustrated. First, PEG-dM is attached to a gold substrate in a Tris buffer (0.3 M, pH = 8.5) solution or a Tris-MeOH mixture (0.3 M Tris buffer solution (pH = 8.5) : MeOH = 1 : 1) at ambient temperature **(B)**. In a second step, the remaining –OH groups were protected employing TBDMS as a protection group **(C)** in order to suppress a nucleophilic attack at the maleimide moiety during PEG-Cp release in the rDA reaction.

Subsequently, a rDA reaction at 90 °C,[114] followed by a DA reaction at ambient temperature was performed, but did not deliver any positive results for the re-conjugation of PEG-Cp in a further DA reaction. Most likely, the -OH moieties generated in the attachment step function as nucleophiles and attack the maleimide when it is released in the rDA reaction. Therefore, the PEG-dM coated surface **(B)** was treated with *tert*-butyldimethylsiliyl chloride (TBDMS-Cl) and 1,8-diaza-bicycloundec-7-ene (DBU) in acetonitrile at ambient temperature prior to the rDA reaction **(C)** in order to protect the remaining -OH groups (**Figure 26**).

Thereafter, the protected surface **(C)** was employed in a rDA reaction at 90 °C. In order to investigate the switching abilities of the system in several consecutive DA/rDA

cycles, **(D)** was exposed to PEG-Cp **(2)** (M_n = 2200 g·mol^{-1}) in DCM at ambient temperature to perform the DA conjugation on the substrate **(C*)**, whilst the subsequent rDA reaction was conducted in toluene at 90 °C **(D*)**, as specified before (**Figure 27 b**). Owing to the previous protection of any residual catechol groups, the desired rDA and DA reactions proceed smoothly without any disturbing nucleophilic attacks on the designated dM-functionality, which will be discussed in detail in the following paragraph. Thus, the base for a reversibly switchable surface technology with a DA/rDA switch system was established.

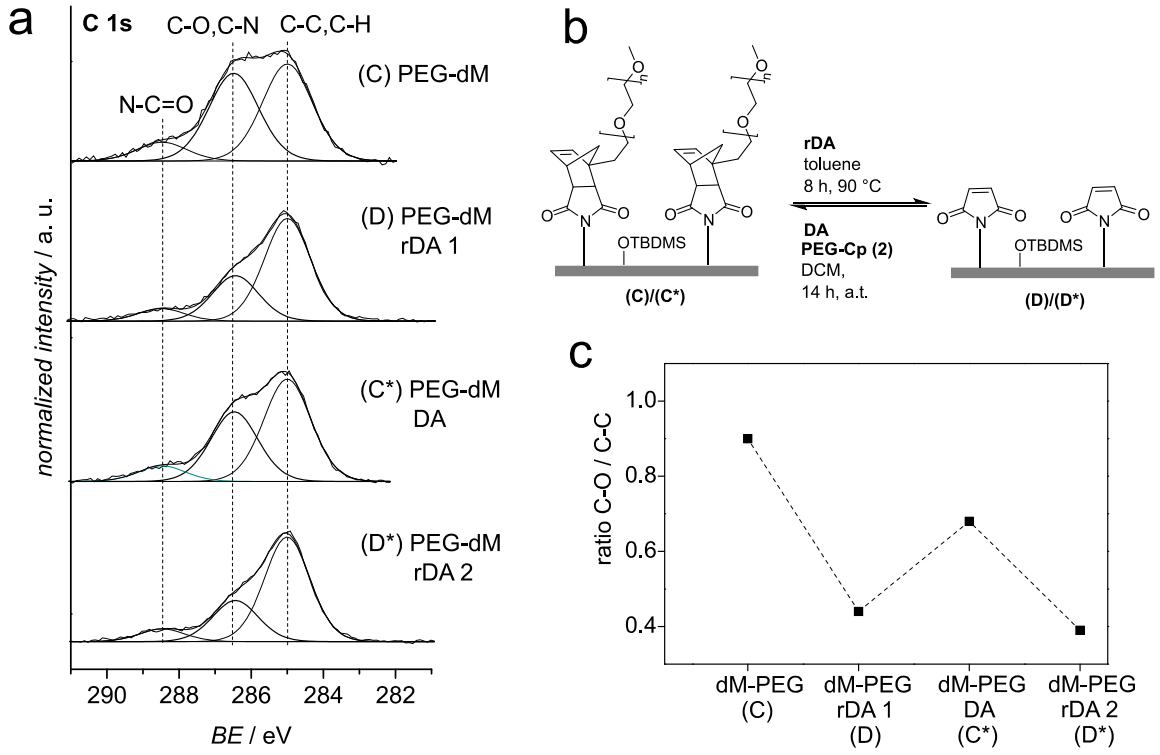

Figure 27: Overview of the rDA/DA cycles, implying the detachment and attachment of PEG-Cp **(2)** from the surface **(C/C*)** or to the surface **(D/D*)**. a) The XPS C 1s spectra of several rDA/DA cycles is depicted. After rDA, the signal assigned to the C-O bonds of PEG at 286.5 eV decreases **(D/D*)**, whereas a following DA reaction with PEG-Cp **(2)** evokes an increase of the same **(C/C*)**. b) The corresponding reaction scheme, including the reaction conditions of the rDA/DA cycles, is illustrated. c) The appropriate C-O/C-C ratios (■) of the C 1s of the rDA/DA reactions are presented and further underline the successful preparation of a switching system.

The successful preparation of the switchable surface **(C)**, as well as the applicability of several rDA/DA switching cycles, indicating the conjugation and release of PEG-Cp **(2)** from a surface **(C/C*)** or to a surface **(D/D*)**, were evidenced *via* XPS characterization (**Figure 27 a**).

The signal assigned to the C-O bonds of PEG at 286.5 eV[161] in the C 1s spectrum decreases after the first rDA reaction **(D)**, increases after a subsequent DA reaction with PEG-Cp **(2)** to form **(C*)** and, finally, declines again after the secondary rDA reaction **(D*)**. Hence, these findings confirm the presence or absence of PEG-Cp on the dM-coated surface. The intensity ratios of the C-O (286.5 eV) and C-C/C-H bonds (285.0 eV) of the C 1s for every surface **(C to D*)** were calculated and are depicted in **Figure 27 c**. The zigzag-shaped trend further emphasizes the previously found results, as it clearly illustrates the decrease and increase of the amount of PEG on the surfaces. Since the ratio of C-O and C-C/C-H bonds after the surface DA reaction **(C*)** is lower than the one previously observed for surface **(C)**, the additional DA reaction seems not to have proceeded to full extend, which is possible caused by the steric requirements of the polymer coil due to different conditions provided on surfaces in comparison to reactions in solution.

3.3. Summary and Outlook

A novel rDA/DA switching system was presented within this chapter. The precursor macro-catechol molecule for the desired surface reactions **(3)** was previously generated in a DA ligation in solution and subsequently attached to substrates. Thereafter, the surface was proven to operate as a switch for covalent linkage and de-linkage employing Cp-carrying PEG as a polymer on gold surfaces. Thus, the present project established the base for an on-demand switching technology for simplified surface modification. As maleimide-Cp conjugation systems were proven to even operate in water,[162] the presented technique is envisioned to be adaptable for applications where aqueous media is required. In addition, variable types of Cp-bearing polymers or biomacromolecules could be applied in such systems in order to change the surface's properties in a reversible fashion, for instance, from hydrophilic to hydrophobic. Moreover, thinking of test-stripes for the control of water quality in rural regions or developing countries, the presented system could serve to attach receptors for monitoring noxious substances (e. g. pesticides, bacteria, insecticides) in drinking water. Furthermore, owing to the reversibility of the Diels–Alder reaction at elevated temperature, recycling of such detectors by simply applying heat and subsequent immersion into a novel or the same solution of a Cp-carrying receptor molecule, could help to create a low cost, independent and on-demand method that serves the desired purposes. However, it needs to be considered that the elevated temperatures in the rDA step represent a limit for the applicability of biomolecules.
Moreover, the reversibility of the novel adherent DA protocol could also be exploited for the remove of undesired art-work, e.g. graffiti, from walls that were previously coated with such a technique, by simply applying heat and consecutive renewal with a suitable Cp-polymer. In addition, the maleimide groups available on the surface can also be employed in thiol-ene reactions or light-induced cycloadditions with photoenol-capable or tetrazole-based compounds in order to create permanently coated substrates and, potentially, spatially resolved patterning on surfaces. In general, the applicability of this technique is expected to be relevant for a wide variety of fields that are dominated by interfacial effects.

The following section further engages in catechol-based thermal DA cycloadditions on surfaces. For this purpose, a new dithio-based HDA precursor was synthesized, which is, besides its adhesion abilities and HDA reactivity, also capable of performing RAFT polymerization in solution.

4

Fusing Polymer Hetero-Diels–Alder Ligation with Bio-Inspired Catechol Attachment

Dithioester compounds are known as well-established controlling agents in RAFT polymerizations, a RDRP technique (2.2.3). Besides their controlling properties, the C=S double bond in the dithioester moiety is also applicable as a dienophile in rapid HDA cycloadditions,[23,163,164] which was yet adapted to polymeric systems (2.3.2).[23,27] For this purpose, Cp-capped molecules or polymers were identified as suitable and highly reactive dienes, implying that the catalyzed conjugation reaction with activated dithioesters operates within seconds at ambient temperature.[26,27] Depending on the type of Z-group (2.2.3), different types of catalysts are employed, however, some systems do not even require a catalyst.[120-122]

Parts of the chapter were reproduced with permission from Preuss, C. M.; Zieger, M. M.; Rodriguez-Emmenegger, C.; Zydziak, N.; Trouillet, V.; Goldmann, A. S.; Barner-Kowollik, C. *ACS Macro Letters* **2014**, *3*, 1169. Copyright (2014) American Chemical Society. XPS characterization was performed by V. Trouillet.

Herein, the activation of the C=S double bond is dependent on the electron-withdrawing abilities of the pyridinyl moiety that serves as Z-group. Thus, TFA is employed as a catalyst in order to protonate the nitrogen in the pyridine ring and consequentially increase the electron withdrawing properties of the Z-group. Within the present project, the already described strong adhesion abilities of catechol anchors are merged with the above described HDA ligation of such a pyridinyl dithioester compound. A new molecule, which exhibits a catechol unit, as well as a dithioester moiety, was synthesized and attached to silicon surfaces under relatively mild and non-toxic conditions, employing a Tris buffer-ethanol mixture at ambient temperature. Consecutive HDA ligations with different polymers bearing a Cp functionality at the α-end, namely PEG and PTFEMA, were conducted in a one-pot rHDA/HDA reaction on the corresponding surface at elevated temperature. PEG was chosen due to its biocompatibility,[158] whereas PTFEMA exhibits excellent detection properties for XPS characterization due to the fluorine present in its backbone. In addition, the HDA-ligation was also investigated in solution to verify the desired reaction path and the rapidness of the conjugation. Furthermore, an intermediate of the new HDA capable catechol was identified to be able to control RAFT polymerizations with styrene or *iso*-bornyl acrylate (*i*BA) as monomers.

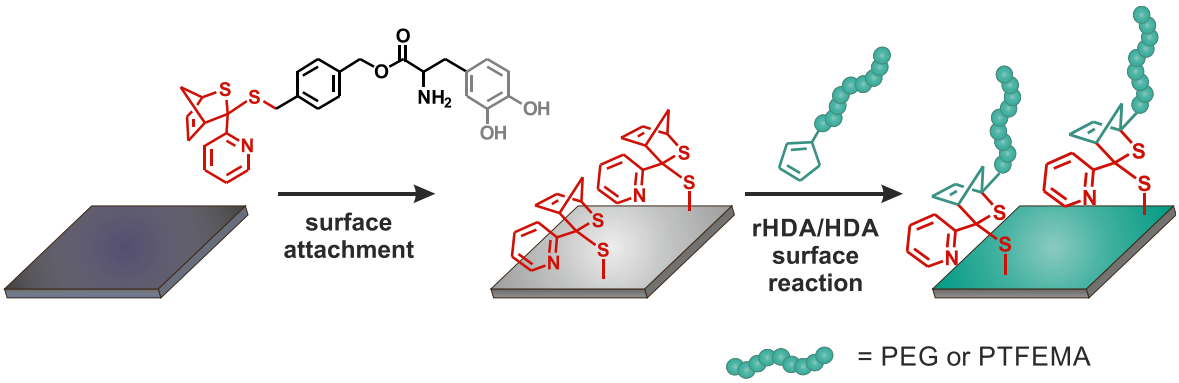

Figure 28: Schematic overview of the surface reaction sequence. A novel dithioester functionalized DOPA-derivative was synthesized and was attached to a silicon wafer under mild conditions. Subsequently, a one-pot rHDA/HDA reaction was conducted in order to tether PEG-Cp or PTFEMA-Cp to the surface.

Characterization of the small molecules was performed by ESI-MS and NMR spectroscopy, whilst surface characterization was executed by XPS and ellipsometry.

The HDA ligations in solution were monitored *via* UV/Vis spectroscopy. Polymer characterization was conducted employing size exclusion chromatography (SEC).

The experimental details and results are described in the following sections.

4.1. Synthesis of HDA-DOPA-Cp

To generate a novel surface modification method combining the strong adhesion abilities of catechols and HDA ligation capability, a new molecule exhibiting both moieties – a DOPA and a dithioester group – was generated. **Figure 29** depicts the full reaction sequence of the small molecule synthesis of the described molecule HDA-DOPA-Cp **(8)**. First, Dithio-OH **(4)**, a pyridinyl-based dithioester that is known for its HDA capability under TFA catalysis at ambient temperature,[165] was coupled to a *tert*-butyldimethylsilyl (TBDMS) and *tert*-butyloxycarbonyl (Boc) protected DOPA-derivative (DOPA-TBDMS$_2$-Boc) **(5)** in a EDC-coupling reaction to generate HDA-DOPA-TBDMS$_2$-Boc **(6)**.

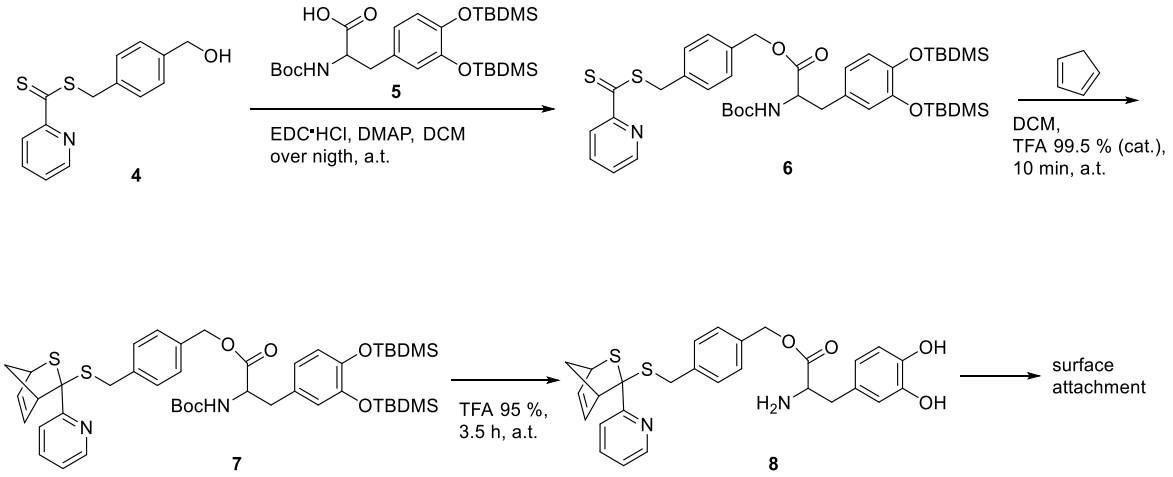

Figure 29: Full reaction sequence for the synthesis of HDA-DOPA-Cp **(8)**. HDA-DOPA-TBDMS$_2$-Boc **(6)** was generated by esterification of Dithio-OH **(4)** and DOPA-TBDMS$_2$-Boc **(5)** utilizing EDC as coupling reagent at ambient temperature. Afterwards, the dithioester group of **(6)** was protected in a HDA ligation with pure cyclopentadiene (Cp) under TFA catalysis in DCM at ambient temperature. The following deprotection step of the -OH and -NH_2 moieties was conducted by exposing **(7)** to TFA (95 %) for 3.5 h in order to achieve HDA-DOPA-Cp **(8)**, which was attached to plasma cleaned Si wafers immediately.

Characterization of **(6)** was performed by ^{1}H and ^{13}C NMR spectroscopy, ESI-MS (**Figure 30**) and UV/Vis spectroscopy (**Figure 32**). Both NMR spectra exhibit the expected signals for **(6)**. The successful coupling of **(5)** and **(4)** is supported by the appearance of the resonances stemming from the aromatic hydrogens in the DOPA unit (16-18), as well as the ones originating from the protection groups (Boc: 13-15, TBDMS: 19-28) in the ^{1}H NMR spectrum. Additionally, the successful synthesis of **(6)** was further evidenced by the detection of its exact mass (*m/z* [**6**+Na]$^+_{exp}$ = 805.4;

m/z [**6**+Na]$^{+}_{theo}$ = 805.3*)* *via* ESI-MS. Furthermore, an absorption maximum at λ_{max} = 348 nm originating from the C=S double bond in the dithioester moiety was detected by UV/Vis spectroscopy (**Figure 32**, left). The corresponding pink color is common for such pyridinyl-dithioesters.

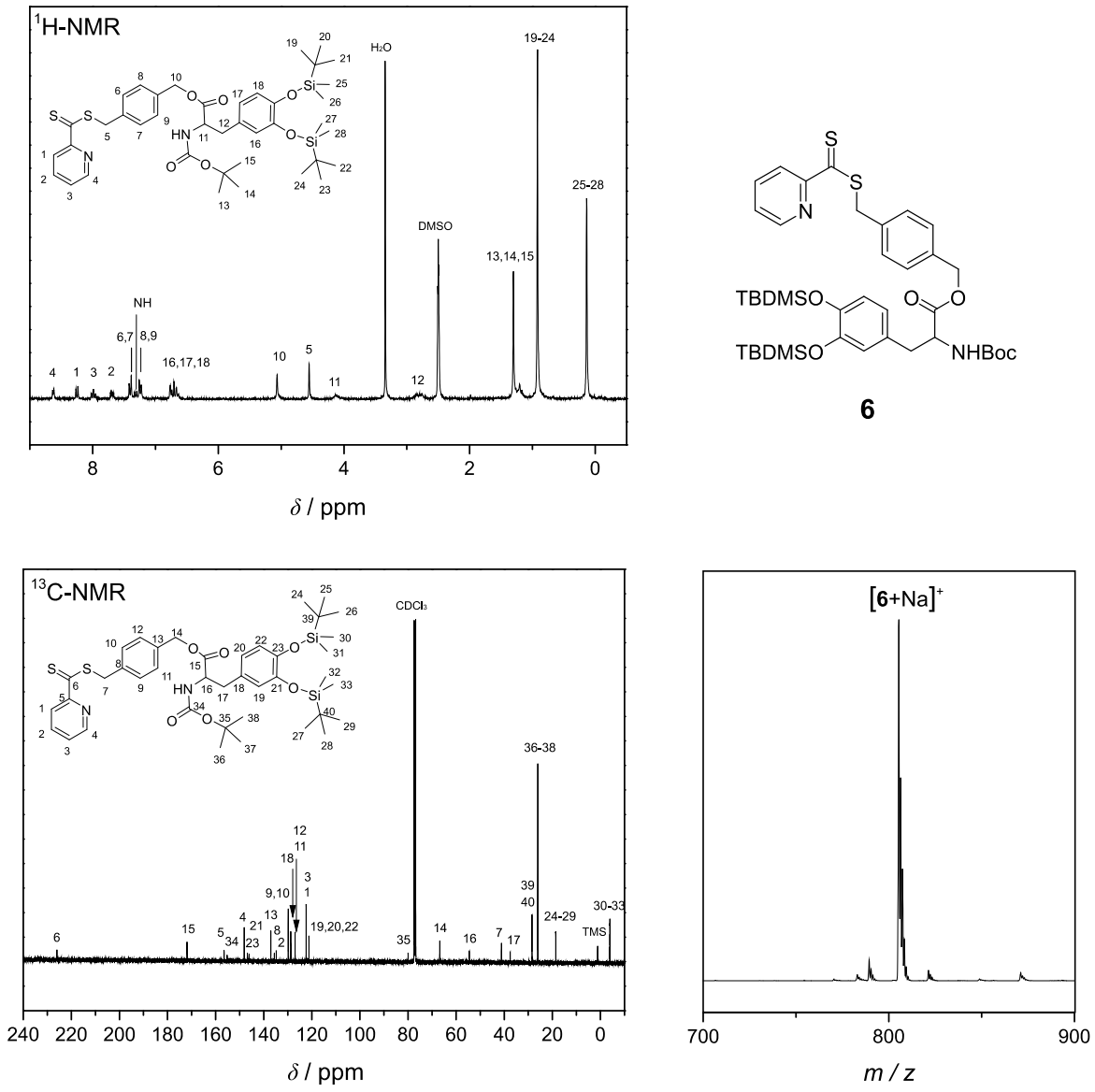

Figure 30: Characterization of HDA-DOPA-TBDMS$_2$-Boc **(6)**. The ^{1}H and ^{13}C NMR spectra are depicted at the top and bottom left and exhibit the expected signals. At the bottom right, the ESI-MS spectrum is illustrated, exhibiting the required mass at *m/z* [**6**+Na^{+}]$_{exp}$ = 805.4 (*m/z* [**6**+Na^{+}]$_{theo}$ = 805.3).

In order to protect the C=S double bond of **(6)** from nucleophilic attacks during the successional surface attachment, HDA-DOPA-TBDMS$_2$-Boc-Cp **(7)** was generated by conjugating **(6)** with pure Cp under TFA catalysis in a HDA reaction. The rapidness of the conjugation is observable by the loss of the pink color of the solution within

seconds (**Figure 32**, the QR code of the corresponding Video 1 is provided in the experimental Section 9.4.2). Consequently, the absorption maximum of **(6)** at λ_{max} = 348 nm in the UV/Vis spectrum was not detectable for the HDA product **(7)** and is, therefore, a supplemental proof for the effectively performed HDA cycloaddition (**Figure 32**, left).

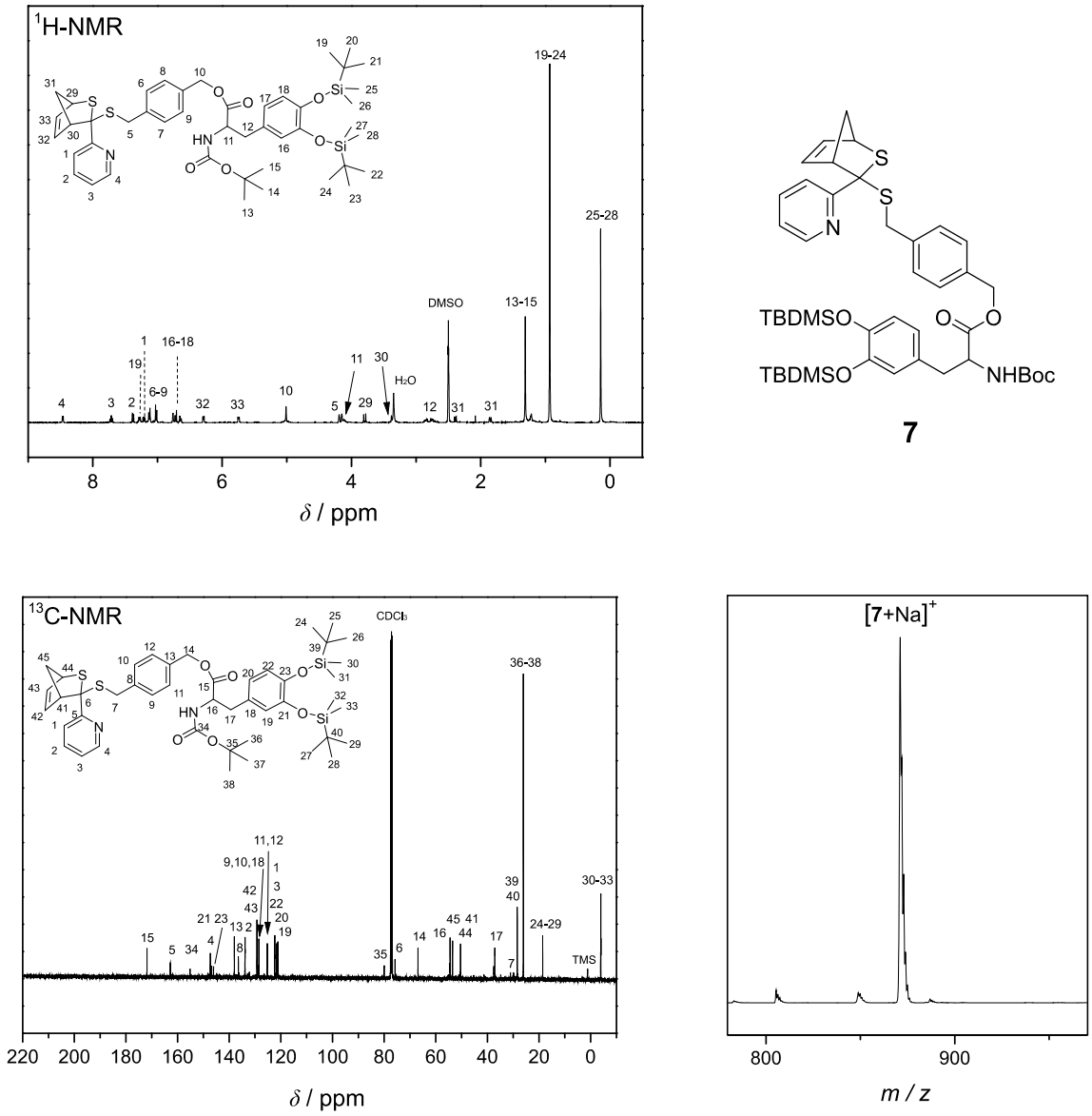

Figure 31: Characterization of HDA-DOPA-TBDMS$_2$-Boc-Cp **(7)**. The respective ^{1}H and ^{13}C NMR spectra are shown at the top and bottom left and exhibit the expected signals. The signal assigned to the carbon atom of the C=S double bond of **(6)** in the ^{13}C NMR in **Figure 30** at 226.02 ppm was shifted to 75.75 ppm for **(7)**, which indicates the loss of the double bond and the formation of a -S-**C**-S- species. At the bottom right, the ESI-MS spectrum of **(7)** is depicted, exhibiting the required mass at *m/z* [**7**+Na]$^+_{exp}$ = 871.1 (*m/z* [**7**+Na]$^+_{theo}$ = 871.3).

In addition, the appearance of the peaks of the hydrogen nuclei of the Cp-unit in the ^{1}H NMR spectrum (29-33) support the findings. Furthermore, the ^{13}C signal assigned to the carbon atom in the dithioester functionality –S-**C**=S at 226.02 ppm in the ^{13}C spectrum of **(6)** (**Figure 30**) was shifted to 75.75 ppm (**Figure 31**) after the HDA ligation **(7)** owing to the loss of the double bond (-S-**C**-S-). The successful results were further underlined by ESI-MS (m/z [**7**+Na]$^{+}_{exp}$ = 871.1; m/z [**7**+Na]$^{+}_{theo}$ = 871.3).

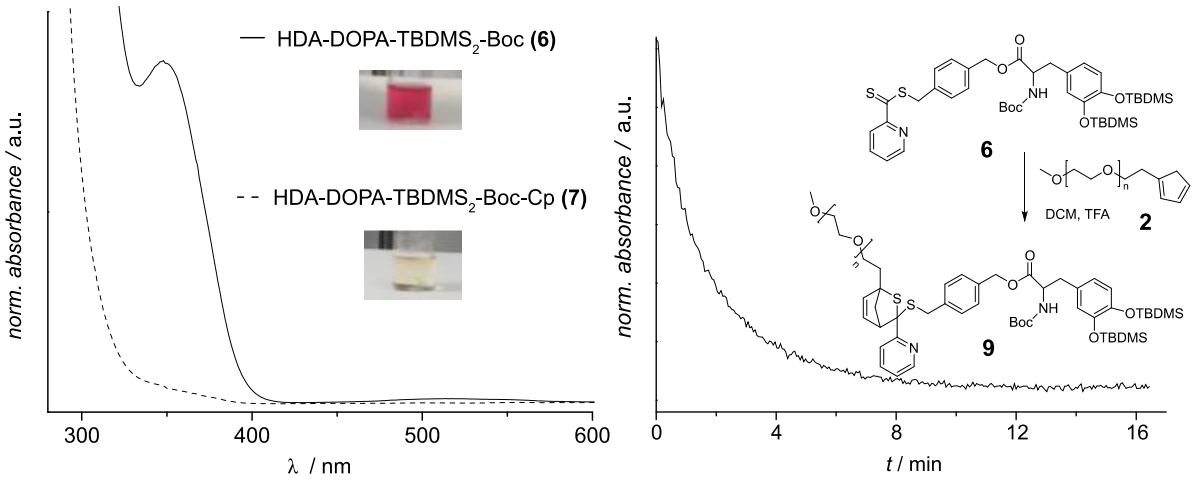

Figure 32: UV/Vis characterization of **(6)** and the conjugation product **(7)** (left), as well as the absorption *versus* time UV/Vis development of the HDA ligation of **(6)** with PEG-Cp **(2)** (right) to form **(9)** are illustrated in this figure. The absorption maximum at λ_{max} = 348 nm for **(6)** vanishes after the successful conjugation with Cp **(7)** (left). Furthermore, the corresponding color change of the solution from pink to clear is also depicted. The HDA polymer ligation ability of **(6)** was proven by conjugation with PEG-Cp (M_n = 2200 g·mol^{-1}) (right) (monitored at λ = 348 nm). Full conversion was achieved within minutes.

The capability of **(6)** to undergo HDA ligations with Cp-capped polymers, which is essential for the later HDA polymer conjugation on the surfaces, was tested by exposing **(6)** to PEG-Cp **(2)** (M_n = 2200 g·mol^{-1}) under TFA catalysis in DCM at ambient temperature (**Figure 32**, right). The formation of the ligation product **(9)** was monitored by a UV/Vis absorption *versus* time experiment. The absorption decreased rapidly within the first 2 minutes. Within 10 minutes, full conversion was reached. Thus, the HDA ability of **(6)** for Cp-polymer conjugation was verified and, therefore, anticipated to be also applicable on surfaces that exhibit a suitable dithioester moiety. In order to transfer the system to surfaces, the Boc- and TBDMS-groups were required to be deprotected, thus, **(7)** was exposed to 95 % TFA for 3.5 hours at ambient temperature (**Figure 29**). The resulting deprotected species HDA-DOPA-Cp **(8)** was identified *via* ESI-MS spectrometry (m/z [**8**+Na]$^{+}_{exp}$ = 543.0 and m/z [**8**+H]$^{+}_{exp}$ = 521.0,

m/z [**8**+Na]$^{+}_{theo}$ = 543.1 and m/z [**8**+H]$^{+}_{theo}$ = 521.1) and immediately applied on the surface of the silicon wafers due to stability reasons.

The subsequent surface attachment and ligation steps will be presented in the following chapter.

4.2. Surface Modification by HDA-Polymer Ligation

As previously described, the novel molecule HDA-DOPA-Cp **(8)** was attached to a plasma cleaned silicon substrate in a mixture of ethanol : Tris-buffer (0.1 M, pH = 8.5) = 1 : 1 at ambient temperature **(E)**, straight after the deprotection of the OH- and NH_2-moieties. The reaction step for the surface attachment, as well as the following synthetic modifications are illustrated in **Figure 33**.

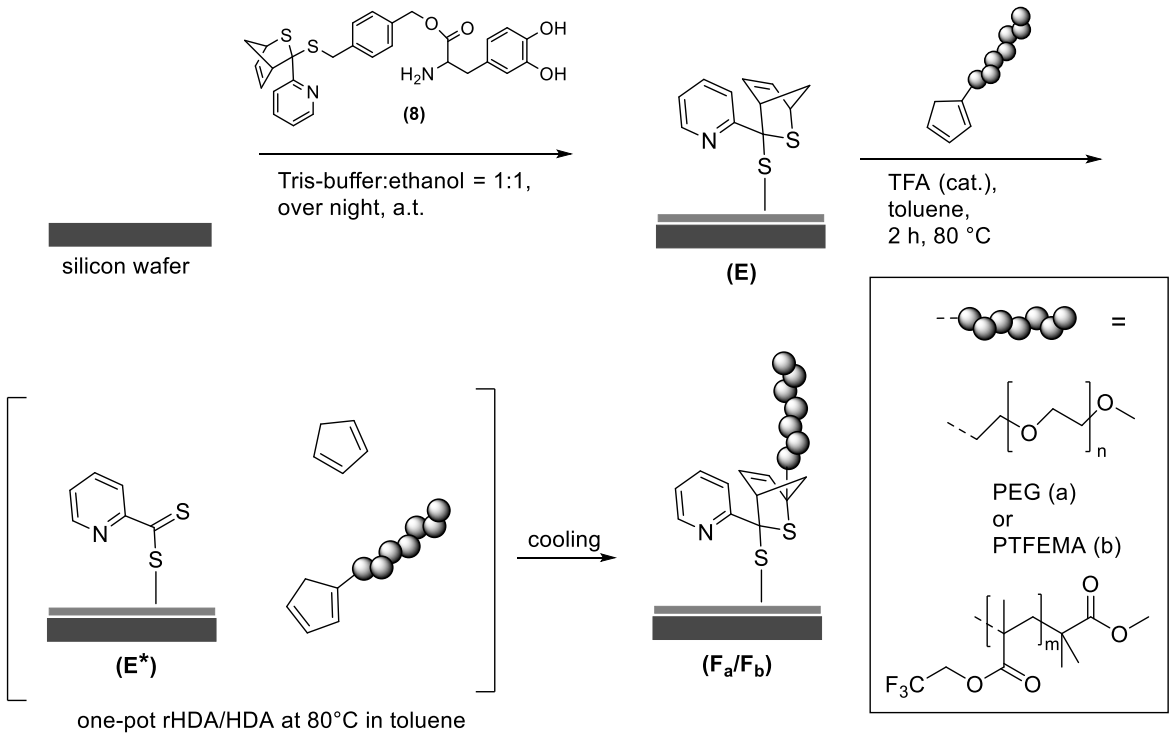

Figure 33: Step-by-step surface modification sequence. First, HDA-DOPA-Cp **(8)** was attached to a silicon wafer **(E)**, before the readily modified substrate was employed in a one-pot rHDA/HDA reaction **(E*)**, where Cp was released upon heating and the subjoined Cp-bearing polymer (either PEG (M_n = 2200 g·mol^{-1}) **(a)** or PTFEMA (M_n = 5200 g·mol^{-1}) **(b)**) underwent a HDA conjugation upon cooling **(F_a/F_b)**.

The dithioester functionalized surfaces **(E)** were further applied in a one-pot rHDA/DA reaction sequence in presence of either PEG-Cp (M_n = 2200 g·mol^{-1}) **(2)** or PTFEMA-Cp (M_n = 5200 g·mol^{-1}) **(10)**, respectively, additionally containing toluene and TFA (catalytic amount) at 80 °C. During the one-pot reaction, Cp was released in a rHDA step and the earlier protected C=S double bond was freed **(E*)**, whereas the appropriate Cp-polymers reconjugated to the dithioester moiety in a HDA reaction

upon cooling **(F_a/F_b)**. In order to demonstrate the rHDA ability in solution, a video (Video 2, QR code available in the experimental Section 9.4.2) of the Cp release at 80 °C was recorded, exhibiting a color change from colorless to pink within one minute due to the reformation of the C=S double bond. The previously described one-pot surface reaction was maintained at 80 °C for 2 h. During cooling, the Cp bearing polymer strands, which were available in excess, underwent the desired HDA ligation.

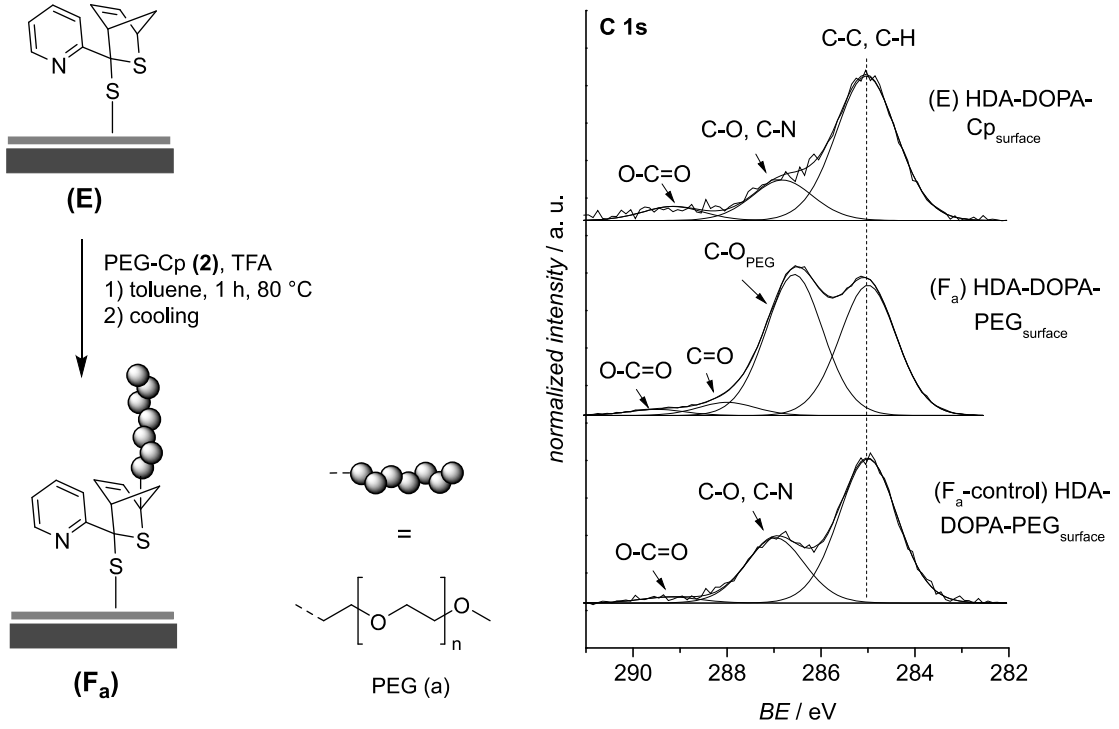

Figure 34: The surface attachment of PEG-Cp **(2)** in a one-pot rHDA/HDA reaction (left) and the corresponding XPS C 1s characterization (right) are shown. The C 1s spectrum of the HDA-DOPA-Cp modified surface **(E)** exhibits the expected signals. After PEG-Cp **(2)** conjugation, the signal assigned to the PEG C-O bonds increases strongly, which proofs the successful attachment *via* HDA **(F_a)**. In addition, an appropriate control experiment **(F_a-control)** was conducted, employing unfunctionalized PEG that showed no attachment of the same, which further underlines the applicability of the method.

In order to evidence that the ligation on the surface proceeded solely *via* HDA conjugation and not simply by adsorption, non-Cp carrying polymers were employed in control experiments, namely $PEG(OMe)_2$ and PTFEMA-Br, which were exposed to the same conditions as their Cp-bearing counterparts in the presence of a substrate **(E)**. Characterization of the prepared surfaces was performed by XPS (**Figure 34**, **Figure 35**) and ellipsometry.

The corresponding C 1s XPS spectra of the surface attachment of PEG-Cp **(F_a)** and the respective control sample **(F_a-control)** are illustrated in **Figure 34**. After surface HDA conjugation of PEG-Cp, the substrate exhibits a strong increase of the signal assigned to the C-O bonds at 286.6 eV in the C 1s spectrum, which originates from the PEG backbone and, hence, verifies the successful attachment.[166] In addition, the performed control experiment **(F_a-control)** underpins that the reaction only operates in the presence of a Cp moiety and no adsorption occurs, as no increase in the signal appertained to the PEG C-O bonds was detected. Furthermore, the results were also confirmed *via* ellipsometry, which presents an increase of about 9 nm in thickness on the PEG-containing substrate **(F_a)** in comparison to **(E)** and **(F_a-control)**.

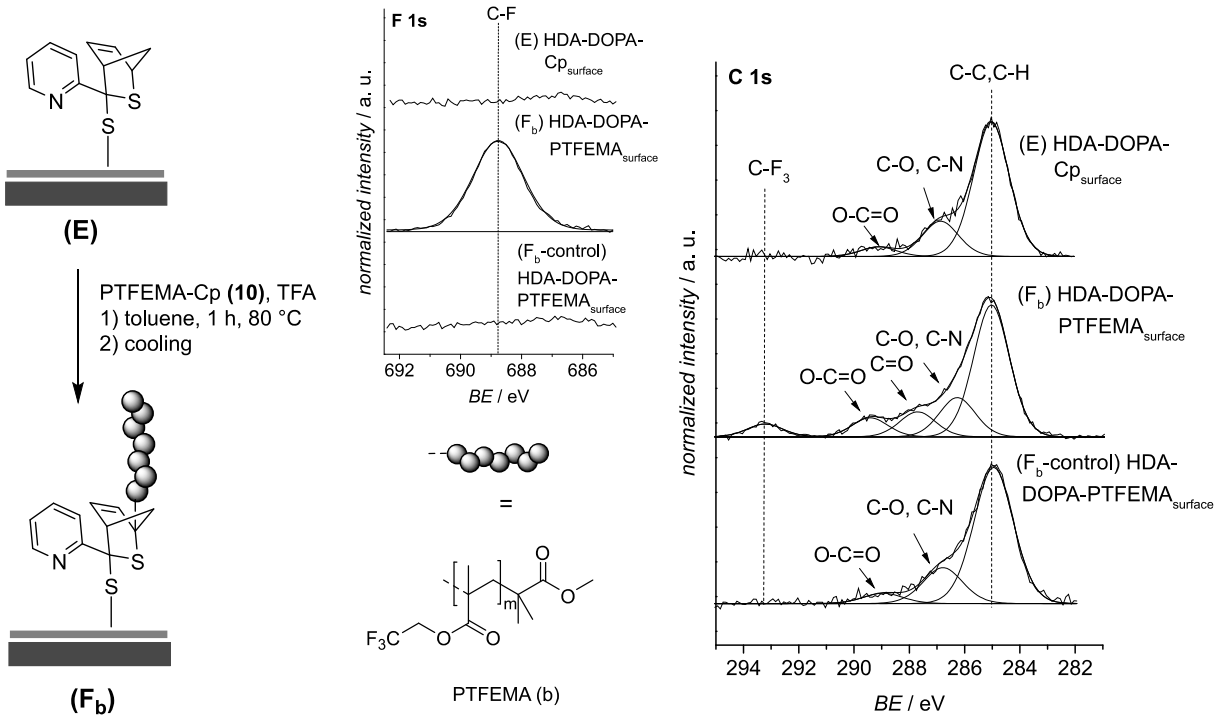

Figure 35: The surface attachment of PTFEMA-Cp **(10)** (or **(b)** for the PTFEMA chain attached to Cp) in a one-pot rHDA/HDA reaction (left) and the appropriate C 1s and F 1s XPS characterizations (right and center top) are depicted. The C 1s spectrum of the HDA-DOPA-Cp modified surface **(E)** exhibits the expected signals. After PTFEMA-Cp **(10)** conjugation, the signal assigned to the C-F bonds in the $-CF_3$ moiety at 293.2 eV appeared **(F_b)** in the C 1s spectrum, which proofs the successful attachment. Furthermore, the F 1s spectrum shows the emergence of a fluorine signal only for **(F_b)** at 688.8 eV. In addition, an appropriate control experiment **(F_b-control)** was performed, employing PTFEMA-Br, displaying no attachment of the same, which further underpins the applicability of the system.

To confirm the HDA ligation of PTFEMA-Cp with the *in situ* released dithioester moiety provided on the substrate **(E)**, the C 1s and the F 1s XPS spectra of **(F_b)** were compared to the ones of **(E)** and the appropriate control sample **(F_b-control)** (**Figure 35**),

respectively. The appearance of an additional peak in the C 1s of **(F_b)** at 293.2 eV, which can be assigned to the C-F bonds in the CF_3 moiety of the PTFEMA backbone, indicates the attachment of the same.[167] Additionally, the F 1s spectrum of **(F_b)** also presents a signal at 688.8 eV, which clearly originates from the C-F bonds in the conjugated PTFEMA backbone, and further verifies the previous findings.[167] Furthermore, the ratio of the quantity of carbon provided in the $-CF_3$ functionality in the C 1s and the amount of fluorine available in the F 1s was identified to equal 1:3 (1×C : 3×F), and thus, serves as additional proof for the previously discussed results. Moreover, the respective C 1s and F 1s XPS spectra of the control samples **(F_b-control)** do not exhibit any attachment of PTFEMA and are, therefore, additional evidence that no adsorption of the polymer strand occurred. Paying attention to the ellipsometry measurements, the increase of thickness on substrate **(F_b)** in comparison to **(E)** or **(F_b-control)** does not turn out as strong as for the corresponding PEG surface **(F_a)**, most likely owing to the steric hindrance in the PTFEMA backbone.

In the present chapter, the novel dithioester-based HDA conjugation system, which was described in Section 4.1 was successfully applied to surfaces. Different Cp-bearing polymer strands were tethered to the modified substrates. The described method can be envisioned to be extended to a wide variety of Cp-polymers to change the properties of various surfaces on demand.

In order to present a rough estimation of the theoretically assumed grafting density of a polymer strand in such a *grafting-to* system, the following simplified calculations were performed for the prepared PEG surface **(F_a)**. For this purpose, it was assumed that the surface is perfectly flat and homogeneous. Furthermore, it was assumed that the density of the polymer chains on the surface $\rho_{PEG,surface}$ (note: not the chain density) would be similar to the one of the bulk material (ρ_{bulk} = 1.08 g·mol^{-1} at 25 °C, $PEG(OMe)_2$, M_n ≈2000.0 g·mol^{-1}, Aldrich, see section 9.1.1), which will deliver an approximate value. Thus, the chain density σ_{chains} was defined as

$$\sigma_{chains} = \frac{N_{PEG,surface}}{A_{surface}} \tag{4.1}$$

where $N_{PEG,surface}$ is the number of chains on the PEG-grafted surface and $A_{surface}$ is the surface's area. As

$$N_{PEG,surface} = n_{PEG,surface} \cdot N_A \tag{4.2}$$

where N_A depicts the Avogadro's number and $n_{PEG,surface}$ the amount of substance, and

$$n_{PEG,surface} = \frac{m_{PEG,surface}}{M_{n,PEG,surface}} \tag{4.3}$$

with $m_{PEG,surface}$ as the mass auf the PEG chains on the surface and $M_{n,PEG,surface}$ as the number average molecular mass of the same, the chain density equals:

$$\sigma_{chains} = \frac{m_{PEG,surface} \cdot N_A}{M_{n,PEG,surface} \cdot A_{surface}} \tag{4.4}$$

Further, the mass $m_{PEG,surface}$ can be determined *via*

$$m_{PEG,surface} = V_{PEG,surface} \cdot \rho_{PEG,surface} \tag{4.5}$$

where $V_{PEG,surface}$ is the Volume of the PEG chains on the surface and $\rho_{PEG,surface}$ is the density of PEG, which gives

$$\sigma_{chains} = \frac{\rho_{PEG,surface} \cdot V_{PEG,surface} \cdot N_A}{M_{n,PEG,surface} \cdot A_{surface}} \tag{4.6}$$

The volume $V_{PEG,surface}$ equals

$$V_{PEG,surface} = A_{surface} \cdot t_{PEG,surface} \tag{4.7}$$

where $t_{PEG,surface}$ depicts the thickness of the PEG layer. After inserting this term and canceling out of the surface area $A_{surface}$ the chain density is found to be:

$$\sigma_{chains} = \frac{\rho_{PEG,surface} \cdot t_{PEG,surface} \cdot N_A}{M_{n,PEG,surface}} \tag{4.8}$$

With $\rho_{PEG,surface}$ = 1.08 g·cm^{-3}, $t_{PEG,surface}$ = 9·10^{-7} cm (from ellipsometry measurements), N_A = 6.022·10^{23} mol^{-1} and $M_{n,PEG,surface}$ = 2200 g·mol^{-1} ($M_{n,PEG,surface}$ = $M_{n,PEG\text{-}Cp}$), the chain density equals:

$$\sigma_{chains} = \frac{1.08\ g \cdot cm^{-3} \cdot 9 \cdot 10^{-7} cm \cdot 6.022 \cdot 10^{23} mol^{-1}}{2200\ g \cdot mol^{-1}} \tag{4.9}$$

$$\sigma_{chains} = 2.66 10^{14} cm^{-2} = \underline{\underline{2.66\ nm^{-2}}}$$

Thus, the calculated grafting density of PEG chains σ_{chains} on the surface equals 2.66 chains per nm^2. Previously, grafting densities in a dimension of 0.1-0.67 chains/nm^2 were reported.[168-170] Hence, the grafting density for the PEG covered surface **(F_a)** exceeds the previously reported values, which is certainly partially caused by the assumptions made prior to the calculation. However, such high grafting densities can only be achieved with highly efficient and very fast *grafting-to* methods. Thus, the thermal HDA system presented herein appears to provide excellent abilities in this regard.

In order to assess the brush-like nature of the grafted PEG film on the surface the reduced tether density Σ was determined by the following equation:[171]

$$\Sigma = \sigma_{chains} \cdot \pi \cdot R_G^2 \tag{4.10}$$

With R_G as the radius of gyration, which was achieved from data provided in Ref. 45, and adjusted by the scaling principle to give R_G = 2.02 nm in water. Thus, the reduced tethering density equals:

$$\Sigma = 2.66\ nm^{-2} \cdot \pi \cdot (2.02\ nm)^2 \tag{4.11}$$

$$\Sigma = \underline{\underline{34.1}}$$

Brittain *et al*. reported that if Σ exceeds 5, the tethered polymer chains on the surface exhibit "true brushes" characteristics,[171] which is provided by the presented surface **(F_a)**. Thus, the grafted polymer chains exhibit an extremely stretched brush regime.

As previously pointed out, the intermediate molecule HDA-DOPA-TBDMS$_2$-Boc **(6)** was identified to function as a controlling agent in RAFT polymerizations of styrene or *iso*-bornyl acrylate (*i*BA). The following chapter examines these findings.

4.3. RAFT Polymerizations Controlled by HDA-DOPA-TBDMS$_2$-Boc (6)

Besides their HDA ability, dithioesters are also well-known as controlling agents in RAFT polymerizations. For this reason, the intermediate HDA-DOPA-TBDMS$_2$-Boc **(6)** was tested for its controlling ability in a kinetic study employing styrene, as well as *i*BA as monomers. The bulk polymerizations were initiated with AIBN and conducted at 60 °C. Samples were taken at different points of time as outlined in the corresponding Figures (**Figure 36**, **Figure 37**).

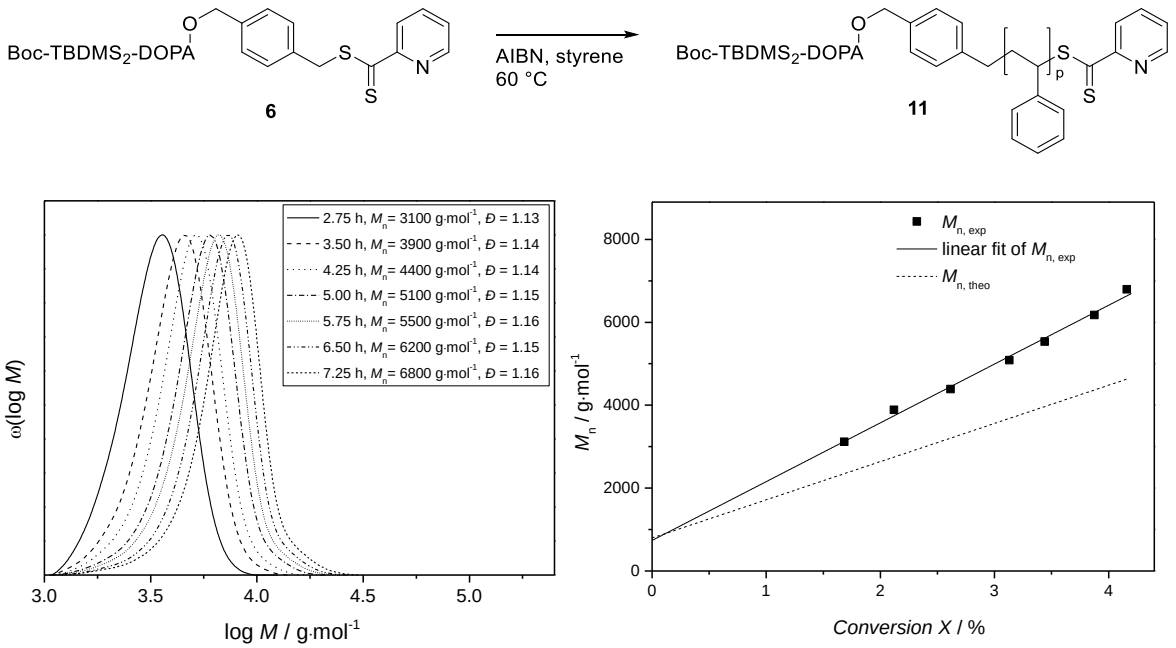

Figure 36: RAFT polymerization and kinetic study of styrene, employing HDA-DOPA-TBDMS$_2$-Boc **(6)** as controlling agent. The polymerization conditions and the chemical structures are depicted at the top. Seven samples were taken at different points of time between 2.75 h and 7.25 h of polymerization time as depicted in the inset (left). On the left, the corresponding SEC traces are shown. On the right, the achieved molecular weights (number average) (■) are plotted against conversion *X*. The appropriate theoretically calculated molecular mass development is presented as a dashed line (---).

The RAFT polymerization of styrene was conducted for 7.25 hours. Seven different samples of the polystyrene (PS) **(11)** were taken, beginning with the first one after 2.75 h (**Figure 36**, **left**). The corresponding SEC traces of the samples, as well as the detected dispersities (*Đ*) and molecular weights (number averages) (M_n) lead to the assumption that the polymerization proceeds with living characteristics. In addition, the experimentally found molecular weights M_n (■) were compared to the theoretically

calculate values (---) (**Figure 36**, right) and plotted against conversion *X*. Linear correlation is shown, which is one of the main criteria of RDRPs, apart from narrow dispersities *Đ* (also provided) and reactivation of chain ends (Section 2.2.1).

The theoretical values for M_n were calculated *via* the following simplified equation adapted from Ref. 172 and extended by the addition of the molecular weight of the RAFT agent M_{RAFT}

$$\overline{M}_n = \frac{[S]_0 - [S]_t}{[RAFT]_0} M_S + M_{RAFT} \tag{4.12}$$

where $[S]_0$ and $[S]_t$ describe the concentration of styrene at the beginning (t = 0) and after a certain time t, $[RAFT]_0$ represents the concentration of the RAFT agent at t = 0, M_S and M_{RAFT} are the molecular masses of styrene or **(6)**, respectively. The linear fit of the experimental M_n values exhibits a high gradient in comparison to the graph of the calculated values, which is caused by the approximations made for equation (4.12), as well as the error of the SEC measurements,[173] where the experimental M_n values were obtained from.

In order to survey the controlling abilities of **(6)** for a different monomer, namely *iso*-bornyl acrylate (*i*BA), an additional experiment was performed, taking four samples at different instants of time as depicted in **Figure 37**.

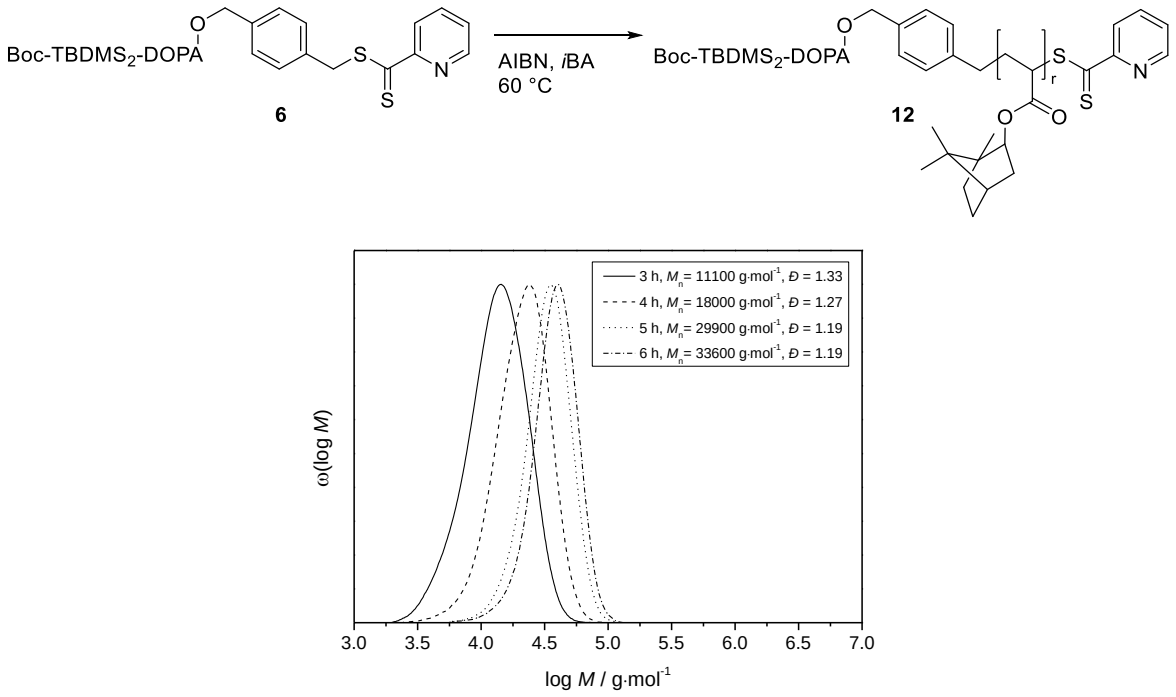

Figure 37: RAFT polymerization and kinetic study of *iso*-bornyl acrylate (*i*BA), employing HDA-DOPA-TBDMS$_2$-Boc **(6)** as controlling agent. The polymerization conditions and the chemical structures are depicted at the top. Four samples were taken at different points of time between 3 h and 6 h of polymerization time as shown in the inset (bottom). At the bottom, the corresponding SEC traces, as well as the achieved molecular weights M_n and dispersities $Đ$, are depicted.

The controlling skills of **(6)** were also confirmed for the described system, even though the dispersities $Đ$ of poly(*i*BA) (P*i*BA) **(12)** were not as low as the ones of PS. Nevertheless, the adaptability of the designed RAFT agents **(6)** to other monomer systems was verified.

4.4. Summary and Outlook

The current chapter described the establishment of a thermal HDA conjugation based modular surface modification method. A novel catechol-bearing and HDA-capable molecule was designed and successfully applied on silicon substrates. The attachment of different types of polymers (PEG, PTFEMA) was achieved. Furthermore, one of the intermediate molecules **(6)** was identified to be capable of operating as a controlling agent in RAFT polymerizations with styrene and *i*BA.

The present approach provides the base for future efforts with regard to the generation of hierarchical structures on virtually any surface by simply grafting of Cp-bearing compounds that exhibit a second but orthogonal ligating moiety, to the substrate in a one-pot rHDA/HDA reaction, followed by a subsequent second conjugation step with a suitably functionalized polymer. Besides the attachment of additional macromolecules, bioreceptors could also be ligated in the second conjugation step – given that mild conditions are provided – in order to generate surfaces for biosensing purposes. With regard to this, the present system needs to be improved and, ideally, be transferred to aqueous media.

Moreover, a second route for preparing hierarchical structures can be envisioned by further benefiting from the already available, but protected, dithioester moiety on the surfaces **(E)**. The novel RAFT agent **(6)** was proven to operate as controlling agent in RAFT-polymerizations in bulk. Thus, the deprotection of the Cp-protected dithio-moiety on the surface **(E)** and a subsequent SI-RAFT polymerization with a selected monomer could generate a novel *grafting-from* approach. However, in case this approach is conducted, it needs to be assured that no side reactions, such as nucleophilic attacks, are interfering after the release of the dithio-moiety. After polymerization of a certain monomer, a second block could be prepared from a different monomer, for instance MeOEGMA in order to achieve non-fouling properties, in a consecutive RAFT polymerization or by exploiting the HDA-capability of the dithioester for the thermal HDA ligation of a second block. However, the present method still requires TFA as a catalyst for the successful HDA conjugation. Thus, the improvement of the system could be achieved by employing a cyano moiety as a Z-group, which was already applied in catalyst-free HDA protocols.[121,122] Furthermore,

synthesis protocols for the preparation of complex structures in aqueous environment are widely desired. Therefore, by employing water-soluble polymers, the current approach is envisioned to be merged with the recently presented ultra-fast catalyst-free macromolecular ligation protocol by Glassner *et al.*, which allows HDA reactions of dithioesters in water at ambient temperature.[120]

In addition, the capability of **(6)** to function as a RAFT agent in bulk polymerizations of styrene and *i*BA could be further employed for the preparation of defined polymer strands from other monomers or for the generation of block copolymers in solution. A consecutive deprotection step that releases the catechol moiety (deprotection from TBDMS-groups) offers novel routes for the attachment of precisely designed polymer strands to surfaces or nanoparticles *via* their catechol-unit. The presented system establishes new path for the design of versatile macromolecular structures.

In a summary, these HDA-based surface ligation methods are envisioned to be applicable for the fabrication of biosensors or simple point-of-care devices, for instance for the detection of individual bacteria or pesticide species. The preparation of more complex material – in terms of spatially control – can be achieved by light-triggered conjugation techniques, which are also in the scope of the current thesis (Chapter 5-6).

The previous and present chapter summarized the results accomplished for versatile catechol anchor-based surface modification techniques conducted by thermal polymer cycloadditions protocols. Gazing into a different area of [4+2]-cycloadditions, the following chapter introduces the combination of catechol anchors and photo-induced DA cycloadditions for spatially controlled surface design.

5

Photoenol Ligation Fused with Catechol Anchoring for Spatially Controlled Surface Modification

Contrary to the described thermal Diels–Alder systems within this thesis, which were based on the [4+2]-cycloaddition of available dienes with dienophiles, in the upcoming approach, the reacting diene needs to be generated first by a light-induced isomerization, before conjugation with a dienophile. The described photo-induced diene moiety, namely photoenol, was already introduced to polymer science by Gruendling *et al.* (2.3.2).[22] By irradiation of such a *o*-methylphenyl ketone or aldehyde, herein a 2-formyl-3-methylphenoxy (FMP) moiety, with UV light (320 nm),[28] a photoenol functionality is generated by isomerization and can subsequently react with highly reactive dienes such as maleimides, for instance.

Parts of the chapter were reproduced from Preuss, C. M.; Tischer, T.; Rodriguez-Emmenegger, C.; Zieger, M. M.; Bruns, M.; Goldmann, A. S.; Barner-Kowollik, C. *Journal of Materials Chemistry B* **2014**, *2*, 36 by permission of The Royal Society of Chemistry (Copyright 2014). Tof-SIMS analysis was performed by Dr. M. Bruns. Mal-peptide was supplied by Prof. H. Börner and K. Linkert (HU Berlin).

In comparison to the previously reported 2-methylbenzophenone derivative,[22] FMP exhibits an ether moiety at one *ortho*-position, which was identified as a far more efficient precursor for the photo-induced DA reaction.[28] As light-triggered conjugation reactions serve as perfect systems for the generation of spatially controlled polymer ligations on surfaces,[28,29] the described method was fused with the principle of catechol anchoring, inspired by the strong adhesion properties of marine mussels. For this purpose, a novel molecule that bears a catechol and a FMP moiety was designed. The molecule was then attached to several different substrates and a variety of maleimide terminated macromolecules, such as PEG-Mal, PTFEMA-Mal and a model peptide sequence (PEP-Mal) was attached by irradiation in a so-called photoenol reaction. PEG was used owing to its significance in medical and pharmaceutical areas based on its passivating character against non-specific adhesion,[158,174] whereas the peptide was utilized to demonstrate the method's ability to ligate biomolecules. In order to achieve spatial control, the previously prepared FMP bearing substrate was covered with a meander-shaped shadow mask to ensure that irradiation and, therefore, the desired DA reaction only occurs in the uncovered (meander shaped) area. As dienophile, PTFEMA-Mal was employed due to its excellent detectability in time-of-flight secondary ion mass spectrometry (ToF-SIMS) analysis, originating from the fluorine in its backbone. Furthermore, photoenolization proved as a convenient tool as no side-products nor fluorescence is generated in the conjugation process.

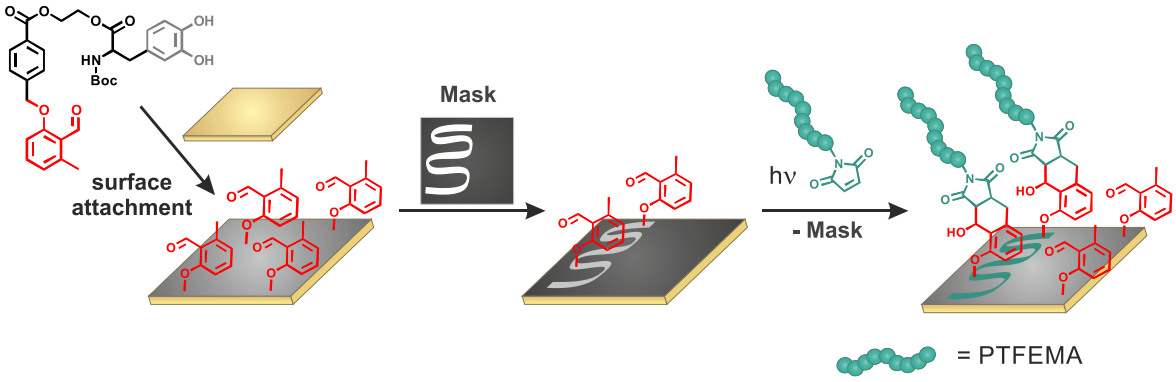

Figure 38: Reaction sequence of the light-induced DA reaction (photoenol reaction) of an *o*-quinodimethane derivative and a maleimide bearing macromolecule. The catechol carrying photoenol precursor was first attached to different substrates before the photo-induced DA reaction was conducted. To demonstrate that spatial control is achievable, a meander shaped shadow mask was employed on the surface during irradiation, which leads to attachment of the model polymer PTFEMA-Mal only in the uncovered areas of the meander shape.

Characterization of the small molecules was conducted *via* ESI-MS and NMR spectroscopy, whilst surface characterization was performed by XPS and ToF-SIMS analysis, as well as contact angle measurements. Polymer characterization was conducted employing SEC. The detailed experiments and results are described in the following chapters.

5.1. Synthesis of the Catechol-based Photoenol Precursor

A novel small molecule, Photo-DOPA **(16)**, bearing a catechol unit, for surface attachment, as well as a FMP moiety, for photoenolization purposes, was designed. The full reaction sequence is provided in **Figure 39**.

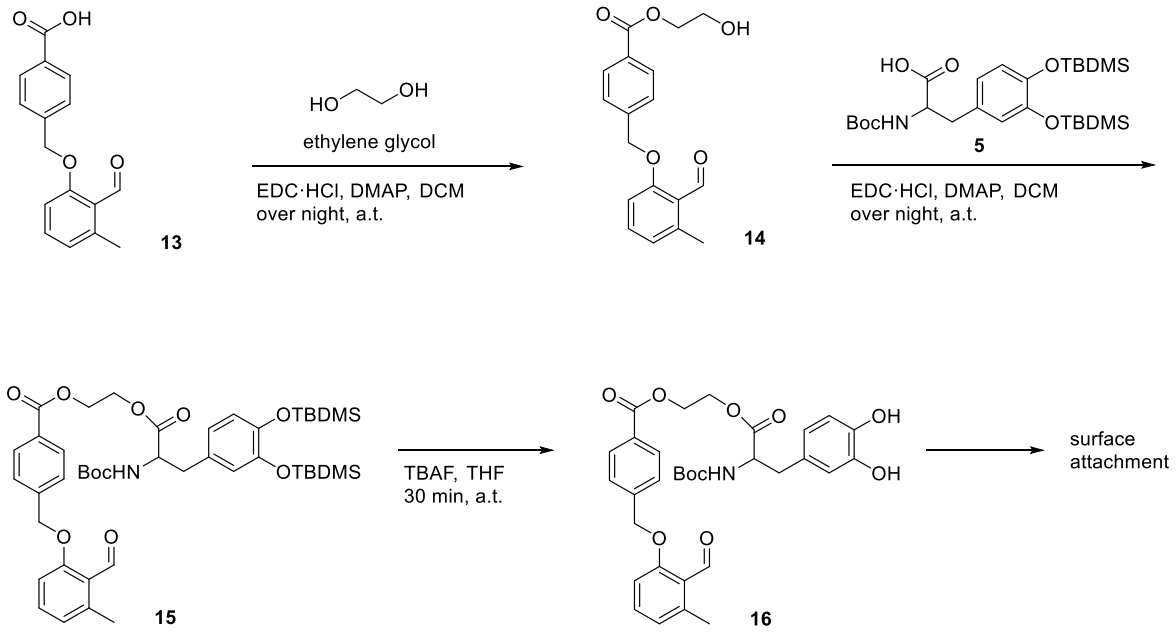

Figure 39: The full reaction scheme for the formation of Photo-DOPA **(16)** is depicted. First, a Steglich-type coupling reaction was performed, employing Photo-COOH **(13)** and ethylene glycol, which serves as linker that provides an additional –OH unit, to generate Photo-Gly **(14)**. In a second esterification step, **(14)** was reacted with a previously Boc- and TBDMS-protected DOPA **(5)** at the carboxylic acid moiety at ambient temperature. In order to remove the TBDMS-protection groups, Photo-DOPA-$TBDMS_2$ **(15)** was exposed to TBAF in THF for 30 minutes. The achieved deprotected substance Photo-DOPA **(16)** was subsequently employed in surface attachment reactions.

Starting from methyl Photo-COOH **(13)**,[28] an ethylene glycol spacer was attached in a Steglich esterification type reaction with 1-ethyl-3-(3-dimethylaminopropyl) carbodiimide hydrochloride (EDC·HCl) in DCM under DMAP catalysis at ambient temperature in order to provide a -OH moiety for the next step, to form Photo-Gly **(14)**. The corresponding ^{1}H and ^{13}C NMR spectra, as well as the ESI-MS spectrum are depicted in **Figure 40**. In the ^{1}H-NMR spectrum, the attachment of the ethylene glycol linker was verified by the appearance of signal 11 and 12 at 3.98 ppm and 2.59 ppm, respectively, which represent the H nuclei of the CH_2 groups of the same (**Figure 40**, top left). The ^{13}C NMR spectrum exhibits all desired resonances and further supports

the successful attachment of the ethylene glycol linker. Furthermore, an ESI-MS spectrum was recorded, demonstrating the desired exact mass at *m/z* [**14**+Na]$^{+}_{exp}$ = 337.16. The experimentally found value is suitable with the theoretically calculated one at *m/z* [**14**+Na]$^{+}_{theo}$ = 337.10.

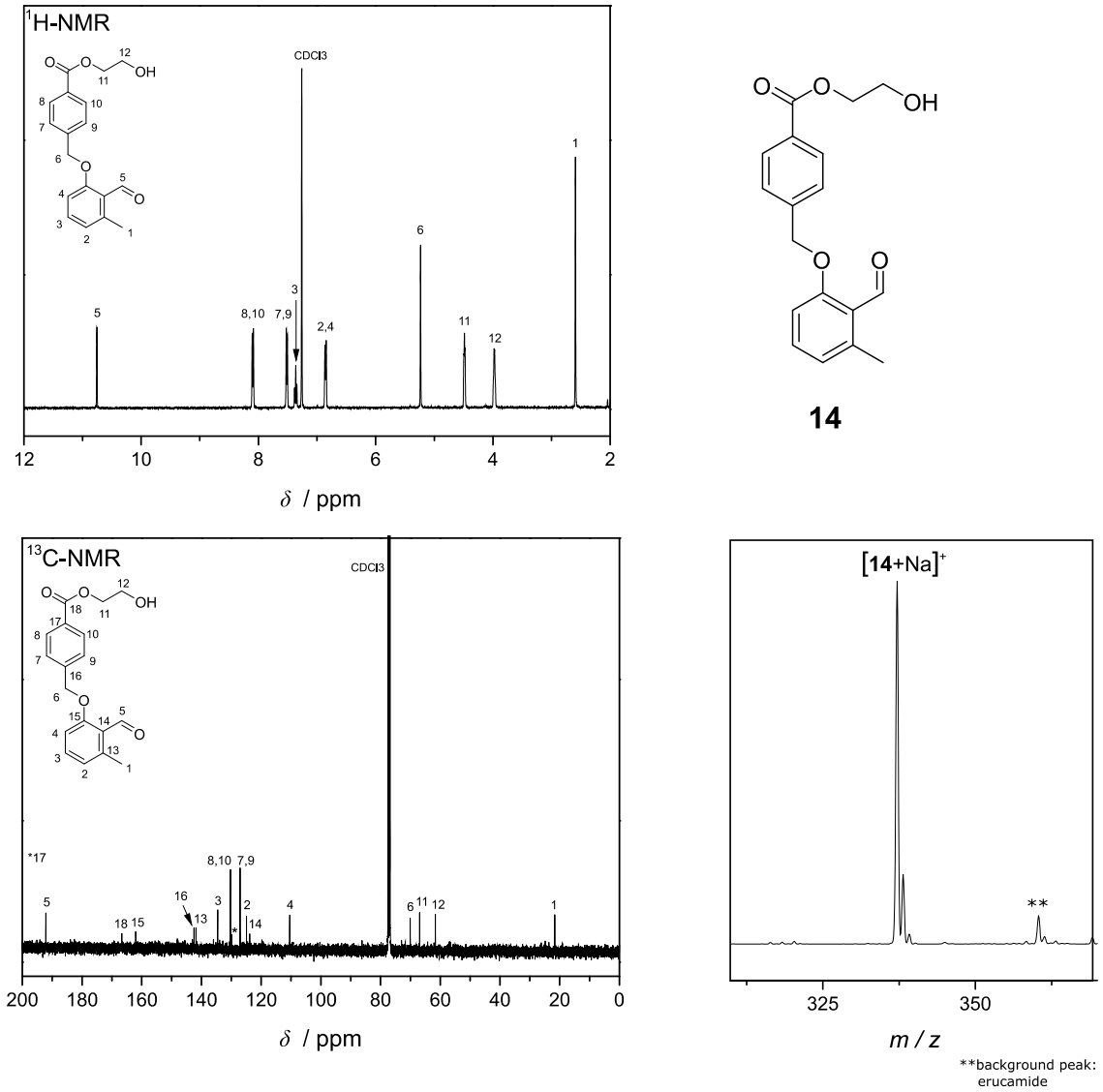

Figure 40: ^{1}H and ^{13}C NMR characterization of Photo-Gly **(14)**, as well as ESI-MS data. In the ^{1}H NMR, the addition auf the linker molecule (ethylene glycol) is achieved as evidenced by peak 11 and 12 (top left). The ^{13}C NMR spectrum exhibits all expected resonances (bottom left). *Via* ESI-MS, the expected exact mass was detected at *m/z* [**14**+Na]$^{+}_{exp}$ = 337.16, which agrees with the theoretically deduced value (bottom right).

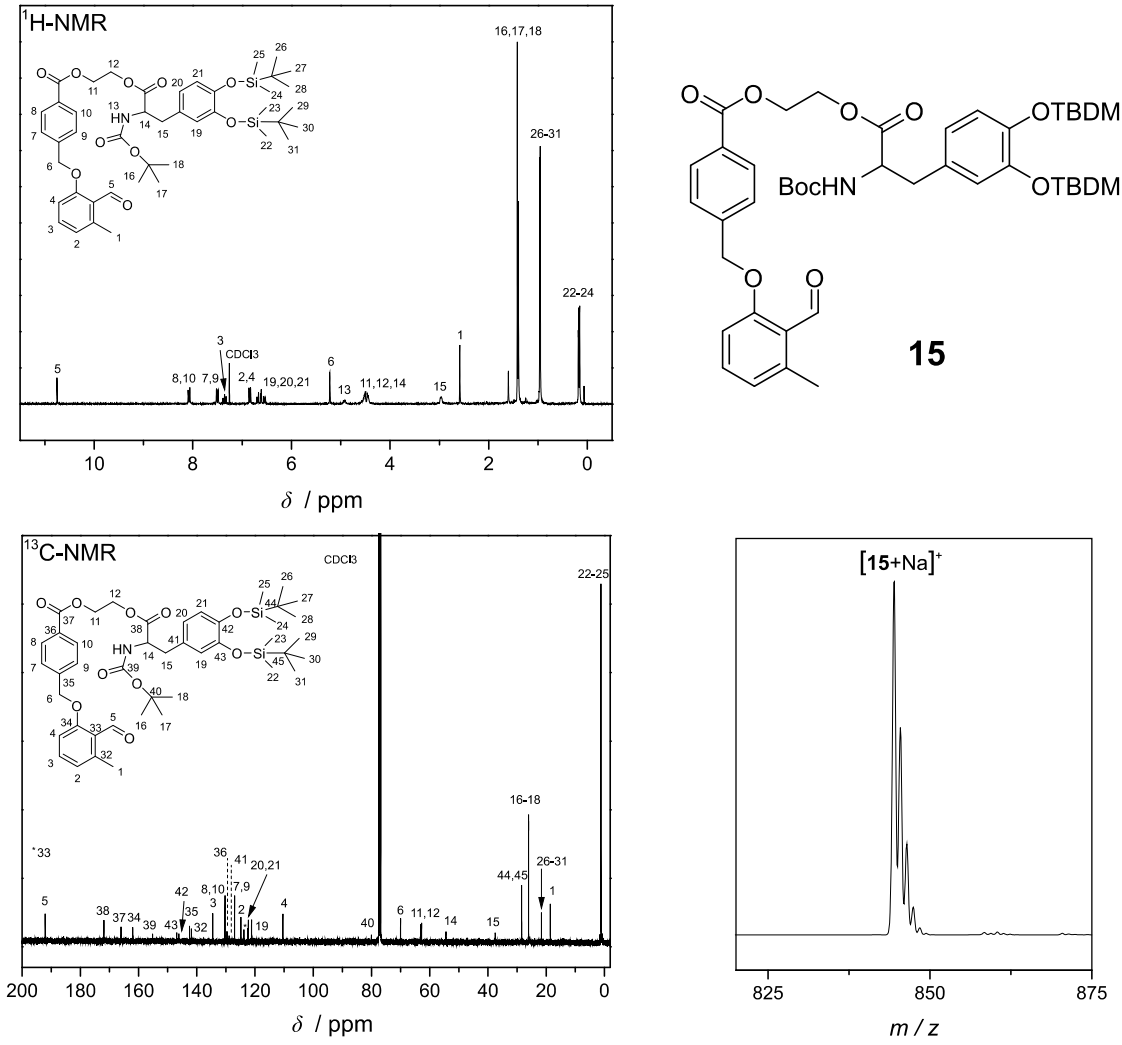

Figure 41: ^{1}H and ^{13}C NMR characterization of Photo-DOPA-$TBDMS_2$ **(15)**, as well as ESI-MS data. In the ^{1}H NMR, the successful esterification to achieve Photo-DOPA-$TBDMS_2$ **(15)** is proven by the additional peaks originating from DOPA (14,15,19-21), as well as the significant signals of the protection groups (Boc: 16-18, TBDMS: 22-31) (top left). The ^{13}C NMR spectrum exhibit all expected resonances, including the additional ones of the DOPA derivative (bottom left). *Via* ESI-MS, the expected exact mass was detected at *m/z* [**15**+Na]$^{+}_{exp}$ = 844.41, which matches the theoretically calculated value (bottom right).

In a consecutive Steglich esterification, Photo-Gly **(14)** was linked to the DOPA-based catechol precursor **(5)** that was previously protected with TBDMS at the hydroxyl and Boc at the amino units in order to prevent side reactions, to generate Photo-DOPA-$TBDMS_2$ **(15)** (**Figure 39**). The esterification was conducted between the carboxylic acid group of **(5)** and the hydroxyl unit of **(14)**, employing EDC·HCl as coupling agent and DMAP as a catalyst in DCM at ambient temperature. **Figure 41** summarizes the analytic data of Photo-DOPA-$TBDMS_2$ **(15)** in the corresponding ^{1}H and ^{13}C NMR spectra and the ESI-MS spectrum. The ^{1}H NMR spectrum of **(15)** (**Figure 41**, top left)

depicts additional peaks compared to the previous one of **(14)** (**Figure 40**, top left) that can be allocated to the just introduced DOPA unit. For instance, the three aromatic H nuclei between 6.71-6.49 ppm, as well as significant resonances of the protons stemming from the protection groups, are characteristic for this DOPA-based molecule. The signals in the ^{1}H NMR spectrum corresponding to the TBDMS moieties are originating at 0.97 ppm (*t*Bu) and 0.17 ppm (Me), whereas the peak of the *tert*-butyl-group in the Boc unit were detected at 1.41 ppm. The appropriate ^{13}C NMR spectrum further underpins the formation of **(15)** (**Figure 41**, bottom left). Firstly, the additionally expected peaks are exhibited and, secondly, the peaks of the carbon nuclei in the ethylene glycol linker (11 and 12) approach, in comparison to **(14)** (**Figure 40**, bottom left), due to the formation of the additional ester group and the resulting similar chemical environment. Furthermore, the appropriate exact mass of **(15)** was detected by ESI-MS at *m/z* $[\mathbf{15}+Na]^{+}_{exp} = 844.41$ and matches the theoretical value of *m/z* $[\mathbf{15}+Na]^{+}_{theo} = 844.39$.

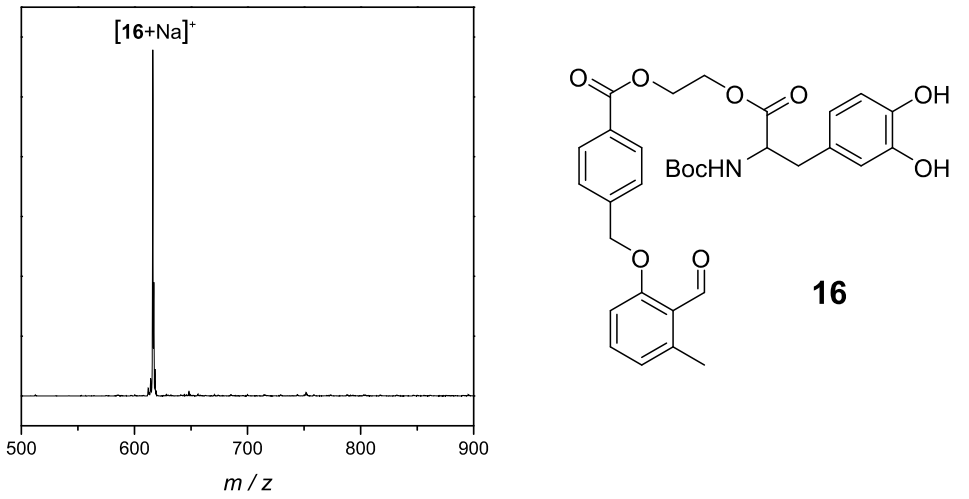

Figure 42: The ESI-MS spectrum of the deprotected photoenol precursor Photo-DOPA (left), as well as the corresponding chemical structure (right) is depicted. Full deprotection was achieved as the peak of previously protected species at *m/z* $[\mathbf{15}+Na]^{+}_{exp} = 844.41$ was shifted to *m/z* $[\mathbf{16}+Na]^{+}_{exp} = 616.25$ after deprotection, which equals the mass of the target peak **(16)**. The freshly prepared molecule was directly applied in subsequent reactions.

After the successful formation of the protected DOPA-bearing and photo-capable molecule **(15)**, the last step in the synthesis strategy involved the deprotection of the hydroxyl units in order to provide free catechols for the consecutive surface attachment step. In the reaction referred to **(15)** was exposed to a 1 M solution of tetra-*n*-butylammonium fluoride (TBAF) in THF for 30 minutes (**Figure 39**).

Characterization was performed *via* ESI-MS (**Figure 42**). The exact mass of the target molecule **(16)** was detected at *m/z* [**16**+Na]$^{+}_{exp}$ = 616.25, which agrees with the theoretical value that was calculated at *m/z* [**16**+Na]$^{+}_{exp}$ = 616.22. Furthermore, the peak of the precursor molecule **(15)**, at *m/z* [**15**+Na]$^{+}_{exp}$ = 844.41, completely disappeared in the recorded ESI-MS spectrum of **(16)**. The newly designed catechol-bearing photoenol precursor **(16)** was immediately employed in the subsequent reactions.

After the successful synthesis of a new photoenol precursor that also carries a catechol unit for the purpose of surface attachment, the following chapters discusses the applicability of such a compound for cycloadditions with suitable maleimide-bearing macromolecules in solution (5.2) and on surfaces (5.3). Moreover, spatial resolution on surfaces was achieved employing this technique, which is described in detail in the context of the cycloadditions on surfaces (5.3).

5.2. Photoenol-Ligation in Solution

As a preliminary experiment for the later photoenol-conjugation with maleimide-capped polymers on different surfaces, a suitable photo-triggered DA ligation was conducted in solution and characterized *via* ESI-MS (**Figure 43**), as previously described by Pauloehrl *et al.*[28]

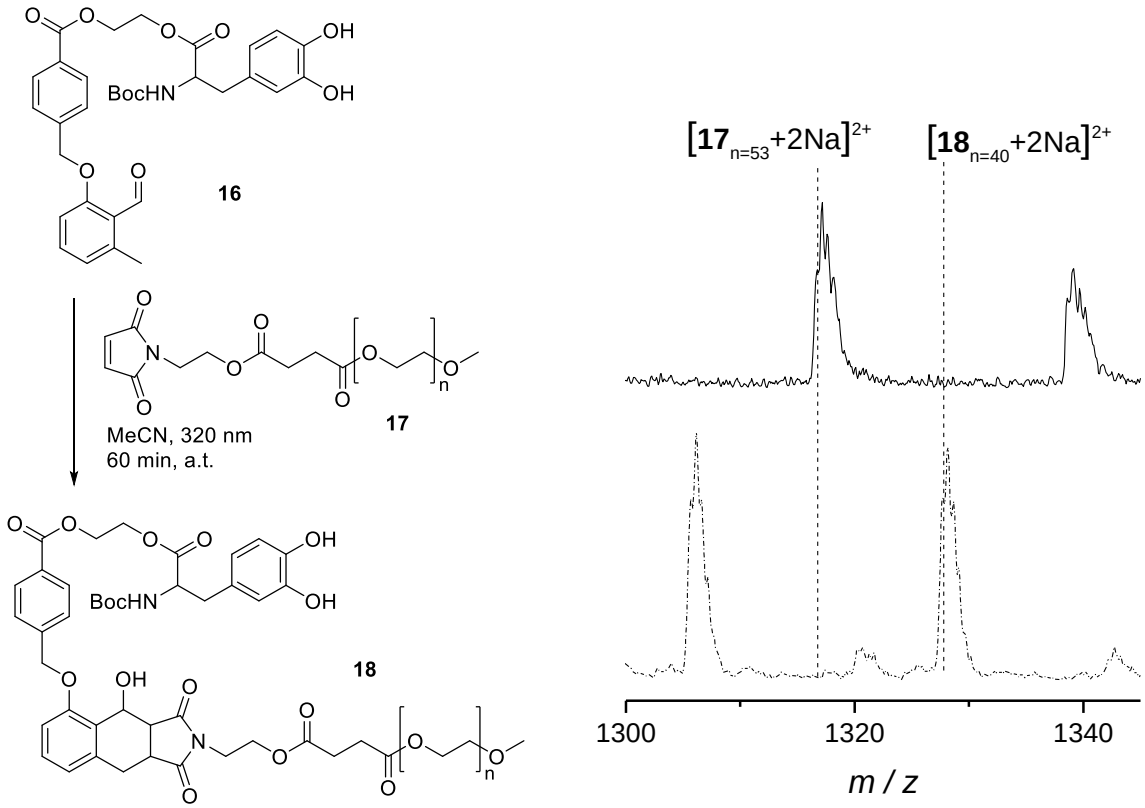

Figure 43: Photo-induced DA reaction (λ_{max} = 320 nm) of **(16)** with maleimide-carrying PEG (PEG-Mal) **(17)** was performed in acetonitrile (MeCN) at ambient temperature. The corresponding reaction scheme is depicted on the left. On the right, the results of the ESI-MS characterization is shown, comparing the double charged signals of PEG-Mal (*m/z* [**17**$_{n=53}$+2 Na]$^{2+}_{exp}$ = 1317.32) and the photoenolization product **(18)** (*m/z* [**18**$_{n=40}$+2 Na]$^{2+}_{exp}$ = 1327.65) of the polymer distribution, which supports the successful conversion.

The novel molecule Photo-DOPA **(16)** was employed as the photo-inducible diene-species in a solution with PEG-Mal **(17)** at ambient temperature during irradiation (λ_{max} = 320 nm) to give the resulting conjugation product **(18)** (**Figure 43**, left). The corresponding double charges in the ESI-MS analysis (**Figure 43**, right) verify the full conjugation of PEG-Mal **(17)** with **(16)** as the signals of the PEG-Mal **(17)** distribution (*m/z* [**17**$_{n=53}$+2 Na]$^{2+}_{exp}$ = 1317.32, *m/z* [**17**$_{n=53}$+2 Na]$^{2+}_{theo}$ = 1317.22) completely disappear after ligation and a new range of signals stemming from the conjugation

product **(18)** appears (*m/z* [**18**$_{n=40}$+2 Na]$^{2+}_{exp}$ = 1327.65, *m/z* [**18**$_{n=40}$+2 Na]$^{2+}_{theo}$ = 1327.65). The distance between the masses of the repeating units of the PEG backbone equals 22.02, which is expected for doubly charged PEG signals in ESI-MS.

As the photo-induced ligation of the new photoenol-capable compound **(16)** with a maleimide-capped polymer **(17)** was proven to operate quantitatively, the described reaction was assumed also to be applicable for the analogous photo-triggered surface conjugation. The next section examines these photoenol reactions on surfaces employing, besides PEG-Mal **(17)**, different maleimide-carrying macromolecules (PTFEMA and a peptide).

5.3. Surface Modification *via* Light-Triggered DA Cycloadditions

In order to generate photo-reactive surfaces based on light triggered DA conjugations, the novel DOPA-based photoenol-precursor Photo-DOPA **(16)** was dissolved in ethanol, applied on various substrates (Au (I), PET (II), graphite (III)), and the same amount of Tris-buffer (0.3 M, pH = 8.5) was subsequently added (**Figure 44**). After 12 h of incubation in the aqueous solution, the PET (II) and Au (I) substrates exhibited a visible change in color ascribed to the successful attachment of the starting material **(16)**. Moreover, the contact angles of the PET (II) or Au (I) surfaces with initially very different surface energy (advancing water contact angle of Au 53 °, and PET 79 °) become the same (~87 °), which further corroborates the findings.

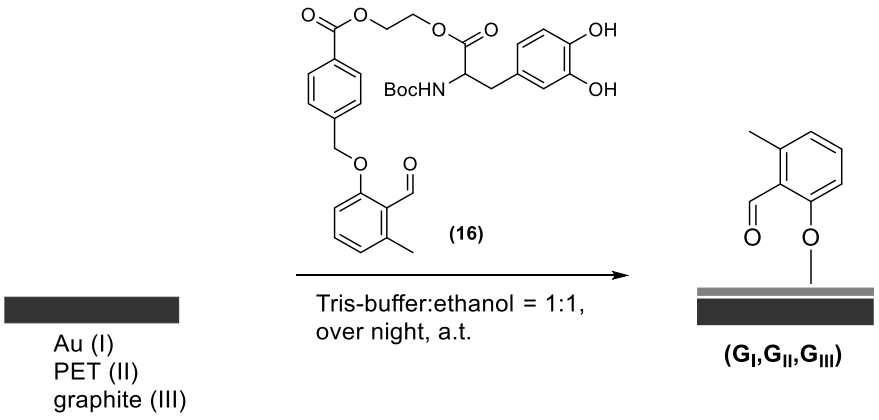

Figure 44: The surface attachment step of Photo-DOPA **(16)** onto three substrates (Au (I), PET (II), graphite (III)) is depicted. The reaction was conducted in a Tris-buffer (0.3 M, pH = 8.5)/ethanol mixture over night at ambient temperature. The prepared substrates **(G_{I-III})** exhibit a photoenolization-capable unit, which was further employed for surface modification with different macromolecules.

Furthermore, the chemical composition, determined *via* XPS, underpins the adhesion abilities of **(16)** on variable substrates and will be discussed in detail in the context of the subsequent photo-induced surface conjugation with maleimide-carrying macromolecules in the following sections. Au substrates were chosen as surfaces for the model systems, as Au does not exhibit organic functionalities that possibly interfere with characterization and, moreover, due to the relevance of Au surfaces for biomedical and biosensing applications. In addition, PET was particularly employed in

order to demonstrate photo-ligation of peptide sequences on a flexible substrate, which is commonly applied in biomedical devices.

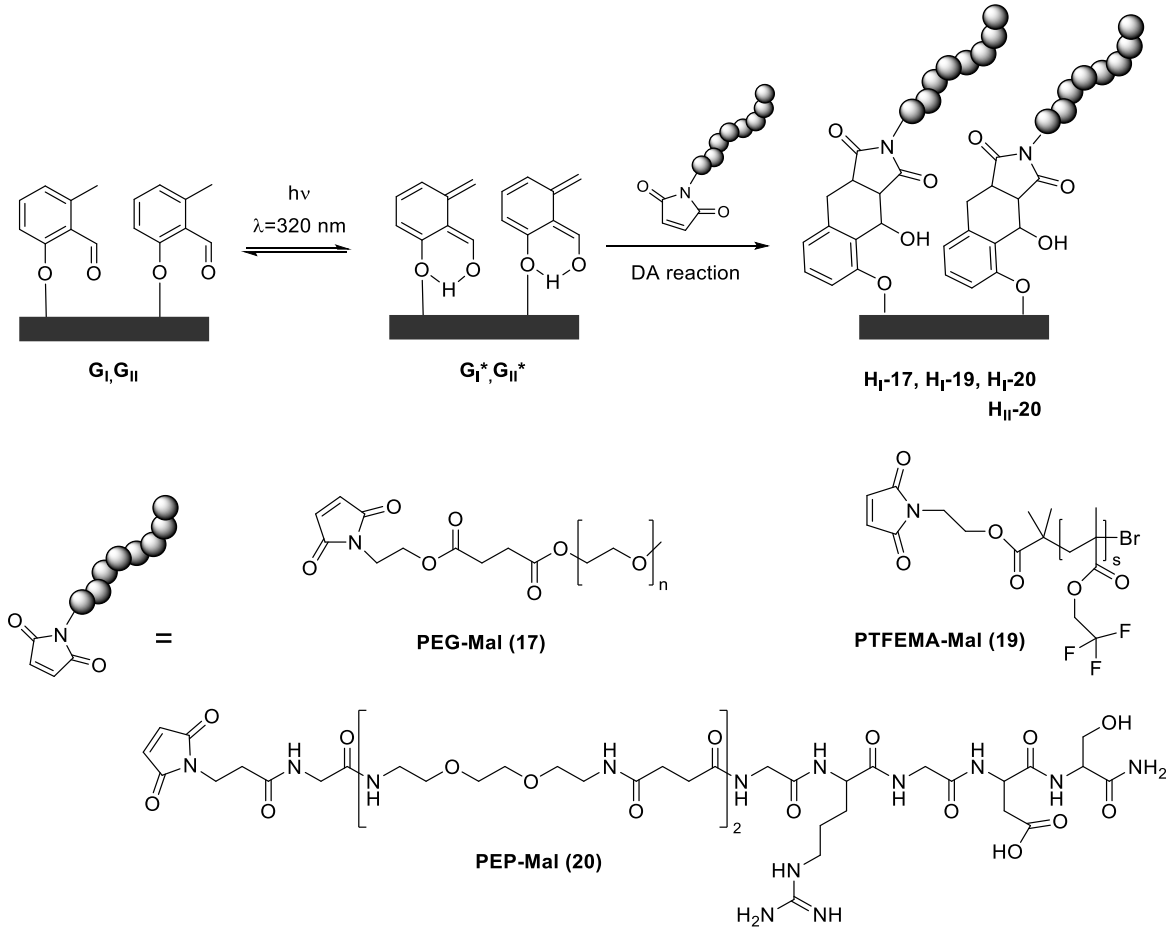

Figure 45: Photo-induced DA cycloaddition reaction on photo-reactive surfaces **(G_I, G_{II})**. The samples **(G_I, G_{II})** were irradiated ($\lambda_{max} \approx 320$ nm) in a solution of the corresponding maleimides, namely PEG-Mal **(17)** ($M_n \approx 2200$ g·mol^{-1}), PTFEMA-Mal **(19)** ($M_{n,SEC} = 3700$ g mol^{-1}, $Đ_{SEC} = 1.27$) and PEP-Mal **(20)** ($M = 1157.53$ g·mol^{-1}). The irradiation generates an intramolecular hydrogen abstraction, followed by a bond reorganization to form an *o*-xylylene intermediate, which subsequently exhibits the ability to undergo a [4+2]-cycloaddition (DA reaction) with a maleimide-carrying polymer **(17, 19)** or peptide **(20)**. Au-based photo-reactive surfaces **(G_I)** were employed for all types of macromolecules, whereas PET-based ones **(G_{II})** were applied for peptide immobilization only.

After the photo-reactive surfaces **(G_I, G_{II}, G_{III})** were successfully generated, different light triggered photoenol ligations were conducted employing various maleimide-bearing macromolecules – polymers and a peptide – as dienophiles (**Figure 45**). As polymer species, PEG-Mal **(17)** ($M_n \approx 2200$ g·mol^{-1}) and PTFEMA-Mal **(19)** ($M_{n,SEC} = 3700$ g mol^{-1}, $Đ_{SEC} = 1.27$) were conjugated, whereas the maleimide-capped peptide PEP-Mal **(20)** ($M = 1157.53$ g·mol^{-1}) was composed of the amino acid sequence Gly-Arg-Gly-Asp-Ser. The photo-triggered DA reaction was induced by irradiating the

prepared substrates **(G_I,G_{II})** with an Arimed B6 UVA lamp ($\lambda_{max} \approx 320$ nm, for emission spectrum refer to the experimental Section 9.3.2) in order to generate an *o*-xylylene intermediate **(G_I*,G_{II}*)** that is formed by an intramolecular hydrogen abstraction and a subsequent bond reorganization, in the corresponding solution of polymer-maleimides (acetonitrile) or peptide-maleimide (acetonitrile : milli-Q water = 3 : 1) after degassing with nitrogen. The successive DA conjugations occurred immediately after generation of the reactive species **(G_I*, G_{II}*)** in the described setting. The photo-reactive Au substrates **(G_I)** were employed as the model system to demonstrate the effective ligation of all the envisaged maleimide-macromolecules on the surfaces, as well as for the spatially controlled surface grafting of PTFEMA-Mal in a micro-scale. PTFEMA was utilized due to the excellent detectability of the F^- and CF_3^- ions originating from the polymer backbone in the ToF-SIMS analysis. The photoenol capable PET substrate **(G_{II})** was employed for the purpose of evidencing peptide attachment on a flexible substrate. The corresponding XPS and ToF-SIMS characterization is described on the following pages.

The conjugation of PEG-Mal **(17)** to the previously modified surface **(G_I)** to form **(H_I-17)** was evidenced by comparing the chemical composition of the different carbon bonded species in the C 1s spectrum of the same (**Figure 46**). The C 1s of the photo-reactive Au surface **(G_I)** depicts all expected signals that confirm the grafting of **(16)**. After the light-induced DA ligation with PEG-Mal **(17)**, a strong increase of the signal assigned to the C-O bonds provided by the PEG backbone at 286.6 eV occurred, which verifies the attachment.[166] Furthermore, the amount of the C-O bonds compared to the total number of C-C and C-O bonds increases from 20 % before **(G_I)** to 66 % after the photo-induced ligation **(H_I-17)** and thus, further supports the applicability of the method.

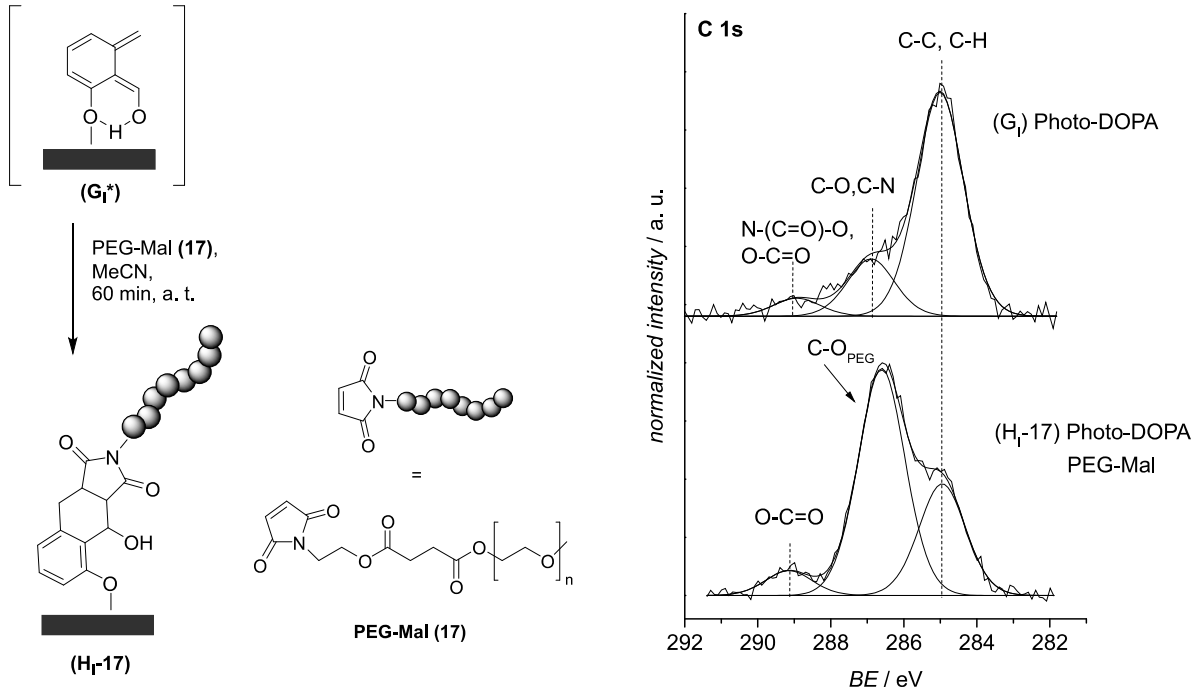

Figure 46: C 1s XPS spectra (right) of the surface conjugation of PEG-Mal **(17)** ($M_n \approx 2200$ g·mol^{-1}) to the photo-reactive gold substrate **(G_I)** after irradiation ($\lambda_{max} \approx 320$ nm) **(G_I*)** and detailed reaction conditions (left). The readily prepared Photo-DOPA substrate **(G_I)** (right top) exhibits all desired signals to verify the attachment of **(16).** Furthermore, after conjugation, the strong increase of the signal assigned to the C-O bonds of the PEG backbone at 286.6 eV in the C 1s spectrum of **(H_I-17)** (right bottom) evidences the grafting of the polymer.

The XPS characterization of the attachment of PTFEMA-Mal **(19)** to **(G_I)** to form **(H_I-19)** is illustrated in **Figure 47**. After photo-induced ligation, the C 1s spectrum of the newly modified substrate **(H_I-19)** exhibits an additional peak at 293.7 eV (compared to the former substrate **(G_I)**), which is characteristic for C-F bonds and can, therefore, be assigned to the CF_3-moieties presented in the PTFEMA backbone. [175,176] Furthermore, the grafting of PTFEMA-Mal **(19)** to the surface was also evidenced by the formation of a signal in the F 1s XPS spectrum (**Figure 47**, middle top) at 689.3 eV, which stems from the already mentioned CF_3-units in the PTFEMA strands.

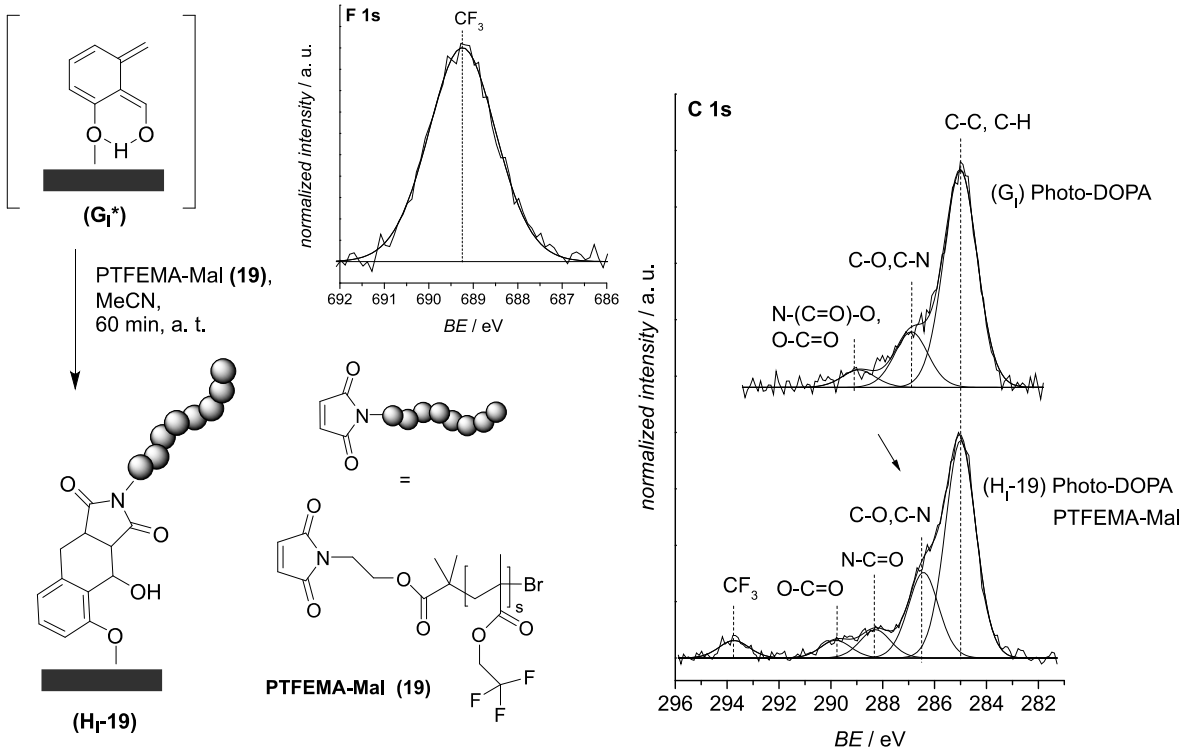

Figure 47: The C 1s XPS spectra (right) and the F 1s spectrum (middle top) of the surface ligation of PTFEMA-Mal **(19)** to the photo-reactive gold substrate **(G_I)** after irradiation ($\lambda_{max} \approx 320$ nm) **(G_I*)** and the detailed reaction conditions (left) are depicted herein. The previously prepared Photo-DOPA substrate **(G_I)** (right top) exhibits all expected signals to evidence the attachment of **(16).** After ligation, the appearance of an additional signal assigned to the CF_3 bonds stemming from the PTFEMA backbone at 293.7 eV in the C 1s spectrum of **(H_I-19)** verifies the grafting of the polymer. Moreover, the F 1s spectrum (middle top) after the photo-induced DA reaction shows a strong signal at 689.3 eV that also originates from the CF_3 moieties in the PTFEMA backbone.

In order to achieve spatial control of the photoenol reaction, a photo-reactive substrate **(G_I)** was applied in a metal sample holder that features a rectangular opening (**Figure 48**, top left) where the sample is exposed to irradiation, whereas the remaining parts of the substrate are covered. A meander shaped shadow mask was placed on top of the sample before covering (**Figure 48**, top right) and the entire setup **(G_I+mask)** was exposed to similar reaction conditions as described for the grafting of PTFEMA to the entire surface.

After irradiation, the freshly prepared substrate **(J_I-19)** was washed with several solvents and dried with nitrogen, before it was characterized by ToF-SIMS analysis. The ToF-SIMS overlay of the negatively charged F^- and CF_3^- fragments, originating from the grafted PTFEMA strand, unambiguously evidences the ability of the current system to generate patterning on surfaces (**Figure 48**, bottom right).

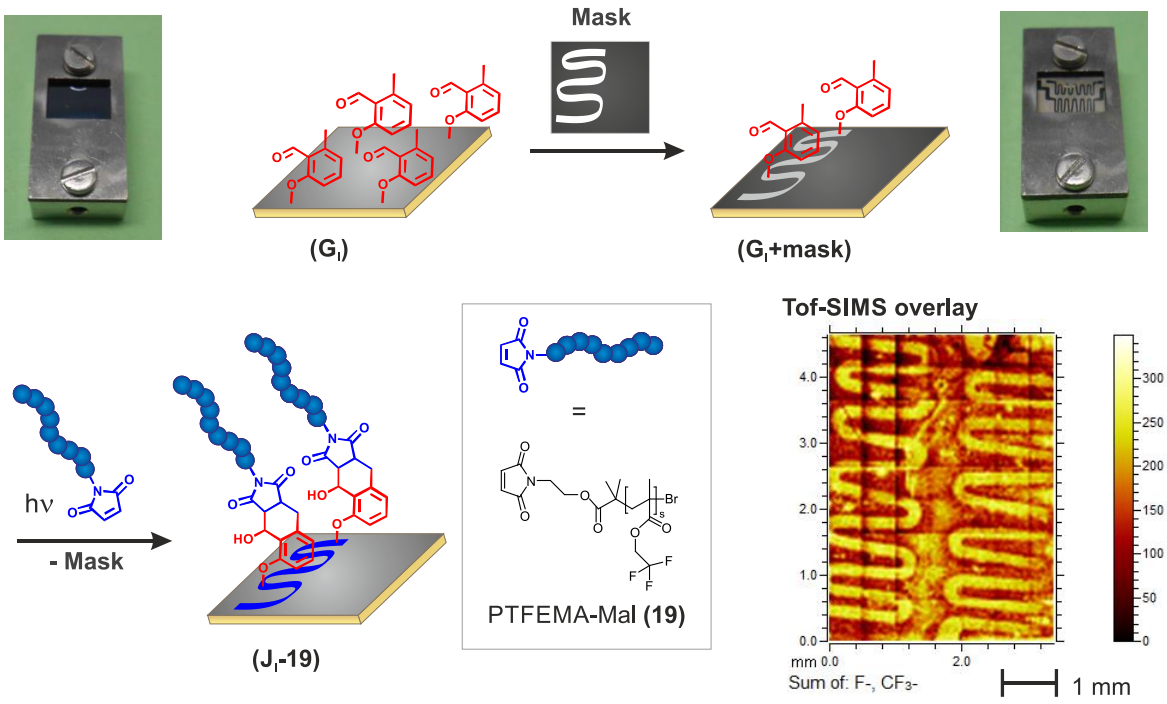

Figure 48: A schematic overview of the spatially controlled photo-triggered photoenol reaction on a gold substrate is presented. The photo-reactive gold substrate **(G_I)** was placed in a metal holder (top left) that possesses a window inset where light can reach the surface. A meander shaped shadow mask (top right) was added before covering **(G_I+mask)** and the partially covered substrate was exposed to the same reaction conditions as described before, employing PTFEMA as the corresponding maleimide-capped polymer. After irradiation, the freshly prepared substrate **(J_I-19)** was characterized *via* ToF-SIMS. The meander shaped grafting of PTFEMA was verified by the overlay of F^- and CF_3^- ions. The pictures of the sample holders were reprinted with permission from Ref. 29. Copyright (2013) American Chemical Society.

In a second approach, the maleimide-peptide sequence Mal-spacer-Gly-Arg-Gly-Asp-Ser (Mal-PEP) **(20)** was grafted onto photo-reactive substrates based on gold **(G_I)** or PET **(G_{II})** in an acetonitrile/water mixture (3:1) in 60 minutes. The corresponding C 1s and N 1s spectra before **(G_I/G_{II})** and after grafting **(H_I-20/H_{II}-20)** are depicted in **Figure 49**. The C 1s of the Au-based substrate exhibits an increase of the signals assigned to the C-N and amide bonds (peptide) at 286.5 eV and 288.4 eV after the attachment of **(20)** (**Figure 49**, center top).[177] The changes in the C 1s XPS spectrum of the PET substrates are not visible due to the strong organic structures stemming from the substrate itself. Therefore, the most significant data for the peptide attachment provides the N 1s spectrum. The N 1s spectrum of **(H_I-20)** shows the appearance of a nitrogen signal (**Figure 49**, right top) assigned to the grafted peptide at 400.3 eV,[161] which further supports the peptide attachment. In addition, similar, but slightly shifted,

results were obtained for the PET substrate. Thus, the grafting of a peptide sequence on different substrates, including PET as a flexible surface, were confirmed.

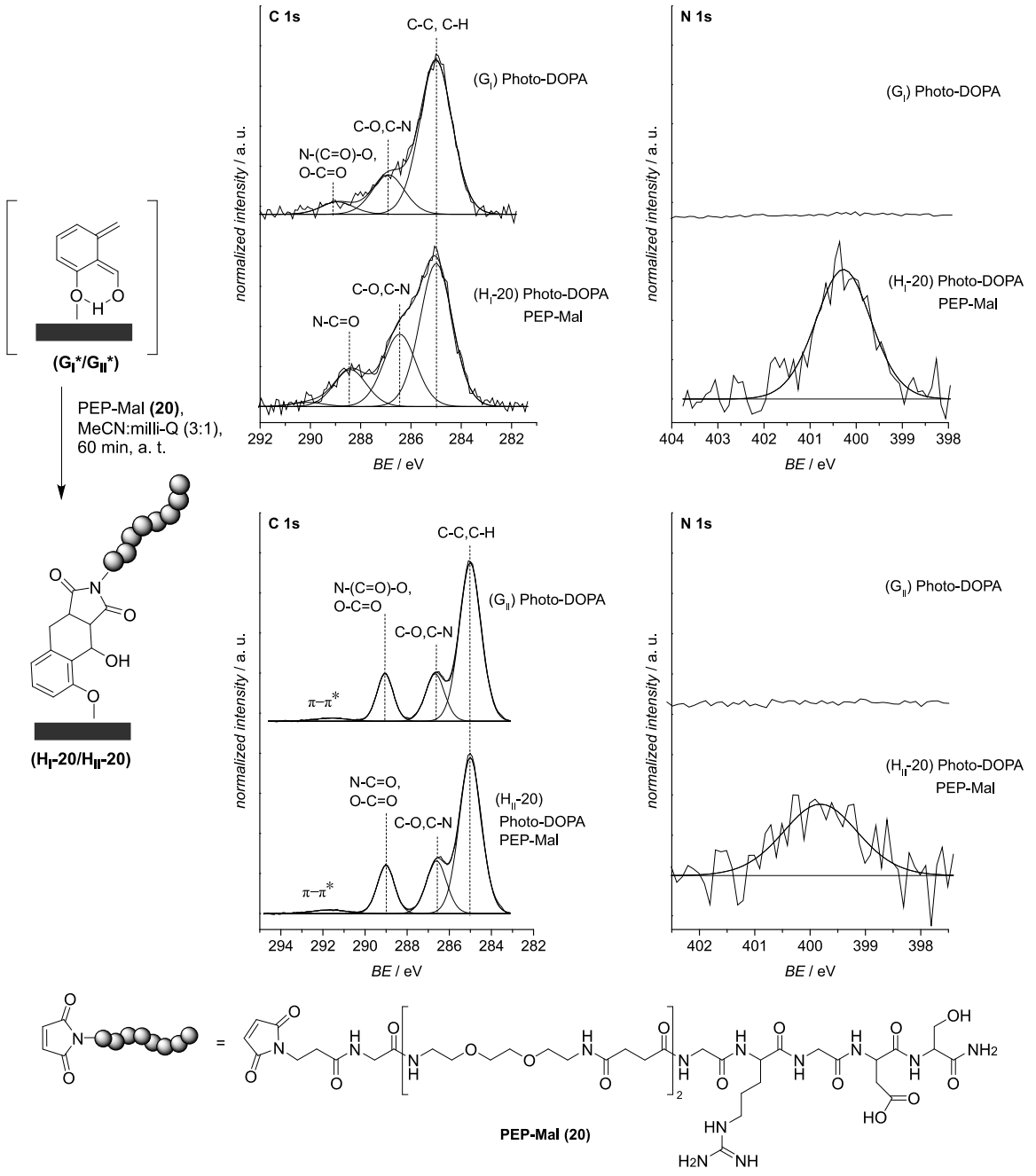

Figure 49: C 1s XPS spectra (center) and N 1s spectra (right) of the surface grafting of PEP-Mal (Mal-spacer-Gly-Arg-Gly-Asp-Ser) **(20)** to the photo-reactive gold substrate **(G_I)** or PET (**G_{II})** after irradiation ($\lambda_{max} \approx 320$ nm) **(G_I*)** or **(G_{II}*)**, respectively, and detailed reaction conditions (left). The former prepared Au-based Photo-DOPA substrate **(G_I)** (center top) exhibits all expected signals in the C 1s XPS spectrum to confirm the attachment of **(16)**. Furthermore, the signals assigned to the C-N and amide bonds (peptide) increase after ligation, which is mainly visible for the Au substrate **(H_I-20)**. Due to the dominance of the organic structures in the PET substrate itself, changes in the C 1s are not significant. Most importantly, after ligation, the N 1s spectrum exhibits a strong signal originating from the peptides' amide bonds as well as from the functionalities of the amino acids on both substrates (Au and PET) **(H_I-20/ H_{II}-20)** (right top and center).

In order to complete the investigations on the attachment of **(16)** on different substrates to generate a universal photo-reactive surface, the C 1s spectrum of the modified graphite surface is depicted in **Figure 50**.

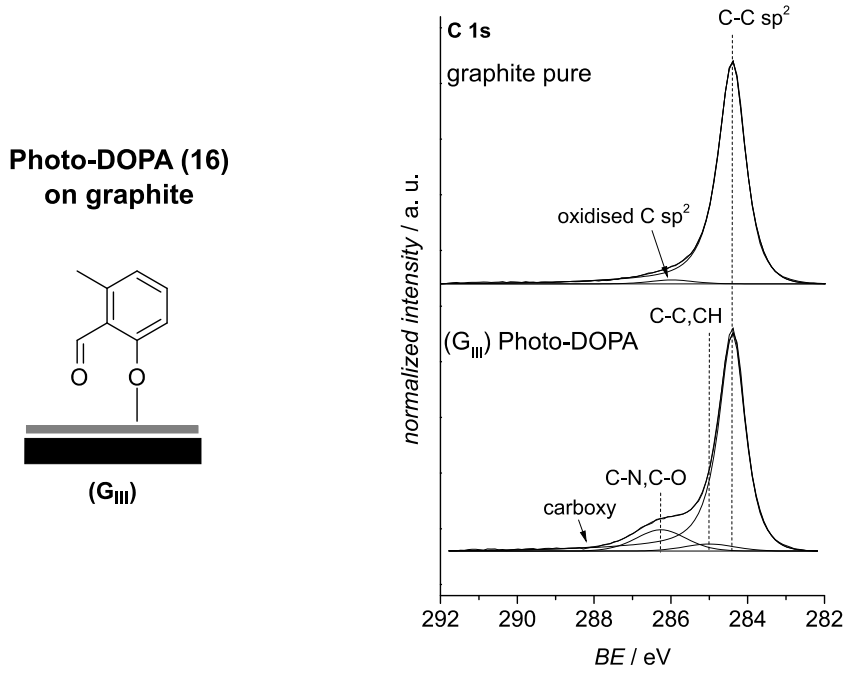

Figure 50: The attached **(16)** on a pure graphite surface **(G_{III})** and the corresponding C 1s spectrum is depicted. The signal for the C-C sp2 of the graphite substrate at 284.4 eV serves as reference peak. Additional signals stemming from the grafted organic molecule, such as the signal assigned to C-C and C-H bonds at 285.0 eV and the C-O and C-N signal at 286.3 eV, support the successful ligation. The signal assigned to the corresponding carboxyl groups most likely vanishes in the characteristic tail originating from the graphite substrate.

After the attachment of **(16)** to pure graphite, the C 1s spectrum shows additional peaks originating from the organic molecule that was attached, which can be deconvoluted into C-H/C-C and C-O/C-N bond contributions with the appropriate bonding energies at 285 eV and 286.3 eV, respectively. The signal for the corresponding carboxyl groups most likely vanishes in the characteristic tail caused by the graphite substrate. The dominate signal at 284.4 eV stems from the sp^2-C-C bonds of the graphite's conjugated π-system.[128]

5.4. Summary and Outlook

The current section emphasized the applicability of the previously designed Photo-DOPA **(16)** as a suitable photo-reactive surface modification precursor for the grafting of suitable maleimide-bearing (bio)macromolecules – polymers and a peptide – to variable surfaces. The attachment of **(16)** was adapted on Au, PET and graphite. The gold substrates were applied as model systems for all consecutive modification steps, including the important spatial resolved patterning of PTFEMA-Mal **(19)** on the microscale, owing to the absence of any disturbing organic material and the relevance of Au surfaces for biosensing and biomedical applications. Furthermore, PET was employed in the peptide grafting study due to its flexibility and its use in biomedical devices. In this context, the photoenol reaction was performed in an acetonitrile-water mixture (3 : 1), which opens even more perspectives with regard to biomedical applications, where aqueous systems and mild conditions play a key role.

In this regard, the photoenol capable surfaces could be employed to tether protein tags, such as a biotin-bearing compound, to surfaces in order to capture specific proteins (in case of biotin: streptavidin). Furthermore, owing to the spatial control the current method offers, the attachment of such a biotin tag can be dictated to selective areas by employing a suitable shadow mask during the photo-ligation. This further allows conjugation of different other protein tags in specific regions by irradiation, in order to generate surfaces that can capture a certain selection of proteins. The same concept is also pictured to be applied for immunoassays, in case the detection of different analytes is targeted. Moreover, as the compatibility of proteins or DNA strands and light-triggered photoenol ligations has already been reported by Bauer *et al.*,[140] the present system is envisioned to be utilized to tether, for instance, single DNA strands on substrates, which could further operate as biosensor for the immobilization of enzymes based on the pairing of the single strand DNA with a complementary DNA attached to the enzyme.[178] However, all the sensing systems just mentioned need to meet additional requirements, such as the absence of any non-specific adsorption (see introduction), and thus, further enhancements are required. Gazing into a different field, spatially controlled patterning of maleimide carrying polymers could also be

beneficial with regard to the attachment of conducting polymers, such as P3HT, in specific areas in order to create a precise patterning for electronic devices.
Thus, the outcomes of the present approach are likely to be considered for the development of smart systems with spatially resolved functions for a plethora of applications.

Moving away from DA conjugation systems and *grafting-to* approaches, the next chapter describes an area resolved *grafting-from* approach for the preparation of non-fouling polymer brushes based on NITEC attachment of a suitable ATRP initiator and the following SI-ATRP. The non-fouling properties were demonstrated by different cell adhesion studies.

6

NITEC as Ligation Tool for Surface-Initiated ATRP from PDA

1,3-dipolar cycloadditions or [3+2] cycloadditions represent conjugation methods employing a 1,3-dipole and a dipolarophile to form five-membered rings. In the present chapter, light-induced nitrile imine-mediated tetrazole-ene cycloaddition (NITEC) (2.3.3) was chosen as the suitable conjugation system for the attachment of an ATRP initiator to a PDA surface in order to grow non-fouling polymers, namely poly(oligoethylene glycol methyl ether methacrylate) (PMeOEGMA) brushes to achieve controlled cell adhesion in a spatially resolved fashion.

Parts of the chapter were reproduced from Rodriguez-Emmenegger, C.;* Preuss, C. M.;* Yameen, B.; Pop-Georgievski, O.; Bachmann, M.; Mueller, J. O.; Bruns, M.; Goldmann, A. S.; Bastmeyer, M.; Barner-Kowollik, C. *Advanced Materials* **2013**, *25*, 6123 by permission from the John Wiley and Sons (Copyright 2013). *: both first authors. The concept was planned by CR and CMP. PDA surfaces were provided by O. Pop-Georgievski. The procedure for the tetrazole-chloride was developed by J. O. Mueller. Small molecule synthesis was conducted by CMP and CR. Surface conjugation reactions were conducted by CR and CMP. SI-ATRP was performed by CR. XPS characterization was executed by CMP. Contact angle and ellipsometry measurements were performed by O. Pop-Georgievski. ToF-SIMS analysis was conducted by M. Bruns. Cell adhesion studies were performed by M. Bachmann. Compounds for the cell experiments were obtained from K. Martin and O. Pertz, University of Basel.

The generation of micro-patterned structures has proven as a powerful tool to create surfaces with encode properties to confine cells and study their behavior upon different stimuli.[179,180] A suitable patterning strategy has to be developed to meet miscellaneous requirements. Besides microscale resolution, the fabrication of spatially and time resolved structures from a material that prevents adhesion of proteins or cells is mandatory. Furthermore, modularity, as well as orthogonality to biomolecules in conjugation with applicability to different substrates regardless of the surfaces' shape, topography or surface energy, is desirable. Therefore, NITEC was chosen as a light based method that allows activation in defined areas at variable times. Owing to its relatively mild conditions, as well as its bioorthogonality, NITEC was already applied in conjugation reactions with bacteria,[147] and proteins.[146] In addition, NITEC-based approaches regarding surface modification by grafting polymers or peptides to silicon wafers or biosubstrates, such as cellulose, have been reported.[148] As previously noted, the independence on the type of substrate provides a key advantage for generating versatile patterning protocols. Thus, PDA films were selected to serve as surface coatings as they possess the ability to adhere to virtually any substrate exerting various forces ranging from covalent to van der Waals interactions,[14,45] as well as providing post-functionalizable moieties such as amino- or hydroxyl units (2.1.3). Furthermore, PDA films were identified to enhance attachment, phenotypic maintenance and proliferation of cells,[181,182] which was an additional criterion for its selection as an adlayer for precise cell adhesion.

To develop interfaces with specific control of cell adhesion three main concepts, implying highly efficient NITEC reactions, superior resistance of PMeOEGMA brushes and versatility of bio-inspired PDA coatings, were merged (**Figure 51**). A PDA film on a silicon wafer was functionalized with a suitable tetrazole, which serves as a NITEC precursor. Subsequently, a shadow mask was applied to the surface and a maleimide carrying ATRP initiator was attached solely in the uncovered areas during irradiation. The consecutive SI-ATRP, employing oligoethylene glycol methyl ether methacrylate (MeOEGMA) as monomer, yielded a meander-shaped patterning of PMeOEGMA brushes. The non-fouling properties of which were further investigated in several cell adhesion studies. For this purpose, rat embryonic fibroblasts (REFs) were seeded and the cell adhesion and proliferation was monitored.

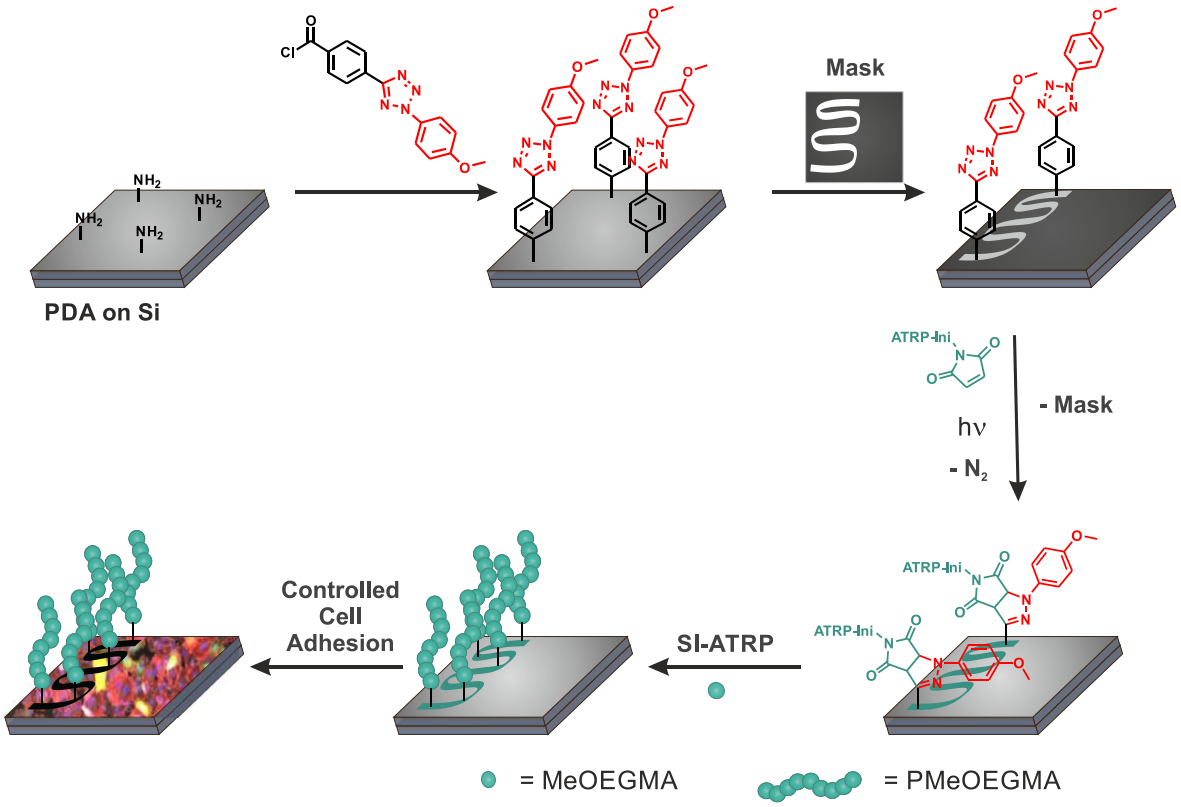

Figure 51: Schematic overview of the reaction sequence to prepare non-fouling polymer brushes (PMeOEGMA) in a spatially controlled fashion to generate surfaces with controlled cell adhesion abilities. On a silicon wafer assembled with a PDA film, a NITEC precursor molecule is attached employing the amino moieties provided on PDA, before a subsequent area controlled photo-induced NITEC reaction with a maleimide that carries an ATRP initiator during the application of a shadow mask is conducted. Consequently, a SI-ATRP employing MeOEGMA as a monomer to generate non-fouling polymer strands is performed. The following cell adhesion studies are expected to solely exhibit cell adhesion in the none-grafted regions.

Characterization of the small molecules was conducted by NMR spectroscopy, whilst surface characterization was performed by XPS analysis, ToF-SIMS analysis, ellipsometry and contact angle measurements.

The detailed experiments and results are described in the following sections.

6.1. Preparation of Non-Fouling Spatially Resolved Surfaces

For the generation of a microscale architecture in order to control cell adhesion on variable surfaces, a tetrazole acid chloride (Tet-Cl) **(24)** was synthesized. The procedure was supplied by J. O. Mueller (AK Barner-Kowollik) and is illustrated in **Figure 52**.

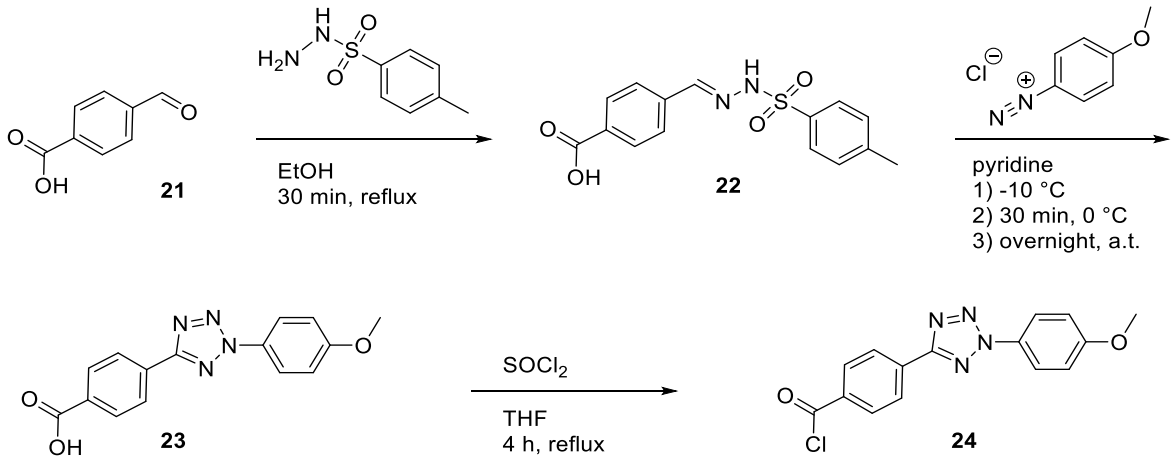

Figure 52: Reaction scheme for the generation of a suitable tetrazole precursor, Tet-Cl **(24)**, for the attachment to PDA films. The procedure was provided by J. O. Mueller (AK Barner-Kowollik). First, 4-formyl benzoic acid **(21)** was reacted with *p*-toluenesulfonylhydrazide to yield the hydrazone **(22)**, which was further converted to the tetrazole acid (Tet-COOH) **(23)** by employing a freshly prepared diazonium salt. The following transformation to the Tet-Cl **(24)** was performed owing to its increased reactivity in the following surface amidation reaction.

The novel tetrazole acid chloride Tet-Cl **(24)** was synthesized in a three step procedure, starting from 4-formyl benzoic acid, which was refluxed in ethanol for 30 minutes in the presence of *p*-toluenesulfonylhydrazine to generate the hydrazone **(22)**. In order to generate a new and more biocompatible tetrazole that undergoes NITEC reactions under milder conditions – implying that it operates at longer wavelengths – than previously reported ones,[148] the tetrazole acid (Tet-COOH) **(23)** was synthesized by the addition of an *in situ* generated diazonium salt from *p*-anisidine to the previously prepared hydrazone **(22)** in pyridine at -10 °C within 30 minutes, before the mixture was stirred overnight at ambient temperature. Earlier publications report that the reactivity of the nitrile-imine dipole, which is generated by nitrogen release during irradiation of a tetrazole, can be increased towards the NITEC conjugation reaction by elevating the energy of the dipole's HOMO, in order to reduce

the energy gap to the dipolarophile's LUMO.[183,184] For this reason, an electron-donating group (EDG), a methoxy moiety, was introduced in *para*-position of the phenyl-group attached to the nitrogen atom of the tetrazole ring. It is worth mentioning that the addition of such a unit at the *ortho*- or *meta*-position of the same phenyl group induces the opposite effect and increase the gap between the two orbitals.[183] In comparison to the previously reported tetrazole by Blasco et al.,[51] which was simply carrying an unsubstituted phenyl group (**Figure 53,** bottom right), the addition of a methoxy moiety at the *para*-position in the *N*-phenyl ring enables a shift of the excitation wavelength from the UVC/UVB region ($\lambda_{max,}$ = 277 nm, for tetrazole from Ref. 51) to the UVA/UVB region for **(23)**. It needs to be noted that **(23)** reaches its absorption maximum at approximately 295 nm but the overlap with the emission spectrum of the employed light source between approximately 290 and 340 nm (UVA lamp Arimed B6, 36 W, λ_{max} = 320 nm) is still sufficient for the desired reaction (**Figure 53**). Thus, the modification of more sensitive (bio)systems can be achieved owing to the milder conditions provided in the NITEC reaction with the novel tetrazoles **(23)** or **(24),** respectively.

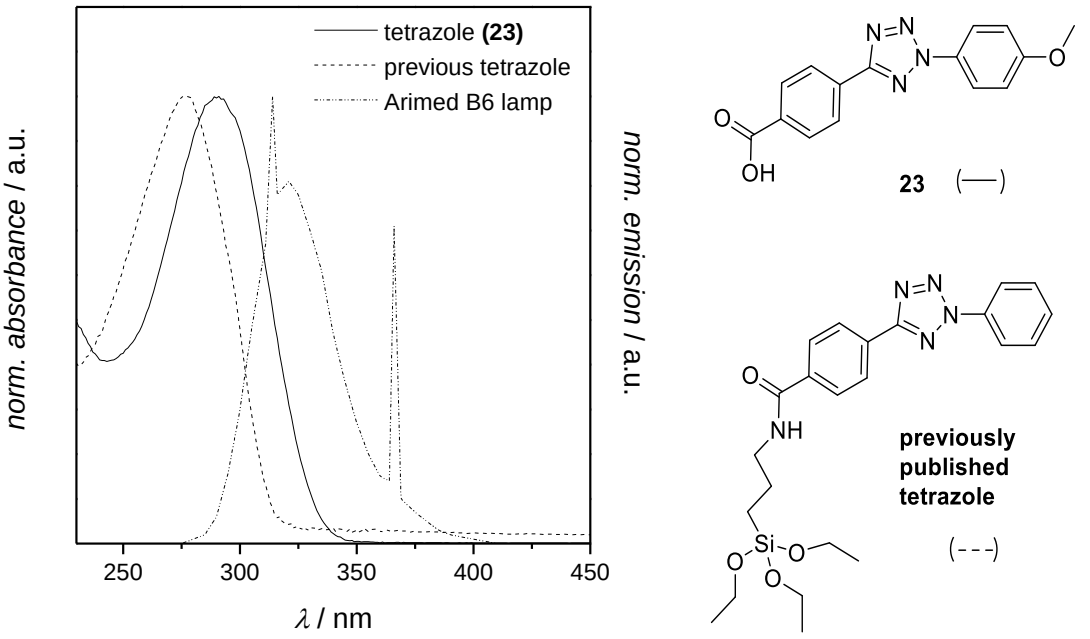

Figure 53: The UV/Vis spectra of the novel tetrazole **(23)** (—), a previously reported tetrazole (---) and the emission spectrum of the employed Arimed B6 UVA lamp (····) are depicted on the left. The corresponding chemical structures of the tetrazoles are presented on the right. An addition of a methoxy-moiety at the *para*-position of the *N*-phenyl ring results in a shift of the excitation wavelength from the UVB/UVC region (previously published tetrazole, bottom) to the UVA/UVB region for **(23)**. Thus, milder irradiation can be applied, which is crucial for the application in more sensitive systems. The UV spectrum of the previously prepared tetrazole was kindly provided by Dr. Eva Blasco and already published in Ref. 51. The UV spectrum of **(23)** was recorded by J. O. Mueller.

To increase the reactivity of the tetrazole acid **(23)** with respect to the attachment to the previously generated PDA by amidation, transformation of the carboxyl unit to the corresponding acid chloride Tet-Cl **(24)** was achieved by exposing **(23)** to thionyl chloride for four hours in THF under reflux. Characterization was performed *via* ^{1}H and ^{13}C NMR spectroscopy, which is provided in the experimental section (9.4.1). A more detailed description of the system is currently in preparation and will be further discussed in the dissertation of J. O. Mueller (expected in July 2015).

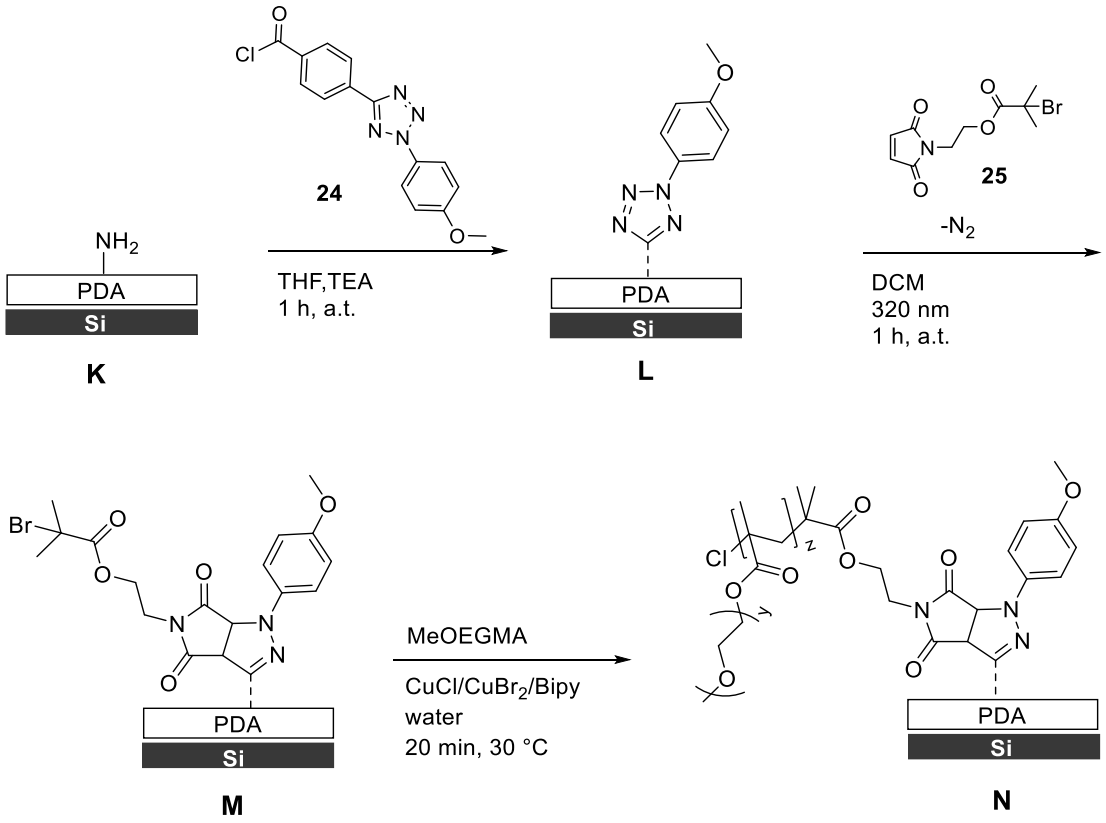

Figure 54: Schematic overview of the surface reactions conducted on the entire surfaces (first) and area resolved (later). In an amidation reaction, the novel molecule Tet-Cl **(24)** was attached to a previously prepared PDA surface **(K)**. The following NITEC reaction was performed under UV irradiation (λ_{max} = 320 nm) with an appropriate light source (Arimed B6, 36 W) in the presence of an electron-deficient double bond (maleimide), which conjugates with the *in situ* generated 1,3-dipole and exhibits an ATRP-initiating moiety for further modification of the substrate **(M)**. Subsequently, a non-fouling polymer, namely PMeOEGMA, was grown from the surface *via* SI-ATRP **(N)**.

In order to generate a tetrazole-based and thus, NITEC capable surface, a PDA surface **(K)** was prepared by the spontaneous polymerization of dopamine on a silicon wafer in a Tris buffer solution (pH = 8.5), before the novel tetrazole acid chloride **(24)** was attached to the provided amine functionalities on the PDA surface **(K)** in the presence of TEA in THF for 1 hour at ambient temperature **(L)** (**Figure 54**). Subsequently, a light-triggered NITEC ligation is performed by irradiation (Arimed B6 UV lamp, 36 W,

λ_{max} = 320 nm) of **(L)**, where nitrogen is released from the tetrazole moieties and a nitrile imine is generated (Section 2.3.3), which spontaneously cyclizes with the provided maleimide-carrying (electron deficient double bond) ATRP initiator[185] (dipolarophile) in DCM to form a stable pyrazoline-based cycloadduct **(M)** (**Figure 54**).[25] In order to investigate the surface properties by XPS, contact angle measurements and ellipsometry, the entire substrates were modified first, before the patterned surfaces were created in a second approach.

The chemical composition of the prepared substrates was analyzed *via* XPS (**Figure 55**, **Figure 56**) and the wettability and thickness data of the surfaces was determined by dynamic contact angle measurements and ellipsometry (**Table 1**), respectively.

	Dynamic water contact angle		Thickness
	θ_a	θ_r	(nm)
PDA **(K)**	70.8 ± 5.1	56.1 ± 2.1	27.7 ± 0.6
PDA-tetrazole **(L)**	77.8 ± 0.8	50.7 ± 4.5	1.3 ± 0.2
PDA-tetrazole-initiator **(M)**	66.6 ± 2.3	33.5 ± 3.7	1.4 ± 0.1
PDA-SI-ATRP PMeOEGMA **(N)**	46.9 ± 1.6	23.8 ± 2.2	15.3 ± 0.5

Table 1: Wettability and thickness data of the surfaces **(K)-(N)**, determined by dynamic contact angle measurements and ellipsometry, respectively

The C 1s spectra of the first two surface modification steps **(K-L)** do not exhibit significant changes owing to the dominant signals of the PDA film and the addition of only small molecules with similar molecular structures (**Figure 55**, top, middle left). However, the appearance of doublet peaks originating from the bromine-containing ATRP initiator in the corresponding Br 3d spectrum of **(L)** confirm the successful photo-triggered NITEC reaction (**Figure 55**, right). The detection of an additional signal located at 67.7 eV in the Br 3d spectrum may result from the formation of bromide ions by decomposition during the XPS analysis.[126,186,187] Additional evidence of the successful NITEC reaction was obtained by an increase of 1.4 nm in thickness and changes in the wettability (**Table 1**). Importantly, in a control experiment **($M_{control}$)** no signals corresponding to the initiator were detected *via* XPS (C 1s and Br 3d) when a substrate coated with pure PDA, without tetrazole, was irradiated in the presence of the maleimide-carrying ATRP initiator **(25)**, ruling out any feasible attachment to PDA *via* hydrophobic effects or other weak forces (**Figure 55**).

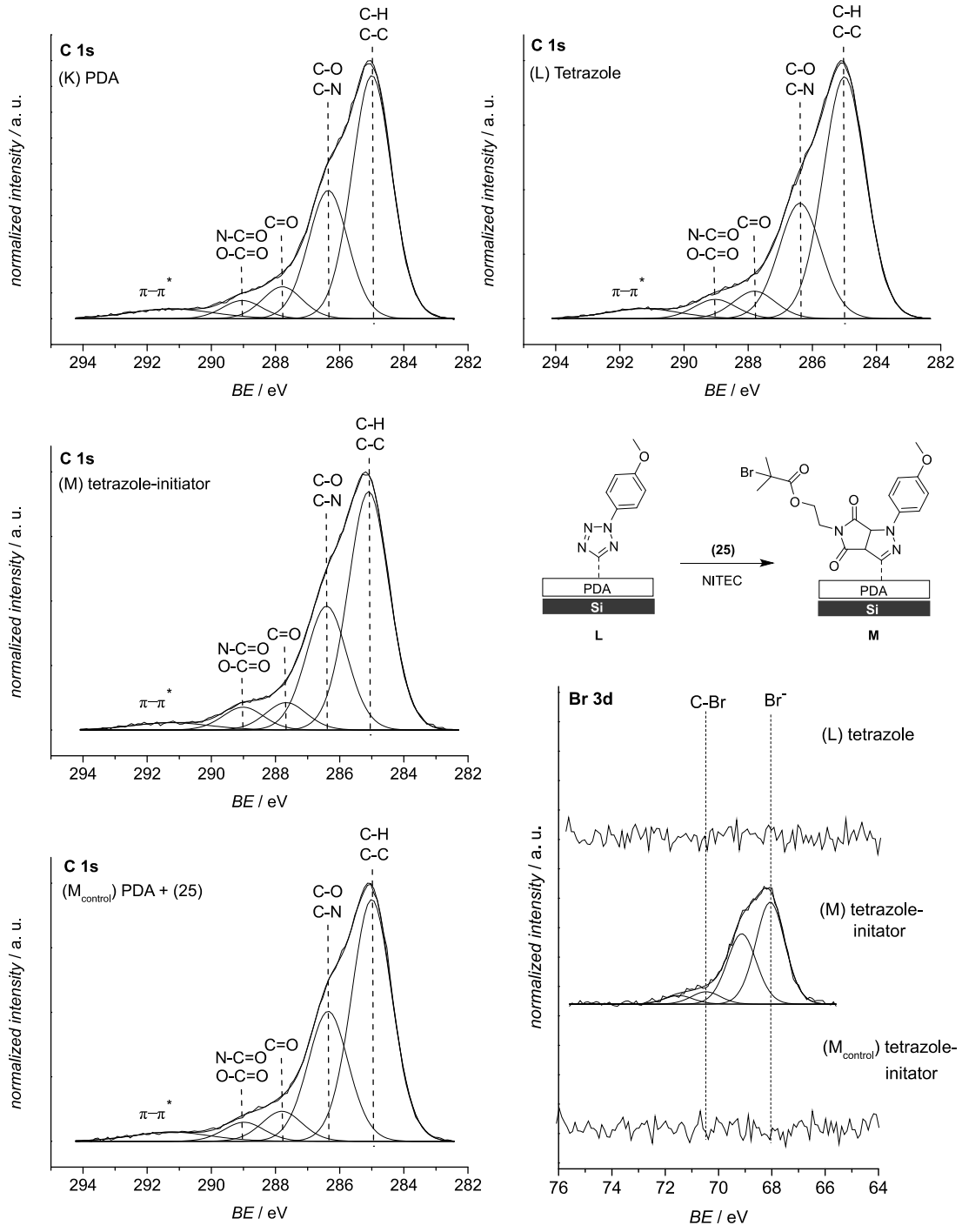

Figure 55: Corresponding XPS spectra of the step-by-step generation of a surface capable of polymerizing non-fouling polymers, namely PMeOEGMA brushes, *via* SI-ATRP **(L)**. Owing to the dominating PDA **(K)** signals in the C 1s spectra (top, middle left), the addition of small molecules to the surfaces, i.e. the attachment of the tetrazole **(L)** and the conjugation of the ATRP initiator **(M)**, does not cause significant changes. Therefore, the Br 3d spectra (bottom right) of the conjugation of the bromine-carrying ATRP initiator **(25)** to the tetrazole surface **(L)** was also recorded and exhibits the expected signals assigned to the C-Br and Br^- bonds **(M)**, which confirm the successful NITEC reaction. Furthermore, a control experiment was conducted employing a sole PDA coated substrate under NITEC reaction conditions **($M_{control}$)**. The appropriate Br 3d spectrum exhibits no signals stemming from bromine (bottom right) and, hence, underpins the former results.

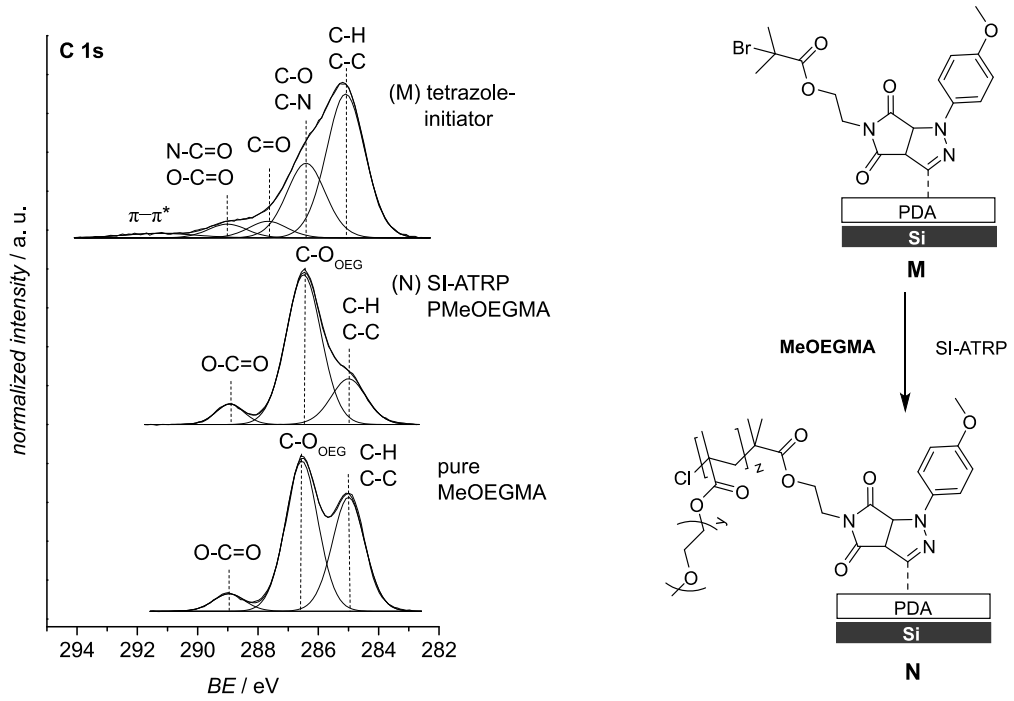

Figure 56: The grafting of PMeOEGMA brushes *via* SI-ATRP **(N)** from the previously modified surface **(M)** (right), as well as the associated C 1s XPS spectra (left) are presented. Due to the polymerization of MeOEGMA, the signal assigned to the C-O bonds at 286.4 eV, which stems from the oligo(ethylene glycol) (OEG) side chains in the PMeOEGMA backbone, increases strongly with respect to the C-C and C-H bonds at 285.0 eV. Owing to the disappearance of the signals that were formerly assigned to the surface **(M)**, the PMeOEGMA brushes must completely shield the surface. Furthermore, the XPS C 1s spectrum of pure MeOEGMA is depicted in order to compare the measured signals to the ones observed for the appropriate C 1s spectrum of the polymer.

After the ATRP initiator **(25)** was successfully attached, SI-ATRP was performed in water, employing a composition of CuCl/$CuBr_2$/Bipy as catalytic system (including 2,2'-bipyridyl (Bipy) as a ligand) (**Figure 54**). Within 30 minutes of polymerization, PMeOEGMA brushes of 15 nm thickness were generated as determined by ellipsometry **(N)** (**Table 1**). The C 1s spectrum of the entire surface after SI-ATRP **(N)** exhibits a strong increase of the signals that can be assigned to the C-O bonds of the oligo(ethylene glycol) (OEG) side chains in the MeOEGMA backbone at 286.4 eV, confirming the growth of the non-fouling polymer brushes (**Figure 56**). Noteworthy, the 15 nm brushes fully shield the PDA film as evidenced by disappearance of the π-π* signal in the C 1s of **(N)** in comparison to **(M)** and the C/O ratio close to 2:1 as expected for OEG. Furthermore, pure MeOEGMA was also characterized by XPS in order to compare the detected signals to the ones found for the polymer on the surface (**Figure 56**). Similar results were achieved. Moreover, comparing the contact angles of the present PMeOEGMA surface **(N)** to polymer brushes grown from a SAM of

ω-mercaptoundecylbromo-isobutyrate that exhibit resistance towards protein fouling,[6] similar values were detected (46.9° advancing and 23.8° receding water contact angles, respectively) (**Table 1**).[104] Hence, the similar wettability indicates that the surfaces possess comparable surface energies and, therefore, similar conformation and resistance to protein fouling of the polymer brushes is expected.

In the second approach, the tetrazole-carrying surfaces **(L)** were covered with a meander-shaped shadow mask **(L+mask)** in a metal holder (refer to Section 5.3.1). To force the spatially resolved NITEC conjugation of the maleimide-ATRP initiator solely in the irradiated regions of the substrate (**Figure 57**). The same reaction conditions as for the global graftings were applied. Thereafter, the substrate **(O)** was exposed to the described SI-ATRP conditions in order to generate non-fouling PMeOEGMA brushes in the previously initiator-attached areas (meander shape) **(P)** (**Figure 57**). The formation of the area resolved PMeOEGMA was evidenced by ToF-SIMS analysis (**Figure 57**, bottom).

The resulting ToF-SIMS images of the negatively and positively charged fragment ions of **(P)** are presented in **Figure 57**. All typically observed positively and negatively charged fragment ions originating from the OEG side chains PMeOEGMA (CH_3O^+, $C_2H_5O^+$, $C_4H_7O_2^+$ and C_2HO^-, $C_2H_3O^-$, $C_2H_2O_2^-$) were detected and accurately match the shape of the meander-shaped shadow mask (**Figure 57**, left, middle left).[188,189] In addition, the ToF-SIMS image of the CN^- fragment ions, typical for PDA,[190] displays the non-irradiated masked region. In **Figure 57**, the overlay of the negative ToF-SIMS images of the OEG fragments and the CN^- fragments is depicted on the right. Thus, the successful area resolved attachment of the ATRP initiator and the consecutive SI-ATRP were evidenced.

After the generation of a meander-shaped patterning of PMeOEGMA brushes in a grafting-from approach, the non-fouling properties of the new system are tested in appropriate cell adhesion experiments, which is investigated in the upcoming section.

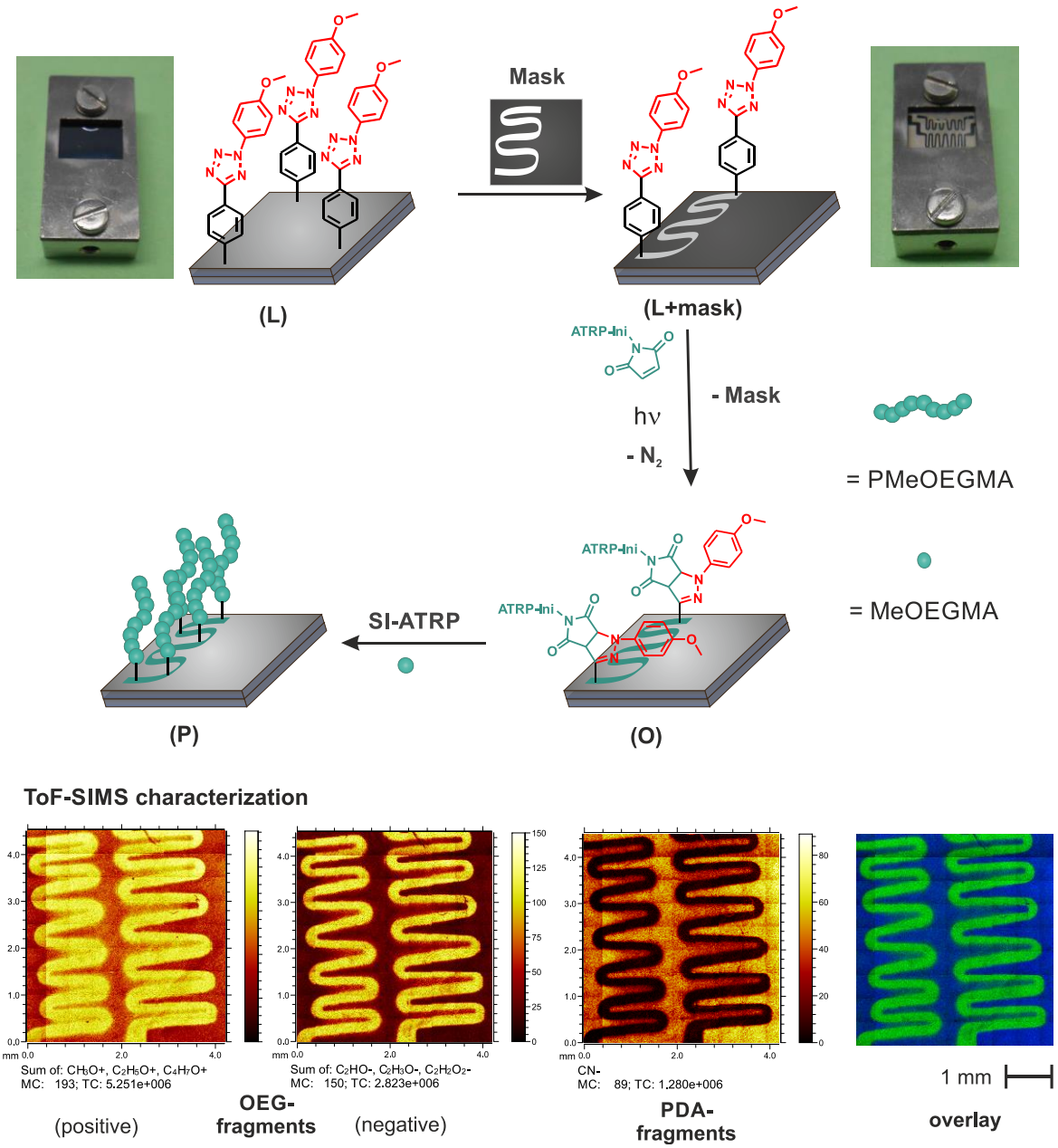

Figure 57: The schematic overview of the spatially resolved patterning and consecutive SI-ATRP is depicted on top, whereas the appropriate ToF-SIMS characterization results are presented on the bottom. The tetrazole-bearing surface **(L)** was covered with a meander shaped shadow mask **(L+mask)** in order to only conjugate the maleimide-carrying ATRP initiator **(25)** in the meander shaped area **(O)**. Thereafter, SI-ATRP was performed employing MeOEGMA as monomer to generate non-fouling PMeOEGMA brushes in a meander shaped fashion **(P)**. The successful preparation of the spatially resolved PMeOEGMA strands was verified by ToF-SIMS analysis (bottom). The signals assigned to the OEG moieties in the PMeOEGMA side chains (CH_3O^+, $C_2H_5O^+$, $C_4H_7O_2^+$ and C_2HO^-, $C_2H_3O^-$, $C_2H_2O_2^-$) (left, middle left) are only available in the meander shaped area, whereas the fragments stemming from the former PDA surface (CN^-) (middle, right) are not present in this region. An overlay of both ToF-SIMS images of the negatively charged ions is depicted on the right. Photographs of holders reprinted with permission from Ref. 29 copyright (2013) American Chemical Society.

6.2. Controlled Cell Adhesion on PMeOEGMA Patterned Surfaces

The cell adhesion studies presented in the current chapter were conducted by Michael Bachmann (AK Bastmeyer, Zoologisches Institut, KIT). In order to study the cell adhesion on the modified surfaces **(K,N,P)**, a defined number of rat embryonic fibroblasts (REFs) was seeded on bare PDA **(K)**, on PMeOEGMA grown on the whole surface **(N)** or patterned PMeOEGMA **(P)** substrates. Given that silicon substrates are not transparent, conventional light microscopy cannot be applied and thus, special REFs that are stably transfected with a vasodilator-stimulated phosphoprotein (VASP) green fluorescent protein construct were employed. VASP is a marker for focal contacts that indicates physiological cell matrix adhesion. Consequently, if the prepared substrate surface repels cell adhesion, the focal contacts are not available, hence, cells cannot spread and, as a result, the cells stay roundish.

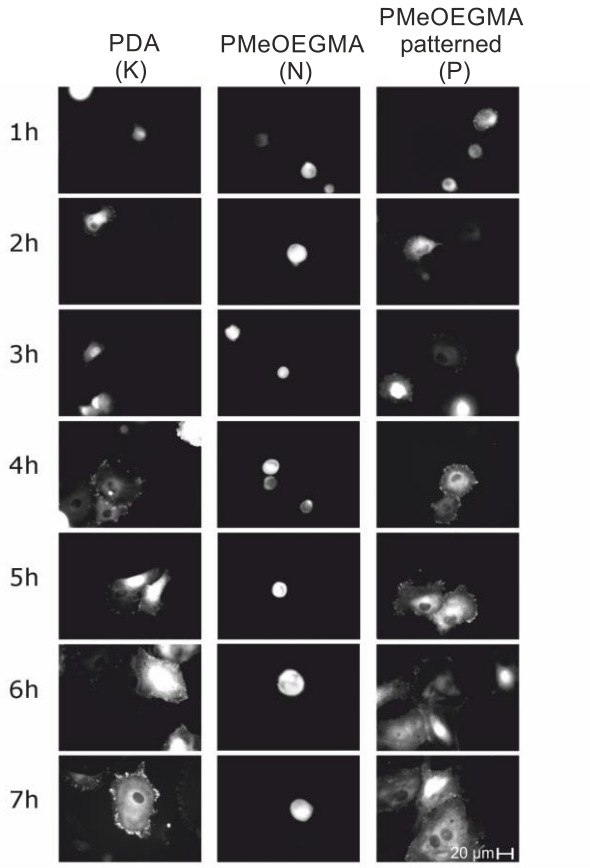

Figure 58: Monitoring of cell attachment on a bare PDA control surface **(K)** (left) and surfaces where PMeOEGMA brushes were grafted on the whole surface **(N)** (middle) or in a patterned fashion **(P)** (right). The attachment was performed for 7 hours and monitored in intervals of 1 hour. In the meantime, the cells were left in an incubator.

The attachment of the cells was monitored for 7 hours, and was imaged at 1 hour intervals. Within less than 2 hours, the cells were widely spread on the bare PDA surface **(K)** as verified by the focal contacts (**Figure 58**). In contrast, in case of the fully PMeOEGMA covered surface **(N)**, the cells stayed roundish during the entire exposure time and no focal contacts were detectable, implying that the cells were not capable of adhering to the surface (**Figure 58**). In addition, the patterned substrate **(P)** exhibited remarkable resistance to REFs adhesion in the areas where PMeOEGMA was previously grown.

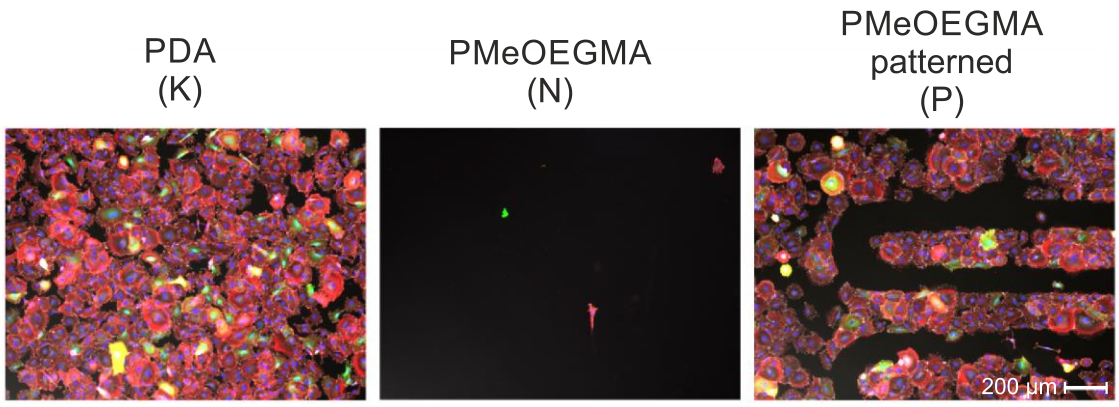

Figure 59: Stained cells after 7 hours in touch with different functionalized substrates, namely bare PDA **(K)**, PMeOEGMA on the entire surface **(N)** and patterned PMeOEGMA **(P)**. As depicted, the cells spread over the whole PDA surface, whereas they are not visible on the substrate that was completely covered with PMeOEGMA **(N)** or in the appropriate PMeOEGMA containing patterned area of **(P)**. REFs were stained for nuclei (blue), actin (red) and paxillin (gray).

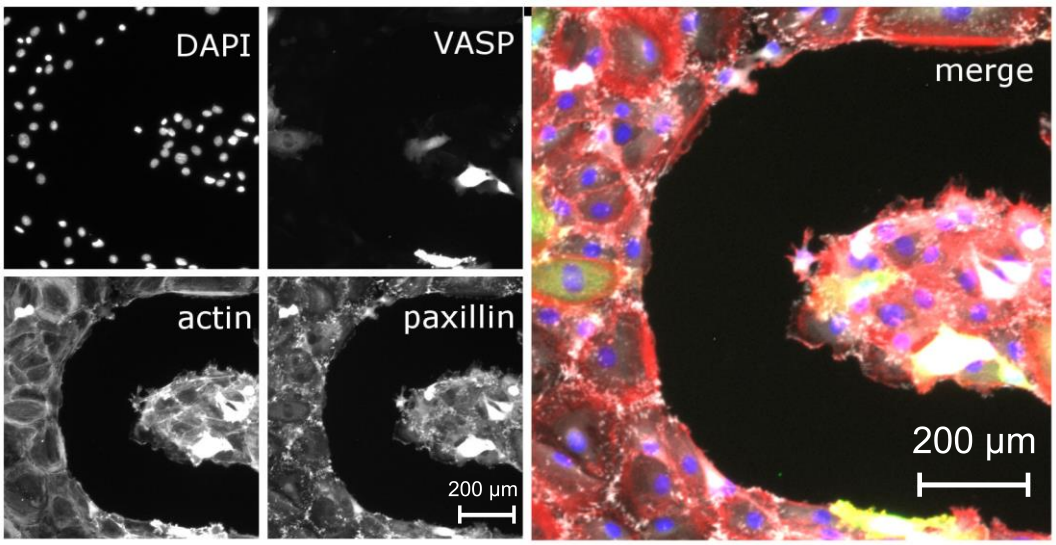

Figure 60: Close up images of fixed cells on the photo-patterned PMeOEGMA substrate **(P)**. Top left: nuclei marked with 4´,6-diamidino-2-phenylindole (DAPI); bottom left: stained actin cytoskeleton; top and bottom middle: stained VASP and paxillin as markers for focal contacts. The merged image on the right shows the precision of the pattern. In the merged figure nuclei, actin, VASP and paxillin are illustrated in blue, red and grey respectively.

After 7 hours of contact, the adhered cells were fixed. Only a certain fraction of cells that were employed in this study expressed VASP which allows their detection on the substrate utilizing fluorescence microscopy. In order to observe all adhered cells, they were stained for cell nuclei with 4´,6-diamidino-2-phenylindole (DAPI) (blue), actin, which is a main component of the cytoskeleton, as well as an indicator of cellular morphology (red) and for paxillin (gray) to detect focal contact in those cells that do not express VASP **Figure 59**). The stained image of the patterned surface **(P)** depicts that the REFs cells almost perfectly follow the pattern of the non-fouling polymer PMeOEGMA (**Figure 59**). Additionally, antibody staining protocols included copious rinsing and washing steps in order to remove the unbound cells.

In **Figure 60**, close up images of the patterned surface **(P)** present the spreading of the different species (DAPI, VASP, actin, paxillin) (left and middle) and a stained and merged image (right) of all of them. The REFs have spread and exhibit multiple focal contact points (VASP, actin) only to the areas where no PMeOEGMA is provided, implying the direct exposure to the PDA-tetrazole surface. Therefore, no cells were observed in the region where PMeOEGMA brushes were grown from, which proves the non-fouling properties of the polymer.

6.3. Summary and Outlook

In the current and final chapter of the results and discussion part, a previously prepared PDA film was modified in several steps, also including a light-triggered cycloaddition method – NITEC – in order to generate an area resolved patterning of a suitable SI-ATRP initiator. Within this microscale patterning, non-fouling PMeOEGMA brushes were grown, which exhibited extraordinary resistance towards cell attachment. Hence, controlled cell adhesion was achieved in spatially defined regions. The presented concept exhibits high significance for the fabrication of micropatterns on the microscale that can be employed to lock cells in specific areas in order to (i) control their shape and (ii) to test their behavior on changes in their microenvironment. The described investigations are of major importance for understanding cellular mechanism or testing drugs.[33] Furthermore, the preparation of non-fouling material that prevents interfaces from protein fouling and thus, from undesired effects, such as thrombosis in cardiovascular devices or non-specific response in affinity biosensors, is essential for such (bio)medical and (bio)chemical applications.[34] For this purpose, different polymeric materials, including non-fouling polymer brushes (e.g. PMeOEGMA, PHEMA) have already been widely employed.[33,34] Thus, the present system is envisioned to entail new advantages to this field owing to its independence on the type of substrate and, especially, the spatial control that can be achieved on the microscale. However, the application of copper salts as catalysts is an issue in biological systems. Thus, the present approach could be improved by performing the SI-polymerization by SET-LRP, as previously presented by Tischer *et al.*[35] Speaking of polymer brushes, an additional approach could give access to hierarchical structure by simply generating a second, but different, polymer block on top of the first one, exploiting the reactivation abilities of such RDRG systems. The novel polymer block could further be designed to provide protein tags in its backbone in order to capture particular proteins. Moreover, the additional block copolymer is also envisioned to function as precursor for even more complex hierarchical structures by providing, for instance, functionalities able to undergo light-triggered ligations with polymer strands or biomolecules. Obviously, the outstanding ability of the present protocol to generate precise polymer brushes from surfaces employing a versatile

method (SI-ATRP) that can access a vast amount monomers, as well as its independence towards the types of surfaces employed and, particularly, its spatial control establishes the base for further developments in a plethora of fields, not restricted to biomedical devices.

In the following chapter (Chapter 7), the different presented approaches (Chapter 3-6) will be compared in terms of their different surface attachment strategies, as well as the employed ligation protocols and further criteria.

7

Comparing the Systems

Within this chapter, the presented systems are compared regarding to specific aspects, such as the attachment *via* catechol anchoring or PDA film manipulation, *grafting-from versus grafting-to* approaches and the different thermal and light-induced ligation protocols that were employed.

Catechol Anchors versus PDA Films

Three approaches employing a catechol anchor system (Chapter 3-5) and one based on PDA post-modification (Chapter 6) were presented. The advantages of such catechol based systems, as they were prepared herein, lies in the covalent linkage of the corresponding ligation moiety with the catechol unit, which ensures the availability of functionalities ready to undergo thermal or light-triggered cycloadditions on the substrate. However, as the precise topology of the catechol-bearing molecules on the surfaces (formation of SAMs, partial formation of SAMs, or any different arrangement) remains elusive, the systems need to be further investigated and testing of more distinct substrates is required. In contrast, PDA films have already proven to serve as

versatile, widely applicable and post-modifiable coatings for virtually any substrate.[14,15] After the PDA film formation, the hydroxyl- or amino-groups available on the PDA film can be further modified and employed for subsequent reactions, in this case for the attachment of a tetrazole moiety that served for the linkage of an ATRP initiator to the surface in order to perform a consecutive SI-ATRP. The advantage of this approach is its miscellaneousness with regard to the applicable surfaces and the facile and versatile post-functionalization of the films. Nevertheless, the exact amount of available post-attached groups and their distribution on the surface remains uncertain. Yet, the presented approach appears to perform extraordinarily well, as evidenced by the outcome of the subsequent SI-ATRP and the cell adhesion experiments.

Grafting-to versus Grafting-from

The modification of flat substrates with macromolecular material can be achieved by *grafting-to* (Chapter 3-5) or *grafting-from* (Chapter 6) approaches. The former technique benefits from its feasibility to accurately prepare and characterize the polymer strands prior to the attachment to a surface. Thus, the molecular weights and the dispersities are precisely controlled. However, *grafting-to* approaches suffer from a range of limitations, which makes it difficult to achieve high thicknesses or dense polymer graftings.[34,103] Nevertheless, in the presented thermal HDA approach (Chapter 4), comparably high grafting densities were achieved, which proves that the developed systems operates extremely fast and well during the surface ligation process. In *grafting-from* approaches the surface polymerization initiating transfer agent or initiator is usually densely packed on the interface and thicknesses even high than 100 nm can be achieved.[34,103] The determination of grafting densities for *grafting-from* systems is a challenging and widely discussed issue as M_n of the polymer chains on the substrate is not known.[191] Some previous attempts involved the removal of polymer brushes from the surface by utilizing strong chemical substances or certain initiators that would cleave during irradiation of an external source.[191] However, the minute amount of polymer that is achieved by these methods limits the accurate determination of the molecular weights. Besides the described approach, several other attempts were performed to obtain grafting densities for polymers generated by *grafting-from*

approaches, including kinetic models, simultaneous preparation of polymer strands in solution or by the swelling ratio of the polymer brushes, among others.[191-193] Yet, the accuracy of these methods remains questionable. Nevertheless, the selection of the appropriate method – *grafting-from* or *grafting-to* – is strongly dependent on the system or the application it is intended to be employed for.

Thermal versus Light-Triggered Cycloadditions

For the surface modifications with (bio)polymers, thermal (Chapter 3-4) and light-induced (Chapter 5-6) ligation techniques were employed. First, the thermal ligation ability of (H)DA systems was utilize to coat the entire surface area of different substrates with specific polymers (PEG, PTFEMA), which were previously prepared in solution. The major advantage of these techniques is given by their applicability at ambient temperature, as well as the reversibility of the systems. Furthermore, in case of the maleimide-Cp protocol, not even a catalyst is required. However, three major disadvantages become obvious, firstly, the retro-(H)DA temperature (90 °C and 80 °C, respectively) exceeds moderate temperatures for biomolecules, secondly, the ligation groups on the surfaces are endangered to be attacked by, e.g. nucleophiles, when released in a r(H)DA reaction and, finally, only the entire surface can be modified. To overcome the described limitations, light-induced conjugation methods were employed in two projects (Chapter 5-6). The light-induced cycloadditions benefit from their applicability at ambient temperature, the generation of the reactive groups (diene or dipole) *in situ*, which makes them less susceptible to side reactions and, of major importance, their capability of performing the photo-triggered conjugation in a spatially controlled fashion. However, even though these methods seem to serve as perfect ligation tools, it needs to be considered that the described conjugations are not able to be reversed.

8

Concluding Remarks and Outlook

The aim of the current thesis was the development of novel versatile surfaces modification methods that are applicable on a wide variety of substrates, exploiting and mimicking the exceptional ability of marine organisms to adhere to virtually any surface. For this purpose, the described adhesion properties were fused with advanced polymer chemistry and different cycloaddition techniques, including distinguished DA and HDA reactions, as well as a photo-triggered approach of the same (photoenol), and NITEC, a light-induced method based on 1,3-dipolar cycloadditions. In this regard, two general well-established approaches for surface manipulation and the generation of polymer bearing substrates – *grafting-to* and *grafting-from* – were applied. Thus, three *grafting-to* (Chapter 3-5) and one *grafting-from* (Chapter 6) based systems were studied.

First, a novel retro-DA/DA switching system, based on a normal DA reaction between Cp-capped PEG and maleimide-bearing substrates, was developed (Chapter 3). This diene-dienophile pair benefits from its DA capability at ambient temperature. A macro-catechol anchor that was previously generated in a DA reaction between a maleimide

catechol and PEG-Cp, was attached to a substrate under relatively mild conditions. The feasibility of several covalent de-linkage and linkage cycles of the Cp-carrying polymer is envisioned to operate as a useful switching tool to change surface properties on demand, which could be interesting for the development of re-usable test-stripes for, e.g. water quality testing, or for the creation of versatile coatings that possess certain properties, which can be – as an additional tool – undergo changes on demand.

In a second *grafting-to* approach, the HDA capability of a newly designed dithioester derivative, which also exhibits a catechol moiety for surface attachment under mild conditions, was utilized in order to generate an efficient conjugation system with different polymers that are equipped with a Cp-unit (Chapter 4). Owing to the ability of the described system to conjugate varying polymers (PEG and PTFEMA) in a one-pot rHDA/HDA sequence on Si-substrates, the described method is envisaged to be extended to the utilization of further types of polymers, as well as to the preparation of hierarchical structures in order to create more complex application-oriented substrates, for instance, for the design of biosensors in point-of-care devices. Furthermore, the protected intermediate of the target catechol anchor was identified to operate as a controlling agent in RAFT polymerizations with different monomers (styrene, *iso*-bornyl acrylate). These abilities are envisioned to be adaptable for the preparation of well-defined polymer chains or block copolymers *via* RAFT polymerization, followed by the deprotection of the catechol moieties and further attachment to either nanoparticles or variable substrates.

The last *grafting-to* based method involved the manufacturing of a versatile substrate modification technique, where the surfaces are capable to perform photochemically driven DA cycloadditions, in order to generate spatially resolved patterning of macromolecules on the microscale (Chapter 5). A novel catechol-bearing molecule, capable of photoenolization, was synthesized, applied on surfaces under non-toxic and ambient conditions and different maleimide-capped macromolecules (PEG, PTFEMA, peptide) were conjugated under irradiation. Spatial control was achieved and evidenced by employing PTFEMA, especially due to its fluorine-bearing backbone that exhibits exceptional detection sensitivity *via* the applied surface characterization methods (XPS, ToF-SIMS), as a suitable maleimide-polymer. The presented method is envisioned to enable the establishment of novel structured material in fields were

area-defined patterns of certain (bio)macromolecules and their properties are desired, such as for the fabrication of more complex biosensors that allow to detect different types of target analytes in one solution or for the precise pattering of conductive polymers for the manufacturing of small electronic devices.

The successful preparation of a photo-patterned surfaces for the purpose to achieve precisely controlled cell adhesion was demonstrated employing highly adhesive PDA films as substrates for further modification. A successive SI-ATRP was conducted in order to generate the desired non-fouling patterning in a *grafting-from* approach (Chapter 6). The ATRP initiator was attached following the well-established NITEC protocol, whereby the area resolved patterning of the initiator was achieved. The generated cell-repellent polymer brushes (PMeOEGMA) in the patterned, meander-shaped area, withstood all cell adhesion, whereas the remaining substrate exhibited the formation of confluent layers of REFs. The cell-resistance of the PMeOEGMA brushes was monitored for 7 hours, which represents a sufficient time scale for *ex vivo* applications. Furthermore, PMeOEGMA brushes were already reported to be stable during cell cultures for more than 7 days.[33] Hence, the method employed in this project is pictured to be applicable on considerable types of interfaces, due to the exceptional ability of PDA films to adhere to a wide variety of materials. Furthermore, micropatterns have proven as excellent tool for locking cells in defined areas and investigating their behavior on externally caused changes in their microenvironments. Thus, the presented system is envisioned to also serve for this purpose and to give access to the fabrication of even more precise micropatterns.

In the following chart, all the four projects are compared with regard to five criteria: applicability at ambient temperature, catalyst free reaction conditions, spatial control, *in situ* generation of the reactive ligating moiety and reversibility of the conjugation step. The projects are classified *via* the ligation protocol that was employed.

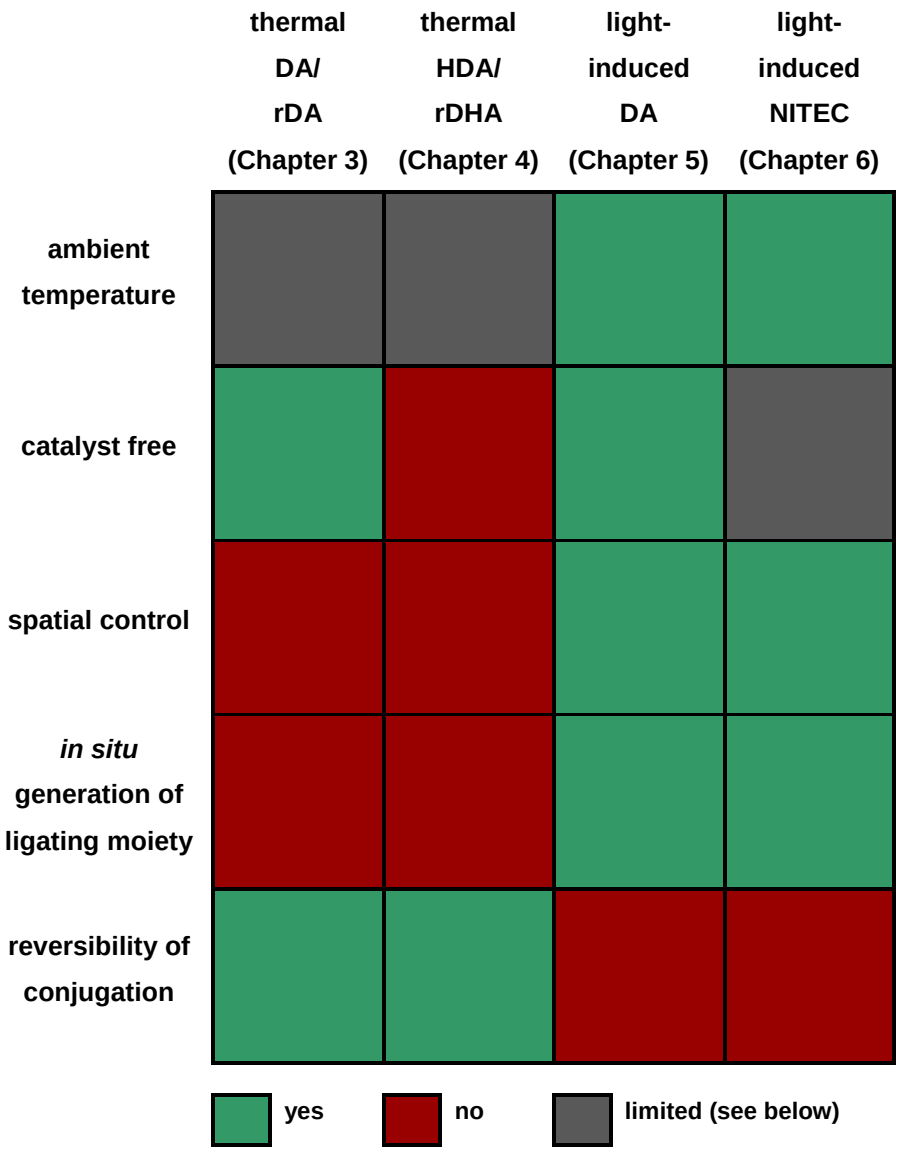

All approaches benefit from the ability to conjugate at ambient temperature. However, the r(H)DA of the thermal systems at elevated temperature still represents an issue with regard to applications involving biomolecules. Furthermore, two catalyst free protocols (thermal DA/rDA and photo-induced DA) were presented, whereas the HDA reaction in the thermal HDA/rHDA system requires TFA as a catalyst. Nevertheless, this issue can be overcome by changing the system, for instance, by employing a different Z-group, such as a cyano moiety. In general, the photo-induced NITEC reaction operates catalyst free, however, in the following SI-ATRP copper salts are employed as catalysts. As copper salts are known to be cytotoxic, other polymerization technique applicable on surfaces, such as SET-LRP, could be utilized in future systems. The photo-induced ligation protocols give access to the precise preparation of defined

micropatterns and immobilization of certain molecules in specific areas of the substrate, whereas in the thermal approaches the entire surface is functionalized. Moreover, the *in situ* generation of the reactive ligating moiety is a major advantage of the photo-triggered reaction in comparison to the thermal approaches as competing side reactions can be minimized. Yet, the ligation of these systems is not reversible and thus, no changes on the surfaces can be conducted in that fashion. In contrast, the thermal conjugation systems are reversible and are, therefore, expected to be suitable for materials where on-demand changes of the surfaces' properties are required.

In conclusion, all projects presented in this thesis successfully combine methodologies from different interdisciplinary fields, such as material science, polymer chemistry, organic synthesis and biology. The surface modification protocols developed herein, show perspectives with regard to novel pathways for the preparation of property-tailored interfaces on various substrates. Yet, some general improvement, such as transferring the methods to aqueous environments or removing catalysts, need to be conducted prior to upscaling. Furthermore, one needs to bear in mind that preparing substrates in a laboratory in a small scale is a different story than fabrication of huge batches of material in industrial production processes.

However, the outcomes of this thesis are based on concepts. Concepts by the real meaning of the word: abstract ideas, plans, intentions.[194] Concepts are always good for improvement but also for gaining new ideals and thus, for developing novel systems. Therefore, the results achieved within this explorative PhD project are envisioned to contribute to the development of more advanced and versatile surface modification procedures that can assist in the preparation of new surface-orientated materials in a (bio)chemical or medical context, as well as in material science, bearing in mind that further development and improvement of the concepts is essential.

9

Experimental Section

All materials, characterization methods and equipment that were applied as well as the syntheses and biological studies that were performed are presented in the following sections.

9.1. Materials

9.1.1. Chemicals

Acetic acid (100%, p.a., Roth), acetonitrile (MeCN) (p.a., Fischer), dry acetonitrile (dry MeCN) (99.5%, extra dry, stored over molecular sieves, Acros), aluminum oxide (Al_2O_3) (active basic and active neutral for column chromatography, Merck), *p*-anisidine (99%, ABCR), 1,8-diazabicyclo[5.4.0]undec-7-ene (DBU) (98 %, Acros), 2,2'-azobisisobutyronitrile (AIBN) (Sigma-Aldrich), *iso*-bornyl acrylate (*i*BA) (inhibited, Aldrich), chloroform (p.a., VWR), chloroform-D1 ($CDCl_3$) (99.8 %, EURISO-TOP), Cu(II)Br_2 (99 %, Fluka), Cu(I)Br (98 %, Fluka), Cu(I)Cl (98 %, Fluka), cyclohexane (p.a., VWR), dichloromethane (DCM) (p.a., VWR), dry dichloromethane (dry DCM) (extra dry, stored over molecular sieve, Acros), dicyclopentadiene (95 %, Aldrich), diethyl ether (p.a., VWR), 4-(dimethyl amino)-pyridine (DMAP) (99 %, Acros), disodium sulfate (≥ 99 %, Roth), dopamine hydrochloride (98 %, Sigma-Aldrich), ethanol (EtOH) (p.a., VWR), dry ethanol (dry EtOH) (extra dry, Acros), ethanol (EtOH, Lachner), ethyl acetate (anal. grade, Merck), 1-ethyl-3-(3-dimethylaminopropyl) carbodiimide hydrochloride (EDC·HCl) (98+ %, Alfa Aesar), 4-formylbenzoic acid (96 %, Acros Organics), hydrochloric acid (HCl) (37 %, Roth), magnesium sulfate ($MgSO_4$) (>99 %, Roth), methanol-D4 (MeOD-D4) (99.96 %, EUROISO-TOP), methanol anhydrous (99.9 %, Alfa Aesar), methanol (p.a., VWR), *N*-methoxycarbonylmaleimide (> 97 %, Sigma-Aldrich), oligo(ethylene glycol) methyl ether methacrylate (MeOEGMA) ($M_n \approx 300$ g·mol^{-1}, Aldrich), *N,N,N',N',N''*-pentamethyldiethylenetriamine (PMDETA) (98 %, Merck), poly(ethylene glycol) dimethyl ether ($PEG(OMe)_2$) ($M_n \approx 2000$ g·mol^{-1}, $\rho_{bulk} = 1.08$ g·mol^{-1} at 25 °C, Aldrich), poly(ethylene glycol) monomethyl ether ($M_n \approx 2000$ g·mol^{-1}, Aldrich), pyridine (99%, ABCR), 2,2'-bipyridyl (BiPy) (> 99 %, Sigma-Aldrich), sand (VWR), silica gel (Merck), sodium bicarbonate (≥ 99 %, Roth), sodium chloride (≥ 99.8 %, Roth), sodium cyclopentadiene solution (NaCp) (2.0 M in THF, Sigma-Aldrich), sodium nitrite ($NaNO_2$) (98 %, Alfa Aesar), styrene (S) (inhibited, Merck), sulfuric acid (H_2SO_4) (≥ 95 %, Roth), *tert*-butyl dimethylchlorosilane (TBDMS-Cl) (97 %, ABCR), tetra-*n*-butylammonium fluoride (TBAF) (1 M in THF, Alfa Aesar), tetrahydrofuran (THF) (p.a., VWR), dry tetrahydrofuran (dry THF) (extra dry, stored over molecular sieve, Acros), thionyl chloride ($SOCl_2$) (99.5 %, Acros Organics),

toluene (p.a., VWR), dry toluene (Acros, 99% and extra dry, stored over molecular sieve), triethyl amine (TEA) (> 99 %, Sigma-Aldrich), *p*-toluenesulfonyl chloride (98 %, ABCR), *p*-toluenesulfonyl hydrazide (98 %, Alfa Aesar), trifluoroacetic acid (TFA) (99.5 %, ABCR), 2,2,2-trifluoroethyl methacrylate (TFEMA) (98 %, TCI), tris(hydroxymethyl)methylamine (Tris) (> 99 %, Acros), dimethyl sulfoxide-D6 (DMSO-D6) (99.8 %, EURISO-TOP) were used as received or treated as stated below.

9.1.2. Previously Synthesized Substances and Treatment of Received Chemicals

Cyclopentadiene (Cp) was prepared by distillation of dicyclopentadiene and stored at -18°C. The Tris-buffer solutions (0.1 M or 0.3 M, pH = 8.5) were prepared before use.[195] Dithio-OH **(4)** was prepared as described by Zydziak *et al.*[165] Poly(ethylene glycol)-Cp (PEG-Cp) **(2)** ($M_n \approx 2200$ g·mol^{-1})* was synthesized as described by Nebhani *et al.*[196] Poly(trifluoro ethyl methacrylate)-Br (PTFEMA-Br) ($M_{n,NMR} \approx 5200$ g·mol^{-1}, $Đ_{SEC} = 1.22$) and poly(trifluoro ethyl methacrylate)-Cp (PTFEMA-Cp) **(10)** ($M_{n,NMR} = 5200$ g·mol^{-1}; $Đ_{SEC} = 1.22$) were prepared following the procedure published by Tischer *et al.* (polymerization time 2 h).[167] 3-(3,4-bis((tert-butyldimethylsilyl)oxy)phenyl)-2-((tert-butoxycarbonyl)-amino) propionic acid (DOPA-TBDMS$_2$-Boc) **(5)** was prepared in a two-step procedure according to Ref. 197. Styrene and *iso*-bornyl acrylate were passed through a column of basic alumina to remove the inhibitor prior to use. 2,2'-Azobisisobutyronitrile (AIBN) was recrystallized twice from methanol before use and stored at -19°C. Photoenol-COOH **(13)** was prepared as described in Ref. 28. PEG-Mal **(17)** ($M_n \approx 2200$ g·mol^{-1})* was synthesized by the reported procedure in Ref. 24. The Maleimide-ATRP initiator **(25)** was synthesized in 3 steps after Ref. 185. PTFEMA-Mal **(19)** ($M_{n,SEC} = 3700$ g mol^{-1}, $Đ_{SEC} = 1.27$) was prepared after Ref. 29.

The maleimide carrying peptide sequence Gly-Arg-Gly-Asp-Ser-linker-maleimide (PEP-Mal) **(20)** ($M = 1157.53$ g·mol^{-1}) was kindly provided by Katharina Linkert and Professor Hans Börner (HU Berlin, Germany).

* M_n values of the modified PEGs were calculate based on the supplier's declared values and rounded.

9.1.3. Surface Data

Silicon wafers (Chapter 3, 4, 6)

Silicon wafers (orientation <100>, B-doped, resistivity 5-20 Ω·cm) with 50 nm thermal silicon dioxide (SiO_2) over-layer were purchased from Siegert Consulting e.K., Germany or Si-Mat, Germany.

Au substrates (Chapter 3, 5)

The gold surfaces (1×1 cm^2) were prepared by sputtering Au on a silicon wafer. Titanium was used as adhesion-promoting agents between the silicon wafer and the gold layer. The silicon wafers (1×1 cm^2) were cleaned with ethanol and dried with air before the titanium-layers (17 nm) and the gold layers (100 nm) were sputtered.

Polyethylene substrates (Chapter 3)

Polyethylene substrates were cut out of a polyethylene sheet purchased from Goodfellow, Germany.

Graphite (Chapter 5)

Graphite substrates were cut out of a graphite sheet purchased from Goodfellow, Germany.

PET substrates (Chapter 5)

Poly(ethylene terephthalate) (PET) substrates were cut out of a PET sheet purchased from Goodfellow, UK.

9.1.4. Biochemicals and Cells

The biochemicals and cells employed for the cell adhesion experiments presented in Section 6.2 were provided by M. Bachmann (AK Bastmeyer, Zoologisches Institut, KIT).

Dulbecco's Modified Eagle Medium (DMEM) containing 4.5 $g \cdot L^{-1}$ D-glucose, L-glutamine and pyruvate, F12 medium and L-glutamine were purchased from Life Technologies. 10% v/v fetal bovine serum, purchased from Thermo Scientific, HyClone, and 1 $\mu g \cdot L^{-1}$ puromycine, purchased from Sigma-Aldrich, were added to DMEM. Penicillin-Streptomycin, also purchased from Sigma-Aldrich, was added to F12 medium. 4-(2-hydroxyethyl)-1-piperazineethanesulfonic acid (HEPES) was purchased from Carl Roth. Mouse anti-paxillin, goat anti-mouse IgG conjugated with Alexa 647, phalloidin Alexa 568 and DAPI were purchased from BD Transduction Labs, Dianove, life technologies, and Carl Roth respectively.
Rat embryonic fibroblasts (REFs) stably transfected for a vasodilator-stimulated phosphoprotein (VASP) green fluorescent protein (GFP) construct with lentiviruses were obtained from Katrin Martin and Olivier Pertz, University of Basel.

9.2. Characterization methods

^{1}H NMR (nuclear magnetic resonance) and ^{13}C NMR spectroscopy were performed using a Bruker Ascend 400 spectrometer, a Bruker AM 250 or a Bruker AM 400 spectrometers (^{1}H, 250 MHz or 400 MHz; ^{13}C, 100 MHz). All samples were dissolved in chloroform-D1, methanol-D4 or DMSO-D6. The δ-scale is referenced to the internal standard trimethylsilane (TMS, δ = 0.00 ppm).

ESI-MS (electrospray ionization-mass spectrometry) spectra were recorded on a LXQ mass spectrometer (Thermo Fisher Scientific) equipped with an atmospheric pressure ionization source operating in the nebulizer-assisted electrospray mode. The instrument was calibrated in the m/z range 195-1822 using a standard comprising caffeine, Met-Arg-Phe-Ala acetate (MRFA), and a mixture of fluorinated phosphazenes (Ultramark 1621, all from Aldrich). A constant spray voltage of 4.5 kV and a dimensionless sweep gas flow rate of 2 and a dimensionless sheath gas flow rate of 12 were applied. The capillary voltage, the tube lens offset voltage, and the capillary temperature were set to 60 V, 110 V, and 275 °C, respectively. The polymer samples were prepared in a THF / methanol solution (ratio 3 : 2) mixed with sodium trifluoroacetate, and were injected directly to the ionization source.

SEC (size exclusion chromatography) measurements were performed on a Polymer Laboratories PL-GPC 50 Plus Integrated System, comprising an autosampler, a PLgel 5 µm bead-size guard column (50 × 7.5 mm) followed by three PLgel 5 µm Mixed-C and one PLgel 3 µm Mixed-E columns (300 × 7.5 mm) and a differential refractive index detector using THF as the eluent at 35 °C with a flow rate of 1 mL·min^{-1}. Calibration was carried out employing linear poly(styrene) standards ranging from 476 to 2.5×10^6 g·mol^{-1} and linear poly(methyl methacrylate) standards ranging from 700 to 2 ×10^6 g·mol^{-1}. The injected polymers were dissolved in THF (HPLC-grade) with a concentration of 2 mg·mL^{-1}. Calculation of the molecular weight proceeded *via* the Mark-Houwink parameters for poly(styrene), *i.e.* K = 14.1×10^{-5} dL·g^{-1}, α = 0.70,[198] or poly(methyl methacrylate) K = 12.8×10^{-5} dL·g^{-1}, α = 0.69.[199]

***SEC-ESI-MS (size exclusion chromatography*-electrospray ionization-mass spectrometr**y) measurements were performed on an LXQ mass spectrometer as described above. The LXQ was coupled to a Series 1200 HPLC-system (Agilent, Santa

Clara, CA, USA) consisting of a solvent degasser (G1322A), a binary pump (G1312A), a high-performance autosampler (G1367B), followed by a thermostated column compartment (G1316A). Separation was performed on two mixed bed size exclusion chromatography columns (Polymer Laboratories, Mesopore 250 × 4.6 mm, particle diameter 3 μm) with precolumn (Mesopore 50 × 4.6 mm) operating at 30 °C. THF at a flow rate of 0.30 mL·min^{-1} was used as eluent. The mass spectrometer was coupled to the column in parallel to an RI-detector (G1362A with SS420xA/D) in a setup described earlier.[200] 0.27 mL·min^{-1} of the eluent were directed through the RI-detector and 30 μL·min^{-1} infused into the electrospray source after postcolumn addition of a 100 μM solution of sodium iodide in methanol at 20 μL·min^{-1} by a micro-flow HPLC syringe pump (Teledyne ISCO, Model 100DM). A 20 μL aliquot of a polymer solution with a concentration of 3 mg·mL^{-1} was injected onto the HPLC system.

UV-Vis spectra were recorded on a Varian Cary 300 Bio spectrophotometer. Spectra were recorded in DCM in a 10 mm path length cell. Spectra were collected between 200 and 800 nm.

***XPS* (X-ray photoelectron spectroscopy)** measurements were performed using a K-Alpha XPS spectrometer (ThermoFisher Scientific, East Grinstead, UK). All samples were analyzed using a microfocused, monochromated Al K-α X-ray source (400 μm spot size). The kinetic energy of the electrons was measured by a 180° hemispherical energy analyzer operating in the constant analyzer energy mode (CAE) at 50 eV pass energy for elemental spectra. Data acquisition and processing using the Thermo Avantage software is described elsewhere.[201] The spectra were fitted with one or more Voigt profiles (BE uncertainty: ± 0.2 eV). The analyzer transmission function, Scofield sensitivity factors,[202] and effective attenuation lengths (EALs) for photoelectrons were applied for quantification. EALs were calculated using the standard TPP-2M formalism.[203] All spectra were referenced to the C 1s peak of hydrocarbon at 285.0 eV binding energy controlled by means of the well-known photoelectron peaks of metallic Cu, Ag, and Au, respectively.

Spectroscopic Ellipsometry (Chapter 5 performed by Vanessa Trouillet) measurements of the thickness of the organic layers were conducted with a single wavelength ellipsometer SE400 (SENTECH Instruments GmbH) equipped with a HeNe laser source of 632.8 nm wavelength and a multiple angle manual goniometer.

Spectroscopic Ellipsometry (Chapter 6, performed by Dr. Ognen Pop-Georgievski) measurements were performed on a Spectroscopic Imaging Auto-Nulling Ellipsometer EP^3-SE (Nanofilm Technologies GmbH, Germany) in the wavelength range of λ = 398.9 – 900 nm (source Xe-arc lamp, wavelength step ~10 nm) prior to and after every deposition/ modification step. To increase the measurement precision, a 5× objective and position calibrated sample stage was utilized to perform repeated measurements from the same area of 1×2 mm^2 on the sample and in this way to exclude the errors from the variations of the layer thicknesses throughout the substrate area. All measurements were performed at an angle of incidence AOI = 70 °. The ellipsometric data were fitted with multilayer models using EP^4-SE analysis software (Accurion GmbH, Germany). The thickness and refractive indices *n* of PDA-tetrazole **(L)** and after functionalization with the initiator were obtained from simultaneous fitting using a Cauchy dispersion function $n = A_n + B_n/\lambda^2$ (Tetrazole: $A_n = 1.728$, $B_n = 5320$ nm^2, tetrazole initiator: $A_n = 1.641$, $B_n = 810$ nm^2) supposing optically transparent layers (*i.e.* $k = 0$). To avoid errors originating from the correlation of thickness and the optical parameters of the thin organic layers, the refractive indices were verified by calculation using the modified Lorentz-Lorenz equation[204]:

$$\frac{n^2 - 1}{n^2 + 2} \times \frac{N_A(\sum_i \Delta V_i)_{r.f.}}{k} = R$$

where $(\sum_i \Delta V_i)_{r.f.}$ and R are the Van-der-Waals volume and molar refraction of the molecules composing the layers supposing coefficient of molecular packing $k = 0.695$. The molar refraction is an additive value; which can be calculated as: $R = \sum_i R_i$, where R_i is the molar refraction of the i-th atom. The accordingly calculated refractive indices for tetrazole and tetrazole initiator were: 1.7414 and 1.6179, respectively. The good agreement between the fitted and calculated optical constants for the ultra-thin organic layers indicates a low correlation between the fitted thicknesses and Cauchy dispersion function parameters. The optical dispersion function of PDA is provided elsewhere.[205] The Si/SiO_2 substrates were modeled using the dispersion functions published by Herzinger *et al.*[206]

ToF-SIMS (time-of-flight secondary ion mass spectrometry) was performed on a TOF.SIMS^5 instrument (ION-TOF GmbH, Münster, Germany), equipped with a Bi cluster liquid metal primary ion source and a non-linear time of flight analyzer. The Bi source

was operated in the "bunched" mode providing 0.7 ns Bi^{1+} ion pulses at 25 keV energy and a lateral resolution of approx. 4 µm. The short pulse length allowed for high mass resolution to analyze the complex mass spectra of the immobilized organic layers. Images larger than the maximum deflection range of the primary ion gun of 500×500 μm^2 were obtained using the manipulator stage scan mode. Negative polarity spectra were calibrated on the C^-, C_2^-, and C_3^- peaks. Positive polarity spectra were calibrated on the C^+, CH^+, CH_2^+, and CH_3^+ peaks. Primary ion doses were kept below 10^{11} ions/cm^2 (static SIMS limit).

Contact Angle (Chapter 5) measurements were conducted by the dynamic water drop method using a custom-made contact angle system. A 10 µL drop was placed on the surface. The volume increase and the advancing contact angle was recorded when the drop was 25 µL. Data was evaluated using a tangent leaning algorithm.

Contact angle goniometry (Chapter 6) of the wettability of the surfaces was examined by the dynamic sessile water drop method using a DataPhysics OCA 20 contact angle system. A 2 µL drop was placed on the surface and advancing and receding contact angles were determined while the volume of the drop was increased up to 4 µL and decreased at a flow rate of 0.2 $\mu L \cdot min^{-1}$. The data was evaluated using the tangent leaning method. The reported values are averages of at least three measurements recorded at different positions on each substrate.

9.3. Equipment

9.3.1. Metal Holder and Shadow Mask

The general setup of the metal holders, which were employed in order to generate the light-induced meander shaped pattering on the corresponding surfaces in Section 5.3 and 6.1 is depicted in **Figure 61**. The pure holder is presented on the left, whereas the holder including the meander shaped shadow mask on top of the to be irradiated substrate is shown on the right.

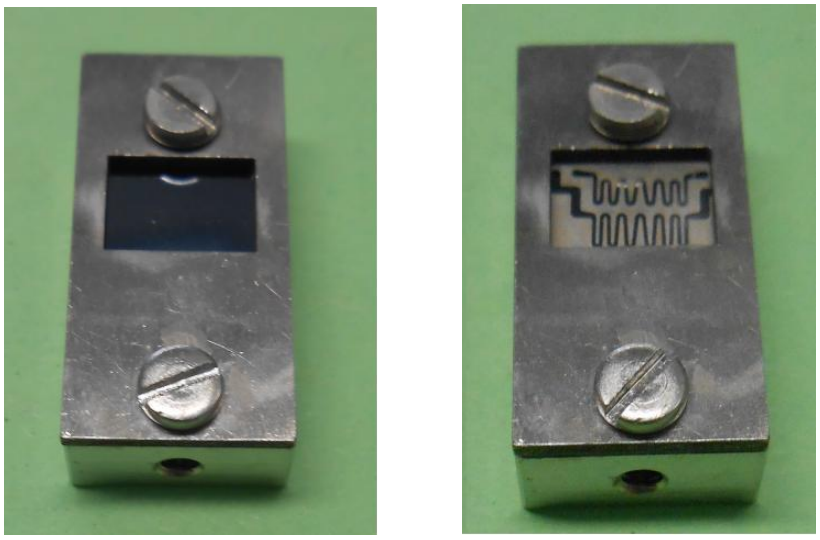

Figure 61: The metal sample holder that is employed in the photo-induced ligation surface modification studies (Section 5.3 and 6.1) is depicted. On the left, the holder that possesses a window inset, is presented, whereas the same setup including the applied meander-shaped shadow mask is shown on the right. Reprinted with permission from Ref. 29. Copyright (2013) American Chemical Society.

9.3.2. Photoreactor

In order to execute photoenol ligations (Chapter 5) or NITEC reactions (Chapter 6), a photoreactor, as described in Ref. 28, was employed (**Figure 63**). The samples were irradiated with a low-pressure fluorescent lamp (Arimed B6, Cosmedico GmbH, Stuttgart, Germany) emitting at 320 nm (± 30 nm, 36 W). The spectrum of the UVA lamp is depicted in **Figure 62**.

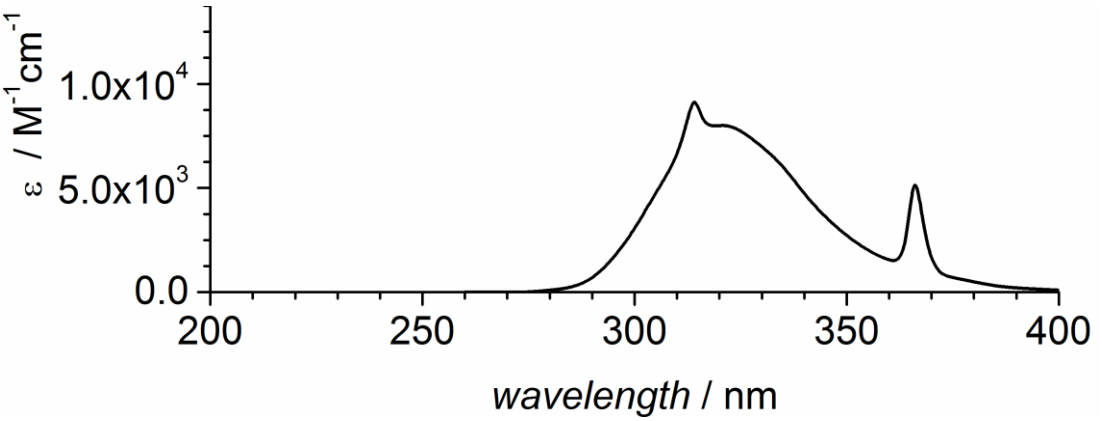

Figure 62: Emission spectrum of the UVA lamp Arimed B6 (36 W, λ_{max} = 320 nm ± 30 nm). Reprinted with permission from Ref. 28. Copyright (2012) John Wiley and Sons.

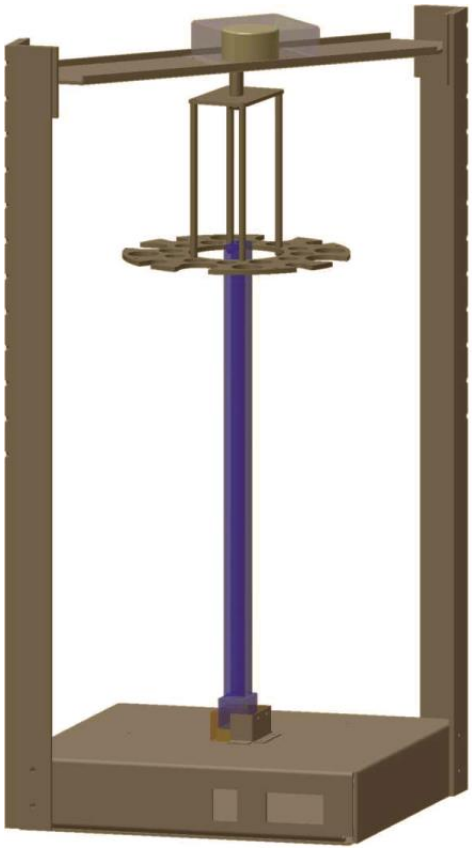

Figure 63: Schematic setting of the photoreactor. The Arimed B6 lamp (Cosmedico GmbH, Stuttgart, Germany) in the middle (blue) emits irradiation in the UVA region ($\lambda \approx 320$ nm). The samples are situated in the wheel-shaped disc in the upper part of the reactor, which rotates while the samples are irradiated. The picture was drawn by Till Gruendling. Reprinted with permission from Ref. 28. Copyright (2012) John Wiley and Sons.

9.4. Syntheses

All manipulations of air-sensitive substances or materials were conducted under rigorous exclusion of moisture and oxygen in Schlenk-type glassware on a dual manifold Schlenk line, connected to a high vacuum line (10^{-3} torr).

9.4.1. Syntheses of Small Molecules

Dopamine-maleimide (dM) (1) was prepared according to a modified procedure described in Ref. 69. In a 250 mL round bottom flask, dopamine·HCl (0.407 g, 2.64 mmol, 1.0 eq.) was dissolved in 20 mL saturated $NaHCO_3$ solution at 0 °C in the absence of light. After the addition of *N*-methoxycarbonylmaleimide (0.496 g, 2.64 mmol, 1.0 eq.) the cooling bath was removed and the mixture was allowed to stir at ambient temperature for 10 minutes, at which point water (70 mL) was added to the solution. The mixture was stirred at ambient temperature for 40 min and the solution was subsequently adjusted to pH = 1.5 with H_2SO_4 (37 %). The resulting aqueous solution was extracted with ethyl acetate (4 × 50 mL). The organic fraction was dried over Na_2SO_4 and the solvent was removed on a rotary evaporator to afford 0.787 g of an orange-yellowish oil and a yellow solid (crude product). The product was purified employing column chromatography (DCM : methanol = 40 : 1, silica gel) to give a yellow-brownish solid, which was further purified by washing with ice-cold chloroform. The product was dried *in vacuo* to give yellow crystals (0.267 g, 43.4 %). ^{1}H NMR (250 MHz, DMSO-D6): δ (ppm) = 8.77 (s, 1 H, Ph-O**H**), 8.67 (s, 1 H, Ph-O**H**), 6.98 (s, 2 H, -CO-C**H**-C**H**-CO-), 6.59 (d, ^3J = 7.9 Hz, 1 H, -CH-C**H**-C(OH)-), 6.52 (d, ^3J = 1.9 Hz, 1 H, -C-C**H**-C(OH)-), 6.36 (dd, ^3J = 8.0, 1.9 Hz, 1 H, -C**H**-CH-C(OH)-), 3.53 (t, 2 H, ^3J = 7.3 Hz, -N-C**H$_2$**-CH$_2$-Ph), 2.61 (t, 2 H, ^3J = 7.3 Hz, -N-CH$_2$-C**H$_2$**-Ph). ^{13}C NMR (100 MHz, DMSO-D6): δ (ppm) = 170.82 (s, -**C**O-CH-CH-**C**O-), 145.10 (s, -CH-**C**(OH)-), 143.71 (s, -CH-CH-**C**(OH)-), 134.44 (s, -CO-**C**H-**C**H-CO-), 128.83 (s, -C(OH)-CH-**C**-CH-CH-C(OH)-), 119.23 (s, -C(OH)-CH-C-**C**H-CH-C(OH)), 115.94 (s, -C(OH)-**C**H-C-CH-CH-C(OH)), 115.52 (s, -C(OH)-CH-C-CH-**C**H-C(OH)), 33.09 (s, -N-**C**H$_2$-CH$_2$-Ph), 30.68 (s, -N-CH$_2$-**C**H$_2$-Ph).

HDA-DOPA-TBDMS$_2$-Boc (6) was prepared under inert conditions. DOPA-Boc-TBDMS$_2$ **(5)** (0.498 g, 0.95 mmol, 1.3 eq.) was dissolved in dry DCM (10 mL). EDC·HCl (0.450 g, 2.19 mmol, 3.0 eq.) was added and the reaction mixture was stirred for 30 minutes at ambient temperature. Dithio-OH **(4)** (0.200 g, 0.73 mmol, 1.0 eq.), previously dissolved in dry DCM (3 ml), and DMAP (0.018 g, 1.46 mmol, 0.2 eq.) were added and allowed to react for 24 hours at ambient temperature. Subsequently, DCM (25 mL) was added and the organic layer was washed with water (6 ×). The DCM fraction was dried over Na_2SO_4 and purified by column chromatography (cyclohexane : ethyl acetate = 5 : 1, R_f = 0.38, silica gel) to give of a pink solid (0.303 g, 53 %). ^{1}H NMR (250 MHz, DMSO-D6): δ (ppm) = 8.63 (d, 1 H, -N-C**H**-CH-), 8.25 (d, 1 H, -N-C-C**H**-), 7.99 (t, 1 H, -N-CH-C**H-**), 7.69 (dd, 1 H, -N-C-CH-C**H-**), 7.40 (d, 2 H, -S-CH$_2$-C-(C**H**-CH-)C**H**-CH-), 7.32 (d, 1 H, -N**H**-), 7.25 (d, 2 H, -S-CH$_2$-C-(CH-C**H**-)CH-C**H**-), 6.80 – 6.61 (m, 3 H, Ar-H (Dopa)), 5.07 (s, 2 H, -O-C**H$_2$**-C-), 4.55 (s, 2 H, -S-C**H$_2$**-C-), 4.14 (s, 1 H, -CH$_2$-C**H**-COO-), 2.92-2.69 (m, 1 H, -C**H**$_2$-CH-COO-), 1.26 (s, 9 H, -CO-C(C**H$_3$**)$_3$), 0.92 (s, 18 H, (-O-Si-C (C**H$_3$**)$_3$)$_2$), 0.14 (s, 12 H, -Si-(C**H$_3$**)$_2$). ^{13}C NMR (100 MHz, $CDCl_3$): δ (ppm) = 226.02 (S=**C**-S-), 171.88 (-CH$_2$-O-(**C**=O)-CH-NH-), 156.48 (-CH-**C**-N-), 154.87 (-NH-(**C**=O)-O-), 148.11 (-C-N-**C**H-CH), 146.83 (-C-CH-**C**(-OTBDMS)-C(-OTBDMS)-CH-CH-), 146.09 (-C-CH-C(-OTBDMS)-**C**(-OTBDMS)-CH-CH-), 137.04 (-**C**-CH$_2$-O-(C=O)-CH-NH-), 135.58 (-S-CH$_2$-**C**-), 134.80 (-C-N-CH-CH-**C**H-CH-), 129.79 (-S-CH$_2$-C-(**C**H-CH)$_2$-), 128.83 (-**C**-CH-C(-OTBDMS)-C(-OTBDMS)-CH-CH-), 126.96 (-S-CH$_2$-C-(CH-**C**H)$_2$-), 122.37 (-C-N-CH-CH-CH-**C**H-, -C-N-CH-**C**H-CH-CH-), 79.99 (-NH-(C=O)-O-**C**-Me$_3$), 66.78 (-**C**H$_2$-O-(C=O)-CH-NH-), 54.53 (-CH$_2$-O-(C=O)-**C**H-NH-), 41.18 (-S-**C**H2-C-(CH-CH)$_2$-), 37.53 (-CH$_2$-O-(C=O)-CH-**C**H$_2$-C-), 28.44 (-O-Si-**C**-(CH$_3$)$_3$), 26.06 (-NH-(C=O)-O-C-(**C**H$_3$)$_3$), 18.55 (-O-Si-C-(**C**H$_3$)$_3$), -3.92 ((-O-Si-(**C**H$_3$)$_2$). *m/z* [**6**+Na]$^+_{exp}$ = 805.4; *m/z* [**6**+Na]$^+_{theo}$ = 805.3. UV/Vis: λ_{max} = 348 nm.

HDA-DOPA-TBDMS2-Boc-Cp (7): HDA-DOPA-TBDMS$_2$-Boc **(6)** (70.0 mg, 0.089 mmol, 1.0 eq.) was dissolved in DCM (2 ml). Cyclopentadiene (Cp) (8.9 mg, 0.134 mmol, 1.5 eq.) and trifluoroacetic acid (TFA) (20.0 mg, 0.179 mmol, 1.33 eq.) were added. The color changed from pink to colorless immediately. The reaction mixture was stirred for 10 minutes at ambient temperature. The crude product was concentrated *in vacuo* and the final purification was carried out by column chromatography (ethyl acetate : cyclohexane = 2 : 1, R_f = 0.33, silica gel) to give of a colorless solid (18 mg, 24 %). ^{1}H NMR (400 MHz, DMSO-D6): δ (ppm) = 8.48 (d, 1 H, -C-N-C**H**-CH-), 7.72 (t, 1 H, -C-N-CH-C**H-**), 7.38 (d, 1 H, -N-C-CH-C**H-**), 7.28 (d, 1H, -O-(C=O)-CH-N**H**-(C=O)-O-), 7.22 (d, 1 H, -N-C-C**H**-), 7.16-7.01 (m, 4 H, -S-CH2-C-(C**H**-C**H**)$_2$-C-), 6.82-6.59 (m, 3 H, -C-C**H**-C**H**-C(-OTBDMS)-C(-OTBDMS)-C**H**-), 6.29 (d ,1 H,-C-CH$_{bridgehead}$-C**H**=CH-), 5.75 (d, 1 H,-C-CH$_{bridgehead}$-CH=C**H**-), 5.00 (s, 2 H, -C-C**H$_2$**-O-(C=O)-CH-NH-), 4.15 (s, 2 H, -S-C**H$_2$**-C-), 4.10 (m, 1 H, -C-CH$_2$-O-(C=O)-C**H**-NH-), 3.79 (d, 1 H, ,-S-C**H**$_{bridgehead}$-CH=CH-), 3.37 (d, 1H, ,-C-C**H**$_{bridgehead}$-CH=CH-), 2.80 (m, 2H, -C-CH$_2$-O-(C=O)-CH-C**H$_2$**-C-), 2.37+1.85 (d, 1 H each, ,-S-CH$_{bridgehead}$-C**H$_2$**-C$_{bridgehead}$-C-), 1.30 (s, 9 H, -O-C-(C**H**$_3$)$_3$), 0.93 (s, 18 H, (-O-Si-C-(C**H$_3$**)$_3$)$_2$), 0.15 (s, 12 H, (-O-Si-C-(C**H$_3$**)$_2$)). ^{13}C NMR (100 MHz, $CDCl_3$): δ (ppm) = 171.84 (-CH$_2$-O-(**C**=O)-CH-NH-), 162.81 (-CH-**C**-N-), 155.17 (-NH-(**C**=O)-O-), 147.31 (-C-N-**C**H-CH)), 146.81 (-C-CH-**C**(-OTBDMS)-C(-OTBDMS)-CH-CH-), 146.07 (-C-CH-C(-OTBDMS)-**C**(-OTBDMS)-CH-CH-), 138.03 (-**C**-CH$_2$-O-(C=O)-CH-NH-), 136.44 (-S-CH$_2$-**C**-), 133.89 (-C-N-CH-CH-**C**H-CH-), 129.28 (-**C**H=**C**H-CH$_{bridgehead}$-), 128.92 (-S-CH2-C-(**C**H-CH)$_2$-), 128.51 (-**C**-CH-C(-OTBDMS)-C(-OTBDMS)-CH-CH-), 125.23 (-S-CH2-C-(CH-**C**H)$_2$-), 122.36 (-C-N-CH-CH-CH-**C**H-), 121.68 (-C-N-CH-**C**H-CH-CH-, -C-CH-C(-OTBDMS)-C(-OTBDMS)-**C**H-**C**H-), 121.16 (-C-**C**H-C(-OTBDMS)-C(-OTBDMS)-CH-CH), 79.95 (-NH-(C=O)-O-**C**-Me$_3$), 75.75 (pyridinyl-**C**-S-CH$_2$-), 66.87 (-**C**H$_2$-O-(C=O)-CH-NH-), 54.50 (-CH$_2$-O-(C=O)-**C**H-NH-), 53.47 (-CH=CH-CH$_{brigdehead}$-**C**H$_2$-CH$_{brigdehead}$-), 50.41 (-**C**H$_{bridgehead}$-CH=CH-**C**H$_{bridgehead}$-S-), 37.14 (-CH$_2$-O-(C=O)-CH-**C**H$_2$-C-), 31.06 (-S-**C**H2-C-(CH-CH)$_2$-), 28.44 (-O-Si-**C**-(CH$_3$)$_3$), 26.07 (-NH-(C=O)-O-C-(**C**H$_3$)$_3$) , 18.56 (-O-Si-C-(**C**H$_3$)$_3$), -3.94 ((-O-Si-(**C**H$_3$)$_2$). *m/z* [**7**+Na]$^+_{exp}$ = 871.1. *m/z* [**7**+Na]$^+_{theo}$ = 871.3.

HDA-DOPA-Cp (8) was prepared as following. HDA-DOPA-TBDMS$_2$-Boc-Cp **(7)** (50 mg, 0.059 mmol) was dissolved in TFA (2 mL, 95 %) and stirred for 3.5 h. TFA was removed under reduced pressure. Diethyl ether was added and removed for washing purposes (3 ×). The product **(8)** was dried and used immediately for the surface reaction. m/z [**8**+Na]$^+_{exp}$ = 543.0. m/z [**8**+H]$^+_{exp}$ = 521.0. m/z [**8**+Na]$^+_{theo}$ = 543.1 and m/z [**8**+H]$^+_{theo}$ = 521.1.

Photo-Gly (14): 4-((2-formyl-3-methylphenoxy)methyl)benzoic acid (Photo-COOH) **(13)** (0.500 g, 1.85 mmol, 1.0 eq.) and EDC·HCl (1.064 g, 5.55 mmol 3.0 eq.) were dissolved in dry DCM (30 mL) under a nitrogen atmosphere. After 20 min, ethane-1,2-diol (0.4 mL, 7.15 mmol, 3.86 eq.) and DMAP (0.045 g, 0.37 mmol, 0.2 eq.) were added. The mixture was stirred overnight at ambient temperature. Water was added and the organic fraction was washed with water (3×), $NaHCO_3$ (1×), brine (3×) and water (3×) again. The organic fraction was dried over $MgSO_4$ and purified *via* column chromatography (cyclohexene : ethyl acetate = 1 : 1, R_f = 0.33, silica gel) to give a white solid (0.070 g, yield: 60.2 %). ^{1}H NMR (400 MHz, $CDCl_3$): δ = 10.76 (s, 1 H, aldehyde), 8.10 (d, ^3J = 7.8 Hz, 2 H, (-CH-C**H**-(C-(C=O)-O-)-C**H**-CH-)), 7.51 (d, ^3J = 7.7 Hz, 2 H, (-C**H**-CH-(C-(C=O)-O-)-CH-C**H**-)), 7.36 (t, ^3J = 8.1 Hz, 1 H, Me-C-CH-C**H**-CH-(C-O-CH_2-)-), 6.85 (d, ^3J = 8.1 Hz, 2 H, Me-C**H**-CH-C**H**-(C-O-CH_2-)-), 5.23 (s, 2 H, CH-(C-CH-)-O-C**H$_2$**-(C-CH-)-CH-), 4.48 (d, ^3J = 2.8 Hz, 2 H, -(C=O)-O-C**H$_2$**-CH_2-OH), 3.98 (d, ^3J = 2.8 Hz, 2 H, -(C=O)-O-CH_2-C**H$_2$**-OH), 2.59 (s, 3H, CH-(C-CH-)-**Me**). ^{13}C NMR (100 MHz, $CDCl_3$): δ = 192.14 (aldehyde), 166.68 (-(**C**=O)-O-CH_2-), 162.02 (-CH-(**C**-O-CH_2)-C-), 142.50 (-CH-(**C**-CH_2-)-CH-), 141.82 (Me-**C**-CH-CH-CH-(C-O-CH_2-)-), 134.55 (Me-C-CH-**C**H-CH-(C-O-CH_2-)-), 130.29 (-CH-**C**H-(C-(C=O)-O-)-**C**H-CH-), 129.84 (-CH-CH-(**C**-(C=O)-O-)-CH-CH-), 127.04 (-**C**H-CH-(C-(C=O)-O-)-CH-**C**H-), 124.90 (Me-C-**C**H-CH-CH-(C-O-CH_2-)-), 123.85 ((H-C=O)-**C**-CH-),110.46 (Me-C-CH-CH-**C**H-(C-O-CH_2-)-), 70.06 (-CH-(C-CH-)-O-**C**H_2-(C-CH-)-CH-), 66.93 (-(C=O)-O-**C**H_2-CH_2-OH), 61.62 (-(C=O)-O-CH_2-**C**H_2-OH), 21.63 (**Me**-C-CH-CH-CH-(C-O-CH_2-)-). m/z [**14**+Na]$^+_{theo}$ = 337.17. m/z [**14**+Na]$^+_{theo}$ = 337.10.

Photo-DOPA-TBDMS$_2$ (15): DOPA-TBDMS$_2$-Boc **(5)** (0.063 g, 0.119 mmol, 1.0 eq.) and EDC·HCl (0.069 g, 0.358 mmol, 3.0 eq.) were dissolved in dry DCM (40 mL). After 20 minutes, Photo-Gly **(14)** (0.045 g, 0.143 mmol, 1.2 eq.) and DMAP (0.015 g, 0.119 mmol, 1.0 eq.) were added. The mixture was stirred for 22 h at ambient temperature. DCM (20 mL) was added and the mixture was washed with brine (3 ×) and water (3 ×). The organic phase was dried over $MgSO_4$ and the solvent was removed. Purification was performed *via* column chromatography (cyclohexane : ethyl acetate = 1 : 1, R_f = 0.65, silica gel) to give a white oil (0.065 g, 66.3 %). ^{1}H NMR (250 MHz, $CDCl_3$): δ = 10.75 (s, 1 H, aldehyde), 8.08 (d, ^3J=8.3 Hz, 2 H, (-CH-C**H**-(C-(C=O)-O-)-C**H**-CH-)), 7.50 (d, ^3J=8.3 Hz, 2 H, (-C**H**-CH-(C-(C=O)-O-)-CH-C**H**-)), 7.35 (t, ^3J = 7.9 Hz, 1 H, Me-C-CH-C**H**-CH-(C-O-CH_2-)-), 6.84 (d, ^3J=8.1, 2 H, Me-C-C**H**-CH-C**H**-(C-O-CH_2-)-), 6.71-6.49 (m, 3 H, arom. H at DOPA-OTBDMS), 5.22 (s, 2 H, CH-(C-CH-)-O-C**H$_2$**-(C-CH-)-CH-), 4.93 (s, 1 H, -N**H**-Boc), 4.64 – 4.38 (m, 5 H, -(C=O)-O-C**H$_2$**-C**H$_2$**-O-, NH-C**H**((C=O)-O-)-CH_2-arom.), 2.96 (s, 2 H, -NH-CH((C=O)-O-)-C**H$_2$**-arom.), 2.59 (s, 3 H, **Me**-C-CH-CH-CH-(C-O-CH_2-)-), 1.41 (s, 9 H, **Boc**), 0.97 (s, 18 H, **tBu** at TBDMS), 0.17 (s, 12 H, **Me** at TBDMS). ^{13}C NMR (100 MHz, $CDCl_3$): δ = 192.07 (aldehyde), 171.93 (-NH-CH((**C**=O)-O-)-CH_2-arom.), 166.03 (arom-(**C**=O)-O-CH_2-CH_2-), 162.03 (-CH-(**C**-O-CH_2)-C-), 155.21 (-NH-(**C**=O)-O-tBu), 146.90 (-C-CH-(**C**-OTBDMS)-(C-OTBDMS)-CH-CH-), 146.16 (-C-CH-(C-OTBDMS)-(**C**-OTBDMS)-CH-CH-), 142.48 (-CH-(**C**-CH_2-)-CH-), 141.84 (Me-**C**-CH-CH-CH-(C-O-CH_2-)-), 134.53 (Me-C-CH-**C**H-CH-(C-O-CH_2-)-), 130.34 (-CH-**C**H-(C-(C=O)-O-)-**C**H-CH-), 129.65 (-CH-CH-(**C**-(C=O)-O-)-CH-CH-), 128.88 (-NH-(CH-(C=O))-CH_2-**C**-) 127.03 (-**C**H-CH-(C-(C=O)-O-)-CH-**C**H-), 124.88 (Me-C-**C**H-CH-CH-(C-O-CH_2-)-), 123.84 ((H-C=O)-**C**-CH-), 122.40 (-C-CH-(C-OTBDMS)-(C-OTBDMS)-CH-**C**H-), 122.29 (-C-CH-(C-OTBDMS)-(C-OTBDMS)-**C**H-CH-), 121.21 (-C-**C**H-(C-OTBDMS)-(C-OTBDMS)-CH-CH-), 110.43 (Me-C-CH-CH-**C**H-(C-O-CH_2-)-), 80.03 ((-NH-(C=O)-O-**C**-Me_3), 70.04 (-CH-(C-CH-)-O-**C**H_2-(C-CH-)-CH-), 63.10 (-(C=O)-O-**C**H_2-CH_2-O-(C=O)-CH), 62.78 (-(C=O)-O-CH_2-**C**H_2-O-(C=O)-CH), 54.43 (-NH-(**C**H-(C=O))-CH_2-C-), 37.50 (-NH-(CH-(C=O))-**C**H_2-C-), 28.43 (-SiMe_2-**C**-Me_3), 26.06 (-NH-(C=O)-O-C-**Me$_3$**), 21.63 (-SiMe_2-C-**Me$_3$**), 18.56 (CH-(C-CH-)-**Me**), 1.16 (-Si**Me$_2$**-tBu). *m/z* [**15**+Na]$^+_{exp}$ = 844.41. *m/z* [**15**+Na]$^+_{theo}$ = 844.39.

Photo-DOPA (16): Photo-DOPA-TBDMS$_2$ **(15)** (0.4 g, 0.487 mmol) was dissolved in THF (2 mL). TBAF (0.973 mL, 0.973 mmol) in THF (1.0 M) was added and the mixture was stirred for 30 minutes at ambient temperature. The solvent was removed. The raw product was dissolved in DCM and washed with water (2 ×), diluted HAc (0.05 M) (2 ×), brine (2 ×) and water (2 ×). The organic fraction was dried over $MgSO_4$ and the solvent was removed. The product was applied for the surface reactions immediately. *m/z* [**16**+Na]$^+_{exp}$ = 616.25. *m/z* [**16**+Na]$^+_{theo}$ = 616.22.

4-((2-tosylhydrazono)methyl)benzoic acid (22): A mixture of 4-formylbenzoic acid (6.558 g, 43.7 mmol, 1.0 eq.) and *p*-toluenesulfonylhydrazide (8.138 g, 43.7 mmol, 1.0 eq.) in ethanol (100 mL) was heated to reflux for 30 minutes. The solution was diluted with water (100 mL) and the precipitate was filtered off. The solid was washed with aqueous ethanol (100 mL). Yield: 14.5 g (98 %).^{1}H NMR (250 MHz, DMSO-D6): δ (ppm) = 13.07 (s, 1 H, -COO**H**), 11.68 (s, 1 H, Ph-C**H**=N-NH-), 7.96 (s, 1 H, Ph-CH=N-N**H**-), 7.94 (d, ^3J = 8.3 Hz, 2 H, -CH-C**H**-C(-COOH)-C**H**-CH-), 7.77 (d, ^3J = 8.2 Hz, 2 H, -C**H**-CH-C(-COOH)-CH-C**H**-), 7.66 (d, ^3J = 8.2 Hz, 2 H, -C**H**-CH-C(-CH_3)-CH-C**H**-), 7.41 (d, ^3J = 8.3 Hz, 2 H, -CH-C**H**-C(-CH_3)-C**H**-CH-), 2.35 (s, 3 H, -CH-CH-C(-C**H$_3$**)-CH-CH-). ^{13}C NMR (100 MHz, DMSO-D6) δ (ppm) = 166.74 (-**C**OOH), 145.63 (Ph-**C**H=N-NH-), 143.49 (-CH-CH-**C**(-SO_2-NH-)-CH-CH-), 137.54 (-CH-CH-**C**(-CH=N-NH-)-CH-CH-), 136.01 (-CH-CH-**C**(-CH_3)-CH-CH-), 131.63 (-CH-CH-**C**(-COOH)-CH-CH-), 129.65 (-**C**H-CH-C(-COOH)-CH-**C**H-, -CH-**C**H-C(-CH_3)-**C**H-CH-), 127.12 (-CH-**C**H-C(-COOH)-**C**H-CH-) 126.69 (-**C**H-CH-C(-CH_3)-CH-**C**H-), 20.91 (-**C**H$_3$). Procedure provided by J.O. Mueller (AK Barner-Kowollik).

4-(2-(4-methoxyphenyl)-2H-tetrazol-5-yl) benzoic acid (Tet-COOH) (23): *p*-Anisidine (4.0 g, 32.5 mmol, 1.0 eq.) was dissolved in a mixture of conc. HCl (8.46 mL), H_2O (26.9 mL) and EtOH (26.9 mL) and cooled to 0 °C. A cooled solution of $NaNO_2$ (2.241 g, 32.5 mmol, 1.0 eq.) in H_2O (13.45 mL) was added dropwise and stirred for 10 minutes at 0 °C.

The *in-situ* generated diazonium salt solution was added dropwise to a solution of hydrazone **(22)** (10.34 g, 32.5 mmol, 1 eq.) in pyridine (200 mL) at -10 °C – -5 °C over a period of 45 minutes. After complete addition, the solution was stirred at 0 °C

for 30 minutes and at ambient temperature overnight. The turbid solution was poured into a HCl solution (10% aq., 500 mL), the precipitate was filtered off and washed with EtOH (250 mL). Yield: 6.2 g (65 %). ^{1}H NMR (400 MHz, DMSO-D6) δ (ppm) = 13.23 (s, 1 H, -COO**H**), 8.24 (d, ^{3}J = 8.1 Hz, 2 H, -CH-C**H**-C(-COOH)-C**H**-CH-), 8.13 (d, ^{3}J = 8.1 Hz, 2 H, -C**H**-CH-C(-OCH_3)-CH-C**H**-), 8.05 (d, ^{3}J = 8.8 Hz, 2 H, -C**H**-CH-C(-COOH)-CH-C**H**-), 7.20 (d, ^{3}J = 8.8 Hz, 2 H, -CH-C**H**-C(-OCH_3)-C**H**-CH-), 3.86 (s, 3 H, -OC**H$_3$**). ^{13}C NMR (100 MHz, DMSO-D6) δ (ppm) = 166.63 (-**C**OOH), 163.43 (Ph-**C**(=N-N-)-N=N-), 160.40 (-CH-CH-**C**(-OCH_3)-CH-CH-), 132.55 (-CH-**C**(-C=N-N-)-N=N-)-CH-), 130.24 (-CH-CH-**C**(-COOH)-CH-CH-), 130.15 (-**C**H-CH-C(-OCH_3)-CH-**C**H-), 129.41 (-CH-CH-**C**(-N(=N-)-N=)-CH-CH-), 126.59 (-CH-**C**H-C(-COOH)-**C**H-CH-) 121.59 (-**C**H-CH-C(-COOH)-CH-**C**H-), 115.02 (-CH-**C**H-C(-OCH_3)-**C**H-CH-), 55.62 (-O**C**H_3). Procedure provided by J.O. Mueller (AK Barner-Kowollik).

4-(2-(4-methoxyphenyl)-2H-tetrazol-5-yl)benzoic acid chloride (Tet-Cl) (24): Tet-COOH **(23)** (1.00 g, 3.374 mmol, 1.0 eq.) was suspended in dry THF and $SOCl_2$ (4.01 g, 2.45 mL, 33.74 mmol, 10.0 eq.) was added under inert atmosphere. The mixture was heated to reflux for 4 h and the volatiles were subsequently removed under reduced pressure. The residue was dissolved in THF (20 mL) and dried *in vacuo* to remove the excess of $SOCl_2$. Yield: 1.05 g (100 %). ^{1}H NMR (400 MHz, DMSO-D6): δ (ppm) = 8.27 (d, ^{3}J = 8.1 Hz, 2 H, -CH-C**H**-C(-COCl)-C**H**-CH-), 8.15 (d, ^{3}J = 8.1 Hz, 2 H, -C**H**-CH-C(-OCH_3)-CH-C**H**-), 8.08 (d, ^{3}J = 8.8 Hz, 2 H, -C**H**-CH-C(-COCl)-CH-C**H**-), 7.22 (d, ^{3}J = 8.8 Hz, 2 H, Ar*H*, -CH-C**H**-C(-OCH_3)-C**H**-CH-), 3.87 (s, 3 H, -OC**H$_3$**). ^{13}C NMR (100 MHz, DMSO-D6): δ (ppm) = 166.58 (-**C**OCl), 163.46 (Ph-**C**(=N-N-)-N=N-), 160.44 (CH-CH-**C**(-OCH_3)-CH-CH-), 132.52 (-CH-**C**(-C=N-N-)-N=N-)-CH-), 130.28 (-CH-CH-**C**(-COCl)-CH-CH-), 130.19 (-**C**H-CH-C(-OCH_3)-CH-**C**H-), 129.44 (-CH-CH-**C**(-N(=N-)-N=)-CH-CH-), 126.64 (-CH-**C**H-C(-COCl)-**C**H-CH-), 121.67 (-**C**H-CH-C(-COCl)-CH-**C**H-), 115.07 (-CH-**C**H-C(-OCH_3)-**C**H-CH-), 55.65 (-O**C**H_3).
Procedure provided by J. O. Mueller (AK Barner-Kowollik).

9.4.2. Video sequences HDA and rHDA

HDA of HDA-DOPA-TBDMS$_2$-Boc (6) with Cp:

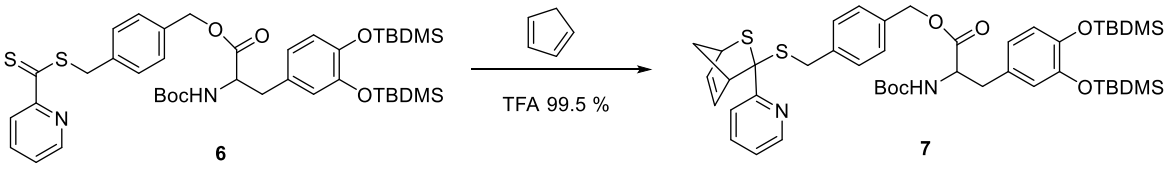

rHDA of HDA-DOPA-TBDMS$_2$-Boc-Cp(7):

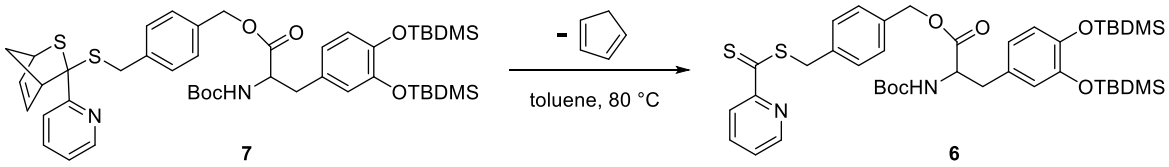

9.4.3. Syntheses of Polymers

RAFT polymerization of styrene (S) to generate poly(styrene) (PS) (11): HDA-Dopa-TBDMS$_2$-Boc **(6)** (75.7 mg, 0.097 mmol, 1.0 eq.) and AIBN (2.7 mg, 0.016 mmol, 0.17 eq.) were dissolved in styrene (9.03 g, 87.0 mmol, 897.0 eq., 10 mL bulk volume). The reaction mixture was distributed in seven flasks and degassed (N_2) for 30 minutes. The polymerization was performed at 60 °C for 2.75 h, 3.5 h, 4.25 h, 5.00 h, 5.75 h, 6.50 h, and 7.25 h. The polymerization was quenched by ice cooling and exposure to atmosphere. The polymers were left to dry under ambient conditions. Conversion was achieved gravimetrically. Polymer characterization was performed *via* SEC.

RAFT polymerization of iso-bornyl acrylate (iBA) to generate poly(iso-bornyl acrylate) (PiBA) (12): HDA-Dopa-TBDMS$_2$-Boc **(6)** (40.0 mg, 0.051 mmol, 1.0 eq.) and AIBN (1.7 mg, 0.010 mmol, 0.20 eq.) were dissolved in *i*BA (9.82 g, 47.1 mmol, 923.0 eq., 10 mL bulk volume). The reaction mixture was distributed in four flasks and degassed (N_2) for 30 minutes. The polymerization was performed at 60 °C for 3 h, 4 h, 5 h and 6 h. Polymerization was quenched by ice cooling and exposure to atmosphere. The polymers were left to dry under ambient conditions. Polymer characterization was performed *via* SEC.

9.4.4. Polymer Conjugation in Solution

PEG-dopamine-maleimide (PEG-dM) (3): Dopamine-maleimide (dM) **(1)** (0.030 g, 0.129 mmol) was added to a solution of PEG-Cp **(2)** (0.189 g, 0.086 mmol) in 5 mL DCM. The mixture was stirred for 18 h at ambient temperature. The solution was concentrated and subsequently precipitated in ice-cold diethyl ether (5 mL). The precipitate was isolated by filtration and dried *in vacuo* to yield a pale brown solid. *m/z* ($[M_{n=34}+Na]^+_{exp}$) = 1877.03; *m/z* ($[M_{n=34}+Na]^+_{theo}$) = 1877.04.

UV/Vis absorption versus time experiment of the HDA reaction of HDA-DOPA-TBDMS$_2$-Boc (6) with PEG-Cp (2) (2200 g·mol^{-1}) in solution: HDA-DOPA-TBDMS$_2$-Boc (1.175 mg, 1.5 µmol, 1.0 eq.) was dissolved in DCM (2 mL) and was placed in a UV/Vis cuvette. A stir bar was added and the cuvette was positioned in the UV/Vis spectrometer. PEG-Cp (3.30 mg, 1.5 µmol, 1.0 eq.) in DCM (1 mL) and TFA (0.98 µL, 0.013 mmol) were added immediately. The UV/Vis measurement was started straight away and the reaction conversion was monitored for 17 minutes at λ_{max} = 348 nm (**Figure 32**).

9.5. Surface Reactions

All manipulations of air-sensitive substances or materials were conducted under rigorous exclusion of moisture and oxygen in Schlenk-type glassware on a dual manifold Schlenk line, connected to a high vacuum line (10^{-3} torr).

Dopamine-maleimide-PEG attachment on gold substrates / silicon wafer / PE substrates, (B): The applied surfaces were first washed with methanol, water and DCM and dried under nitrogen. Dopamine-Maleimide-PEG **(3)** (7 mg, 2.88 µmol) was dissolved in methanol (0.5 mL). The previous solution and a Tris buffer solution, (0.5 mL, 0.3 M, pH = 8.5) were added to a substrate in a snap lid glass. The mixture was shaken for 14 h at ambient temperature (60 shakes / min). The substrate was washed with deionized water and methanol first and shaken in DCM for 2 h at ambient temperature. The substrate was dried with nitrogen and analyzed *via* XPS.

TBDMS-protection of the remaining OH-groups (C): TBDMS-Cl (1.301 mg, 8.63 µmol), DBU (1.288 µL, 8.63 µmol) and acetonitrile (1 mL) were added to the gold substrate with dopamine-maleimide-PEG coating **(B)** in a snap lid glass. The mixture was shaken for 14 h at ambient temperature (90 shakes / min). The substrate was washed with acetonitrile, dried with nitrogen and analyzed *via* XPS.

Retro-Diels-Alder (rDA) reaction on the surface (D/D*): All rDA reactions on the surface were performed in the same manner. A modified gold substrate **(C/C*)** in toluene (2 mL) was heated to 90 °C for 8 h (200 shakes / min). The substrate was washed with toluene and DCM, dried with nitrogen and analyzed *via* XPS. Reaction according to a modified procedure of Ref. 114.

Diels-Alder (DA) reaction on the surface (C*): A maleimide carrying gold substrate, which had undergone a rDA reaction previously **(D)** was shaken (90 shakes / min) in a solution of PEG-Cp (5.00 mg, 2.273 µmol) in DCM (1 mL) for 14 hours at ambient temperature. The substrate was washed with DCM, dried with nitrogen and analyzed *via* XPS.

Surface decoration with of HDA-DOPA-Cp (8) to achieve (E): The silicon wafers were washed with acetone, ethanol, milli-Q water and DCM, dried with nitrogen, plasma cleaned (25 W) for 10 minutes and used immediately. An ethanolic solution of HDA-DOPA-Cp **(8)** (5 mg, 9.6 µmol in 30 µL ethanol) was placed on each substrate (1 × 1 cm^2). A 30 µL drop of Tris buffer (0.1 M, pH = 8.5) was added. The surfaces were place in a chamber saturated with a water/ethanol atmosphere to prevent evaporation and left overnight in the dark. The surfaces were immersed in ethanol (10 min), Milli-Q water (10 min) and afterwards washed with ethanol, methanol, Milli-Q water, toluene and dichloromethane and dried with nitrogen. XPS analysis and ellipsometry were performed. The surfaces were employed immediately for the HDA reaction.

***One-pot retro-Hetero-Diels–Alder/Hetero-Diels–Alder reaction on the surface (F_a/F_b)*:** The surface was placed upright into a Schlenk-tube. PEG-Cp **(2)** ($M_n \approx 2200$ g·mol^{-1}) (10 mg, 4.55 µmol) was dissolved in dry toluene (1 mL) and added to the surface. After addition of TFA (0.088 mmol, 75 µmol of a 1.17 M TFA solution in toluene) the flask was heated to 80 °C and left for 2 h. After cooling, the surface was immersed in toluene (10 min), DCM (10 min) and washed with toluene, ethanol, methanol, DCM and dried with nitrogen. A similar procedure was employed for the surface HDA reaction with PTFEMA-Cp ($M_{n,NMR}$ = 5200 g·mol^{-1}; $Đ_{SEC}$ = 1.22) **(10)**. The control samples underwent the same reaction conditions, employing poly(ethylene glycol) dimethyl ether (MeO-PEG-OMe) (MeO-PEG-OMe) ($M_n \approx 2000$ g·mol^{-1}) for the control experiment of the PEG attachment and PTFEMA-Br ($M_{n,NMR} \approx 5200$ g·mol^{-1}; $Đ_{SEC}$ = 1.22) for the control experiment of the attachment of PTFEMA, respectively. All surfaces were analyzed *via* XPS analysis and ellipsometry.

Surface attachment of Photo-DOPA (16) on gold substrates (G_I), PET (G_{II}) and graphite (G_{III}): Gold substrates, PET substrates and graphite substrates were employed. The gold substrates were washed with ethanol, milli-Q water, acetone, DCM, dried with nitrogen, and exposed to air plasma for 10 minutes (25 W) just before deposition. The PET substrate was washed with ethanol and milli-Q water and dried with nitrogen. The graphite substrates were treated with nitrogen.
In a saturated atmosphere of ethanol and water (1:1), the substrates were placed in a petri-dish and freshly prepared Tris-buffer solution (60 µL) was added to each surface. Straight afterwards, Photo-DOPA **(16)** (2.7 mg, 4.55 µmol) was dissolved in dry EtOH (60 µL) (per sample) and added to each surface employing an Eppendorf pipette. The surfaces were left for 12 hours at ambient temperature under ethanol/water atmosphere. Afterwards, the surfaces were washed with milli-Q water, ethanol and were left in DCM for 15 minutes before they were washed with DCM again. The samples were dried in a nitrogen stream. Surface characterization was performed *via* XPS spectroscopy and contact angle measurements.

Photoenol ligation reaction of PEG-Mal (17) and PTFEMA-Mal (19) on the surface (G_I) to generate (H_I-17, H_I-19): The prepared photo-reactive surfaces **(G_I)** were placed (upright) in a headspace vial (Pyrex, diameter 20 mm). PEG-Mal **(17)** (5 mg, 2.27 µmol) or PTFEMA-Mal **(19)** (5 mg, 1.35 µmol) were dissolved in dry acetonitrile (4 mL) and the mixture was added to the vial. The vial was crimped air-tight using SBR seals with PTFE inner liner and was degassed with nitrogen for 30 minutes, before it was placed into the photo reactor (refer to Section 9.3.2) and irradiated (λ_{max} = 320 nm) for 60 minutes. The surface was washed with acetonitrile, milli-Q water, left in DCM for 20 minutes and washed with DCM. The samples were dried in a nitrogen stream. Characterization was performed *via* XPS spectroscopy.

Photoenol ligation reaction of PEP-Mal (20) on the surfaces (G_I, G_{II}) (H_I-20, H_{II}-20): The prepared photo-reactive surfaces ***(G_I, G_{II})*** were placed (upright) in a headspace vial (Pyrex, diameter 20 mm). PEP-Mal **(20)** (4 mg, 3.46 µmol) were dissolved in an acetonitrile/milli-Q water mixture (3:1) (4 mL) and the mixture was added to the vial. The vial was crimped air-tight using SBR seals with PTFE inner liner and was degassed with nitrogen for 30 minutes, before it was placed into the photo reactor (refer to Section 9.3.2) and irradiated (λ_{max} = 320 nm) for 60 minutes. The surface was washed with acetonitrile, milli-Q water, left in milli-Q water for 20 minutes and washed with acetonitrile again. The samples were dried in a nitrogen stream. Characterization was performed *via* XPS spectroscopy.

Area-resolved photo-patterning with PTFEMA-Mal (19) on (G_I) (J_I-19): For the demonstration of area-resolved patterning *via* photo-ligation of a DOPA-photoenol surface and a maleimide-carrying molecule, the Au-Photo-DOPA surface **(G_I)** and PTFEMA-Mal **(19)** were employed as a model system. The freshly prepared Au-PE-DOPA surface **(G_I)** was covered with a shadow mask **(G_I+mask)** and fixed in a holder to prevent irradiation of the whole surface (refer to Section 9.3.1). The unmasked part (meander structure) was irradiated. The experiment was performed with the equipment that was already described by Pauloehrl *et al.*.[28] The prepared photo-reactive surfaces (masked and in the holder) were placed (upright) in a headspace vial (Pyrex, diameter 20 mm). PTFEMA-Mal **(19)** (5 mg, 1.35 µmol) was dissolved in dry acetonitrile (4 mL) and the mixture was added to the vial. The vial was crimped air-tight using SBR seals with PTFE inner liner and was degassed with nitrogen for 30 minutes, before it was placed into the photo reactor (refer to Section 9.3.2) and irradiated (λ_{max} = 320 nm) for 60 minutes. The surface was washed with acetonitrile, milli-Q water, left in DCM for 20 minutes and washed with DCM. The samples were dried in a nitrogen stream. Characterization was performed *via* ToF-SIMS.

Substrate preparation before PDA coating: One side polished silicon wafers with a 50 nm thermal silicon dioxide (SiO_2) over-layer was sonicated in methanol and deionized water (Milli Q system, Millipore) for 15 min, immersed in a mixture of 25 % ammonia, 30 % hydrogen peroxide and water (1:1:5 v/v/v) heated at 70 °C for

10 min and finally thoroughly rinsed with water. Dry samples were exposed to air plasma (25 W) for 5 min just before PDA deposition.
Substrates kindly provided by O. Pop-Georgievski.

Polydopamine (PDA) coating (K): PDA was deposited from a 2 mg·mL^{-1} solution prepared by dissolution of dopamine hydrochloride in an air-saturated 10 mM Tris-HCl (pH 8.5) buffer.[14] The deposition of PDA on the Si-substrates was performed in open glass dishes and under controlled stirring that provided a continuous supply of oxygen through the air/solution interface. In addition, the flat substrates were kept vertical to suppress microparticle sedimentation.[205,207,208] The coated surfaces were finally rinsed with water, sonicated in water for 15 min and dried in a stream of nitrogen. Coatings were prepared by O. Pop-Georgievski. XPS characterization of the PDA coated substrates was performed by C. M. Preuss.

Immobilization of tetrazole chloride (24) on PDA (K) to generate (L): Tet-Cl **(24)** was covalently attached to the surface of PDA films by amidation with surface amino groups.[209209] Substrates freshly coated with PDA were immersed in 15 mL of 0.24 M TEA (364 mg, 502 µL) in THF at ambient temperature. Subsequently, 7.5 mL of a 0.24 M solution of Tet-Cl **(24)** (565 mg) was added drop wise and the samples were placed on a shaker. After 1 h, the substrates were removed and rinsed with THF, ethanol and Milli-Q water and dried with nitrogen. The surfaces were characterized by XPS, ellipsometry and contact angle measurements.

Attachment of the ATRP initiator (25) via photo-triggered NITEC ligation (M) (whole surface) or (O) (patterned surface): The substrates functionalized with PDA-tetrazole **(L)** were placed vertically in individual headspace vials (Pirex) and 2 mg·mL^{-1} solution of maleimide-functional-initiator **(25)** in DCM was added. The vials were subsequently crimped air-tight with SBR seals having a PTFE inner liner and the solution was purged with nitrogen gas for 5 min. The samples to be irradiated were placed in a custom made photo-reactor (refer to Section 9.3.2) as hanging from a metallic disk (diameter 4-5 cm) designed to revolve around a compact low-pressure lamp (Arimed B6, Cosmedico GmbH, Germany) emitting at

λ = 320 nm (± 30 nm, 36 W) as shown in **Figure 63**. The samples were irradiated for 1 hour at ambient temperature. The surfaces were characterized by XPS, ellipsometry and contact angle measurements.
The spatially controlled surface functionalization was conducted in an analogous fashion, yet placing a mask on top of the substrate (refer to Section 9.3.1).

Preparation of PMeOEGMA brushes via SI-ATRP from (M) (whole surface) or (O) (patterned surface to generate (N) and (P)): A solution of $CuBr_2$ (24.3 mg, 109.2 µmol), 2,2´-dipyridyl (435 mg, 2.79 mmol) and MeOEGMA (17.1 g, 57 mmol) in a water : MeOH (2 : 1) mixture (30 mL) was degassed using nitrogen bubbling for 1 hour. CuCl (111 mg, 1.13 mmol) was added under nitrogen atmosphere and the bubbling was carried out for the next 30 minutes. The polymerization mixture was subsequently transferred under inert atmosphere to the reactors containing the substrates functionalized with ATRP initiator **(M, O)**. The polymerization was carried out at 30 °C for 20 min. Samples were taken from the reactors washed successively with copious amounts of methanol and water, and dried with a stream of nitrogen gas. The surface **(N)** was characterized by XPS, ellipsometry and contact angle measurements, whereas the patterned surface **(P)** was analyzed by ToF-SIMS.

9.6. Biological studies

The cell adhesion experiments presented in Section 6.2 and in the current section were conducted by M. Bachmann (AK Bastmeyer, Zoologisches Institut, KIT).

Cell Culture. Rat embryonic fibroblasts (REFs) stably transfected for a vasodilator-stimulated phosphoprotein (VASP) green fluorescent protein (GFP) construct with lentiviruses were cultured in DMEM at 37 °C in a humidified atmosphere of 5 % CO_2.

Live cell imaging and immune staining. The functionalized substrates were incubated in PBS for 12 h. Prior to cell culture, the substrates were placed in 6-well culture plates containing imaging medium (F12 culture medium, 25 mM Hepes, 2 mM L-glutamine, 1% v/v penicillin/streptomycin and 10% v/v FBS). Trypsinized cells were re-suspended in imaging medium and 150 000 cells were seeded onto each substrate. Imaging was performed on a Zeiss Apotom Imager Z1 microscope with a 40×/0.75 Zeiss water immersion objective in hourly intervals. Cells were fixed after 7 h with 4% w/v paraformaldehyde in PBS at ambient temperature for 10 min and permeabilised by washing three times with PBS containing 0.1% v/v Triton X-100. The samples were incubated one hour at ambient temperature with primary antibodies (mouse anti-paxillin). Incubation of secondary antibodies (goat anti-mouse Alexa 647), phalloidin Alexa 568, and 4´,6-diamidino-2-phenylindole (DAPI) was also performed for one hour at ambient temperature. After each incubation step, the samples were washed 3× with PBS-Triton. The samples were mounted on slides by covering them with Mowiol and cover slips, and imaged using 5x/0.25 or 10x/0.3 Zeiss objectives.

References

[1] Lin, P.-C.; Weinrich, D.; Waldmann, H. *Macromol. Chem. Phys.* **2010**, *211*, 136.

[2] Williams, D. F. *Biomaterials* **2009**, *30*, 5897.

[3] Zollfrank, C. *Scripta Mater.* **2014**, *74*, 3.

[4] de Araújo, A. D.; Palomo, J. M.; Cramer, J.; Köhn, M.; Schröder, H.; Wacker, R.; Niemeyer, C.; Alexandrov, K.; Waldmann, H. *Angew. Chem. Int. Ed.* **2006**, *45*, 296.

[5] Liu, Q.; Wu, C.; Cai, H.; Hu, N.; Zhou, J.; Wang, P. *Chem. Rev.* **2014**, *114*, 6423.

[6] Rodriguez-Emmenegger, C.; Hasan, E.; Pop-Georgievski, O.; Houska, M.; Brynda, E.; Alles, A. B. *Macromol. Biosci.* **2012**, *12*, 525.

[7] Rodriguez Emmenegger, C.; Brynda, E.; Riedel, T.; Sedlakova, Z.; Houska, M.; Alles, A. B. *Langmuir* **2009**, *25*, 6328.

[8] Kuzmyn, A. R.; de los Santos Pereira, A.; Pop-Georgievski, O.; Bruns, M.; Brynda, E.; Rodriguez-Emmenegger, C. *Polym. Chem.* **2014**, *5*, 4124.

[9] Zou, Y.; Yeh, P.-Y. J.; Rossi, N. A. A.; Brooks, D. E.; Kizhakkedathu, J. N. *Biomacromolecules* **2009**, *11*, 284.

[10] Bernard, A.; Renault, J. P.; Michel, B.; Bosshard, H. R.; Delamarche, E. *Adv. Mater.* **2000**, *12*, 1067.

[11] Sgarbi, N.; Pisignano, D.; Di Benedetto, F.; Gigli, G.; Cingolani, R.; Rinaldi, R. *Biomaterials* **2004**, *25*, 1349.

[12] Alonso, J. M.; Reichel, A.; Piehler, J.; del Campo, A. *Langmuir* **2007**, *24*, 448.

[13] Barthlott, W.; Koch, K. *Beilstein J. Nanotechnol.* **2011**, *2*, 135.

[14] Lee, H.; Dellatore, S. M.; Miller, W. M.; Messersmith, P. B. *Science* **2007**, *318*, 426.

[15] Lee, B. P.; Messersmith, P. B.; Israelachvili, J. N.; Waite, J. H. *Annu. Rev. Mater. Res.* **2011**, *41*, 99.

[16] Fan, X.; Lin, L.; Dalsin, J. L.; Messersmith, P. B. *J. Am. Chem. Soc.* **2005**, *127*, 15843.

[17] Ye, Q.; Zhou, F.; Liu, W. *Chem. Soc. Rev.* **2011**, *40*, 4244.

[18] Waite, J. H.; Tanzer, M. L. *Science* **1981**, *121*, 1038.

[19] Bilic, G.; Brubaker, C.; Messersmith, P. B.; Mallik, A. S.; Quinn, T. M.; Haller, C.; Done, E.; Gucciardo, L.; Zeisberger, S. M.; Zimmermann, R.; Deprest, J.; Zisch, A. H. *Am. J. Obstet. Gynecol.* **2010**, *202*, 85 e1.

[20] Black, K. C. L.; Yi, J.; Rivera, J. G.; Zelasko-Leon, D. C.; Messersmith, P. B. *Nanomedicine (Lond)* **2013**, *8*, 17.

[21] Haller, C. M.; Buerzle, W.; Brubaker, C. E.; Messersmith, P. B.; Mazza, E.; Ochsenbein-Koelble, N.; Zimmermann, R.; Ehrbar, M. *Prenat. Diagn.* **2011**, *31*, 654.

[22] Gruendling, T.; Oehlenschlaeger, K. K.; Frick, E.; Glassner, M.; Schmid, C.; Barner-Kowollik, C. *Macromol. Rapid Commun.* **2011**, *32*, 807.

[23] Sinnwell, S.; Inglis, A. J.; Davis, T. P.; Stenzel, M. H.; Barner-Kowollik, C. *Chem. Commun.* **2008**, 2052.

[24] Glassner, M.; Kempe, K.; Schubert, U. S.; Hoogenboom, R.; Barner-Kowollik, C. *Chem. Commun.* **2011**, *47*, 10620.

[25] Wang, Y.; Rivera Vera, C. I.; Lin, Q. *Org. Lett.* **2007**, *9*, 4155.

[26] Inglis, A. J.; Stenzel, M. H.; Barner-Kowollik, C. *Macromol. Rapid Commun.* **2009**, *30*, 1792.

[27] Inglis, A. J.; Sinnwell, S.; Stenzel, M. H.; Barner-Kowollik, C. *Angew. Chem. Int. Ed.* **2009**, *48*, 2411.

[28] Pauloehrl, T.; Delaittre, G.; Winkler, V.; Welle, A.; Bruns, M.; Börner, H. G.; Greiner, A. M.; Bastmeyer, M.; Barner-Kowollik, C. *Angew. Chem. Int. Ed.* **2012**, *51*, 1071.

[29] Tischer, T.; Claus, T. K.; Bruns, M.; Trouillet, V.; Linkert, K.; Rodriguez-Emmenegger, C.; Goldmann, A. S.; Perrier, S.; Börner, H. G.; Barner-Kowollik, C. *Biomacromolecules* **2013**, *14*, 4340.

[30] Sun, J.; Xianyu, Y.; Jiang, X. *Chem. Soc. Rev.* **2014**, *43*, 6239.

[31] Yetisen, A. K.; Akram, M. S.; Lowe, C. R. *Lab on a Chip* **2013**, *13*, 2210.

[32] Paek, S.-H.; Lee, S.-H.; Cho, J.-H.; Kim, Y.-S. *Methods* **2000**, *22*, 53.

[33] Krishnamoorthy, M.; Hakobyan, S.; Ramstedt, M.; Gautrot, J. E. *Chem. Rev.* **2014**, *114*, 10976.

[34] Zamfir, M.; Rodriguez-Emmenegger, C.; Bauer, S.; Barner, L.; Rosenhahn, A.; Barner-Kowollik, C. *J. Mater. Chem. B* **2013**, *1*, 6027.

[35] Tischer, T.; Rodriguez-Emmenegger, C.; Trouillet, V.; Welle, A.; Schueler, V.; Mueller, J. O.; Goldmann, A. S.; Brynda, E.; Barner-Kowollik, C. *Adv. Mater.* **2014**, *26*, 4087.

[36] Thery, M. *J. Cell Sci.* **2010**, *123*, 4201.

[37] Braun, S.; Salaneck, W. R.; Fahlman, M. *Adv. Mater.* **2009**, *21*, 1450.

[38] Yameen, B.; Rodriguez-Emmenegger, C.; Preuss, C. M.; Pop-Georgievski, O.; Verveniotis, E.; Trouillet, V.; Rezek, B.; Barner-Kowollik, C. *Chem. Commun.* **2013**, *49*, 8623.

[39] Lee, H.; Scherer, N. F.; Messersmith, P. B. *Proc. Natl. Acad. Sci. U.S.A.* **2006**, *103*, 12999.

[40] Dalsin, J. L.; Messersmith, P. B. *Mater. Today* **2005**, *8*, 38.

[41] Waite, J. H.; Qin, X. *Biochemistry* **2001**, *40*, 2887.

[42] Pop-Georgievski, O.; Rodriguez-Emmenegger, C.; Pereira, A. d. l. S.; Proks, V.; Brynda, E.; Rypacek, F. *J. Mater. Chem. B* **2013**, *1*, 2859.

[43] Pop-Georgievski, O.; Verreault, D.; Diesner, M.-O.; Proks, V.; Heissler, S.; Rypáček, F.; Koelsch, P. *Langmuir* **2012**, *28*, 14273.

[44] Luo, R.; Tang, L.; Zhong, S.; Yang, Z.; Wang, J.; Weng, Y.; Tu, Q.; Jiang, C.; Huang, N. *ACS Appl. Mater. Interfaces* **2013**, *5*, 1704.

[45] Pop-Georgievski, O.; Popelka, S. t. p. n.; Houska, M.; Chvostová, D.; Proks, V. r.; Rypáček, F. e. *Biomacromolecules* **2011**, *12*, 3232.

[46] Proks, V.; Jaroš, J.; Pop-Georgievski, O.; Kučka, J.; Popelka, Š.; Dvořák, P.; Hampl, A.; Rypáček, F. *Macromol. Biosci.* **2012**, *12*, 1232.

[47] Prime, K. L.; Whitesides, G. M. *J. Am. Chem. Soc.* **1993**, *115*, 10714.

[48] Sileika, T. S.; Kim, H.-D.; Maniak, P.; Messersmith, P. B. *ACS Appl. Mater. Interfaces* **2011**, *3*, 4602.

[49] Gu, R.; Xu, W. Z.; Charpentier, P. A. *J. Polym. Sci., Part A: Polym. Chem.* **2013**, *51*, 3941.

[50] Ulman, A. *Chem. Rev.* **1996**, *96*, 1533.

[51] Blasco, E.; Piñol, M.; Oriol, L.; Schmidt, B. V. K. J.; Welle, A.; Trouillet, V.; Bruns, M.; Barner-Kowollik, C. *Adv. Funct. Mater.* **2013**, *23*, 4011.

[52] Yang, Z.; Galloway, J. A.; Yu, H. *Langmuir* **1999**, *15*, 8405.

[53] Rodriguez-Emmenegger, C.; Brynda, E.; Riedel, T.; Houska, M.; Šubr, V.; Alles, A. B.; Hasan, E.; Gautrot, J. E.; Huck, W. T. S. *Macromol. Rapid Commun.* **2011**, *32*, 952.

[54] Paripovic, D.; Klok, H.-A. *Macromol. Chem. Phys.* **2011**, *212*, 950.

[55] Tugulu, S.; Klok, H.-A. *Biomacromolecules* **2008**, *9*, 906.

[56] McGovern, M. E.; Thompson, M. *Anal. Commun.* **1998**, *35*, 391.

[57] Kallury, K. M. R.; MacDonald, P. M.; Thompson, M. *Langmuir* **1994**, *10*, 492.

[58] Fadeev, A. Y.; McCarthy, T. J. *Langmuir* **2000**, *16*, 7268.

[59] Kassam, A.; Bremner, G.; Clark, B.; Ulibarri, G.; Lennox, R. B. *J. Am. Chem. Soc.* **2006**, *128*, 3476.

[60] Dalsin, J. L.; Hu, B.-H.; Lee, B. P.; Messersmith, P. B. *J. Am. Chem. Soc.* **2003**, *125*, 4253.

[61] Zobrist, C.; Sobocinski, J.; Lyskawa, J.; Fournier, D.; Miri, V.; Traisnel, M.; Jimenez, M.; Woisel, P. *Macromolecules* **2011**, *44*, 5883.

[62] Yah, W. O.; Xu, H.; Soejima, H.; Ma, W.; Lvov, Y.; Takahara, A. *J. Am. Chem. Soc.* **2012**, *134*, 12134.

[63] Wach, J.-Y.; Malisova, B.; Bonazzi, S.; Tosatti, S.; Textor, M.; Zürcher, S.; Gademann, K. *Chem. Eur. J.* **2008**, *14*, 10579.

[64] Gao, T.; Wang, X.; Yu, B.; Wei, Q.; Xia, Y.; Zhou, F. *Langmuir* **2013**, *29*, 1054.

[65] Han, H.; Wu, J.; Avery, C. W.; Mizutani, M.; Jiang, X.; Kamigaito, M.; Chen, Z.; Xi, C.; Kuroda, K. *Langmuir* **2011**, *27*, 4010.

[66] Wei, Q.; Yu, B.; Wang, X.; Zhou, F. *Macromol. Rapid Commun.* **2014**, *35*, 1046.

[67] Wei, Q.; Pei, X.; Hao, J.; Cai, M.; Zhou, F.; Liu, W. *Advanced Materials Interfaces* **2014**, *1*, DOI:10.1002/admi.201400035.

[68] Amstad, E.; Gillich, T.; Bilecka, I.; Textor, M.; Reimhult, E. *Nano Lett.* **2009**, *9*, 4042.

[69] Geiseler, B.; Fruk, L. *J. Mater. Chem.* **2012**, *22*, 735.

[70] Xie, J.; Xu, C.; Kohler, N.; Hou, Y.; Sun, S. *Adv. Mater.* **2007**, *19*, 3163.

[71] Goldmann, A. S.; Schödel, C.; Walther, A.; Yuan, J.; Loos, K.; Müller, A. H. E. *Macromol. Rapid Commun.* **2010**, *31*, 1608.

[72] Jenkins, A. D.; Jones, R. G.; Moad, G. *Pure Appl. Chem.* **2009**, *82*, 483.

[73] Hawker, C. J. *Science* **2005**, *309*, 1200.

[74] Kamigaito, M.; Ando, T.; Sawamoto, M. *Chem. Rev.* **2001**, *101*, 3689.

[75] Otsu, T.; Yoshida, M. *Makromol. Chem., Rapid Commun.* **1982**, *3*, 127.

[76] Otsu, T.; Yoshida, M.; Tazaki, T. *Makromol. Chem., Rapid Commun.* **1982**, *3*, 133.

[77] Chiefari, J.; Chong, Y. K.; Ercole, F.; Krstina, J.; Jeffery, J.; Le, T. P. T.; Mayadunne, R. T. A.; Meijs, G. F.; Moad, C. L.; Moad, G.; Rizzardo, E.; Thang, S. H. *Macromolecules* **1998**, *31*, 5559.

[78] *Handbook of RAFT Polymerization*; Barner-Kowollik, C., Ed.; Wiley-VCH: Weinheim, 2008; Vol. 1.

[79] Odian, G. *Principles of Polymerization*; Wiley-Interscience: Hoboken, NJ, 2004; Vol. 4.

[80] Matyjaszewski, K.; Xia, J. *Chem. Rev.* **2001**, *101*, 2921.

[81] Wang, J.-S.; Matyjaszewski, K. *J. Am. Chem. Soc.* **1995**, *117*, 5614.

[82] Kato, M.; Kamigaito, M.; Sawamoto, M.; Higashimura, T. *Macromolecules* **1995**, *28*, 1721.

[83] Moineau, G.; Dubois, P.; Jérôme, R.; Senninger, T.; Teyssié, P. *Macromolecules* **1998**, *31*, 545.

[84] Jakubowski, W.; Matyjaszewski, K. *Macromolecules* **2005**, *38*, 4139.

[85] Matyjaszewski, K.; Dong, H.; Jakubowski, W.; Pietrasik, J.; Kusumo, A. *Langmuir* **2007**, *23*, 4528.

[86] Queffelec, J.; Gaynor, S. G.; Matyjaszewski, K. *Macromolecules* **2000**, *33*, 8629.

[87] Percec, V.; Guliashvili, T.; Ladislaw, J. S.; Wistrand, A.; Stjerndahl, A.; Sienkowska, M. J.; Monteiro, M. J.; Sahoo, S. *J. Am. Chem. Soc.* **2006**, *128*, 14156.

[88] Percec, V.; Popov, A. V.; Ramirez-Castillo, E.; Weichold, O. *J. Polym. Sci., Part A: Polym. Chem.* **2003**, *41*, 3283.

[89] Levere, M. E.; Nguyen, N. H.; Leng, X.; Percec, V. *Polym. Chem.* **2013**, *4*, 1635.

[90] *Handbook of RAFT Polymerization*; Barner-Kowollik, C., Ed.; Wiley-VCH: Weinheim, 2008; Vol. 1, p 235.

[91] *Handbook of RAFT Polymerization*; Barner-Kowollik, C., Ed.; Wiley-VCH: Weinheim, 2008; Vol. 1, p 106.

[92] *Handbook of RAFT Polymerization*; Barner-Kowollik, C., Ed.; Wiley-VCH: Weinheim, 2008; Vol. 1, p 237.

[93] Charmot, D.; Corpart, P.; Adam, H.; Zard, S. Z.; Biadatti, T.; Bouhadir, G. *Macromol. Symp.* **2000**, *150*, 23.

[94] Destarac, M.; Brochon, C.; Catala, J. M.; Wilczewska, A.; Zard, S. Z. *Macromol. Chem. Phys.* **2002**, *203*, 2281.

[95] *Handbook of RAFT Polymerization*; Barner-Kowollik, C., Ed.; Wiley-VCH: Weinheim, 2008; Vol. 1, p 239.

[96] *Handbook of RAFT Polymerization*; Barner-Kowollik, C., Ed.; Wiley-VCH: Weinheim, 2008; Vol. 1, p 237.

[97] Moad, G.; Rizzardo, E.; Thang, S. H. *Aust. J. Chem.* **2009**, *62*, 1402.

[98] Moad, G.; Rizzardo, E.; Thang, S. H. *Aust. J. Chem.* **2005**, *58*, 379.

[99] *Handbook of RAFT Polymerization*; Barner-Kowollik, C., Ed.; Wiley-VCH: Weinheim, 2008; Vol. 1, p 39.

[100] *Handbook of RAFT Polymerization*; Barner-Kowollik, C., Ed.; Wiley-VCH: Weinheim, 2008; Vol. 1, p 192.

[101] Keddie, D. J.; Moad, G.; Rizzardo, E.; Thang, S. H. *Macromolecules* **2012**, *45*, 5321.

[102] Balazs, A. C.; Singh, C.; Zhulina, E.; Chern, S.-S.; Lyatskaya, Y.; Pickett, G. *Prog. Surf. Sci.* **1997**, *55*, 181.

[103] Barbey, R.; Lavanant, L.; Paripovic, D.; Schüwer, N.; Sugnaux, C.; Tugulu, S.; Klok, H.-A. *Chem. Rev.* **2009**, *109*, 5437.

[104] Rodriguez-Emmenegger, C.; Kylián, O. e.; Houska, M.; Brynda, E.; Artemenko, A.; Kousal, J.; Alles, A. B.; Biederman, H. *Biomacromolecules* **2011**, *12*, 1058.

[105] Rühe, J.; Knoll, W. *J. Macromol. Sci. C* **2002**, *42*, 91.

[106] Matyjaszewski, K.; Miller, P. J.; Shukla, N.; Immaraporn, B.; Gelman, A.; Luokala, B. B.; Siclovan, T. M.; Kickelbick, G.; Vallant, T.; Hoffmann, H.; Pakula, T. *Macromolecules* **1999**, *32*, 8716.

[107] Sedjo, R. A.; Mirous, B. K.; Brittain, W. J. *Macromolecules* **2000**, *33*, 1492.

[108] Matyjaszewski, K.; Shipp, D. A.; Wang, J.-L.; Grimaud, T.; Patten, T. E. *Macromolecules* **1998**, *31*, 6836.

[109] Clayden, J.; Greeves, N.; Warren, S.; Wothers, P.; Oxford University Press: Oxford, 2001; Vol. 1, Chap. 35, 905.

[110] Goldmann, A. S.; Glassner, M.; Inglis, A. J.; Barner-Kowollik, C. *Macromol. Rapid Commun.* **2013**, *34*, 810.

[111] Sauer, J.; Sustmann, R. *Angew. Chem., Int. Ed. Engl.* **1980**, *19*, 779.

[112] Mizawa, T.; Takenaka, K.; Shiomi, T. *J. Polym. Sci., Part A: Polym. Chem.* **2000**, *38*, 237.

[113] Glassner, M.; Blinco, J. P.; Barner-Kowollik, C. *Macromol. Rapid Commun.* **2011**, *32*, 724.

[114] Blinco, J. P.; Trouillet, V.; Bruns, M.; Gerstel, P.; Gliemann, H.; Barner-Kowollik, C. *Adv. Mater.* **2011**, *23*, 4435.

[115] Glassner, M.; Blinco, J. P.; Barner-Kowollik, C. *Polym. Chem.* **2011**, *2*, 83.

[116] Paulöhrl, T.; Inglis, A. J.; Barner-Kowollik, C. *Adv. Mater.* **2010**, *22*, 2788.

[117] Inglis, A. J.; Barner-Kowollik, C. *Polym. Chem.* **2011**, *2*, 126.

[118] Inglis, A. J.; Nebhani, L.; Altintas, O.; Schmidt, F. G.; Barner-Kowollik, C. *Macromolecules* **2010**, *43*, 5515.

[119] Langer, M.; Brandt, J.; Lederer, A.; Goldmann, A. S.; Schacher, F. H.; Barner-Kowollik, C. *Polym. Chem.* **2014**, *5*, 5330.

[120] Glassner, M.; Delaittre, G.; Kaupp, M.; Blinco, J. P.; Barner-Kowollik, C. *J. Am. Chem. Soc.* **2012**, *134*, 7274.

[121] Oehlenschlaeger, K. K.; Guimard, N. K.; Brandt, J.; Mueller, J. O.; Lin, C. Y.; Hilf, S.; Lederer, A.; Coote, M. L.; Schmidt, F. G.; Barner-Kowollik, C. *Polym. Chem.* **2013**, *4*, 4348.

[122] Oehlenschlaeger, K. K.; Mueller, J. O.; Brandt, J.; Hilf, S.; Lederer, A.; Wilhelm, M.; Graf, R.; Coote, M. L.; Schmidt, F. G.; Barner-Kowollik, C. *Adv. Mater.* **2014**, *26*, 3561.

[123] Yameen, B.; Puerckhauer, T.; Ludwig, J.; Ahmed, I.; Altintas, O.; Fruk, L.; Colsmann, A.; Barner-Kowollik, C. *Small* **2014**, *10*, 3091.

[124] Nebhani, L.; Barner-Kowollik, C. *Macromol. Rapid Commun.* **2010**, *31*, 1298.

[125] Yameen, B.; Rodriguez-Emmenegger, C.; Ahmed, I.; Preuss, C. M.; Dürr, C. J.; Zydziak, N.; Trouillet, V.; Fruk, L.; Barner-Kowollik, C. *Chem. Commun.* **2013**, *49*, 6734.

[126] Yameen, B.; Zydziak, N.; Weidner, S. M.; Bruns, M.; Barner-Kowollik, C. *Macromolecules* **2013**, *46*, 2606.

[127] Zydziak, N.; Hubner, C.; Bruns, M.; Vogt, A. P.; Barner-Kowollik, C. *Polym. Chem.* **2013**, *4*, 1525.

[128] Zydziak, N.; Hübner, C.; Bruns, M.; Barner-Kowollik, C. *Macromolecules* **2011**, *44*, 3374.

[129] Goldmann, A. S.; Tischer, T.; Barner, L.; Bruns, M.; Barner-Kowollik, C. *Biomacromolecules* **2011**, *12*, 1137.

[130] Tischer, T.; Goldmann, A. S.; Linkert, K.; Trouillet, V.; Börner, H. G.; Barner-Kowollik, C. *Adv. Funct. Mater.* **2012**, *22*, 3853.

[131] Kaupp, M.; Vogt, A. P.; Natterodt, J. C.; Trouillet, V.; Gruendling, T.; Hofe, T.; Barner, L.; Barner-Kowollik, C. *Polym. Chem.* **2012**, *3*, 2605.

[132] Sammes, P. G. *Tetrahedron* **1976**, *32*, 405.

[133] Charlton, J. L.; Alauddin, M. M. *Tetrahedron* **1987**, *43*, 2873.

[134] Segura, J. L.; Martín, N. *Chem. Rev.* **1999**, *99*, 3199.

[135] Altintas, O.; Willenbacher, J.; Wuest, K. N. R.; Oehlenschlaeger, K. K.; Krolla-Sidenstein, P.; Gliemann, H.; Barner-Kowollik, C. *Macromolecules* **2013**, *46*, 8092.

[136] Oehlenschlaeger, K. K.; Mueller, J. O.; Heine, N. B.; Glassner, M.; Guimard, N. K.; Delaittre, G.; Schmidt, F. G.; Barner-Kowollik, C. *Angew. Chem. Int. Ed.* **2013**, *52*, 762.

[137] Kaupp, M.; Tischer, T.; Hirschbiel, A. F.; Vogt, A. P.; Geckle, U.; Trouillet, V.; Hofe, T.; Stenzel, M. H.; Barner-Kowollik, C. *Macromolecules* **2013**, *46*, 6858.

[138] Winkler, M.; Mueller, J. O.; Oehlenschlaeger, K. K.; Montero de Espinosa, L.; Meier, M. A. R.; Barner-Kowollik, C. *Macromolecules* **2012**, *45*, 5012.

[139] Glassner, M.; Oehlenschlaeger, K. K.; Gruendling, T.; Barner-Kowollik, C. *Macromolecules* **2011**, *44*, 4681.

[140] Bauer, D. M.; Rogge, A.; Stolzer, L.; Barner-Kowollik, C.; Fruk, L. *Chem. Commun.* **2013**, *49*, 8626.

[141] Stolzer, L.; Ahmed, I.; Rodriguez-Emmenegger, C.; Trouillet, V.; Bockstaller, P.; Barner-Kowollik, C.; Fruk, L. *Chem. Commun.* **2014**, *50*, 4430.

[142] Quick, A. S.; Rothfuss, H.; Welle, A.; Richter, B.; Fischer, J.; Wegener, M.; Barner-Kowollik, C. *Adv. Funct. Mater.* **2014**, *24*, 3571.

[143] Richter, B.; Pauloehrl, T.; Kaschke, J.; Fichtner, D.; Fischer, J.; Greiner, A. M.; Wedlich, D.; Wegener, M.; Delaittre, G.; Barner-Kowollik, C.; Bastmeyer, M. *Adv. Mater.* **2013**, *25*, 6117.

[144] Stolzer, L.; Quick, A. S.; Abt, D.; Welle, A.; Naumenko, D.; Lazzarino, M.; Wegener, M.; Barner-Kowollik, C.; Fruk, L. *Chem. Commun.* **2015**, *51*, 3363.

[145] Clovis, J. S.; Eckell, A.; Huisgen, R.; Sustmann, R. *Chem. Ber.* **1967**, *100*, 60.

[146] Song, W.; Wang, Y.; Qu, J.; Madden, M. M.; Lin, Q. *Angew. Chem. Int. Ed.* **2008**, *47*, 2832.

[147] Song, W.; Wang, Y.; Qu, J.; Lin, Q. *J. Am. Chem. Soc.* **2008**, *130*, 9654.

[148] Dietrich, M.; Delaittre, G.; Blinco, J. P.; Inglis, A. J.; Bruns, M.; Barner-Kowollik, C. *Adv. Funct. Mater.* **2012**, *22*, 304.

[149] de Hoog, H.-P. M.; Nallani, M.; Liedberg, B. *Polym. Chem.* **2012**, *3*, 302.

[150] Dürr, C. J.; Lederhose, P.; Hlalele, L.; Abt, D.; Kaiser, A.; Brandau, S.; Barner-Kowollik, C. *Macromolecules* **2013**, *46*, 5915.

[151] Mueller, J. O.; Guimard, N. K.; Oehlenschlaeger, K. K.; Schmidt, F. G.; Barner-Kowollik, C. *Polym. Chem.* **2014**, *5*, 1447.

[152] Mueller, J. O.; Voll, D.; Schmidt, F. G.; Delaittre, G.; Barner-Kowollik, C. *Chem. Commun.* **2014**, *50*, 15681.

[153] Hiltebrandt, K.; Pauloehrl, T.; Blinco, J. P.; Linkert, K.; Börner, H. G.; Barner-Kowollik, C. *Angew. Chem. Int. Ed.* **2015**, *54*, 2838.

[154] Hufendiek, A.; Barner-Kowollik, C.; Meier, M. A. R. *Polym. Chem.* **2015**.

[155] Klemm, D.; Heublein, B.; Fink, H.-P.; Bohn, A. *Angew. Chem. Int. Ed.* **2005**, *44*, 3358.

[156] Durmaz, H.; Karatas, F.; Tunca, U.; Hizal, G. *J. Polym. Sci., Part A: Polym. Chem.* **2006**, *44*, 499.

[157] Gandini, A. *Prog. Polym. Sci.* **2013**, *38*, 1.

[158] French, A. C.; Thompson, A. L.; Davis, B. G. *Angew. Chem. Int. Ed.* **2009**, *48*, 1248.

[159] Borgens, R. B.; Bohnert, D. *J. Neurosci. Res.* **2001**, *66*, 1179.

[160] Sun, G.; Hovestädt, M.; Zhang, X.; Hinrichs, K.; Rosu, D. M.; Lauermann, I.; Zielke, C.; Vollmer, A.; Löchel, H.; Ay, B.; Holzhütter, H.-G.; Schade, U.; Esser, N.; Volkmer, R.; Rappich, J. *Surf. Interface Anal.* **2011**, *43*, 1203.

[161] Bruns, M.; Barth, C.; Brüner, P.; Engin, S.; Grehl, T.; Howell, C.; Koelsch, P.; Mack, P.; Nagel, P.; Trouillet, V.; Wedlich, D.; White, R. G. *Surf. Interface Anal.* **2012**, *44*, 909.

[162] Meijer, A.; Otto, S.; Engberts, J. B. F. N. *The Journal of Organic Chemistry* **1998**, *63*, 8989.

[163] Bastin, R.; Albadri, H.; Gaumont, A.-C.; Gulea, M. *Org. Lett.* **2006**, *8*, 1033.

[164] Heuzé, B.; Gasparova, R.; Heras, M.; Masson, S. *Tetrahedron Lett.* **2000**, *41*, 7327.

[165] Zydziak, N.; Preuss, C. M.; Winkler, V.; Bruns, M.; Hübner, C.; Barner-Kowollik, C. *Macromol. Rapid Commun.* **2013**, *34*, 672.

[166] Preuss, C. M.; Goldmann, A. S.; Trouillet, V.; Walther, A.; Barner-Kowollik, C. *Macromol. Rapid Commun.* **2013**, *34*, 640.

[167] Tischer, T.; Claus, T. K.; Oehlenschlaeger, K. K.; Trouillet, V.; Bruns, M.; Welle, A.; Linkert, K.; Goldmann, A. S.; Börner, H. G.; Barner-Kowollik, C. *Macromol. Rapid Commun.* **2014**, *35*, 1121.

[168] Zhu, X. Y.; Jun, Y.; Staarup, D. R.; Major, R. C.; Danielson, S.; Boiadjiev, V.; Gladfelter, W. L.; Bunker, B. C.; Guo, A. *Langmuir* **2001**, *17*, 7798.

[169] Holmberg, K.; Tiberg, F.; Malmsten, M.; Brink, C. *Colloids and Surfaces A: Physicochemical and Engineering Aspects* **1997**, *123–124*, 297.

[170] Zdyrko, B.; Klep, V.; Luzinov, I. *Langmuir* **2003**, *19*, 10179.

[171] Brittain, W. J.; Minko, S. *J. Polym. Sci., Part A: Polym. Chem.* **2007**, *45*, 3505.

[172] Mayadunne, R. T. A.; Rizzardo, E.; Chiefari, J.; Krstina, J.; Moad, G.; Postma, A.; Thang, S. H. *Macromolecules* **2000**, *33*, 243.

[173] Hofe, T., PSS, http://www.pss-polymer.com/infocenter/gpcsec-tippstricks-germandeutsch/.

[174] Sauter, A.; Richter, G.; Micoulet, A.; Martinez, A.; Spatz, J.; Appel, S. *Biointerphases* **2013**, *8*, 1.

[175] Chebbi, R.; Beicha, A.; Daud, W. R. W.; Zaamouche, R. *Appl. Surf. Sci.* **2009**, *255*, 6367.

[176] Agraharam, S.; Hess, D. W.; Kohl, P. A.; Bidstrup-Allen, S. A. *J. Electrochem. Soc.* **1999**, *146*, 1960.

[177] Massia, S. P.; Stark, J. *J. Biomed. Mater. Res., Part A* **2001**, *56*, 390.

[178] Shtenberg, G.; Massad-Ivanir, N.; Moscovitz, O.; Engin, S.; Sharon, M.; Fruk, L.; Segal, E. *Anal. Chem.* **2013**, *85*, 1951.

[179] Connelly, J. T.; Gautrot, J. E.; Trappmann, B.; Tan, D. W.-M.; Donati, G.; Huck, W. T. S.; Watt, F. M. *Nat. Cell. Biol.* **2010**, *12*, 711.

[180] Gautrot, J. E.; Wang, C.; Liu, X.; Goldie, S. J.; Trappmann, B.; Huck, W. T. S.; Watt, F. M. *Biomaterials* **2012**, *33*, 5221.

[181] Wang, J.-L.; Ren, K.-F.; Chang, H.; Jia, F.; Li, B.-C.; Ji, Y.; Ji, J. *Macromol. Biosci.* **2013**, *13*, 483.

[182] Ku, S. H.; Park, C. B. *Biomaterials* **2010**, *31*, 9431.

[183] Wang, Y.; Song, W.; Hu, W. J.; Lin, Q. *Angew. Chem. Int. Ed.* **2009**, *48*, 5330.

[184] Wang, Y.; Hu, W. J.; Song, W.; Lim, R. K. V.; Lin, Q. *Org. Lett.* **2008**, *10*, 3725.

[185] Mantovani, G.; Lecolley, F.; Tao, L.; Haddleton, D. M.; Clerx, J.; Cornelissen, J. J. L. M.; Velonia, K. *J Am Chem Soc* **2005**, *127*, 2966.

[186] Al-Bataineh, S. A.; Britcher, L. G.; Griesser, H. J. *Surf. Interface Anal.* **2006**, *38*, 1512.

[187] Al-Bataineh, S. A.; Britcher, L. G.; Griesser, H. J. *Surf. Sci.* **2006**, *600*, 952.

[188] Kingshott, P.; McArthur, S.; Thissen, H.; Castner, D. G.; Griesser, H. J. *Biomaterials* **2002**, *23*, 4775.

[189] Norrman, K.; Papra, A.; Kamounah, F. S.; Gadegaard, N.; Larsen, N. B. *J. Mass Spectrom.* **2002**, *37*, 699.

[190] Kang, S. M.; You, I.; Cho, W. K.; Shon, H. K.; Lee, T. G.; Choi, I. S.; Karp, J. M.; Lee, H. *Angew. Chem. Int. Ed.* **2010**, *49*, 9401.

[191] Patil, R. R.; Turgman-Cohen, S.; Šrogl, J.; Kiserow, D.; Genzer, J. *Langmuir* **2015**, DOI:10.1021/la5044766.

[192] Bhairamadgi, N. S.; Pujari, S. P.; Leermakers, F. A. M.; van Rijn, C. J. M.; Zuilhof, H. *Langmuir* **2014**, *30*, 2068.

[193] Zhou, D.; Gao, X.; Wang, W.-j.; Zhu, S. *Macromolecules* **2012**, *45*, 1198.

[194] Oxford Dictionaries, http://www.oxforddictionaries.com/definition/english/concept.

[195] Ryou, M.-H.; Lee, Y. M.; Park, J.-K.; Choi, J. W. *Adv. Mater.* **2011**, *23*, 3066.

[196] Nebhani, L.; Sinnwell, S.; Lin, C. Y.; Coote, M. L.; Stenzel, M. H.; Barner-Kowollik, C. *J. Polym. Sci., Part A: Polym. Chem.* **2009**, *47*, 6053.

[197] Lee, B. P.; Huang, K.; Nunalee, F. N.; Shull, K. R.; Messersmith, P. B. *J. Biomater. Sci., Polym. Ed.* **2004**, *15*, 449.

[198] Wagner, H. L. *J. Phys. Chem. Ref. Data* **1985**, *14*, 1101.

[199] Stickler, M.; Panke, D.; Wunderlich, W. *Macromol. Chem. Phys.* **1987**, *188*, 2651.

[200] Gruendling, T.; Guilhaus, M.; Barner-Kowollik, C. *Anal. Chem.* **2008**, *80*, 6915.

[201] Parry, K. L.; Shard, A. G.; Short, R. D.; White, R. G.; Whittle, J. D.; Wright, A. *Surf. Interface Anal.* **2006**, *38*, 1497.

[202] Scofield, J. H. *J. Electron. Spectrosc. Relat. Phenom.* **1976**, *8*, 129.

[203] Tanuma, S.; Powell, C. J.; Penn, D. R. *Surf. Interface Anal.* **1994**, *21*, 165.

[204] Askadskii, A. A. *Physical Properties of Polymers: Prediction and Control*; Gordon and Breach Publ.: Amsterdam, 1996; Vol. 2.

[205] Pop-Georgievski, O.; Popelka, S.; Houska, M.; Chvostova, D.; Proks, V.; Rypacek, F. *Biomacromolecules* **2011**, *12*, 3232.

[206] Herzinger, C. M.; Johs, B.; McGahan, W. A.; Woollam, J. A.; Paulson, W. *Journal of Applied Physics* **1998**, *83*, 3323.

[207] Pop-Georgievski, O.; Neykova, N.; Proks, V.; Houdkova, J.; Ukraintsev, E.; Zemek, J.; Kromka, A.; Rypaček, F. *Thin Solid Films* **2013***, 543,* 180.

[208] Pop-Georgievski, O.; Verreault, D.; Diesner, M. O.; Proks, V.; Heissler, S.; Rypáček, F.; Koelsch, P. *Langmuir* **2012**, *28*, 14273.

[209] Rodriguez-Emmenegger, C.; Kylian, O.; Houska, M.; Brynda, E.; Artemenko, A.; Kousal, J.; Bologna Alles, A.; Biederman, H. *Biomacromolecules* **2011**, *12*, 1058.

List of Publications

[11] *Fusing Catechol-Driven Surface Anchoring with Rapid Hetero Diels-Alder Ligation*

Preuss, C. M.; Zieger, M.; Rodriguez-Emmenegger, C.; Zydziak, N.; Trouillet, V.; Goldmann, A. S.; Barner-Kowollik, C. ***ACS Macro Lett.*** **2014**, *3*, 1169.

[10] *Suppressing Pseudomonas aeruginosa Adhesion via Anti-Fouling Polymer Brushes*

Rodriguez-Emmenegger, C.; Decker, A.; Surman, F.; **Preuss, C. M.**; Sedlákova, Z.; Zydziak, N.; Barner-Kowollik, C.; Schwartz, T.; Barner, L. ***RSC Adv.*** **2014,** *4,* 64781.

[9] *A Bioinspired Light Induced Avenue for the Design of Patterned Functional Interfaces*

Preuss, C. M.; Tischer, T.; Rodriguez-Emmenegger, C.; Zieger, M. M; Bruns, M.; Goldmann, A. S.; Barner-Kowollik, C. ***J. Mater. Chem. B*** **2014**, *2*, 360.

[8] *Controlled Cell Adhesion on Poly(dopamine) Interfaces Photo-Patterned with Non-Fouling Brushes*

Rodriguez-Emmenegger, C.;*** Preuss, C. M.**;***** Yameen, B.; Pop-Georgievski, O.; Bachmann, M.; Mueller, J. O.; Bruns, M.; Goldmann, A. S.; Bastmeyer, M.; Barner-Kowollik, C. ***Adv. Mater.*** **2013**, *25*, 6123.

[7] *A Facile Avenue to Conductive Polymer Brushes via Cyclopentadiene-Maleimide Diels–Alder Ligation*

Yameen, B.; Rodriguez-Emmenegger, C.; **Preuss, C. M.**; Pop-Georgievski, O.; Verveniotis, E.; Trouillet, V.; Rezek, B.; Barner-Kowollik, C. ***Chem. Commun.*** **2013**, *49*, 8623.

[6] *A Facile One-Pot Route to Poly(carboxybetaine acrylamide) Functionalized SWCNTs*

Yameen, B.; Rodriguez-Emmenegger, C.; Ahmed, I.; **Preuss, C. M.**; Dürr, C. J.; Zydziak, N.; Trouillet, V.; Fruk, L.; Barner-Kowollik, C. ***Chem. Commun.*** **2013**, *49*, 6734.

[5] *Hetero Diels-Alder Chemistry for the Functionalization of Single-Walled Carbon Nanotubes with Cyclopentadienyl End-Capped Polymer Strands*

Zydziak, N.; **Preuss, C. M.**; Winkler, V.; Hübner, C.; Bruns, M.; Barner-Kowollik, C. ***Macromol. Rapid Commun.*** **2013**, *34*, 672.

[4] *Biomimetic Dopamine-Diels-Alder Switches*

Preuss, C. M.; Goldmann, A. S.; Trouillet, V.; Walther, A.; Barner-Kowollik, C. ***Macromol. Rapid Commun.*** **2013**, *34*, 640.

[3] *Chiral Benzamidinate Ligands in Rare-Earth-Metal Coordination Chemistry*‡

Benndorf, P.; Kratsch, J.; Hartenstein, L.; **Preuss, C. M.**; Roesky, P. W. ***Chem. Eur. J.*** **2012**, *18*, 14454.

[2] *The Influence of a Potential Diffusion Control on the Outcome of Modular Polymer-Polymer Click Conjugations*†

Preuss, C. M.; Barner-Kowollik, C. ***Macromol. Theory Simul.*** **2011**, *20*, 700.

[1] *Synthesis of Enantiomeric Pure Lithium and Potassium Benzamidinate Complexes*‡

Benndorf, P.; **Preuß, C.**; Roesky, P. W**. *J. Organom. Chem.*** **2011,** *696*, 1150.

* both authors contributed in equally

†Publication resulting from the Diploma thesis.

‡Results from the Vertieferarbeit in collaboration with Professor P. W. Roesky.

Conference Contributions

[7] *Spatially Resolved Photochemical Biosurface Design*

A. S. Goldmann, C. M. Preuss, T. Tischer, C. Rodriguez-Emmenegger, M. Bastmeyer, C. Barner-Kowollik, ***4th International Conference on Multifunctional, Hybrid and Nanomaterials***, Sitges, Spain, March **2015**.

[6] *Advanced (Photo)-Click Conjugation on Bioinspired Mussel Adhesives for Complex Surface Design and Controlled Cell Adhesion*

C. M. Preuss, C. Rodriguez-Emmenegger, V. Trouillet, M. Bruns, A. S. Goldmann, C. Barner-Kowollik, ***4th Zing Polymer Conference 2014***, Cancun, Mexico, December **2014**.

[5] *Advanced (Photo)-Click Conjugation on Bioinspired Mussel Adhesives for Complex Surface Design*

C. M. Preuss, C. Rodriguez-Emmenegger, V. Trouillet, M. Bruns, A. S. Goldmann, C. Barner-Kowollik, ***MRS Fall Meeting and Exhibit 2013***, Boston, USA, December **2013.**

[4] *Functional (Bio) Surfaces for Reversible Coatings*

A. S. Goldmann, C. M. Preuss, T. Tischer, Barner-Kowollik et al., ***Australian Polymer Symposium (34APS) Darwin***, Australia, July **2013**.

[3] *Modular Biosurface Design*

T. Tischer, A. S. Goldmann, C. M. Preuss, A. Walther, G. Delaittre, L. Barner, M. Bruns, H. G. Börner, **C. Barner-Kowollik**, ***EPF 2013***, Pisa, Italy, June **2013**.

[2] *Biomimetic Click-Surfaces*

C. M. Preuss, A. S. Goldmann, V. Trouillet, A. Walther, C. Barner-Kowollik, ***MacroBEGE***, Houffalize, Belgium, December **2012**.

[1] *Orthogonal Mussel Inspired Surface Modification*

C. M. Preuss, **A. S. Goldmann**, V. Trouillet, A. Walther, C. Barner-Kowollik, ***International Conference on Bioinspired and Biobased Chemistry and Materials***, Nice, France, October **2012.**

Danksagung

Zuerst möchte ich mich bei Prof. Dr. Christopher Barner-Kowollik dafür bedanken, dass er mir die Möglichkeit gegeben hat, diese Doktorarbeit auf einem interessanten interdisziplinären Thema in seiner Gruppe durchzuführen. Vielen Dank für die Inspiration, Diskussionen und Unterstützung, auch wenn es manchmal knifflig wurde!

Herzlichen Dank auch an Dr. Anja Goldmann, die mich neben meiner wissenschaftlichen Arbeit auch bei administrativen Fragen stets unterstützt hat und immer eine Lösung gefunden hat.

Ich möchte mich außerdem bei der Deutsche Telekom Stiftung für die Finanzierung meiner Doktorarbeit, aber vor allem auch für die Chancen bedanken, die mir im Zusammenhang mit diesem Stipendium eröffnet wurden. Die Stipendiatentreffen und Seminare haben nicht nur zum interdisziplinären Austausch mit anderen Stipendiaten beigetragen, sondern auch eine wissenschaftliche Gemeinschaft geformt, die auch in Zukunft bestehen wird. Hier möchte ich insbesondere unserer Stipendiatenbetreuerin und Projektleiterin Frau Frense-Heck danken, die neben den organisatorischen Aufgaben auch immer ein offenes Ohr für die Belange der Stipendiaten hatte. Ein ganz besonderes Dankeschön auch an unseren langjährigen Vorstand Dr. Klaus Kinkel, der wie ich aus dem schönen “Schwobaländle” kommt.

Des Weiteren möchte ich mich bei der Landesgraduiertenförderung für die finanzielle Unterstützung im ersten Jahr meiner Doktorarbeit bedanken.

Ich danke Dr. Michael Bruns, Vanessa Trouillet, Vanessa Oberst, Udo Geckle und Volker Winkler aus meinem „zweiten” Arbeitskreis am Campus Nord für die schöne Zeit, die ich bei ihnen am Anfang meiner Promotion verbringen durfte.

Außerdem möchte ich meinen Kooperationspartnern und Co-Autoren für die ausgezeichnete Zusammenarbeit danken, die viele wertvolle Publikationen hervorgebracht hat.

Vielen Dank an Professor Dr. Peter W. Roesky für seine Unterstützung wenn immer ich danach gefragt habe und die Beratung bezüglich unserer Weihnachtsexperimentevorführung.

Außerdem möchte ich Herrn Prof. Michael A. R. Meier für die Unterstützung bei der Bewerbung auf das Stipendium der Deutsche Telekom Stiftung danken.

Thanks to the following people for proof reading my thesis: Dr. César Rodriguez-Emmenergger, Dr. Ognen Pop-Georgievsky, Dr. Christiane Lang, Dr. Michael Kaupp, Dr. Thomas Tischer and Dr. Anja S. Goldmann.

Ich danke meinen Meistern Michi und Thomas (ich hab jetzt mal die Größenbezeichnungen weggelassen ;-)) : es war mir eine Ehre euer Padawan zu sein! Ich habe viel von euch beiden gelernt, vor allem fürs Leben! Vielen Dank für eure Freundschaft und die unzähligen Male, in denen ihr mich einfach „entschleunigt" habt als es bitternötig war. "Come to the dark side – We have cookies!"

Vielen Dank an Christiane – die Chefin. Du hast mir von Anfang an das Gefühl gegeben, willkommen zu sein und mich an die Hand genommen. Danke für deine Freundschaft und die Unterstützung, die ich nicht nur im wissenschaftlichen Zusammenhang von dir bekommen habe. Ich werde dich vermissen!

Außerdem möchte ich meinen „Kleinen" Markus, Nils und Kai H. (adoptiert) für die Zusammenarbeit, das gemeinsame Kämpfen und die Freundschaft danken.

Danke an meine früheren und jetzigen „Labmates" und meine „Mitinsassen" im großen Büro. Ganz besonderen Dank an Nathalie, César, Elena, Markus, Quicky, Thomas G., Thomas T., Mathias G., Kai H. und Jan. Vielen Dank außerdem an Frau Schneider, Vincent, Astrid und Doris.

¡Muchas gracias a mis compañeros, a los profesores y sobretodo a un muy buen amigo, el Dr. César Rodríguez-Emmemegger por todo lo que ha hecho por mí. César, ¡gracias por tu amistad, tu paciencia y tu tiempo! I also would like to thank Nina for being such a good friend and for always making me feel welcome.

Chère Vanessa, je vous remercie de tout cœur pour les nombreuses conversations merveilleuses et de précieux conseils que tu m'as donné. Merci, que tu es toujours là pour moi!

Susanne, tack för din vänskap, glädje och lite galen tid i labbet! Jag kommer alltid att minnas vår fina tid tillsammans i Karlsruhe! Pussar, Cookie

Vielen Dank an meine Studienfreunde und Dienstagsmittagessensgruppe (auch „der Harem" genannt) Matthias und Ulrike und deren Partner Karola und Kevin. Erster Tag in Karlsruhe im OCF: „Ich hätte niemals ohne euch beide die Etherdestille aufgebaut bekommen!" sagt die OC-Biene zu den PC-Freaks. ;-)

An meine Tübinger Mädels, Susi und Sabine: Danke für die schöne Zeit mit euch im Grundstudium!

Außerdem möchte ich meinen neu in Karlsruhe gewonnenen Freunden Steffi, Thomas, Michi, Yvonne, Nico und Strubbel für die schönen Spieleabende, Kinobesuche und ihre Freundschaft danken. Zitat Strubbel: „Auf einmal war sie da!"

An meine (sehr) große Verwandtschaft: Danke, dass ihr immer an mich geglaubt habt. Ganz besonderen Dank an Bene, Hebe, Irina, Regi, Maike und Anike.

An dieser Stelle ist es mir besonders wichtig, mich an meinen Opa Siegfried zu erinnern, der letztes Jahr im Dezember verstorben ist. Ich war immer sein ganzer Stolz und es hätte mich glücklich gemacht, wenn er den Abschluss meiner Doktorarbeit noch hätte miterleben können. Herzlichen Dank, dass du und Oma immer für mich da wart!

Vielen Dank auch an meine Freundin Rebecca, die ich auf ganz schicksalhafte Weise kennengelernt habe. Hätten sich unsere Wege nicht zweimal zufällig gekreuzt, würde ich dich heute nicht kennen. Danke für deine Freundschaft, für das viele Reden und Zuhören und unsere Teeabende.

Nun, die Geschichte ist etwas länger, aber ohne meine Freundin Chrissi hätte ich viele Situationen in den 18 Jahren (Ja, Chrissi, es ist so lang und im Sommer werden es 19) die wir uns schon kennen, nicht so gut gemeistert. Chrissi, ich weiß gar nicht wo ich genau anfangen soll, aber ich danke dir für alles, was du jemals für mich getan hast: Für die Unterstützung, das Kopf Zurechtrücken, das Zuhören, die stundenlangen Telefonate, die unzähligen schönen Mädelsabende, … Danke, dass es dich gibt!

Zuletzt und am allermeisten danke ich meiner Familie. Meinem Papa, meiner Mama und meinem kleinen Bruder Steffen. Ihr seid die allerbeste Familie, die man sich wünschen kann und ohne euch wäre ich heute niemals wo ich jetzt bin. Danke, dass ihr immer für mich da seid und mich unterstützt! Ich hab euch lieb!